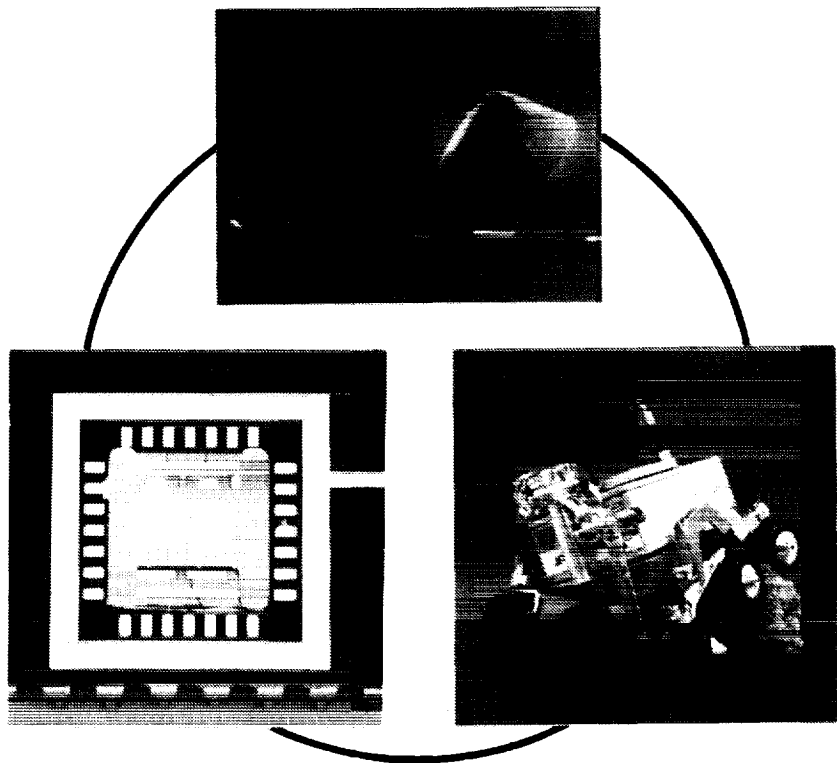


Proceedings of the Workshop on Microtechnologies and Applications to Space Systems

Held at the Jet Propulsion Laboratory on
May 27 and 28, 1992



June 15, 1993

NASA

National Aeronautics and
Space Administration

Jet Propulsion Laboratory
California Institute of Technology
Pasadena, California

This publication was prepared by the Jet Propulsion Laboratory, California Institute of Technology, under a contract with the National Aeronautics and Space Administration.

**WORKSHOP PROCEEDINGS:
MICROTECHNOLOGIES AND APPLICATIONS TO SPACE SYSTEMS**

ABSTRACT

Study Coordinator and Proceedings Editor: B.A. Wilson
Jet Propulsion Laboratory, California Institute of Technology

Workshop Chairs: F.Y. Hadaegh, W.J. Kaiser and B.A. Wilson
Jet Propulsion Laboratory, California Institute of Technology

During FY'92, the NASA Code RS System Analysis RTOP funded a study to evaluate the potential impact of emerging microtechnologies on future space missions. As part of this study, a workshop, "Microtechnologies and Applications to Space Systems" was held May 27-29th, 1992, in Pasadena, CA. This volume serves as the Proceedings of this workshop. It contains the manuscripts provided by plenary and parallel session presenters, and summary reports generated from this material and from information presented during the panel discussions. Where manuscripts were not provided, extended abstracts, if available, have been included. The order of the papers follows the original workshop agenda.



**WORKSHOP PROCEEDINGS:
MICROTECHNOLOGIES AND APPLICATIONS TO SPACE SYSTEMS**

FOREWORD

Study Coordinator and Proceedings Editor: B.A. Wilson
Jet Propulsion Laboratory, California Institute of Technology

Workshop Chairs: F.Y. Hadaegh, W.J. Kaiser and B.A. Wilson
Jet Propulsion Laboratory, California Institute of Technology

During FY'92, the NASA Code RS System Analysis RTOP funded a study to evaluate the potential impact of emerging microtechnologies on future space missions. As part of this study, a workshop, "Microtechnologies and Applications to Space Systems," was held May 27-29th, 1992, in Pasadena, CA. There were three main goals of the workshop:

- Provide a forum for the fruitful exchange of ideas on emerging and future microtechnologies, and stimulate the development of a NASA-wide microtechnology community
- Provide an overview of emerging microtechnology capabilities, and evaluate their potential for future NASA applications
- Identify important near-term NASA applications of these emerging technologies, and develop an integrated technology development plan to meet these requirements by the target dates

Pre-workshop discussions involving JPL, LaRC, LeRC and GSFC personnel, as well as interactions with non-NASA funding agencies including NSF, SDI, DARPA, AFOSR and the Gas Research Institute, led to the identification of six key applications areas. Panels were convened as part of the workshop to focus attention on these key areas:

| Application Area | Panel Chairs |
|---------------------------------------|---|
| Science Instruments | Ben Clark (Martin Marietta), Gregg Vane (JPL) |
| Microrovers | Ken Gabriel (NRL), Subramani Venkataraman (JPL) |
| Guidance and Control | John DiBattista (NASA), Fred Hadaegh (JPL), Claude Keckler (LaRC) |
| Space Station, Shuttle and Propulsion | W.T. Powers (MSFC), Gerald Voecks (JPL) |
| Microspacecraft | Denis Connolly (LeRC), Ross Jones (JPL) |
| Microtechnologies of the Future | Frank Grunthaner (JPL), John Hines (ARC), Brent Mott (GSFC) |

The charge of the first four panels was to evaluate the potential of emerging device concepts such as microsensors and actuators in their respective application areas. The Microspacecraft Panel had a somewhat different charter. They started with a first-generation microspacecraft defined as the "microtechnology" element, and examined the subsystem and integration requirements for a near-term implementation. Their charge was to identify areas requiring further development, regardless of the nature of the technologies involved. Finally, the Microtechnologies of the Future Panel attempted to identify microtechnology development areas of the future which offer the most revolutionary new possibilities for enhancing the science return of NASA space missions. Panel membership is detailed in the Appendix.

The three-and-a-half-day workshop consisted of a day and a half of plenary sessions, an afternoon of focused parallel sessions, and a third morning of panel discussions. The plenary session topics, listed below, were deemed relevant to all applications areas.

| Plenary Session Topics | Speakers |
|-------------------------------|--|
| Future Visions | Charles Elachi (JPL), George Hazelrigg (NSF), Kurt Petersen (Lucas NovaSensor) |
| Mission and Science Goals | Corinne Buoni (SAIC), Lonnie Lane (JPL), Paul Henry (JPL), Jim Randolph (NASA), Aldo Bordano (JSC) |
| Microtechnology Programs | Stephen Jacobsen (Univ. of Utah), Mick Blackledge (SDI), Al Wheatley (DARPA), Dave Lavery (NASA), Ned Godshall (Sandia), Robert Warrington (Louisiana Tech. Univ.), Bill Kaiser (JPL), Richard White (UC Berkeley), Noel Macdonald (Cornell Univ.), Henry Guckel (Univ. of Wisconsin-Madison), Wilfrid Veldkamp (Lincoln Laboratory), Joseph Stetter (Transducer Research, Inc.) |
| Applications Overviews | Bill Trimmer (Princeton Univ.), Jan Iwanczyk (Xsirius, Inc.), Jim Tillman (Univ. of Washington), Ken Gabriel (NRL), Marc Madou (Teknekron), M.G. Littman (Princeton Univ.), Dave Miller (MIT), Charles Kyriacou (JPL), Ross Jones (JPL), Glen Kissel (JPL), Stephen Johnson (Martin Marietta) |

Parallel sessions were held in each of the six key applications areas, and were moderated by the associated panel chairs. These sessions consisted of a mixture of presentations and open discussions. During the final morning sessions, which were restricted to panel members and designated guests, the panels reviewed the information presented at the workshop, and generated a set of recommendations to NASA on key technology developments in their respective areas.

This Proceedings contains the manuscripts provided by plenary and parallel session presenters, and summary reports generated from this material and from information presented during the panel discussions. Where manuscripts were not provided, extended abstracts, if available, have been included. The order of the papers follows the original workshop agenda. The full workshop agenda is provided in the Appendix.

**WORKSHOP PROCEEDINGS:
MICROTECHNOLOGIES AND APPLICATIONS TO SPACE SYSTEMS**

CONTENTS

| | PAGE |
|--|-------------|
| ABSTRACT | iii |
| <i>B.A. Wilson, F.Y. Hadaegh and W.J. Kaiser</i> | |
| FOREWORD | v |
| <i>B.A. Wilson, F.Y. Hadaegh and W.J. Kaiser</i> | |
| FUTURE VISIONS | 1 |
| Future Trends in Small Missions and the Need for Microtechnology | 3 |
| <i>Charles Elachi</i> | |
| The NSF Microtechnology Program, or Robots on the Head of a Pin | 5 |
| <i>George Hazelrigg</i> | |
| Silicon Micro-Instrumentation | 7 |
| <i>Kurt Petersen</i> | |
| NASA MISSION & SCIENCE GOALS | 9 |
| The Solar System Exploration Program: Goals, Strategy, and Plans | 11 |
| <i>Carl Pilcher</i> | |
| The Pluto Fast Flyby Mission: Completing the Reconnaissance of the Solar System | 13 |
| <i>Paul K. Henry</i> | |
| MICROTECHNOLOGY PROGRAM OVERVIEWS | 15 |
| DoD Advanced Space Technology Program Challenge | 17 |
| <i>Major Al Wheatley</i> | |
| Micromechanics Program at Sandia: Micromechanical Sensors, Actuators, and Devices | 19 |
| <i>Ned A. Godshall</i> | |
| Micromanufacturing: Recent Developments in this Country and Abroad | 21 |
| <i>Robert O. Warrington, Craig R. Friedrich, Robert X. Gao and Gang Lin</i> | |
| Microsensors and Microinstruments: New Measurement Principles and New Applications | 29 |
| <i>W. J. Kaiser, T. R. VanZandt, T. W. Kenny, W. B. Banerdt and D. Crisp</i> | |
| Micro-Sensors, -Actuators, and -Systems: Accomplishments and Prospects | 31 |
| <i>Richard M. White</i> | |
| National Nanofabrication Facility and Nanoelectromechanics | 33 |
| <i>Noel C. MacDonald</i> | |
| Microactuator Production Via High Aspect Ratio, High Edge Acuity Metal Fabrication Technology | 35 |
| <i>H. Guckel and T.R. Christenson</i> | |
| Overview of Microoptics: Past, Present, and Future | 43 |
| <i>Wilfrid B. Veldkamp</i> | |
| Microsensors, Smart Sensors, Sensor Arrays, and the Artificial Nose | 55 |
| <i>Joseph R. Stetter</i> | |

| | |
|--|---------|
| APPLICATION OVERVIEWS | 57 |
| Micromechanical Actuators | 59 |
| <i>William Trimmer</i> | |
| In situ Meteorological Sensors for Earth and Mars | 61 |
| <i>James E. Tillman</i> | |
| Silicon Flexural Microelectromechanical Devices | 63 |
| <i>K.J. Gabriel</i> | |
| Micromachining the Future | 65 |
| <i>Marc Madou</i> | |
| Learning From Biology—Motor Systems at All Scales | 67 |
| <i>M.G. Littman</i> | |
| Micro-Software for Micro-Robots | 69 |
| <i>David P. Miller</i> | |
| Spacecraft Telecommunications Technology for Microspacecraft Applications | 71 |
| <i>K. Kellogg and C. Kyriacou</i> | |
| Microspacecraft: A Concept | 73 |
| <i>Ross M. Jones</i> | |
| Micro Guidance and Control Technology Overview | 75 |
| <i>Glen J. Kissel and Fred Y. Hadaegh</i> | |
| SCIENCE INSTRUMENTS | 83 |
| Miniaturization in X-Ray and Gamma-Ray Spectroscopy | 85 |
| <i>Jan S. Iwanczyk, Yuzhong J. Wang and James G. Bradley</i> | |
| Backscatter Mössbauer Spectrometer (BaMS) for Extraterrestrial Applications | 95 |
| <i>D.G. Agresti, T.D. Shelfer, M.M. Pimperl, E.L. Wills, M.H. Shen and R.V. Morris</i> | |
| A Sub-cm Micromachined Electron Microscope | 99 |
| <i>A.D. Feinerman, D.A. Crewe, D.C. Perng and S.E. Shoaf</i> | |
| Differential Scanning Calorimetry (DSC) for Planetary Surface Exploration | 121 |
| <i>James L. Gooding and Douglas W. Ming</i> | |
| Micro-Sensors for in-situ Meteorological Measurements | 123 |
| <i>David Crisp, William J. Kaiser, Thomas R. VanZandt and James E. Tillman</i> | |
| A Broad-Band Microseismometer for Planetary Applications | 125 |
| <i>W.B. Banerdt, T. VanZandt, W.J. Kaiser and T.W. Kenny</i> | |
| Imaging Spectrometry of the Earth and Other Solar System Bodies | 127 |
| <i>Gregg Vane</i> | |
| Smart Focal-Plane Technology for Micro-Instruments and Micro-Rovers | 129 |
| <i>Eric R. Fossum</i> | |
| Evolution of Miniature Detectors and Focal Plane Arrays for Infrared Sensors | 131 |
| <i>Louis A. Watts</i> | |
| MICROSPACECRAFT | 141 |
| Asteroid Investigation with Microspacecraft (AIM) | 143 |
| <i>Christopher G. Salvo</i> | |
| Development of MMIC Technology for SATCOM Applications | 145 |
| <i>John J. Berenz</i> | |
| Power Subsystem State-of-the-Art Assessment and Miniaturization Technology Needs | 147 |
| <i>R.C. Detwiler</i> | |
| The Application of Microtechnology to Spacecraft On-Board Computing | 149 |
| <i>Leon Alkalaj</i> | |

| | |
|---|-----|
| Electronic Packaging for Microspacecraft Applications | 151 |
| <i>David Wasler</i> | |
| Microspacecraft Attitude Control | 153 |
| <i>George E. Sevaston</i> | |
| Lightweight Structures and Mechanisms for Microsatellites | 155 |
| <i>Robert Wendt</i> | |
| Advanced Microfabrication Technologies for Microspacecraft | 157 |
| <i>M. Ghezzi, B. Bagepalli, S. Kodiyalam, C. Korman, K. Browall and Norman Alexander</i> | |
| Microspacecraft for Space Science in ISAS, Japan | 159 |
| <i>Hirobumi Saito</i> | |
| SPACE STATION, SHUTTLE & PROPULSION | 161 |
| Microfabricated Silicon Biosensors for Microphysiometry | 163 |
| <i>L.J. Bousse, J.M. Libby and J.W. Parce</i> | |
| MICROROVERS | 183 |
| Robotic Vehicles for Planetary Exploration | 185 |
| <i>Brian H. Wilcox</i> | |
| Difficulties Inherent in Miniaturizing Current Rover Technologies for Use as Planetary Explorers | 187 |
| <i>Gerald P. Roston</i> | |
| Micromachining Technologies for Automotive Applications | 189 |
| <i>William C. Tang</i> | |
| Toward Milli-Newton Electro- and Magneto-Static Microactuators | 191 |
| <i>Long-Sheng Fan</i> | |
| Micro Structures and Micro Actuators for Implementing Sub-Millimeter Robots | 193 |
| <i>R.S. Fearing</i> | |
| MICROTECHNOLOGIES OF THE FUTURE | 203 |
| Micromachined Electron Tunneling Infrared Sensors | 205 |
| <i>T.W. Kenny, W.J. Kaiser, J.A. Podosek, H.K. Rockstad and J.K. Reynolds</i> | |
| Macro, Mini, Micro and Nano (M ³ N) Technologies for the Future | 213 |
| <i>Craig R. Friedrich, Robert O. Warrington, Robert X. Gao and Gang Lin</i> | |
| GUIDANCE & CONTROL | 223 |
| Control of Micromachined Deformable Mirrors | 225 |
| <i>M.L. Agronin, R. Bartman, F.Y. Hadaegh, W. Kaiser and P.K.C. Wang</i> | |
| Emerging Technologies in Microguidance and Control | 247 |
| <i>Marc S. Weinberg</i> | |
| Integrated Microgyroscope | 257 |
| <i>Timothy J. Hawkey and Richard P. Torti</i> | |
| GEC Ferranti Piezo Vibratory Gyroscope | 265 |
| <i>J.D. Nuttall</i> | |
| The Application of Micromachined Sensors to Manned Space Systems | 279 |
| <i>Aldo Bordano, Gary Havey, Jerry Wald and Hatem Nasr</i> | |
| Micro Guidance and Control Synthesis: New Components, Architectures and Capabilities | 289 |
| <i>Edward Mettler and Fred Y. Hadaegh</i> | |

| | |
|---|-----|
| Micro-Opto-Mechanical Devices and Systems Using Epitaxial Lift Off | 305 |
| <i>C. Camperi-Ginestet, Young W. Kim, S. Wilkinson, M. Allen and N.M. Jokerst</i> | |
| Miniature Wide Field-of-View Star Trackers for Spacecraft Attitude | |
| Sensing & Navigation | 317 |
| <i>William McCarty, Eric Curtis, Anthony Hull and William Morgan</i> | |
| Novel Position Sensor Technologies for Micro Accelerometers | 329 |
| <i>T.R. VanZandt, T.W. Kenny and W.J. Kaiser</i> | |
| SUMMARY REPORTS | 331 |
| Report of the Microspacecraft Panel | 333 |
| <i>Ross M. Jones and Denis Connolly</i> | |
| Micro Guidance and Control Panel Recommendations | 339 |
| <i>John DiBattista, Fred Y. Hadaegh and Claude Keckler</i> | |
| Workshop Summary Report | 349 |
| <i>B.A. Wilson, F.Y. Hadaegh and W.J. Kaiser</i> | |
| APPENDIX | 355 |
| Agenda | 357 |
| Workshop Panels | 360 |

Microtechnologies
and
Applications to Space Systems Workshop

FUTURE VISIONS

Future Trends in Small Missions and the Need for Microtechnology

Charles Elachi
Jet Propulsion Laboratory
California Institute of Technology
Pasadena, California 91109

ABSTRACT

During the next decade, the trend will be to emphasize small missions which can be implemented rapidly (2 to 3 years) and are affordable, but still scientifically exciting and publicly engaging. These seemingly contradictory objectives could be accomplished by relying on new advanced technology, particularly microtechnologies that allow significant capability in a low volume/low mass spacecraft.

In this talk I will review some of the most engaging planetary and earth missions which would significantly benefit from microtechnologies and discuss the needs in the areas of remote and in-situ sensors, spacecraft subsystems and rovers.

PRECEDING PAGE BLANK NOT FILMED

The NSF Microtechnology Program,
or
Robots on the Head of a Pin

George Hazelrigg
National Science Foundation
Washington, DC

Researchers at AT&T Bell Labs, the University of California at Berkeley, and other institutions have recently developed techniques for fabricating fully released mechanical and electromechanical parts on silicon substrates using techniques of microelectronics fabrication. Mechanical mechanisms including gears and gear trains, pneumatic turbines, and linkages on a scale of 50 to 500 microns have been successfully fabricated. A variety of electrostatic rotating and resonant motors have been fabricated and operated. A major breakthrough has been the development of methods for fabricating such devices fully assembled, that is, such that they require no further assembly prior to operation. Thus, in mass production, microelectromechanical devices hold the potential for extremely low cost. Gears and motors could be fabricated for as little as \$0.001. This presentation will discuss the state-of-the-art of this emerging technology, and the role that the National Science Foundation is playing in its emergence.

Silicon Micro-Instrumentation

Kurt Petersen
Lucas NovaSensor
Fremont, CA

ABSTRACT

Silicon micromachining technology is creating new research and development opportunities for innovation and astonishing new products, seemingly not far removed from science fiction. Japanese researchers have even proposed microrobots which roam the body's vascular system, searching for and destroying invading microorganisms. Whole new industries are evolving and growing, from high volume automotive components to specialty scientific, medical, and biological instruments, in an atmosphere of intense international competition. This presentation will discuss the fundamentals of the technology as well as practical commercial applications. Devices demonstrated are as diverse as automotive crash detectors controlling air-bag deployment, to instruments for operating on eyes, blood vessels, and even individual cells, to microvalves for fluid control, to pressure and acceleration sensors for aerospace, industrial, and consumer applications. Several futuristic micro-electro-mechanical systems and/or instruments will also be proposed and discussed.

PRECEDING PAGE BLANK NOT FILMED

Microtechnologies
and
Applications to Space Systems Workshop

NASA MISSION & SCIENCE GOALS



The Solar System Exploration Program:
Goals, Strategy, and Plans

Carl Pilcher, Chief
Solar System Exploration Division
NASA Headquarters

ABSTRACT

The planetary exploration program, spanning three decades of exciting and successful planetary achievements included the visitation of American spacecraft to every planet in the solar system except Pluto. NASA's current plans provide for completing the reconnaissance of our own solar system; the continued systematic exploration of the inner planets, outer planets, and small bodies; and the expansion of the horizon to include the search for planets around other stars. The goals, strategy, and the structure and plans for the FY 1994 - 2003 time frame are presented in the context of the current programmatic and technical imperatives, including the foreseen opportunities for and contributions of microtechnologies.

PRECEDING PAGE BLANK NOT FILMED



THE PLUTO FAST FLYBY MISSION:
COMPLETING THE RECONNAISSANCE OF THE SOLAR SYSTEM

Paul K. Henry

Jet Propulsion Laboratory
California Institute of Technology
Pasadena, CA 91109

ABSTRACT

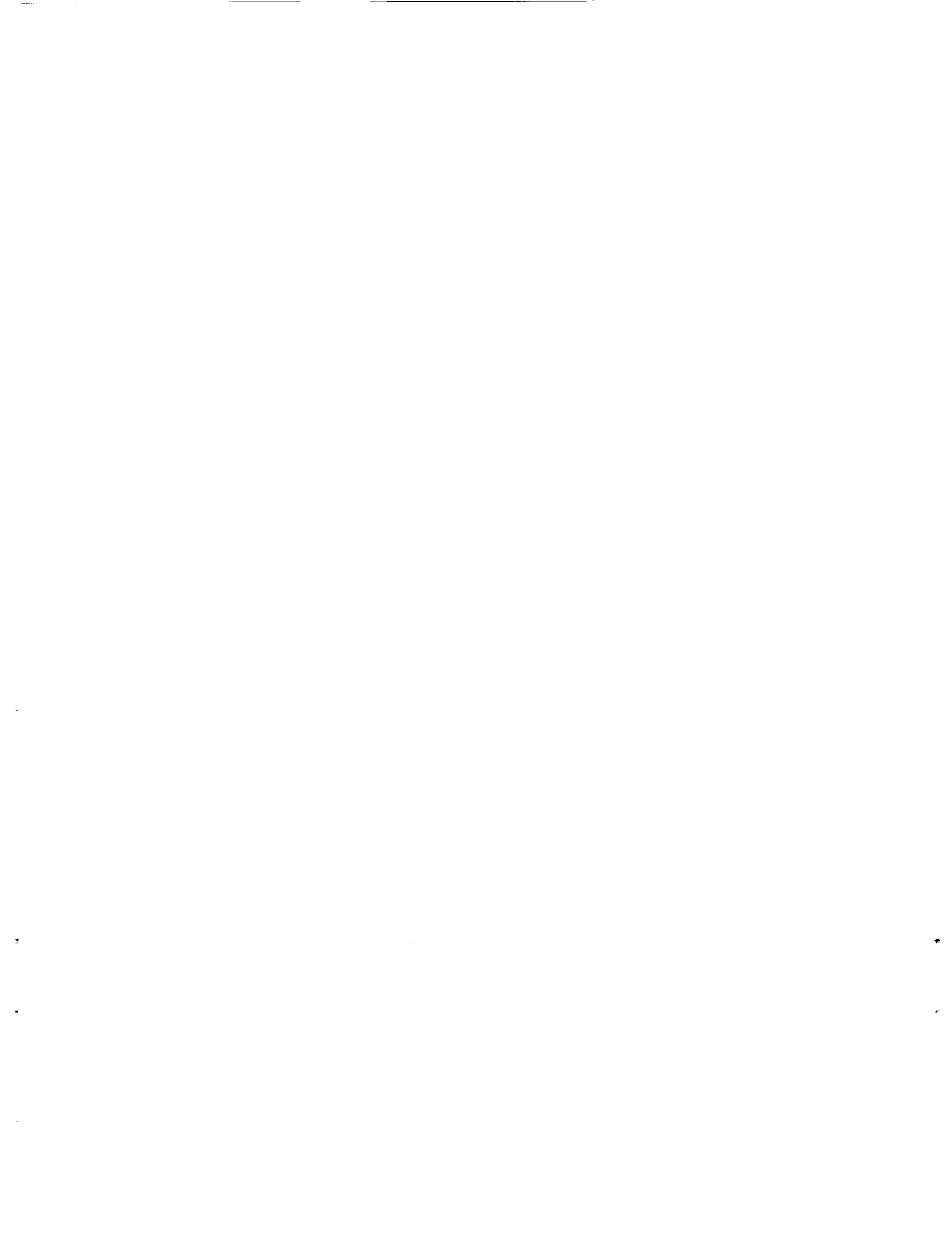
The concept of a fast flyby mission to Pluto has been advanced as a means to complete the reconnaissance of the known solar system. In order to acquire data on the Pluto system at the earliest possible time, and within the professional lifetime of investigators now active in the field, concepts are being developed for relatively small spacecraft in the mass range of 70 Kg to 350 Kg with flight times to Pluto of 7 to 13 years.

Necessarily, the science complement on such a mission will be very mass and power limited. The challenge will be to define a spacecraft and an instrument package that will maximize the scientific return within these limitations.

Cost, of course, will be a major consideration, and funds for new technology development specific to this mission will not be extensive. Consequently, innovative ways to incorporate elegant simplicity into the designs must be found.

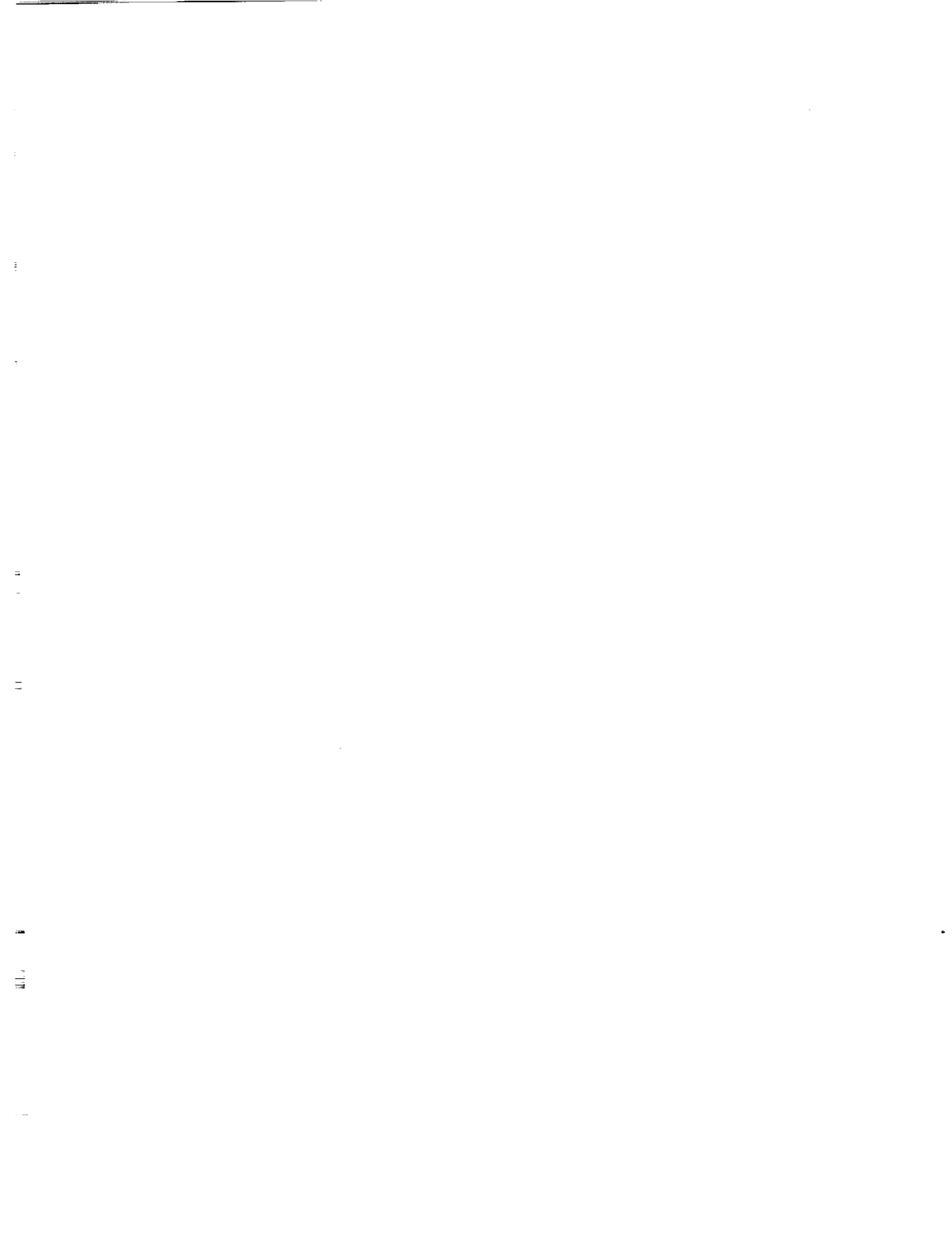
In order to facilitate exploration of the Pluto-Charon system, fully integrated science payloads must be developed. Two proposed mission designs involving limited mass and power science payloads have been presented to the Outer Planets Science Working Group (OPSWG). These payload mass allocations range from 5 to 30 kilograms with power allocations as low as 5 watts. The drivers behind these low mass and power allocations are that they enable developing missions to fit within the moderate mission cost profile and allow fast flight times to Pluto (7 to 13 years).

The OPSWG has prioritized science goals for this class of reconnaissance mission. Three specific science objectives were identified as the highest priority required for the first Pluto mission. These goals were: 1) Study of the neutral atmosphere, 2) Geology and morphology, and 3) Surface compositional mapping. In order to achieve these science goals within the constraints of low mass, power and cost, it may be necessary to combine the functions of 3 conventional instruments (CCD camera, Ultra-Violet Spectrometer, and Infrared Spectrometer) into one fully integrated payload. Where possible, this payload would share optics, mechanisms, electronics and packaging.



Microtechnologies
and
Applications to Space Systems Workshop

**MICROTECHNOLOGY
PROGRAM OVERVIEWS**



DoD Advanced Space Technology Program Challenge

Major Al Wheatley
Defense Advanced Research Projects Agency

Micro and miniature technologies provide the military with the ability to build highly capable small satellites. Small satellites require shorter development times, allow procurement flexibility and provide rapid technology insertion for affordable modernization of DoD space systems. The Defense Advanced Research Projects Agency's (DARPA) Advanced Space Technology Program is a comprehensive technology program which is developing a broad spectrum of advanced technologies, responsive and economical launch vehicles, and demonstrating advanced technologies and concepts using Lightstats as a demonstration vehicle.

In this talk, ASTP's progress over the past three years and challenges for the future will be presented. Small launch vehicles, Lightstats, and miniature and microtechnologies for satellite subsystems, communications systems, optical systems and submarine laser communications are highlighted.



Micromechanics Program at Sandia:
Micromechanical Sensors, Actuators, and Devices

Ned A. Godshall, PhD
Sandia National Laboratories
Microelectronics and Photonics Center

The '*micromachining*' of silicon-based materials is a rapidly growing field that allows the fabrication of extremely small, three-dimensional, mechanical and electromechanical structures by utilizing present microelectronic processes and equipment. '*Micromechanics*', like '*microelectronics*', are devices which are batch-fabricated on silicon wafers, and thus enjoy the same high reproducibility, small size, and low-cost economics of scale historically present in the microelectronics industry. The two technologies are strongest when integrated together to make '*smart sensors*': micromechanical sensors with on-chip integrated microelectronics. The applications of micromechanics lie principally in the fields of physical sensors, chemical sensors, electromechanical actuators, and advanced microelectronic packaging. Specific examples of micromechanical devices are pressure transducers, accelerometers, microgears, micromotors, and microvalves. The ubiquitous emphasis on miniaturization is driving the rapid growth of micromechanics, for both weapon and commercial applications.

The dimensions of micromechanical devices are typically on the order of 10 to 100 μm (0.0004" to 0.004"), or about the size of a human hair width. These dimensions are much smaller than manufacturable by conventional machining techniques -- yet they are easily manufactured with present photolithographic equipment, since they are larger than typical microelectronic critical dimensions. As size decreases, the reliability of sensor components can be greatly increased through the use of sensor redundancy -- since several micromachined sensors can be placed on a single die. Current micromechanics projects within Sandia's *Microelectronics and Photonics Center* include development of 1) a micromachined quartz resonator, 2) micromachined polysilicon microgears and actuators for surety components, 3) a non-contact micromachined Atomic Force Sensor, 4) a solid state hydrogen sensor, and 5) very small field emission structures for vacuum microelectronics and flat panel displays.



Micromanufacturing: Recent Developments in this Country and Abroad

Robert O. Warrington, Director Craig R. Friedrich, Associate Professor
Robert X. Gao, Research Associate Gang Lin, Visiting Assistant Professor

**Institute for Micromanufacturing
Louisiana Tech University
Ruston, Louisiana 71272
(318) 257-2357**

Introduction

Often defined as an "emerging" technology, the microelectromechanical systems (MEMS) technologies have their roots in research activities back to the early 60s, as the first micro pressure sensors were fabricated using the anisotropic etching method [1]. Since then, the fabrication techniques developed in microelectronics have begun to directly impact the progress in micromechanics. During these years, pioneer research work in electrostatically-driven microstructures has been performed [2] which a decade later found its further development in surface micromachining for sensor formation [5].

During the 1970s, numerous industrial companies were involved in the efforts to commercialize the existing microfabrication technologies for a new generation of products featuring light weight, small volume and high efficiency. Among those pioneers, Texas Instruments succeeded in marketing micro printing elements in computer accessories and terminal products [3]. At the end of the 70s, the controlled anisotropic undercut etching technique was further developed which resulted in microcantilever beams and similar micromechanical structures.

The continuing exploitation of VLSI processing methods in the 1980s has opened considerable opportunities for the further invention of unique silicon-based micromechanical devices as well as the creation of new markets [4]. In response to the growing need for application specific integrated circuit chips (ASICs), custom design and fabrication facilities have been implemented. The concept of the "IC Foundry" quickly found its expression as the "Silicon Micromechanics Foundry" in the development and production of micromechanical structures [6]. Also during this time, based on a combination of deep-etch lithography and subsequent high-precision replication, a new micromachining technique, known as the "LIGA" process, was introduced in Germany for producing three dimensional microstructures [7]. Innovative improvement and modification to this process have subsequently been made by researchers at the University of Wisconsin [17]. Besides conventional electromagnetic actuators, various types of electrostatic motors and actuators featuring simple structure, micro size and high force/volume ratio were developed worldwide [8] - [11]. Also, different materials were investigated for possible applications in the micro robot domain, such as the shape memory alloy (SMA) [12].

Parallel to the endeavors of pushing ahead the micromanufacturing technique down to the order of submicron and nanometer scales, there have been numerous activities reported which focus on applying different micromachining technologies to fabricate end products which are mainly mini with microcomponents, such as the microcompact heat exchangers produced with diamond bit cutting [13]. To meet the increasing need for metrology and products inspection in the submicron and nano scale, atomic-force microscopes are under further development [14]. Also, micro EDM, molding, plating and many other new techniques are emerging to augment the microsensor and actuator fabrication [16]. It is evident that micromanufacturing technologies will lead to commercialization of revolutionary devices which will dramatically change our lives in the 21st century.

This paper will describe recent activities in high aspect ratio MEMS, the Louisiana initiatives in MEMS through the newly formed Institute for Micromanufacturing at Louisiana Tech University and their collaboration with the Center for Advanced Microstructures and Devices at Louisiana State University, and a brief discussion of MEMS activities in Russia.

The Louisiana Initiatives in MEMS

The Center for Advanced Microstructures and Devices (CAMD) at Louisiana State University was established in 1987 by a grant from the Department of Energy. The facility currently consists of an electron storage ring with a linac injector, two beamlines which are under construction, and ancillary equipment. The Institute for Micromanufacturing (IfM) at Louisiana Tech University was established in 1991 by grants from the Department of Energy. This institute consists of a research building for multiple process micromachining, cleanrooms, process equipment, and state-of-the-art metrology and testing equipment. Additional equipment and line item funding for personnel, operating and supplies, for both facilities has been provided by the state of Louisiana. CAMD synchrotron is very close to being operational with the first beamlines due to be installed shortly. The institute building is currently under architectural design and construction should start by late 1992 or early 1993. Staffing for both facilities is underway. A more complete description of CAMD and IfM are given below.

The Institute for Micromanufacturing

The Institute for Micromanufacturing will be composed of three components. The focal point for the Institute for Micromanufacturing will be the component for research and development located on the Louisiana Tech University campus in Ruston. A second component will be associated with the Center for Advanced Microstructures and Devices (CAMD) at Louisiana State University in Baton Rouge. This component will perform research associated with the X-ray lithography micromachining capability at CAMD. The third and final component of the Institute is Technology Transfer. This component will be located in Shreveport/Bossier in order to take advantage of the unique opportunities and resources offered in this region. There will be a strong inter-

action among the three components of the proposed Institute and each of the components will interact, to varying degrees, with universities, industries and research centers within the state and region.

A major strength of the institute will be the complete integration of multiple process microtechnologies which will span the spectrum from nano to macro. Macro, mini, micro and nano are all a part of MEMS or micromanufacturing. An important component of the institute will be the development of minidevices with microcomponents requiring nanomeasurements with connections to the macroworld. These minidevices could very well become the economic drivers of the technology well into the next century.

Research and Development Component

This component will consist of a new 40,000 sq. ft. building which will accommodate institute faculty, graduate students, visiting scientists and engineers. Almost 20,000 sq. ft. of laboratory space will include space for metrology and testing (2,700 sq. ft.), lithography (initially over 3,000 sq. ft. of class 1000 cleanroom space will be available, expandable to 5,500 sq. ft.), and alternative micromachining technologies such as energy beams. The entire floor of the laboratory area will be isolated from the structure and, in addition, many areas within the laboratory space will be isolated from the main floor pad. The laboratory bay will be kept at 68 ± 1 °F and $45 \pm 5\%$ relative humidity. Four areas of concentration will be developed within the facility at Louisiana Tech University. They are:

- * The design and fabrication of microdevices, such as micro-motors, actuators, sensors, pumps, valves, and connectors.
- * The design and fabrication of microstructures, such as micro-heat exchangers, filters, distillation columns and supports for micro-devices and systems.
- * Research related directly to the manufacturing processes, including fabrication, metrology assembly and testing of the microproducts mentioned above.
- * Microsystem research involving the integration of these microdevices/structures and interfacing of these systems with the macroworld.

Several technologies will be developed and used for the fabrication of these micro devices and structures. First, the existing capabilities in diamond bit machining at Louisiana Tech University will be enhanced. Micro electrical discharge machining capabilities are being acquired and power beam micromachining (excimer laser and focused ion beam) will be developed. Second, conventional photo lithography and chemical etch will be developed and used for the fabrication of low aspect ratio devices and structures. Third, as X-ray lithography technology becomes available at CAMD, Louisiana Tech and LSU researchers will utilize a dedicated beam line to fabricate high aspect ratio devices and structures. Finally, research and development will be

performed on small machines techniques that can build and assemble these microproducts.

X-ray Lithography Component and CAMD

This component consists of a dedicated beam line (off of the electron storage ring at CAMD and associated equipment specifically for the fabrication of high aspect ratio structures and devices. Researchers from Louisiana Tech and Louisiana State University will work at CAMD on research directly related to the fabrication of microdevices and structures using selective etch techniques and the X-ray depth lithography available at CAMD. Direct communication with the component of the Institute in Ruston, will facilitate the design and fabrication of the structures and devices at the CAMD facility. This type of machining is currently available at only a few locations worldwide.

Of course, one of the key components of the institute will be the synchrotron light source. This electron storage ring has been optimized for soft X-ray lithography [15]. The CAMD storage ring has an energy of 1.2 GeV with 400 Ma circulating current. The ring can operate at 1.4 GeV with a decrease in circulating current to 200 Ma. The mean radius of the ring is 8.78 m with a circumference of 55.2 m. The ring has been designed with four straight sections, one of which is used for the 200 MeV low energy injection for the linac. The other three sections will be used for insertion devices such as undulators and wigglers.

The beamline for the micromachining application is currently being designed. Preliminary specifications for the line are that the line must transmit photons of 2 - 8.5 KeV and the high energy transmission must be less than 15% at 10 KeV. The photons must be incident vertically over a field of view of 50 mm horizontally with a uniformity of $\pm 3\%$ and with a beam spot of less than 3 mm height. The beamline must be capable of exposing 100 micron thick 50 mm x 25 mm PMMA resists to a minimum of 4 kj/cc and a maximum of 20 kj/cc in less than 120 seconds with the CAMD storage ring being operated at nominal conditions. The beamline will have a calorimeter and beam position sensor which has a resolution of better than .05 mm for the vertical direction. The beryllium window must be of variable thickness and the transverse window size must be 10 mm x 50 mm. The beamline must be compatible for operation with a superconducting wiggler insertion device.

In addition to micromachining the following uses are anticipated for the facility:

- * X-ray lithography for sub - .05 micron featured integrated circuits (the ring was optimized for this application).
- * Electronic structure, surface science, etc.
- * Geometrical structure, crystallography, etc.

- * Imaging, microscopy, tomography, etc.
- * Medical technology.
- * Education of engineers, scientists and technicians.

Technology Transfer Component

This facility is intended to help existing manufacturers obtain and use new and existing technologies to modernize their manufacturing processes and improve their productivity. Existence of such a facility should be helpful in attracting new industry as well. Staff members would conduct training at the facility or off-site, as needed, as well as using computer and video linkages to efficiently serve industry. In addition, they would seek to develop markets for existing products, look for new products to be developed.

Two facilities will be available for this activity. Space and limited conferencing facilities will be available at the research and development building on the Louisiana Tech University campus. A larger facility is being planned for Shreveport, Louisiana. This proposed facility of 30,000 sq. ft. will be used for conferencing, technology transfer and for close interaction with the Louisiana State University-Shreveport Biomedical Research Center.

MEMS Activities in Russia

A United States-Russia forum on manufacturing, factories of the future, and productivity enhancement was held in St. Petersburg, Russia from 18 to 21 May, 1992. The first author presented a paper on micromanufacturing [18] and interacted with researchers interested in MEMS. In addition to this interaction, several universities and companies were visited in the St. Petersburg area. A follow-on trip to Moscow resulted in a visit and presentation to the recently formed Russian Academy of Sciences (includes engineering and everything else). Several general observations from this visit listed are: 1) the status of MEMS in the United States is not well known in Russia (the reverse is also true); 2) the status of MEMS research in Russia does not seem to be well known by researchers in Russia, particularly what is being done in defense related industries - this is just now becoming available and it appears that everything is opening up; 3) the Russian researchers are eager to collaborate and have initiated some collaborations, particularly with Europe; 4) until the economy stabilizes, their resources (for travel, operating, etc.) appear to be very limited; 5) their higher educational system and structure is currently undergoing major review and it appears that the revisions which will be implemented will incorporate both the US and European (particularly German) systems; and 6) the Russian Academy of Sciences is extremely sensitive and worried about the movement of scientists and bright students from Russia to other parts of the world.

There appears to be considerable activities in MEMS throughout Russia, however, several scientists felt that this was a small field of activity. MEMS interest appeared to be mostly focused on sensors, optics, acoustics, and materials. None of the researchers that were contacted knew of research in micro gears, motors, or systems, however most were interested in extending their work into these areas. Several robotics researchers attended the workshop and indicated that they were interested in micro-robots, although none knew of any current research activities in this area. Listed below are a few current MEMS activities from one large microelectronics firm and one university research center.

- * Avangard (microelectronics company outside of St. Petersburg)
 - Ion sensor (ion-sensitive field effect transistor), chip size 5 x 1 mm.
 - Multiple gas sensor on chip (up to three) with local calorimetric control and heater temperature control.
 - Acoustoelectronic devices with reflector arrays.
 - Approximately 35,000 sq. ft. of class 1000 (?) cleanroom space.

- * Scientific-Educational Center of Microtechnology and Testing (St. Petersburg Electrical Engineering Institute)
 - Bio crystals of phospholipid analogues for sensors and molecular electronics micro actuators.
 - Starting to investigate micromechanical device fabrication.

These facilities were in relatively good shape. Processing equipment used 2-3 inch wafer technology and most of the equipment was of Russian origin. The laboratories were well maintained, however, the cleanrooms were not of high quality. It appears that the many Russian microelectronic industries are not competitive for VLSI but could be very competitive in MEMS.

Summary

This paper has attempted to summarize some recent activities in this country and overseas. The effort in Louisiana is relatively new and growing. The Russian effort is not well coordinated or documented. A conference on Micro Systems Technologies is scheduled for June of 1993 in St. Petersburg, Russia. Serious consideration should be given to developing a strategy to not only participate in this meeting, but also to spend additional time in Russia assessing the technology. MEMS technologies will eventually affect virtually every aspect of our lives and, at least in the near term, mini devices with micro components will probably be the economic drivers for the technology.

References (in chronological order)

- [1] O.N. Tufte, P.W. Chapman and D. Long, "Silicon Diffused-Element Piezoresistive Diaphragms", *J. Appl. Physics*, vol. 33, pp. 3322-3329, 1962.
- [2] H.C. Nathanson, W.E. Newell, R.A. Wickstrom and J.R. Davis, "The Resonant-Gate Transistor", *IEEE Trans. ED*, vol. 14, 117-133, 1967.
- [3] Texas Instruments Thermal Character Print Head, EPN3620, *Bulletin DL-S771-2505*, 1977.
- [4] H. Guckel and D.W. Burns, "A Technology for Integrated Transducers", *Transducers '85. IEEE Int'l Conf. on Solid-State Sensors and Actuators, 90-92*, Philadelphia, PA, 1985.
- [5] R.T. Howe and R.S. Muller, "Resonant-Microbridge Vapor Sensor", *IEEE Trans. Electron Devices*, vol. 33, pp. 499-506, 1986.
- [6] K. Petersen, "The Silicon Micromechanics Foundry", *IEEE*, 87TH0204-8, 1987.
- [7] W. Ehrfeld, P. Bley, F. Götz, P. Hagman, A. Maner, J. Mohr, H.O. Moser, D. Münchmeyer, W. Schelb, D. Schmidt and E.W. Becker, "Fabrication of Microstructures Using the LIGA Process", *IEEE*, 87TH0204-8, 1987.
- [8] S.D. Senturia, "Microfabricated Structures for the Measurement of Mechanical Properties and Adhesion of Thin Films", in *Proc. 4th Int. Conf. Solid-State and Sensors and Actuators (Transducers '87)*, pp. 11-16, Tokyo, 1987.
- [9] W.S. Trimmer and K.J. Gabriel, "Design Consideration for a Practical Electrostatic Micromotor", *Sensors and Actuators*, vol. 11, pp. 189-206, 1987.
- [10] H. Fujita and A. Omodaka, "The Fabrication of an Electrostatic Linear Actuator by Silicon Micromachining", *IEEE Trans. Electron Devices*, vol. 35, pp. 731-734, 1988.
- [11] S.C. Jacobsen, R.H. Price, J.E. Wood, T.H. Rytting and M. Rafaelof, "The Wobble Motor: An Electrostatic Planetary-Armature Microactuator", in *Proc. IEEE Micro Electro Mechanical Systems*, Salt Lake City, Utah, 1989.
- [12] K. Kuribayashi, "Milimeter Size Joint Actuator Using Shape Memory Alloy", *1989 IEEE Micro Electro Mechanical Systems Workshop*, pp. 139-144, Salt Lake City, Utah, 1989.
- [13] C.R. Friedrich and R.O. Warrington, "Machining of Metal Foils for Use in Microcompact Heat Exchangers", in *Proc. Micro System Technologies 90*, pp. 509-514, Berlin, Germany, 1990.

- [14] L.C. Kong, B.G. Orr and K.D. Wise, "A Micromachined Silicon Scan Tip for an Atomic Force Microscope", *Digest IEEE Solid-State Sensor Workshop*, Hilton Head, S.C. pp. 28-31, 1990.
- [15] R.L. Stockbauer, et al, "Center for Advanced Microstructures and Devices at Louisiana State University", *Physica Scripta*, vol. 41, pp. 788-792, 1990.
- [16] J. Simon, G. Engelmann, O. Ehrmann and H. Reichl, "Plating of Microstructures for Sensors", in *Proc. Micro System Technologies 91*, pp. 315-321, Berlin, Germany, 1991.
- [17] H. Guckel, K. Skrobis, T. Christenson, J. Klein, S. Han, B. Choi and E. Lovell, "Fabrication of Assembled Micromechanical Components via Deep X-Ray Lithography", in *Proc. IEEE Micro Electro Mechanical Systems*, pp. 74-79, Nara, Japan, 1991.
- [18] R.O. Warrington, C.R. Friedrich, R.X. Gao and G. Lin, "Micromanufacturing, An Emerging Technology", presented at the *1992 US-Russia Forum on Manufacturing, Factories of the Future and Productivity Enhancement*, St. Petersburg, Russia, 1992.

**MICROSENSORS AND MICROINSTRUMENTS:
NEW MEASUREMENT PRINCIPLES AND NEW APPLICATIONS***

**W. J. Kaiser, T. R. VanZandt, T. W. Kenny, W. B. Banerdt, and D. Crisp
Center for Space Microelectronics Technology
Jet Propulsion Laboratory, California Institute of Technology
Pasadena, California 91109**

ABSTRACT

An important new approach for space science is based on the use of compact, low-mass, low-cost science instruments integrated with their delivery systems. Many advantages of this approach lead to new missions and new science return opportunities. First, many critical investigations of planetary interiors, surfaces, and atmospheres, which require in-situ measurements, may be completed, since the cost in resources to execute in-situ science is reduced. Second, the reduced mass and volume of microinstrument systems allow a greatly expanded distribution of measurement sites. Then, science investigations may be performed simultaneously over large regions. In particular, a major advance in the investigation of planetary interior structure by seismology or atmospheric properties by meteorology is obtained by use of a planetary-wide measurement network.

Advances in microelectronics have enabled the convenient fabrication of compact structures (for example, by silicon micromachining). Many advantages of this approach provide new capabilities for producing sensors and instruments for guidance and control, seismology, meteorology, material and gas analysis, and other in-situ science applications. However, the development of compact sensors and instruments leads to a variety of fundamental sensor sensitivity limits. In particular, the development of compact instruments for many of the most important applications requires a drastic improvement in signal detection sensitivity. Thus, new fabrication techniques may not, alone, yield suitable microinstruments. Instead, improved measurement methods must be developed to enable microsensors and microinstruments. In this presentation, the unique challenges for microsensor and microinstrument technology will be discussed.

Recent developments at JPL, based on novel signal detection principles, have produced a series of ultra-high sensitivity microsensors and microinstruments. Included among the applications demonstrated are a micro-seismometer, micro-accelerometer, micro-magnetometer and a unique, uncooled infrared detector. Also in this presentation, the principles, performance, and unique in-situ science applications of these new devices will be described. It will be shown that the implementation of microinstruments using these principles produces systems having performance equivalent to previous conventional instruments, but, with major reductions in mass, volume, and power consumption.

* Research supported by NASA, DARPA, NADC, ONT, ASTRO, and SDIO/IST.



Micro-Sensors, -Actuators, and -Systems:
Accomplishments and Prospects

Richard M. White
Co-Director, Berkeley Sensor & Actuator Center

and

Professor, Department of Electrical Engineering and
Computer Sciences
University of California
Berkeley, CA 94720

Microsensors and microactuators have been reported in recent years by many researchers worldwide. Most are made with silicon by integrated-circuit processing techniques, often augmented by specialized etching (bulk or surface micromachining), or by electroplating, as in the LIGA and related processes. Deposited films have been used as micromechanical members (examples being polycrystalline silicon and low-stress silicon nitride), or as actuators (such as the thin-film piezoelectrics zinc oxide and lead-zirconate-titanate, and shape-memory alloy thin films). Techniques for bonding together individual die have been developed, and some polymeric structures have been reported. In many cases, integrated circuitry has been included on the sensor/actuator die for signal conditioning, control, test and calibration purposes.

Other devices that have emerged from this work include a microlamp having a gas-tight enclosure, and ultrasonic devices that transport granular solids, pump and mix fluids, measure viscosity, and function as gravimetric sensors for chemical gases and certain biomolecules in liquids. An important indication of the maturity of the field was the 1991 announcement by Analog Devices of its accelerometer, which employs a micromechanical sensing element and much associated integrated circuitry.

One may expect in the future to see: more integrated microsystems having increased functionality; emergence of CAD tools for the entire design of these devices; use of the fabrication techniques developed to make critical parts of milli- and mini-, instead of micro-, devices; expansion into systems that accomplish chemical and biological analysis, and even synthesis; and greater use of optical interactions with these devices.

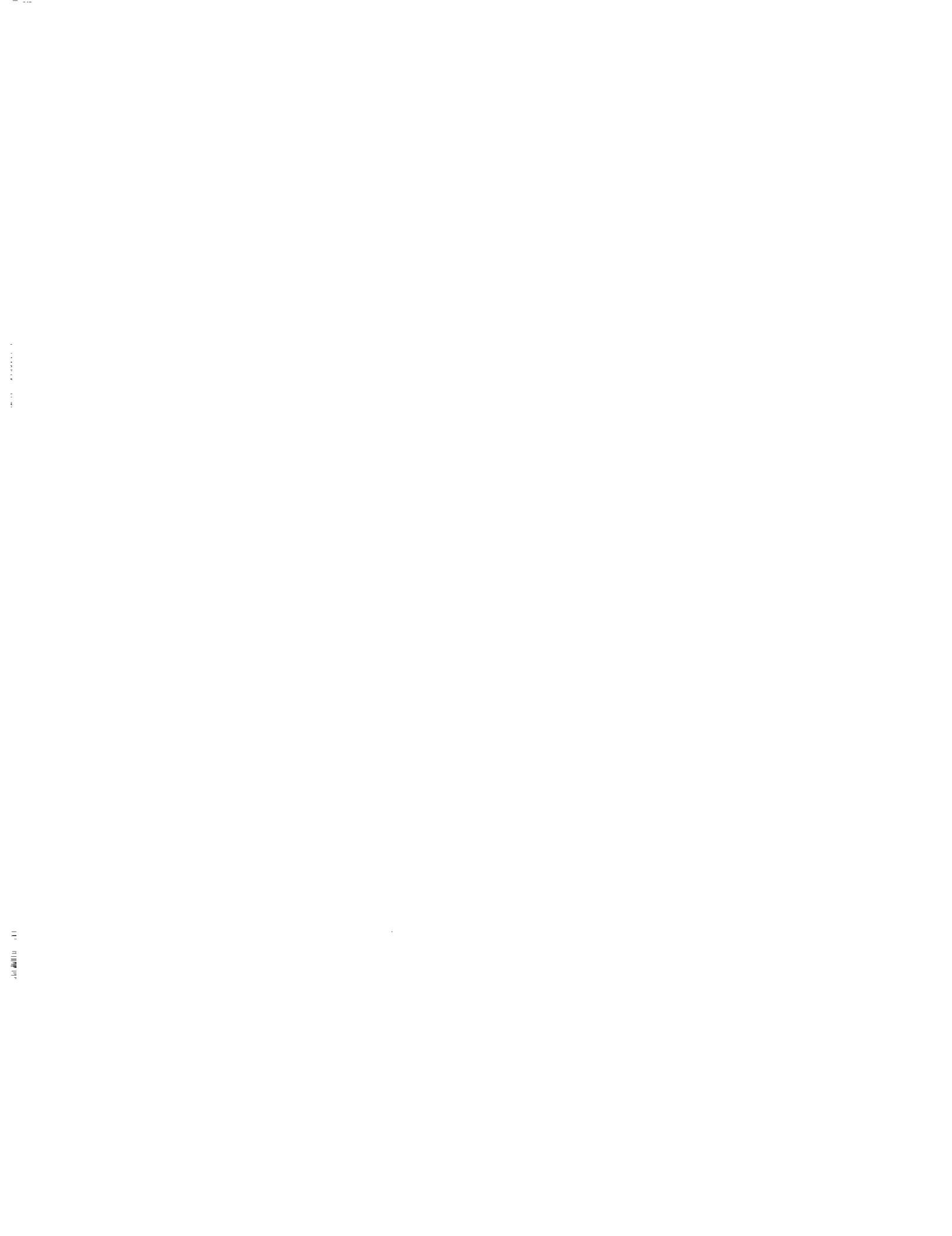
National Nanofabrication Facility and Nanoelectromechanics

Noel C. MacDonald
School of Electrical Engineering and
The National Nanofabrication Facility
Cornell University
Ithaca, NY 14853-5401

The National Nanofabrication Facility at Cornell University (NNF) is a partnership formed by Cornell University, the National Science Foundation, university and government laboratories, and leading American corporations. The NNF mission is to advance the fabrication capabilities at dimensions less than 100 nm (nanofabrication), and advance the applications of micro- and nanofabrication to diverse areas of science and engineering applications.

NNF has become a national focal point for teaching and research in nanofabrication. A sophisticated laboratory facility with complete instrumentation for fabricating structures at submicrometer and nanometer dimensions, NNF provides an ideal hands-on environment for graduate students conducting state-of-the-art thesis research and for industrial scientists and engineers pursuing emerging technologies.

We have developed a nanoelectromechanical scanned probe mechanism using an integrated, single crystal silicon (SCS) process. Suspended SCS structures are used to fabricate x-y capacitive translators and high aspect ratio conical tips for scanned probe devices. The integrated nano-mechanical device includes methods to form integrated tunneling tip pairs and to produce electrical isolation, contacts, and conductors. Each device occupies a nominal area of $40\ \mu\text{m} \times 40\ \mu\text{m}$. These devices include a novel self-aligned tip-above-a-tip tunneling structure and capacitive x-y translators defined by electron beam lithography and the thermal oxidation of silicon. The x-y translators produce a maximum x-y displacement of $\pm 200\ \text{nm}$ for an applied voltage of 55V. The low mass ($2 \times 10^{-13}\ \text{kg}$), rigid structure has a measured fundamental mechanical resonant frequency of 5 MHz.



MICROACTUATOR PRODUCTION VIA HIGH ASPECT RATIO, HIGH EDGE ACUITY METAL FABRICATION TECHNOLOGY

*H. Guckel and T.R. Christenson
Department of Electrical and Computer Engineering
University of Wisconsin
Madison, WI 53706*

ABSTRACT

LIGA is a processing sequence which uses x-ray lithography on photoresist layers of several hundred micrometers to produce very high edge acuity photopolymer molds. These plastic molds can be converted to metal molds via electroplating of many different metals and alloys. The end results are high edge acuity metal parts with large structural heights. The LIGA process as originally described by W. Ehrfeld can be extended by adding a surface micromachining phase to produce precision metal parts which can be assembled to form three-dimensional micromechanisms. This process, SLIGA, has been used to fabricate a dynamometer on a chip. The instrument has been fully implemented and will be applied to tribology issues, speed-torque characterization of planar magnetic micromotors and a new family of sensors.

INTRODUCTION

Microactuators are components which are required for micro electro-mechanical systems or MEMS. These components are typically three-dimensional and involve submicron dimensions. This requirement, submicron geometries, originates from scaling arguments of larger devices. Thus, a shaft which is to be supported in a bushing is typically machined to a nominal diameter of, say, 1 cm with a tolerance of ± 2 micrometer. The implication is that tolerances of better than 100 ppm are being used routinely in the macro-world and are required for low friction, long wear sliding joint performance. If one takes a primitive outlook on microactuators and simply insists that they are miniaturized cousins of their larger counterparts it becomes reasonable to assume that nominal as well as tolerance dimensions must be scaled together. This would then suggest that bushing to shaft tolerances very quickly become submicron issues.

Microactuators are devices which require many materials. The restriction of the material base to those substances which are readily available in integrated circuit technologies is not reasonable and is too confining. This is particularly true for sliding joints where the brittle behavior of silicon and its derivatives is a decided handicap. The exclusion of ferromagnetic metals and their alloys is particularly detrimental because it eliminates an entire class of actuators: magnetic devices. These components in turn profit from multiple metals to provide low loss conductors, hard magnetic materials and the soft counterparts.

Finally there is the issue of manufacturability. The end goal is that of producing highly complex MEMS very much like a VLSI chip. These systems are hopefully candidates for high volume production as for instance in the case of actuators for magnetic recording heads. Reasonable manufacturability with low cost batch processing is required if this type of application of MEMS is to be successful. Special components and proof of concept devices are initially less restricted by these considerations. However, their success as an economically viable system profits also from an early inclusion of manufacturability in the process development cycle.

HIGH ASPECT RATIO PROCESSING VIA LIGA

A possible candidate for high aspect ratio processing and therefore a step in the right direction for three-dimensional fabrication was first suggested by W. Ehrfeld via a processing sequence which he termed LIGA [1]. This process consists of three components. The first part is fundamentally a lithography which can deal with photoresist layers of several hundred micrometer thickness. The implication of a photoresist technology is that of a planar substrate to which the photoresist can be applied. The photoresist thickness requirement cannot be satisfied easily by solvent based systems and spin coating and has been replaced by polymer casting and in situ polymerization. Complete exposure of such thick photoresist layers requires

high energy photons from a well collimated, high brightness source. A synchrotron is nearly perfect for the illuminator and can provide x-ray photons with average wavelengths in the low angstrom range with power densities of several watts/cm² and essentially perfect collimation. This type of exposure has the additional benefit that standing wave difficulties are avoided because of the absorption process which x-ray photons use to interact with the photopolymer. Exposure profiles for critical dimensions above 0.1 micrometer are therefore essentially vertical and do not suffer appreciably from diffraction effects even if large gap proximity printing rather than contact exposures are used. The exposed pattern requires a developer which must show very large dissolution rate sensitivity between exposed and unexposed photoresist areas. A suitable chemical formulation for the polymethylmethacrylate or PMMA system has been found [2,3]. This would imply that the first phase of the LIGA process when coupled with a suitable x-ray mask technology can produce photoresist patterns or a plastic mold with edge acuities of better than 0.1 micrometer/100 micrometer structural height. As in all processes there are some negatives. The exposure resolution, i.e. mask to wafer, is better than can be measured. Thus, submicron dimensions can be accommodated if the mask fabrication allows this. However, free standing submicron photoresist structures cannot be developed because of mechanical strain in the PMMA. Buckling typically results during developing. In this sense this process is not a submicron process.

The second phase of the LIGA process involves the conversion of the plastic mold to a metal mold. This is done by first of all modifying the planar substrate to a planar substrate with a suitable plating base. An example would be a sputtered film of titanium at 150 Å followed by a sputtered film of nickel at 150 Å. The prepared substrate is then processed with the previously explained thick photoresist procedure. The plastic mold is filled with electroplated metals or alloys. The plating process when adjusted properly does not disturb the PMMA and forms a negative metal replicate of the plastic mold. Photoresist removal follows and leads to a metal mold which may be the desired prototype or can serve as a mold for other materials.

The third segment of the LIGA process addresses manufacturing issues. It uses the metal mold as the primary mold for injection molding which substitutes for the x-ray lithography process. The injection molding replaces the PMMA procedure and in turn is followed by electroplating and clean-up. More than 1000 molding cycles have been achieved and lead to mass produced, fully attached, high aspect ratio, high edge acuity metal parts.

SLIGA AND ASSEMBLY

The draw-backs of the basic LIGA process fall into two categories: fully attached parts and submicron tolerances. Both can be removed by suitable process modifications.

The LIGA process as explained above can be furnished with a pre-LIGA and post-LIGA sequence to produce parts which are either fully attached or partially attached or free of the substrate. The concept is that of combining surface micromachining with LIGA which will be termed SLIGA [4].

The pre-LIGA sequence involves substrate modifications. Thus, the planar substrate is first furnished with a suitable sacrificial layer for instance soft polyimide. This layer is patterned with an optical mask. The entire substrate is then covered with the plating base and the LIGA procedure follows. There is conceptionally a minor but technically a major modification in the LIGA procedure: The x-ray mask must be aligned to the pattern on the substrate. The required accuracy is fortunately not excessive and therefore alignment in a double sided aligner and subsequent clamping prior to synchrotron insertion is adequate.

The post-LIGA segment deals with the removal of the plating base in those sections of the substrate which are not covered by PMMA. This is done by wet etching and is followed by wet chemical procedures to remove the sacrificial layer. The end results are metal parts with the stated substrate relationships. The free parts in particular are noted to have the property that they do not exhibit geometric distortion due to the sacrificial process. This is the consequence of the fact that electroplating can be adjusted to produce small built-in tensile strain which is on the average nearly constant because the parts are thick enough to avoid interface strained regions.

The parts of interest can be picked up via micromanipulators which use magnetic or electrostatic needle probes. Assembly is completely feasible and does of course enhance the three-dimensional nature of the process. However, this is only a part of the desired goal. Submicron bearing tolerances can be achieved even though the x-ray masks have critical dimensions above 1 micrometer. Two facts support this. Optical masks with incremental critical dimensions of 0.1 micrometer are not very difficult to produce. Therefore, subtraction of optical patterns from two masks or mask regions can be used to produce submicron incremental features. An example would be a shaft of, say, 50 micrometer diameter which is

rigidly attached to the substrate and a gear with an inside hole diameter of 50.1 micrometer which is free and assembled to the shaft. The result is a bushing clearance of 0.05 micrometer which can be utilized fully if the edge acuity of the process is large enough to produce a run-out free metal structure. Fortunately, LIGA processing allows this and the successful result is exemplified in Fig. 1.

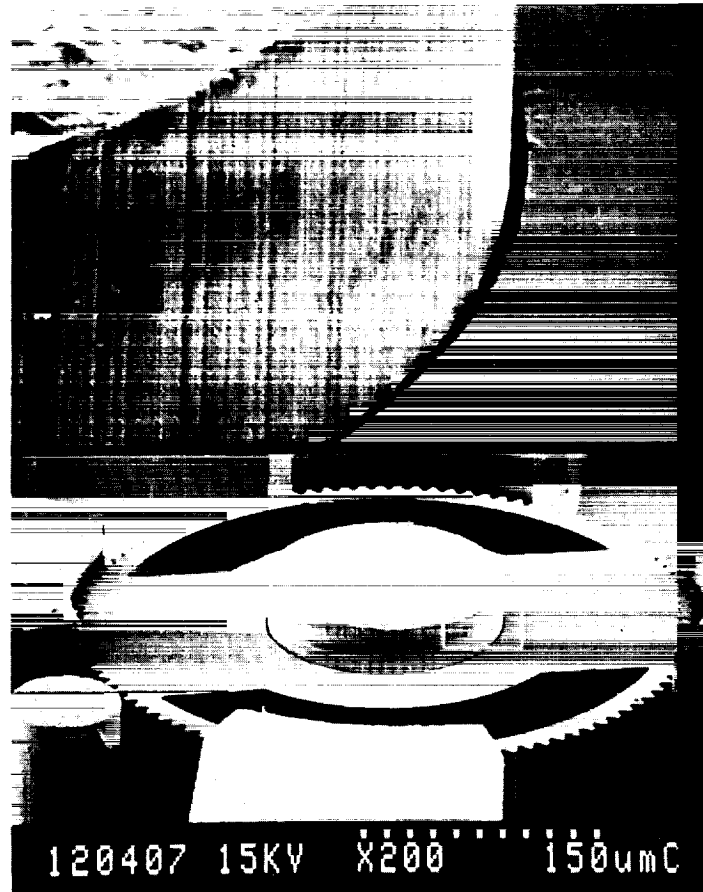


Fig. 1 SEM photograph showing assembled bearing surface for 100 micrometer tall nickel structures and shaft diameter which is 0.5 micrometer smaller than bearing hole.

APPLICATION TO MEMS

Micromechanical components will eventually be used in a MEM system. Since system requirements very often dictate component design the development cycle for MEMS can be shortened by considering a system first and then designing the components which satisfy the system design. For this purpose a detailed investigation of a specific, moderately difficult MEM system has been initiated. The system of choice is a dynamometer which consists of the following parts:

- (1) A Motor
 - (2) An Electric Generator
 - (3) A Motor-Generator Coupler
 - (4) Position Sensors for Rotor Position
 - (5) An Electronic Control Unit.
- and

The first four components are located on the substrate, the control unit is constructed off-chip.

The purpose of this system is found in part in tribology issues such as friction in MEMS which cannot be calculated but must be measured. The speed-torque characteristics of a planar magnetic micromotor are also of interest and profit from the active load which the generator presents. Finally there is an issue which is predicated on success. A micro-dynamometer of this type is in fact a force measurement system with extreme sensitivity and can therefore usher in an entire new family of sensors for nearly all physical quantities.

The implementation of the dynamometer via SLIGA requires magnetics. The electroplated metal must therefore be ferromagnetic and, for the sake of simplicity, should be an element rather than an alloy. Nickel has been selected as the material of choice. The expected behavior is that of square-loop B-H material with a saturation flux density above 6000 gauss. The first order of business is a tribology issue: can nickel on nickel surfaces be used as bearing surfaces without excessive frictional losses. This question has been answered by designing a reluctance motor with gear take-off [5]. Figures 2 and 3 detail the concept.

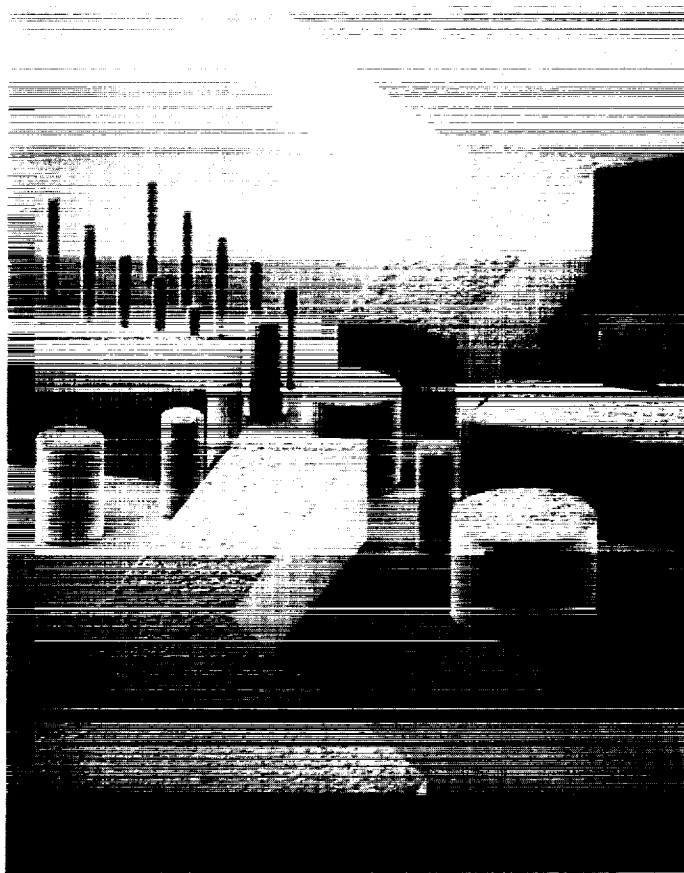


Fig. 2 Nickel stator, height 100 micrometer.

The assembled device as shown in Fig. 3 was tested with an externally supplied rotating magnetic field. Frictional losses required flux densities near 5 gauss for the unloaded rotor. Friction is therefore very low and dynamic ranges of three orders of magnitude can be anticipated. This observation is sufficiently encouraging to proceed with the next phase: coils for current to magnetic field conversion. These coils must of course envelope the pole pieces of the motor and must surround the magnetic circuit of the generator. Figure 4 illustrates the concept.

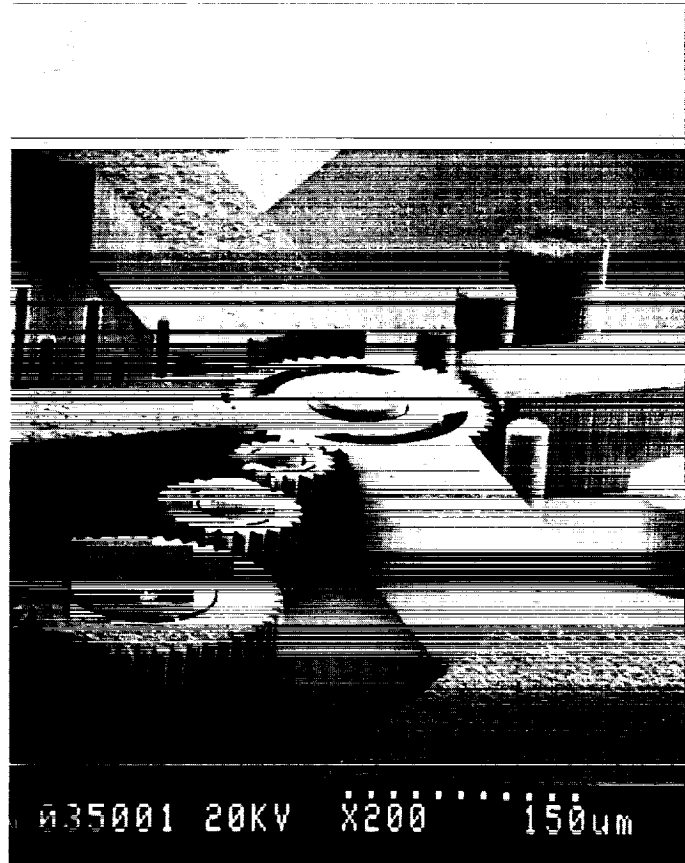


Fig. 3 Assembled magnetic motor with gear train. The reluctance rotor and gear train were assembled on to the stator of Fig. 2. The gears have involute tooth geometry with a tooth length of 9 micrometer.

The coil shapes, "U's", which are dielectrically isolated from the magnetic circuit are visible in Fig. 4. The square holes were intended for coil closure via assembly of staple-like nickel pieces. This approach failed because mechanical instabilities and contact problems occurred due to spring forces. Fig. 5 illustrates coil closure via hybrid bonding of aluminum alloy wire to the nickel pre-forms. This procedure gives satisfactory results for coils with up to 100 or so turns. This construction procedure when applied to the device shown in Fig. 4 indicates that micro-dynamometer construction is fully feasible.

The remaining issue involves a functional device. This requires not only suitable coil construction but also appropriate magnetic behavior of the ferromagnetic segments of the devices. For a reluctance motor a soft magnetic material with high permeability and low coercivity is very desirable. In this respect nickel is non-ideal. Electroplated nickel layers are further complicated by built-in tensile strain which causes a strong degradation of the B-H curve due to magnetostriction [6]. This problem, a material science issue, is slowly disappearing as plating conditions improve and anneal cycles are clarified. Acceptable magnetic behavior has been achieved and functional testing will occur in the near future.

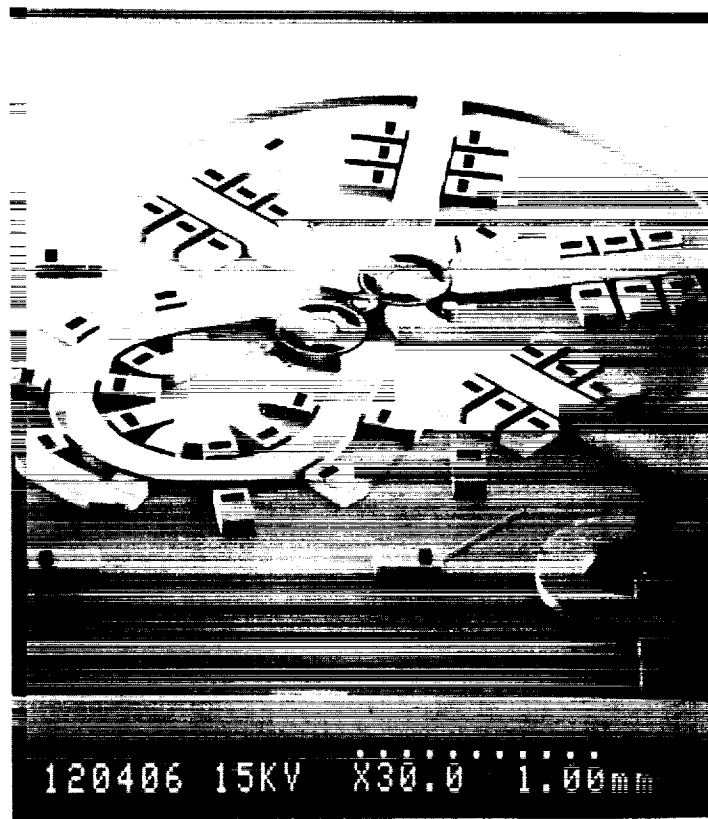


Fig. 4 Assembled microdynamometer with coil forms prior to coil completion. The motor with 6 windings per pole pair is located at the upper right hand side of the SEM photograph and is coupled to a generator at the lower left. The generator has 6 windings which split into a biasing coil and signal coil. Photodiodes have been fabricated underneath the rotors in the silicon substrate.

CONCLUSIONS

High aspect ratio metal fabrication procedures when combined with assembly offer a technology for magnetic and electrostatic actuators with increasing three-dimensionality. Submicron bearing tolerances are particularly noteworthy. They lead to frictional behavior which is lower than expected. The goal: a fully functional micro electro mechanical system appears to be achievable in the very near future.

ACKNOWLEDGEMENTS

This work was in part supported by the National Science Foundation under grant EET-8815285. The help of Mr. T. Martin, Quantum Devices, Inc., Barneveld, Wisconsin with wire bonding issues is deeply appreciated. The support of the staffs of the Center for X-ray Lithography and the Synchrotron Radiation Center for their help and the use of their facilities is acknowledged. The Center for X-ray Lithography is supported by SEMATECH Center of Excellence SRC Grant No. 88-MC-507 and the Department of Defense Naval Research Laboratory Grant No. N00014-91-J-1876. The Synchrotron Radiation Center is supported by the National Science Foundation Grant No. DMR-88-21625.

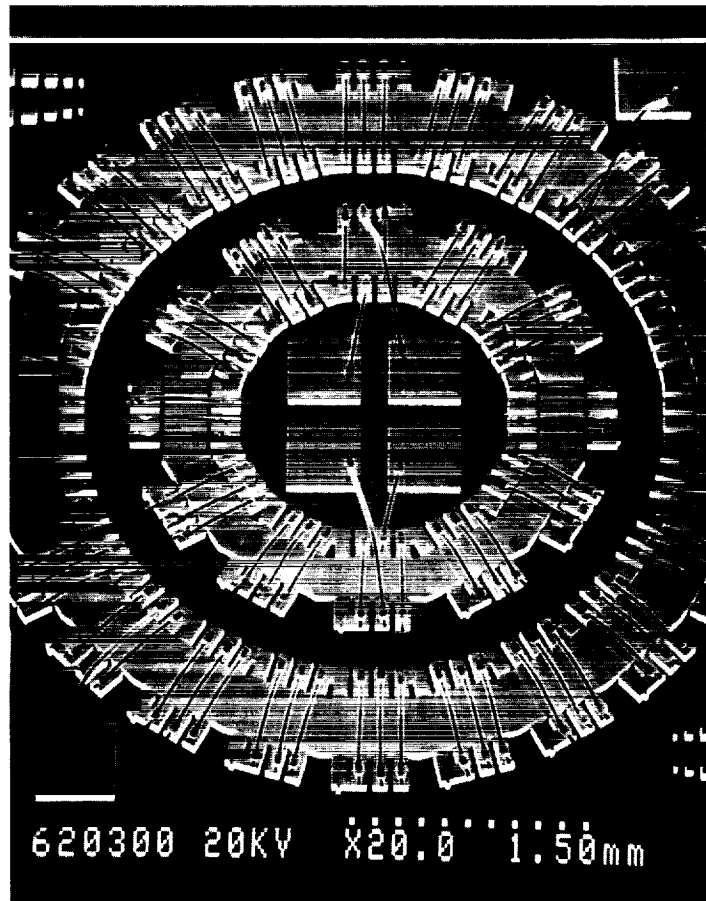


Fig. 5 Coil test construction via hybrid wire bonding. This SEM photograph shows two split wound toroidal windings about a Ni core. The outer toroid contains 72 turns.

REFERENCES

- [1] E.W. Becker, W. Ehrfeld, P. Haggmann, A. Maner, D. Münchmeyer, "Fabrication of Microstructures with High Aspect Ratios and Great Structural Heights by Synchrotron Radiation Lithography, Galvanoformung, and Plastic Moulding (LIGA Process)," *Microelectronic Engineering*, 4, 1986, pp. 35-56.
- [2] V. Ghia and W. Glashauser, "Verfahren für die Spannungsfreie Entwicklung von bestrahlten Polymethylmethacrylat-Schichten," Offenlegungsschrift DE 3039110, Siemens AG, Munich.
- [3] H. Guckel, T.R. Christenson, K.J. Skrobis, D.D. Denton, B. Choi, E.G. Lovell, J.W. Lee, S.S. Bajikar, and T.W. Chapman, "Deep X-Ray and UV Lithographies for Micromechanics," *Technical Digest, Solid-State Sensor and Actuator Workshop*, June 1990, pp. 118-122.
- [4] H. Guckel, K.J. Skrobis, T.R. Christenson, J. Klein, S. Han, B. Choi, E.G. Lovell, T.W. Chapman, "On the Application of Deep X-ray Lithography with Sacrificial Layers to Sensor and Actuator Construction (The Magnetic Motor with Power Takeoffs)," in *Paper Substitutions to Technical Digest of International Conference on Solid-State Sensors and Actuators (Transducers '91)*, June 1991.
- [5] H. Guckel, K.J. Skrobis, T.R. Christenson, J. Klein, S. Han, B. Choi, E.G. Lovell, and T.W. Chapman, "Fabrication and Testing of the Planar Magnetic Micromotor," *J. of Micromechanics and Microengineering*, vol. 1, no.4, 1991, pp. 135-138.
- [6] R.D. Fisher, "The Influence of Stress on Magnetic Characteristics of Electrodeposited Nickel and Cobalt," *J. Electrochem. Soc.*, vol. 109, No. 6, pp. 479-485.

OVERVIEW OF MICROOPTICS: PAST, PRESENT, AND FUTURE

Wilfrid B. Veldkamp
 Lincoln Laboratory, Massachusetts Institute of Technology
 244 Wood Street, Lexington MA 02173-9108

ABSTRACT

Through advances in semiconductor miniaturization technology, microrelief patterns, with characteristic dimensions as small as the wavelength of light, can now be mass reproduced to form high-quality and low-cost optical components. In a unique example of technology transfer, from electronics to optics, this capability is allowing optics designers to create innovative optical components that promise to solve key problems in optical sensors, optical communication channels, and optical processors.

1. INTRODUCTION

Many of the current micro structures in optics are based on binary optics technology. This is an inherently diffractive optics technology that uses computer-generated designs of microscopic relief patterns and electronic circuit etching technology to create novel optical devices and to provide design freedom and new materials choices for conventional refractive optical elements. Over the past ten to twelve years we in the holographic optics community have learned to produce diffractive and mixed refractive-diffractive devices that are highly efficient and of high enough quality to be used in cameras and in medical applications. These devices are fabricated by methods compatible with current lithographic and integrated circuit techniques.

In the early seventies, the Defense Advanced Research Projects Agency (DARPA), the Air Force, and many industrial groups started to drive electronic circuit features to below the one-micron level. This effort led DARPA and the National Science Foundation (NSF) to establish a MOSIS (Metal Oxide on Silicon Integrated Systems) foundry service in 1981. MOSIS aggregates designs from different sources onto one mask set; instead of paying \$60,000 for a dedicated set of masks and a fabrication run, users can get packaged parts for as low as a few hundred dollars. This service dramatically lowers the risk of electronic circuit prototyping. In the late seventies a micromechanics technology piggybacked on the VLSI and VHISIC electronics technologies to develop micromotors, microaccelerometers, microchromatometers and other mechanical devices made by computer lithography and etching technology. Now we see the integration of processing electronics and microsensors and actuators on a common silicon wafer and chips.

Similarly, in the mid eighties, with the support of Jasper Lupo, DARPA started a program called Binary Optics. The goal was to piggyback a new diffractive optics technology on the flourishing micromachining technology with the participation of federal laboratories, universities, and industry. DARPA's programmatic goals then were three-fold:

- (1) Develop an optics technology based on electronic circuit fabrication technology for the purpose of cost and labor savings in military sensor systems, for creating new freedom in designs and materials, and for developing new composite optical functions that could not be created with the current technology,
- (2) promote computer-aided design of total electrooptical systems, and

- (3) launch a broad-based diffractive optics technology in U.S. industry.

Therefore, the key features of the microoptics technology that evolved since 1984 were:

- (1) That it dealt with one of the three ways of manipulating light -- diffraction. Refraction and reflection are the other two. Soon after the startup of the program, diffraction was blended with the other two ways in order to cover broad waveband applications and a mixed macro technology emerged.
- (2) That fabrication be based on holography microlithography, and ion-etching technology.
- (3) That the new technology provide design freedom and materials choices in imaging sensors by diffractively compensating the dispersive properties of infrared, visible, and ultraviolet materials.
- (4) That the arrayed micro components shape, steer, filter, and process light in new ways to produce smart sensors that would be adaptive and agile.

2. THE PAST: LARGE FEATURE APPLICATIONS

In the early days of the binary optics program diffractive optics work proceeded along two approaches. The first was based on planar structures only, where all the optical power was diffractive. It required very high resolution lithography and a full electromagnetic field treatment of the optics in order to describe the efficiency characteristics of the devices accurately (1). These planar devices generally were sensitive to the polarization of the incident fields and were useful only for narrow optical bandwidths and fields-of-view. Later, techniques were developed to circumvent most of these limitations by trading structure depths for lower periodicities and less diffractive power. In other words, quasi planar structures were fabricated where the etch depths were multiple wavelengths deep, and that had characteristics of both refractive and diffractive microoptics. A true Euglina of the refractive and diffractive microoptics fields evolved naturally.

The second approach was based on mixing refractive with diffractive power on macro elements, typically on fast lenses. With mixed optics a spherical surface provides the raw focal power, and the diffractive micro structure corrects the spheric and chromatic aberrations of the element. For such applications one needed only low resolution, and more importantly, low accuracy lithography (generally one-micron accuracy was good enough). Because of the coarse features of the diffractive patterns, the devices generally exhibited little sensitivity to polarization and could be used with wide optical bandwidths and in large field-of-view applications, from infrared to deep ultraviolet wavelengths (2).

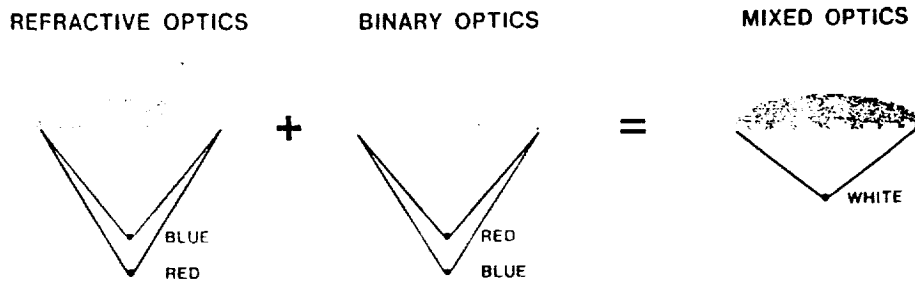


Figure 1. Chromatic Aberration Correction With Binary Optics

From another perspective, mixed refractive and diffractive optics fulfill an alternate complementary role, for not only can diffractive optics be used to fine tune the surface profile of spherical elements and eliminate spherical aberrations, it can also modify the bulk properties of optical materials. The dispersive quality (change of refractive index with wavelength) of all optical materials is a consequence of light absorption in a material as a function of wavelength. Conventional optical designs compensate for dispersive or chromatic aberrations by cementing together different materials with carefully varied radii to produce compensating dispersion characteristics. These lenses need not have dispersions of opposite slope; a mere difference in refractive index is sufficient to null chromatic aberration over a finite bandwidth. Similarly, with binary optics, we can achieve an achromatic balance between a dispersive lens material and a diffractive pattern etched into the surface of that material. Such a binary optics element is an advanced implementation of a highly efficient Fresnel zone pattern in which phase gratings are used to focus light into a corrected spot (see Figure 1).

As a grating, a binary optics element has inherent optical dispersion properties that can be tailored by varying the geometric dimensions of the zone rings in a space-variant manner, i.e., ring widths, depths and spacings, irrespective of the intrinsic properties of the substrate material. The selectable dispersion characteristic can be used to achromatize optical materials over a wide bandwidth. The high efficiency (no undesired scatter) determines the effectiveness of this kind of compensation. In general the diffractive features are much larger than the used wavelength, whereas pattern accuracy must be comparable to the wavelength; in complex system designs the number of needed elements can be cut in half by use of binary optics. Micro machined optical elements can have dramatically improved resolving power and useful bandwidths, as is demonstrated in Figure 2 for a range of wavelengths and lens speeds.

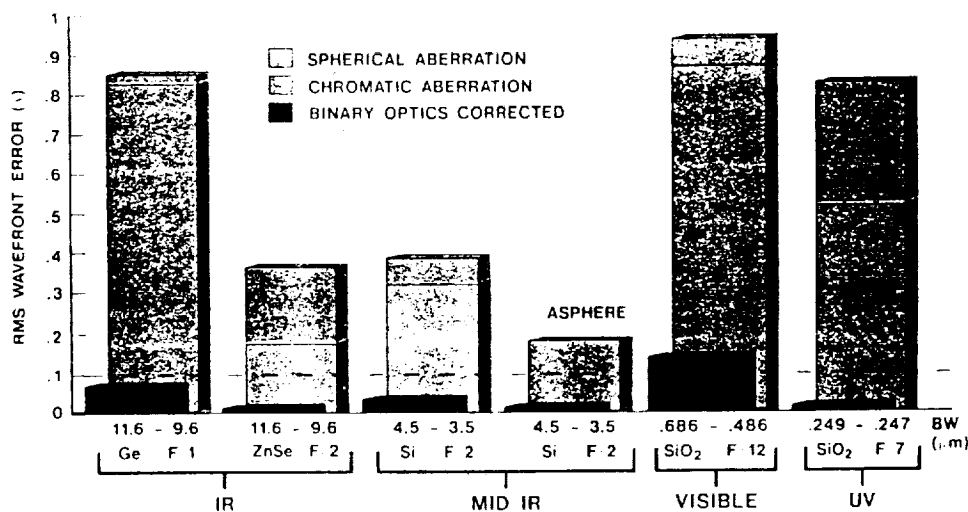


Figure 2. Diffractive Correction of Various Lenses in Four Wavebands

Many companies are now routinely using micro machined and mixed elements in the design of new optical systems. Hughes, Loral, Honeywell, Optical Filter, Rockwell, Texas Instruments, 3M, Polaroid, and many others are active in the field.

As a result of the modest DARPA program that began in 1984, a truly enabling optics technology has evolved. The first generation of the micro optics technology (aberration correction of conventional optics) has been transferred from a federal laboratory to more

than fifty companies and has spawned six U.S. startup companies (see Figure 3). Four years ago we moved in earnest into the second generation of novel devices: arrayed microoptical elements.

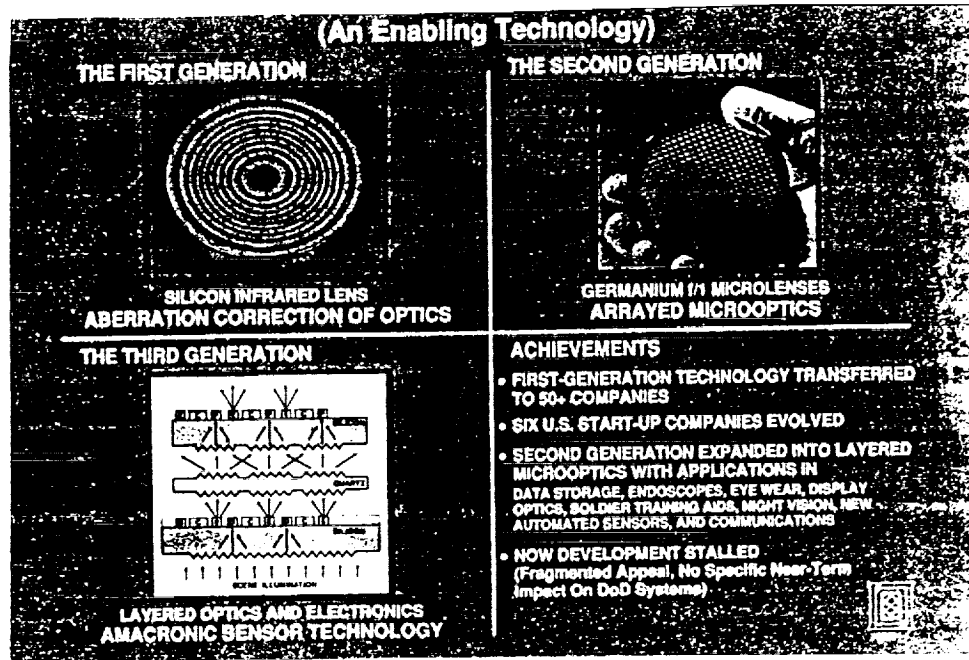


Figure 3. Three Developmental Generations of the Microoptics Technology

3. THE PRESENT: LARGE ARRAYS OF FAST MICROOPTICS

Much of the current research activity centers on the fabrication of microfine arrayed optics. One of the many unique applications of binary optics is microoptics, a technology that produces optical elements such as lenses, multiplexers, and filters that range in diameter from a few tens of microns to one millimeter. The lithographic flexibility in layout and design of the arrays with rectangular, round, or hexagonal close-packed layouts (while maintaining optical coherence over the array) makes this technology unique among all other current fabrication techniques. The optical phase profile of a lenslet, for example, is not restricted by fabrication constraints either; designers can choose optimal surface profiles such as spheric, parabolic, aspheric, astigmatic, and anamorphic, depending on application requirements (3,4).

The use of microoptics in systems is still new, and occurs primarily in laser diode beam shaping, on-chip optical tasks, focal plane imaging, and processing functions. Binary optics with 0.1 micron accuracy and 0.5 micron resolution has been used to demonstrate coherent lenslet arrays of 20,000 elements/cm², f/1 speed, and zero dead spacing (optically inactive areas between the lenses). An individual element can exhibit root-mean-square wavefront errors limited to $\lambda/50$ and strehl ratios of 0.98 (the strehl ratio is defined as the peak field amplitude in the focus normalized to the diffraction-limited amplitude). In other words, with binary optics and very-large-scale integrated step-and-repeat technology, large arrays of micro lenslets can exhibit full diffraction-limited performance. Because this is an inherently planar optics technology, very large segmented apertures can be assembled in etched dielectrics or metals or embossed in plastic-like materials. Current research centers

on extending this microlens technology to broad-waveband (more than 20% fractional bandwidth) applications by deep-etch structuring or by blending refractive and diffractive microoptics on either side of a substrate.

The unique capability of current microoptics technology can be demonstrated by three key example applications to optical imaging sensor systems. These applications were chosen because of our specific interest in optical sensor technology. Throughout the conference we have heard from other organizations about their applications, ranging from optical communications, optical data processing, and data storage to medical implantation devices. Although the current work in microoptics is primarily an enabling technology development, the very nature of an enabling technology means that its success can only be measured in terms of useful applications in many fields, and transcends applications in specific devices.

Our first important application exploiting microoptics technology in sensor systems is with agile and high-speed steering of images and laser beams. The lack of an agile steering element is the Achilles heel of most electrooptical sensor systems. A possible solution uses layers of coherently arrayed afocal microoptics that is moved via piezo or electrostrictive forces to form a programmable beam scanner with a minimum amount of motion (half a lens diameter maximum). Alternatively, layers of confocal microoptics with electrooptic material sandwiched in between can be used to form the optical equivalent of a phased array antenna with high speed steering properties so well known by the radar community.

The second class of applications that has our long-term interest is the formation of arrayed microcavities for one and two dimensional arrays of solid state lasers. These arrays can form extremely bright laser sources by coherently adding the power of the elements in the array. Radiation power densities of today's single diode lasers already exceed those at the surface of the sun, and materials limitations prevent further increases in laser power density. Yet, the very small radiation area of a single laser can reliably produce only about 50 mW. Only coherent addition of sparsely spaced lasers in an array can overcome the thermodynamic barrier to higher laser diode power. Figure 4 shows a collection of six tested microcavity designs using microoptical multiplexers, filters, phase converters, fractional Talbot gratings, and interlaced microelements (5). Some of the elements require interlaced refractive and reflective lens arrays and coherently integrated components on both sides of an optical substrate.

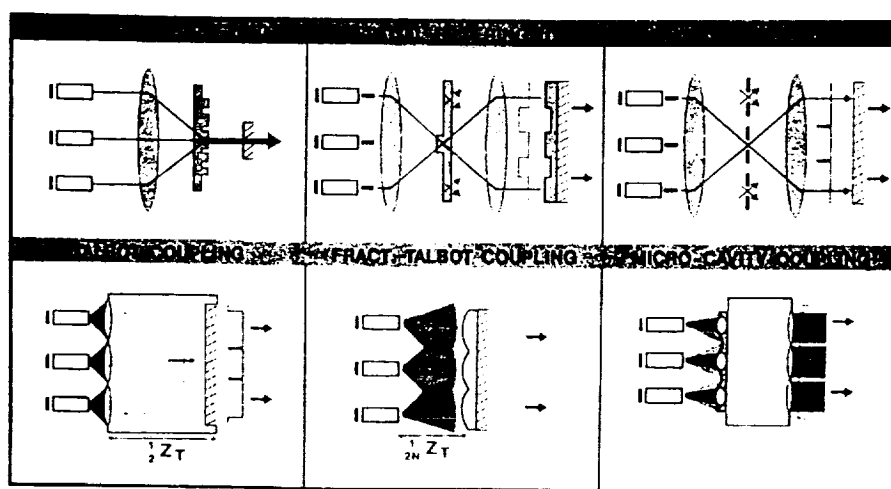


Figure 4. Various Tested Microcavity Designs for Coherent Laser Array Addition

The binary optic elements couple, lock, and control modes of a new generation of coupled-laser microcavities, and the technology will radically change the capabilities of all active optical sensors probably with as much impact as magnetrons had on radars. In less than ten years, square-inch-size power sources producing a hundred watts of coherent laser power will be a reality.

A third and broad class of problems requiring optical microcomponents is in mapping and transforming optical field distributions into a new distribution. During the conference we heard about examples of spatially matched filters for target and fingerprint identification (6), about filters that map cartesian into polar coordinates (Mellin transforms), and about composite matched filters for preprocessing imagery. All these applications have been demonstrated with binary optical components. However, the first generation of mapping devices only requires one planar surface to phase and direct the light. Current research work centers on mapping arbitrary distributions of light into a new one with the minimum number of surfaces and maximum light throughput efficiency. A good demonstration of this technology is the geometric transformer for end-pumping solid state lasers shown in Figure 5. Microoptics aligned on two sides of a bulk substrate maps a linearly segmented array of laser pump diodes into a uniformly filled aperture that is mode matched to a solid state YAG laser rod for maximum pump efficiency. Such a transformer requires a space-variant off-axis microlens array to redirect the light filling the back-plane exit aperture uniformly and a space variant phase corrector to match the mode of the laser cavity.

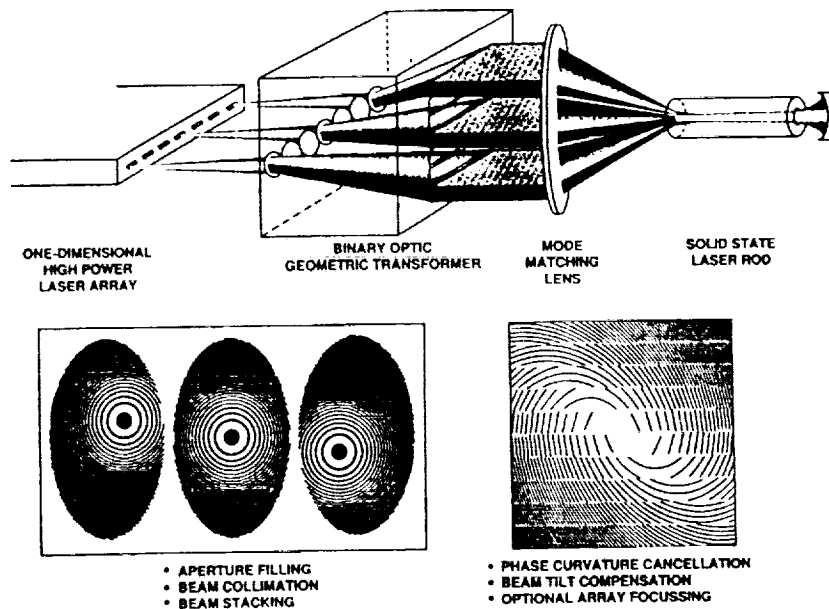


Figure 5. Optical Transformer for End-pumping of Solid-state Lasers

These are only a few examples of the blossoming microoptics technology. Does this mean the road is clear for far more complicated devices? Clearly not: there remain many unsolved technology problems that are impeding broader use of this technology. Let me mention a few. Current support of software for workstations and displays that is adapted for diffractive microstructures is virtually non-existent. Ray-trace programs need to be more consumer friendly for people working in diffractive optics and must be matched to drivers that can write data blocks in polar coordinates. Although mask foundries are now widely used for binary optics mask production, the software that drives the pattern generators or e-beam machines is cumbersome and geared to the cartesian coordinate systems used in the electronics industry. Mebes machine language needs to be developed

to satisfy the needs of optics applications. In terms of device fabrication infrastructure are DARPA supported microoptics MOSIS fabrication foundries on the horizon to drive down the cost and broaden the acceptance of this technology? We also still have a lot to learn about the problems that make microoptics fabrication different from micromechanics and micro electronics. For example, the technology for etching large-area deep-structures (more than 2 μ m deep) and replanarizing the different lithographic layers is still uncharted territory. Dual-sided lithography and layering of the micro optics on different substrate with sub-micron precision has still not been mastered either.

4. THE FUTURE: MIXING ELECTRONICS, OPTICS, AND MECHANICAL STRUCTURES

As microoptics technology matures, we shall see develop a dual role for optics in imaging sensors. Not only is optics required in photon collection processes such as image magnification, agile image scanning, and the segmentation of foveal and peripheral vision or of colors, but optics will play an important role in shaping detection architectures and image preprocessors as well. These high-throughput processing roles may come in the form of optical communication between layered processing wafers, as cross-coupling neighborhoods of clustered detector arrays, and as inter-wafer resonant processing architectures that group moving centroids and segmented texture clusters in robotic vision applications.

Present-day electronic imaging sensors are asked to perform a wide variety of functions, often with contradictory requirements in tracking, surveillance, identification, clutter rejection, or in extraction of textured patterns. But, the image-in/picture-out approach of the past in automated recognition systems is fundamentally flawed. These sensors have evolved from a camera technology developed at the turn of the century and are based on photographic or electronic recording of 2-D images that are presented to the human eye. All post processing then centers on extracting and enhancing detected features in a serially processed single image. This approach leads to very large and high speed computer system requirements.

Systems that can adapt processing architectures or interact with a changing environment do not yet exist. However, most optical sensors in nature did develop complex eye adaptability by necessity for survival. For example, whereas vertebrates have mostly simple or camera eyes, the human corneal type imaging is uncommon outside the land vertebrates. The only other large group with corneal eyes is spiders. Insects have mostly compound eyes, or sometimes their larvae are born with corneal eyes that are discarded as they grow and are replaced by compound eyes. Among the marine mollusks and crustations the most interesting eyes are found (due to photon starvation). Many of the crustation eyes are based on mirrors. Scallops have concave mirrors, others have convex lenses and sometimes one large eye and one small one. Capepod crustations have roving fovea, a linear scanning retina (3x410 elements), and a field-of-view that is a linear strip, as in many of our infrared sensors (7). The variety in foreoptics is great, e.g., male pontella fish have three lenses (one parabola and two spherical lenses), the females have two lenses (one parabola and a spherical lens), but the variety in retinal preprocessing architectures is even greater, although far less understood. Besides simple registry of images, there are retinal processing cells which are particularly interested in movement, regardless of what is moving. It has been known for some years that, in the eyes of some creatures, there are cells which will respond to movement even at levels of light too low to cause them to fire for the illumination as such. For most mammals, this sensitivity to moving objects suits prey and predator functions. Work with rabbits and ground squirrels

showed that not only frogs but mammals have specialized retinas. The squirrel is particularly fitted to detect the direction of motion of small objects (maybe that is why it freezes in on-coming car headlights). The rabbit has "fast" detectors and "slow" detectors far more sensitive than man's. Each of these optical sensors is tuned by evolution to fit a specific set of defense and predator requirements.

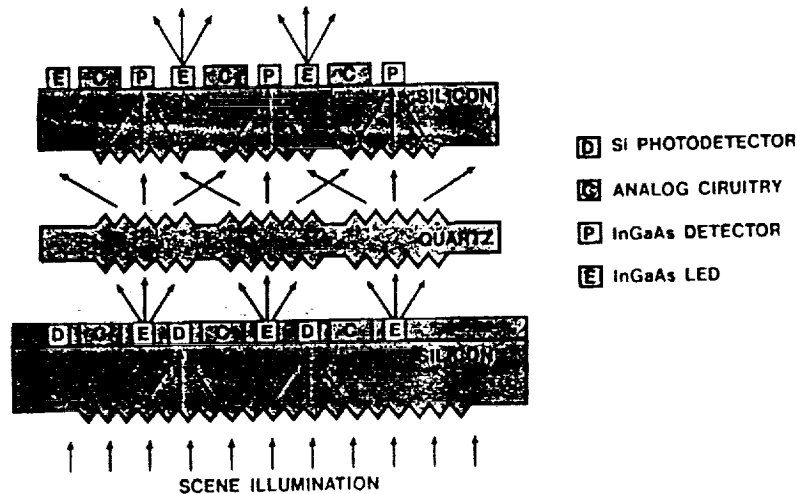


Figure 6. A Multilayer Amacronic Network with Microlenses and Micromultiplexers

Faced with such a wide ranging optical sensor complexity in nature, it is imperious to assume that our optical image-in/electronic image-out (the basis of all cameras) is not deficient for most tracking and recognition tasks. If we are to tackle one of the great remaining challenges in science, namely, robotic vision, we need to start developing focal plane processors for data rate reduction and develop sensor outputs that are fed back to the optical front end. The feedback would give the sensor agility and nonlinearity and would avoid the data overdose that always follows conventional maximum-resolution image-rastering strategies. The new approach will require compact optics and optics integration with focal plane designs (see Figure 6) The new microoptics technology based on lithography and holography can help significantly to provide agility feedback and a high throughput competitive non-linear preprocessing capability.

The first stage of the change in sensor technology requires replacement of detector arrays that consist of densely packed elements and leave no space for processing with integrated focal plane microlenses that concentrate light on smaller pixels and leave enough room for local electronic processing cells. Binary optics can focus pixel-sized signals to more efficient (lower noise) shrunken detectors and it can create sufficient space on the back focal plane to implement primary amacrine type networks and enough space to optically re-emit processed pixel information to the next processing layer. The second stage in amacronics development requires very low power circuitry to be interlaced with the detector grid and to process locally and couple electronically to the nearest detector neighbor. The most rudimentary electronic network can adapt images to changing light levels by space-variant gain settings and by amplifying differences between detectors and local averages. Neighborhood groupings then can compete and adapt away stationary or fixed patterns in space and time.

In the third stage of development each locally processed pixel output must be optically transmitted off the back focal plane to the next processing network level. The multi-

technology integration of microoptics, detectors, analog circuitry, and microlasers in the form of LED's, quantum-well lasers or SEED devices, is very complex. However, the complexity appears necessary in order to handle the inherent high-throughput requirements of image processing.

The term "amacronics" was recently given to optically and competitively coupled focal plane structures with local electronic processing cells. Amacronics derives its name from the biological term for layered "a-macros" or "short-range" interacting networks observed in front of mammalian retinas. Key amacrine functions are motion detection, edge enhancement, and space-variant image dynamic range reduction. With an optically crosslinked detector array, competitive non-linear center-surround designs that form the basis of biological amacrine functions can be implemented. For a description of these micro-sized optical pixel multiplexers, see the paper by Wong in these conference proceedings (8).

Companies like Sony and Hitachi have begun to market the first stage of amacronics technology by integrating microoptics on the front focal plane and electronic processing modules on the free space created between CCD detector arrays. The result is that their cameras have less dark current, one extra f-stop in sensitivity, and a higher dynamic range with electronic shuttering and a reduced fixed-pattern-noise dependence.

5. SUMMARY

In this presentation I have reviewed two generations of macro- and microoptical structures, and, through examples of applications, may have given you a glimpse of what the future may hold for optical sensors that use the new enabling technologies. Clearly, that future is bright with wide ranging implications; however, I would like to make three observations.

The first is that the review I presented is myopic because of my heavy bias toward smart sensor and robotic vision development we in our research group at MIT Lincoln Laboratory are involved in. It is not representative of the true capabilities and the broad ranging applications of microoptics. The technology has as many applications in optical communications in space and in fibers, optical crossbar switching, fiber coupling, mode matching, and filtering. Alternatively, optical computing and high-throughput processing which generically is a quasi-monochromatic optics technology, will also greatly benefit from the flexibility and the microscopic nature of the technology. All these applications fall under the heading of photonics used to describe the sensor, communication, and data processing applications. Photonics has been described as a "critical emerging technology" by the National Research Council and in that context microoptics is seen as an enabling technology.

However, to gain broad acceptance by a systems community not intimately familiar with the microoptics capabilities, the photonics community must actively pursue applications outside the field of optics, for example, in medicine as interocular or corneal devices and as key endoscopic optics components and in miniaturized surgical tools. In the large data storage, retrieval, and printing domain, there are significant microoptics applications in optical disk readers, laser printers, and in optical storage devices. The widest market for microoptics certainly will be in the entertainment domain, where microoptics will be used in flat screen displays, HDTV, artificial reality, and 3-D perception applications (see Figure 7).

The second point has to do with the funding level of the new technology. Microoptics as an enabling technology development is not likely to be funded generously. Yet, it is a high technology field with severe requirements on capital investments in clean rooms, lithographic equipment, high-vacuum etchers, electron-beam writers, microscopes, etc. Governmental agency funding generally, and particularly nowadays, goes to near-term solutions of problems, not to future technology investments.

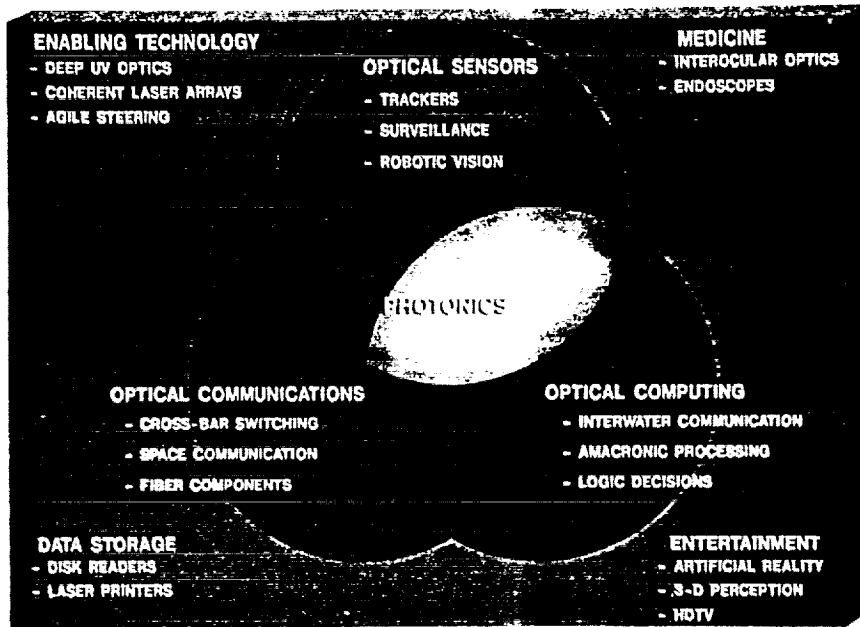


Figure 7. Multiple Binary Optics Application Domains

But microoptics won't be considered as a viable solution to a systems problem until the technology is better understood and further developed. So we must slowly bootstrap ourselves by continually proving the value of the technology with immediate applications. The past approach where passive components could be developed in isolation appears no longer feasible (except for niche applications). We in the microoptics community must cross the threshold into new multi-disciplinary technologies where we must mix optics with analog VLSI, neural network, non-linear material, microlaser, and other technologies. This will require us to forge collaboration with other disciplines in information processing, biology, medicine, data storage, and display fields.

The third and final observation is that the new optics technologies are at a historic crossroad and that many parallels can be drawn between the photonic and the electronic evolution (see Figure 8). Both are building on the same strategic microfabrication technologies of sub-micron lithography and anisotropic etching. We have a tough road ahead but, if we slowly build university trained expertise in both electronics and microoptics fabrication and gain industrial acceptance, then the future will be bright. Microoptics is the quintessential enabling technology.

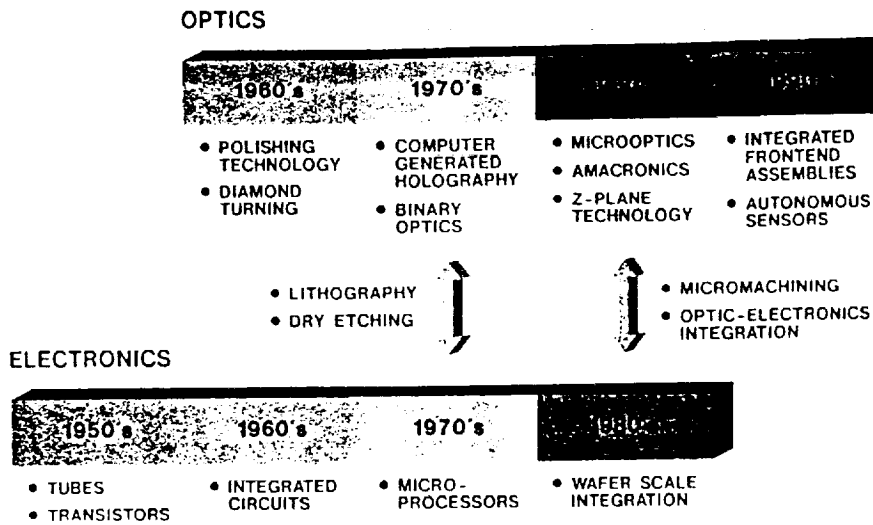


Figure 8. Parallel and Coupled Evolutions in Optics and Electronics

ACKNOWLEDGEMENTS

Over the years of the binary optics program, many people have contributed to the establishment of diffractive macrooptics and subsequently microoptics as a viable and reputable optics technology for systems. Foremost, I acknowledge the foresight of J. Lupo and L. Durvasula of DARPA and E. Wilkinson of the Army/SDC for their support in the various stages of the program. I thank my colleagues at MIT Lincoln Laboratory and numerous coworkers in industry. T. McHugh of Hughes Danbury Optical Systems and M. Riedl of Optical Filter Corp. particularly made significant contributions to the acceptance of the technology in systems. This work was funded by the Defense Advanced Research Project Agency. The views expressed are those of the author and do not reflect the official policy or position of the U.S. Government.

REFERENCES

1. E. Loewen, M. Neviere, and D. Maystre, "Efficiency Optimization of Rectangular Groove Gratings for Use in the Visible and IR Regions", *Appl. Opt.* , 18, p.2262, (1979).
2. G. Swanson, "Binary Optics Technology: The Theory and Design of Multi-level Diffractive Optical Elements", MIT Lincoln Laboratory Technical Report, 854 (1989).
3. M. Holz, M. Stern, S. Medeiros, and R. Knowlden, " Testing Binary Optics: Accurate High-precision Efficiency Measurements of Microlens Arrays in the Visible", These Proceedings, SPIE, San Diego (1991).
4. J. Leger, M. Scott, P. Bundman, and M. Griswold, "Astigmatic Wavefront Correction of a Gain-guided Laser Diode Array Using Anamorphic Diffractive Microlenses", *SPIE Proc.* 884, p. 82, (1988).
5. J. Leger, M. Holz, G. Swanson, and W. Veldkamp, "Coherent Laser Beam Addition An Application of Binary Optics Technology" , *The Lincoln Vol 1*, (2), p.225 (1988).
6. J. Homer, "ASAF Stresses Development of Semiconductor Lasers", *Aviation Week and Space Technology*, p.57, Jan 30, (1989).
7. M. Land, *Handbook of Sensory Physiology*, 8, p 471, (1982), Springer Verlag.
8. V. Wong and G. Swanson, "Binary Optics Interconnects: Design, Fabrication, and Limits on Implementation", These Proceedings, SPIE, San Diego, (1991).

MICROSENSORS, SMART SENSORS, SENSOR ARRAYS, AND THE ARTIFICIAL NOSE

by

Joseph R. Stetter
Transducer Research, Inc.
999 Chicago Avenue
Naperville, IL 60540

ABSTRACT

"Smart" sensors, or sensors connected to computers with intelligent software, offer new capability for chemical detection and monitoring. The human nose contains an array of differently selective receptors and an electronic preprocessing neuron network and is connected to a brain that can perform complex pattern recognition. Smart sensors and sensor arrays are now being developed that can begin to replicate the human olfactory process in function.

The field of microchemical sensors has experienced recent advances that allow the design of a variety of small sensor systems that are both sensitive and reliable. Examples include the thin film chemi-resistors, ISFETs, CHEMFETs, amperometric gas sensors, capacitance sensors, fiber optic [radiant] sensor systems, piezoelectric [mechanical] sensors, and microfabricated biosensors. Applications of microsensors include process control, indoor air quality monitoring, life support systems monitoring, effluent waste control, personal protection, and medical diagnostics.

Recent applications of "smart" sensor arrays include hazardous waste detection and identification and the determination of the quality of food [grain] prior to human consumption. At this time, sensor arrays have used relatively simple signal processing and pattern recognition. A comparison of a K-nearest neighbor [KNN] pattern recognition algorithm and a simple neural network [NN] intelligent system has revealed that the NN is better able to handle sensor array data and provide useful user output. The NN can deal with real applications and problems of sensor arrays such as multidimensional drift, sensor failure, and electronic noise. NNs that employ algorithms based on a "layered-model" of the natural olfactory system and are self-organizing [e.g., Kohonen networks] should be even more powerful [and more selective] than the simple algorithms now in use with sensor systems.

The opportunity exists to combine the microchemical sensors and the microelectronics systems to produce intelligent chemical recognition systems. The above examples are only the beginning.

Microtechnologies
and
Applications to Space Systems Workshop

APPLICATION OVERVIEWS

Micromechanical Actuators

William Trimmer

Princeton University and

Belle Mead Research, Inc

Man has been developing tools and devices on the size scale of his hands for millennia. Cooperative efforts have also made substantially larger mechanical systems such as cranes, ships, and even canals and roads possible. It is interesting then, that substantially smaller systems have not seen the same development. Recent work, however, has demonstrated that micro structures and actuators can be made.

Micro mechanical devices have several advantages, especially when handling small parts. First, small systems tend to be fast, in part because the transit distances are smaller. Second, perturbations due to temperature expansions and vibrations, become smaller as the systems become smaller. Third, small systems have the obvious advantage of consuming less space. Fourth, the smaller forces required to move micro systems are more compatible with handling fragile things. And fifth, because the material costs of small systems scale as the third power (the volume), material costs are reduced, and exotic materials can be used that have desirable properties.

A number of forces scale advantageously into the micro domain. For example, hydraulics, pneumatics, and biological forces scale as the dimension to the second power. These forces become stronger relative to inertial forces that scale as the dimension to the third power (the volume). If the E field is constant, the electrostatic field also scales as the second power. Often the E field can be increased for small systems, and electrostatic forces have an even more advantageous scaling.



In situ Meteorological Sensors for Earth and Mars

by

James E. Tillman, University of Washington, Department of Atmospheric Sciences,
Mail Stop AK-40, Seattle, WA 98195

The requirements for in situ meteorological sensors which measure wind speed, wind direction, pressure, temperature and humidity, the primary variables of Earth and Mars, are presented. Ideal designs maximize accuracy, specificity, resolution, and reliability, while minimizing size, cost, complexity, weight and power. The importance of minimizing contamination of the measurement by the sensor, its support, and the surrounding spacecraft, will be illustrated using the Viking Meteorology Experiment. In some instances, such as Martian applications, the deployment is the driver rather than the lack of adequate sensor characteristics. Deployment, and measuring the very important vertical variation in the lower few meters of the atmosphere, can be greatly improved by microsensor development: other advantages of microsensors will also be described. The general status for each variable is discussed, as are the areas which need improvement. Instrumental enigma's, such as sensitivity to other environmental variables, or multiple types of interaction with the sensing elements, such as are found with water vapor, are outlined. Techniques for determining complex, multi-variable parameters from simpler measurements will be mentioned along with applications. Sensor aspects still requiring major development will be highlighted. Special attention will be directed to humidity measurement on Earth since it is by far the most important greenhouse gas, and it currently can not be satisfactorily measured in some of the most important applications critical to understanding the global climate and its potential for significant change. Without adequate humidity measurements, climate modeling will remain a resource consuming exercise with little chance of reasonable accuracy, until models can be compared with accurate space-time measurements of water vapor, clouds and snow and their effect on the radiative balance of Earth.

PRECEDING PAGE BLANK NOT FILMED

Silicon Flexural Microelectromechanical Devices

K. J. Gabriel
Nanoelectronics Processing Facility
Naval Research Laboratory
Washington, DC 20375

Electrical Computer and Systems Engineering Department,
Biomedical Engineering Department
Boston University
Boston, Massachusetts 02215

Many applications of silicon microelectromechanical systems (MEMS) will require using the batch fabrication as well as the miniaturization of silicon VLSI technology. Silicon microelectromechanical components can be used to implement complex mechanical functions through interconnections among a large number of mechanical components, each of which is relatively simple. Following a review of the design, fabrication and operation of early, discrete microactuators, we discuss the fabrication and operation of some flexural, suspended support, electrostatic microactuators designed as components for multi-actuator systems: a non-resonant, comb-drive actuator with sub-micron, interelectrode gaps achieved without submicron etching; a parallelogram actuator which transforms both the magnitude and direction of the attractive, electrostatic force; and a vertically-deflecting, electrostatic/pneumatic actuator. These flexural microactuators are inherently free from friction/wear evident in continuous-motion microactuators and are capable of producing sufficient motion for envisioned applications in sensors, photonics and biomedicine.



MICROMACHINING THE FUTURE

by Dr. Marc Madou
Vice Chairman and Founder

Teknekron Sensor Development Corporation

ABSTRACT

The impact of microfabrication on the manufacturing industry will be much more profound than just the advent of some new sensors and actuators. Microfabrication constitutes a new way of designing and manufacturing all types of small parts by incorporating technologies borrowed from the semiconductor industry. This method of manufacturing is not limited to parts made out of silicon but involves materials such as ceramics, metals and all types of semiconductors and organic materials. In the first part of this talk, I will try to increase the awareness of the audience about micromachining by giving examples of micromachined parts for a very wide variety of applications. The remainder of the discussion will center on the maturity of various sensor technologies in different application fields and barriers to commercialization. Emphasis is on micromachined parts for biomedical use.

Learning From Biology--Motor Systems at All Scales

M.G. Littman
Princeton University

Human muscle is made up of cells (fibers) that are essentially microactuators. Within each bulk skeletal muscle in man are also thousands of redundant micro-length-sensors (muscle spindle organs). There are also micro-force-sensors (Golgi tendon organs) in the collagenous connecting tissues including tendons and aponeuroses. The muscle fibers themselves are organized in motor units capable of delivering different amounts of force depending on the number of fibers in a unit. As force is required, units fire according to the needed force with the smallest force-producing units firing at smallest required forces, and the largest ones firing at largest forces. This scheme keeps the $\Delta F/F$ (i.e., fractional change in force) roughly constant as new motor units come on-line. Much about the organization of microelements in a macroscopic system can be learned from looking at working biological motor systems. For example, it is interesting that the microactuator in biological muscle is roughly the same from a flea to a whale. The number of microactuators, of course, is very dependent on the scale of the organism. How many actuators is optimal for a given application? Should the actuators be paired with sensors and local processors and, if so, what is a useful ratio of sensors to actuators? How should the mechanical and control system be structured? All of these are questions for which guidance can be obtained by understanding biological motor systems.

In our research we are using SLIM (a six-link planar robot) as a platform to understand principles of the control of movement derived from biology. SLIM is structurally like man and so are his control systems. SLIM is a light-weight redundant system with five joints (ankle, knee, hip, shoulder, elbow) that are controlled by antagonist pairs of muscle-like actuators. The actuators, known as Rubbertuators (Bridgestone Corp.) are soft pneumatic bladders that, when inflated, contract 20% of their length. Like human muscle they are compliant. Length and force sensors are affixed to each artificial muscle.

We are using biologically-inspired algorithms to solve the inverse kinematics problem of the redundant structure and introducing reflex-like joint coordinations to improve posture management. The low-level posture controller is an iterative forward approximation scheme derived from a study of spinal frogs. The algorithm is parallel in nature and we are developing a specialized architecture of parallel digital signal processors (DSP--TI320C25) that mimics the organization of the human spinal cord to implement this algorithm. The parallel controller is being designed so that learning can be included at many different levels of the control hierarchy. The research is proceeding to use neural networks to learn how to integrate many levels of reflex control into smooth and efficient movements. Eventually, we would like to apply microtechnology to replace our crude artificial muscles with ones capable of more detailed control with the goal of efficiently performing the same dexterous and agile movements that man can carry out so well.

Micro-Software for Micro-Robots

David P. Miller*
MIT AI Lab
545 Technology Square
Cambridge, MA 02139

Abstract

Microtechnology has successfully reduced the size of processors, sensors, and actuators orders of magnitude from what they were a few years ago. This has allowed researchers to build a new breed of robots massing only a few kilograms (or in some instances grams) that have all of their functions onboard. This is quite an accomplishment compared to robots of only a decade ago whose cameras or computer would outweigh dozens of these current "micro-robots." Not to be outdone, software engineers and AI researchers have produced new robot programs that are more capable and orders of magnitude larger than the robot software that was available a few years ago. Despite the fact that today's micro-processors are more capable than yesterday's supercomputers, this new software will not fit on today's small robots.

It takes energy to store data in memory or to perform a computer operation. The more operations and data storage, the more energy is needed. Robots must operate in the world, in time to react to changes and events in their environment. The faster the robot needs to operate, the faster it needs to process its program, and the more power it needs for computation. The more power it needs for computation, the larger the power and thermal systems it needs to carry, which mean the larger (and more massive) its structure needs to be. The larger heavier its structure, the larger its actuators need to be, the larger its actuators, the more power they require. For space applications, the amount of software to be processed per second on a robot can have significant impact on the launch mass of the system.

Fortunately, AI research has also produced what has become known as "behavior control programming." Behavior control is an alternative method of programming robots (particularly mobile robots) which requires orders of magnitude less processing than traditional sense-plan-act control of these robots.

This task will review the current state-of-the-art in behavior control. Examples of its capabilities and limitations will be given. The role of behavior control in space robotics will also be explored.

*On leave until 10/92 from the Jet Propulsion Laboratory, 4800 Oak Grove Drive, Pasadena, CA 91109



SPACECRAFT TELECOMMUNICATIONS TECHNOLOGY
FOR MICROSPACECRAFT APPLICATIONS

K. Kellogg and C. Kyriacou
Jet Propulsion Laboratory, California Institute of Technology
Pasadena, California 91109

ABSTRACT

Spacecraft telecommunications systems traditionally consist of Radio Frequency Subsystems (RFS) and Antenna Subsystems. Fundamental trade-offs in system design are between power consumption, frequency and antenna size. Higher frequencies, such as Ka-band, result in systems with higher data rates, and low volume and mass, and enable use of electrically large antennas in a small physical envelope. These systems are at the state of the art for deep space telecommunications and are very costly to implement.

Development and space qualification of the following critical RFS technologies will yield significant savings to mass and volume, with lower cost than is available today. Application and integration with Microwave Monolithic Integrated Circuit (MMIC) devices with improvements in reliability through higher levels of integration, can reduce volume requirements by an order of magnitude; however, this technology is not space qualified at deep space frequencies. Research is also needed into rigorous modeling of MMIC packages and devices to reduce production iterations and to understand device interaction. Increased use of Application Specific Integrated Circuits (ASICs) to implement digital functions within the Transponder, Telemetry Control Unit and Command Detector Unit will likewise reduce mass and volume; however, research is needed to develop low power consumption MMIC and digital devices.

Antenna performance will dramatically benefit by development of space qualified MMICs for active array applications. Active arrays can replace bulky, massive TWTs and their associated high voltage power supplies by placing both the power amplifiers and low noise amplifiers at the aperture. Such arrays have the flexibility to be used as stand-alone small- to medium-sized apertures or to be used as feeds for reflector systems to efficiently realize larger aperture sizes. A key design challenge to implementing this technology is to provide a suitable thermal environment for the active components. Optically Processed Beamforming (OPB) is the ultimate step in

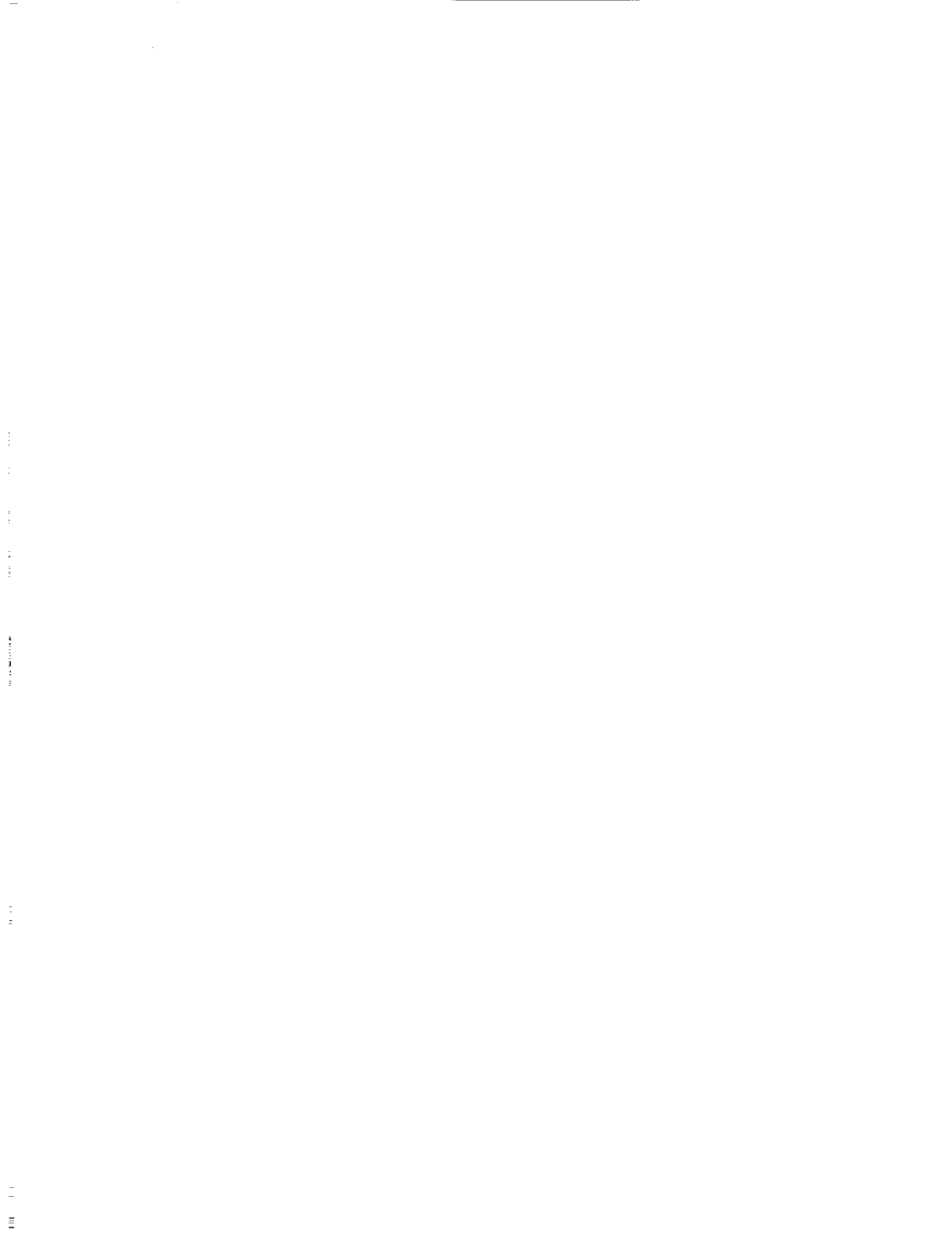
increasing overall telecommunications system flexibility and reducing system mass. OPB removes RF processing and components between the transponder and active aperture; transmission and distribution of signals to and from the aperture is accomplished photonically. Research is needed to develop photonic devices and tools to accurately model them in telecommunication system applications.

MICROSPACECRAFT: A CONCEPT

Ross M. Jones
Jet Propulsion Laboratory
California Institute of Technology
Pasadena, California 91109

ABSTRACT

There is need for smaller, faster, more frequent space science missions. Smaller spacecraft may enable such missions. Technology has been developed by the United States' Department of Defense and other government agencies that can enable smaller spacecraft. This author has developed a generic concept for utilizing advanced technology to create a microspacecraft. A microspacecraft would have a mass on the order of 10 kg. This paper will present this microspacecraft concept.



Micro Guidance and Control Technology Overview

Glen J. Kissel and
Fred Y. Hadaegh
Jet Propulsion Laboratory
California Institute of Technology
Pasadena, CA 91109

Abstract

This paper gives an overview of micro guidance and control technologies and in the process previews of some of the technology/user and systems issues presented in the guidance and control session at the workshop. We first present a discussion of the advantages of using *micro* guidance and control components and then detail six micro guidance and control thrusts that could have a revolutionary impact on space missions and systems. Specific technologies emerging in the micro guidance and control field will be examined. These technologies fall into two broad categories: micro attitude determination (inertial and celestial) and micro actuation, control and sensing. Finally, the scope of the workshop's guidance and control panel will be presented.

1 Introduction

For this paper we define micro guidance and control technology as consisting of two items. First, it includes micro-miniaturized guidance and control components and subsystems (sensors, actuators and control electronics). Second, it includes micro guidance and control architectures realized by integration of micro-machined devices and on-chip VLSI circuits with guidance and control functions.

As with many microtechnologies, *micro* guidance and control components and technologies have numerous advantages over their larger counterparts. These advantages include lower mass, volume and power consumption than components used on today's spacecraft. With solid state reliability, there should be lower risk and more robustness to temperature and vibrations. Lower costs are expected with fewer hands needed to handle the devices and with cost saving potentials inherent in batch processing technologies. Some microsystems could be more capable than today's larger systems because the decreased mass, volume and power consumption would allow redundancy or even massive redundancy of components.

In the Guidance and Control Section at Jet Propulsion Laboratory, we believe that micro guidance and control technologies can have a revolutionary impact on space missions and systems via innovative work in six thrust areas:

1. Massively distributed microsensing for system identification and control to enable space interferometers and large reflectors.
2. Light-powered remote-processing networks for guidance and control microsensing to enable viable distributed identification and control architectures needed to support item 1.
3. Micro guidance and control components for microspacecraft and microrovers to enable essential subsystem functions. These components include micro sun sensors, encoders, star trackers and motors.
4. A six degree of freedom (acceleration and attitude) micro inertial measurement unit for microspacecraft and microrovers to enable guidance

and control navigation functions.

5. Actively controlled micromachined deformable mirrors for adaptive reflectors to provide optical performance not presently feasible.
6. Embedded health sensing for guidance and control effectors to monitor and manage mission effectiveness and lifetime.

Some of the emerging micro guidance and control technologies that will support these thrusts are described in the following section.

2 Micro Guidance and Control Technologies

This section will present an overview of present and emerging micro guidance and control technologies from NASA, private industry and academia [1]. Some systems and users issues will be considered as well. The first broad area of technology to be covered is attitude determination, both celestial and inertial. This is an area where most of the advantages of microtechnologies will hold, with the possible exception of more capability. Microgyroscopes, for example, tend to have much higher drift rates than larger devices flying on today's spacecraft. The second broad area covered will be micro actuation, control and sensing.

2.1 Micro Attitude Determination, Inertial and Celestial

Microfabricated gyroscopes and accelerometers are now being developed at the Charles Stark Draper Laboratory, Cambridge, Massachusetts, using batch processing techniques such as photolithography, diffusion and etching to carve mechanical parts. Draper is working on three distinct devices:

1. Gimballed, vibrating gyroscopes and force rebalance accelerometers constructed from bulk silicon
2. Polysilicon surface machined tuning fork gyroscopes
3. Quartz resonant accelerometers and gyroscopes

One reason Draper is pursuing three separate technologies is in part to lessen the risks associated with emerging technologies.

Satcon Technology Corporation, Cambridge, Massachusetts, is also working on microgyroscopes, in this case electrostatically suspended micromechanical rate gyroscopes based on variable capacitance motors developed at MIT. The device resembles an electrically suspended disk and is controlled to provide rate information. Surface micromachining lithographic techniques are the proposed fabrication processes, and the eventual goal is to develop a microgyroscope suspended in all six degrees of freedom.

Work on gyroscopes is also being done overseas by GEC Ferranti in Edinburgh, Scotland, which is fabricating piezo-electric vibratory angular rate transducers (gyroscopes). They make use of a cylinder of radially poled piezo-electric ceramic, metallized inside and out. The outside is divided into eight electrodes and the inside is earthed. The cylinder vibrates in one of two modes, with rotation causing a coupling of these modes which can be detected. With this kind of microdevice we obtain the kinds of benefits listed earlier - decreases in size, mass, power consumption and cost with increased reliability.

At the JPL Microdevices Laboratory, novel sensor technologies are being developed for micro accelerometers and seismometers. Researchers at the Microdevices Laboratory have made the crucial observation that compactness of devices leads to fundamental physical problems associated with sensor sensitivity and noise, including thermal noise. Some recent devices developed have been based on electron tunneling and have resulted in ultrahigh-sensitivity microaccelerometers with major reductions in mass, volume and power.

The final emerging technology in micro-attitude determination has to do with celestial sensing. OCA (Optical Corporation of America) Applied Optics in Garden Grove, California, has developed a suite of miniature wide field of view star tracker cameras. The original device was developed jointly with Lawrence Livermore National Laboratory for Brilliant Pebbles and has a field of view of 60 degrees. A follow-on camera has a 25 degree field of view and features a dual-redundant camera with a 100 microradian accuracy, 3σ , and is fully autonomous. These devices are also noted for low cost, mass and power.

2.2 Micro Actuation, Control and Sensing

Microtechnologies have also been applied to the actuation, control and sensing functions that are important to spacecraft and space guidance and control subsystems. Recently there has been joint work between JPL and UCLA on micromachined deformable mirrors which could be used on large space interferometers to compensate for distortions in elements of the optical train and in the instrument's field of view. The pixelated capacitive linear actuator is the key microtechnology needed to produce a highly pixelated mirror surface to be controlled. The actuators could be monolithically integrated with the mirror assembly. Research is also being done on the modeling and control of these devices.

Micromachined sensors are a rapidly developing microtechnology that could aid guidance and control systems. An example of this kind of technology, being developed at the Georgia Institute of Technology, Atlanta, Georgia, involves epitaxial lift-off to fabricate thin-film, single crystal, optical quality semiconductor devices. The technique employs surface micromachining and epitaxial growth with sacrificial layers such as aluminum arsenide. Depositions of light-emitting diodes have been made on micromachined movable platforms yielding microoptomechanical devices. Here the potential exists for integrated interferometric sensors and steerable and movable light sources.

From a systems and user's perspective, the Johnson Space Center, Hous-

ton, Texas, and the Honeywell Systems and Research Center, Minneapolis, Minnesota, are examining how micromachined sensors could be used for vehicle health monitoring. The health monitoring task would include manned space vehicles. They have examined requirements that vehicle health monitoring places on micromachined sensors, including requirements on performance, size, mass and fault tolerance. The two centers are also grappling with the issue of how commercial and military sensors can be used to meet space systems requirements.

Some good overview work on micro guidance and control technologies has been done in the JPL Guidance and Control Section. In particular they have noted that Lunar and Mars explorers, space-based interferometers and remote sensing platforms, whether Earth orbiting or planetary flyby or orbiting, could benefit greatly from microelectromechanical technology. They believe that the synergistic use of microminiature sensors, VLSI microelectronics and fiber optic networks will give rise to new guidance, navigation and control capabilities. Six microtechnology products or thrusts have been identified that could enable new guidance and control subsystems. These were listed in the introductory section.

3 Guidance and Control Panel Scope

The Guidance and Control panel will be considering the technologies presented in the previous section as it charts a course for micro guidance and control technology development. At the workshop, the panel will focus on emerging micro guidance and control technologies, users' and systems issues with the following emphases:

- Microdevice guidance and control subsystems for spacecraft with emphasis on component technology, attitude and articulation control and health monitoring and recovery.
 - microsensor and microactuator design including electronics, power and information processing.

- fabrication technologies including silicon processing, micromachining and tunneling technology.
- distributed architecture issues including data handling, power transmission and microsensing.
- Platform applications will include
 - shape control for multi-use vehicles and large instruments like radiometers, and vehicle guidance, navigation and control.
 - system identification, health monitoring and remote sensing applications.
- Science mission applications will include system identification, optical figure control for ground/spaceborne telescopes and interferometers, and instrument pointing/sensing/isolation.

4 Conclusion

In this paper we have briefly reviewed the advantages of using *micro* guidance and control components and architectures and listed six microtechnology thrusts in guidance and control that could have a revolutionary impact on spacecraft and space missions. We also reviewed some of the emerging micro guidance and control technologies. These technologies included micro attitude determination, inertial and celestial, and micro actuation, control and sensing. Finally, we included the guidance and control panel scope that will be used to direct the efforts of the panel as it creates a technology development plan.

References

- [1] Workshop on Microtechnologies and Applications to Space Systems, Workshop Abstracts, Guidance and Control Panel Parallel Session, May 27 and 28, 1992, Jet Propulsion Laboratory, Pasadena, CA.

Microtechnologies
and
Applications to Space Systems Workshop

SCIENCE INSTRUMENTS



MINIATURIZATION IN X-RAY AND GAMMA-RAY SPECTROSCOPY

Jan S. Iwanczyk, Yuzhong J. Wang
Xsirius, Inc., 4640 Admiralty Way, Suite 214, Marina del Rey, CA 90292

James G. Bradley
Jet Propulsion Laboratory, 4800 Oak Grove Drive, Pasadena, CA 91109

Abstract:

The paper presents advances in two new sensor technologies and a miniaturized associated electronics technology which, when combined, can allow for very significant miniaturization and for the reduction of weight and power consumption in x-ray and gamma-ray spectroscopy systems:

1. Mercuric iodide (HgI_2) x-ray technology, which allows for the first time the construction of truly portable, high-energy resolution, non-cryogenic x-ray fluorescence (XRF) elemental analyzer systems, with parameters approaching those of laboratory quality cryogenic instruments.
2. The silicon avalanche photodiode (APD), which is a solid-state light sensitive device with internal amplification, capable of uniquely replacing the vacuum photomultiplier tube in scintillation gamma-ray spectrometer applications, and offering substantial improvements in size, ruggedness, low power operation and energy resolution.
3. Miniaturized (hybridized) low noise, low power amplification and processing electronics, which take full advantage of the favorable properties of these new sensors and allow for the design and fabrication of advanced, highly miniaturized x-ray and gamma-ray spectroscopy systems.

The paper also presents experimental results and examples of spectrometric systems currently under construction. The directions for future developments are discussed.

Mercuric iodide (HgI_2) technology:

Mercuric iodide (HgI_2) occurs in two main phases, tetragonal alpha- HgI_2 and orthorhombic beta- HgI_2 . The tetragonal alpha- HgI_2 is stable at room temperature and undergoes a reversible transition to the orthorhombic phase at about 130°C. Alpha- HgI_2 single crystals usually are grown either by physical vapor transport at temperatures in the range of 100-115°C [1], or in solution at 25°C by decomplexing of dimethylsulfoxide- HgI_2 complexes [2]. Crystals grown from the vapor are characterized by better charge transport properties [3]. Table 1 lists selected properties of HgI_2 crystals. The current, most widely used vapor-growth technique was introduced by Scholz [4], and subsequently modified by different laboratories [1,5]. Another method, also used, is the growth of HgI_2 platelet crystals by polymer-assisted vapor transport [6,7]. The latter method yields relatively small sized single crystals.

Prior to detector fabrication, the as-grown crystals are sawed into slices, polished, and then etched in an aqueous solution of KI. Electrodes are deposited onto both sides of a slice of single crystal HgI_2 . For x-ray applications, usually Palladium of 100-200 Å thickness is used as the electrode material. A guarding structure is employed in order to reduce surface leakage current and improve the electric field distribution in the active part of the detector. The unit is then mounted onto a ceramic substrate for mechanical support. The surface of the detector is passivated and protected from the environment by a very thin (1-3 μm) plastic encapsulant. The Union Carbide Parylene process has been adopted for this purpose. Detectors are produced in different shapes and sizes, ranging from a few mm² up to several cm². Techniques have been developed to fabricate either single or multiple detectors on the same crystal slice. In addition, more complex, multielement detectors have been designed in the form of submodules that can be aggregated into large linear or two-dimensional arrays. A typical detector leakage current is in the range of 0.08-0.5 pA/mm² at room temperature, depending on the specific crystal and applied bias voltage. High-energy-resolution detectors are constructed to exhibit the lowest electronic noise and the

best possible charge collection. Their capacitances are kept below 1 pF. A reduction of the electronic noise level of a spectroscopy system, as well as an enhancement of the charge collection, can be achieved by cooling the detector and the input Field Effect Transistor (FET), which can be accomplished using miniature thermoelectric (Peltier) coolers. These small, single stage coolers are very compact (less than 0.3 cm^3) and use very little power (250 mW) to achieve an effective temperature in the range -10 to 0°C . Properly fabricated detectors show very good long term stability and reliability of their performance under various ambient conditions, including high vacuum and temperature cycling [8]. Also, HgI_2 detectors exhibit excellent radiation damage resistance in comparison to other semiconductor detectors [9,10].

In summary, it has been found that HgI_2 possesses a number of properties that make it very attractive for room temperature x-ray detectors that are capable of high energy resolution.

TABLE 1

| Property | Value |
|------------------------------|--|
| Crystal Structure | Tetragonal (low T, red) Orthorhombic (high T, yellow) |
| Lattice Parameters | $a = b = 4.361 \text{ \AA}$, $c = 12.450 \text{ \AA}$ |
| Density | 6.4 g/cm^3 |
| Melting Point | 259°C |
| Phase Transition Temperature | 127°C |
| Dielectric Constant | $8.80-1.2i$ (at 5461 \AA) |
| Index of Refraction | 2.71 (at 5890 \AA), 2.62 (at 6328 \AA) |
| Band Gap | 2.13 eV |
| Electrical Resistivity | $\sim 10^{13} \text{ ohm-cm}$ |
| Electron Mobility | $\sim 100 \text{ cm}^2/\text{Vs}$ at 300K |
| Hole Mobility | $\sim 4 \text{ cm}^2/\text{Vs}$ at 300K |
| $(\mu\tau)_e$ | $\leq 10^{-3} \text{ cm}^2/\text{V}$ |
| $(\mu\tau)_h$ | $\leq 10^{-5} \text{ cm}^2/\text{V}$ |
| Energy per e-h pair | 4.2 eV (measured) |
| Fano factor | 0.1 |

Avalanche photodiode (APD) technology:

The most common "reach-through" APD structure was introduced by R.J. McIntire over two decades ago [11], and devices based upon it have been produced since then in many commercial companies. This structure allows one to achieve reliable and high performance devices with useful internal gain. These devices have found many applications, including those in short wavelength communications. However, due to their small active areas (limited to only a few square millimeters, at most), they never offered any real competition to PMTs in a wide range of applications.

Recently, though, newer large area avalanche photodiodes have become available [12,13]. These newer APDs are based upon a construction which utilizes a highly uniform, neutron-transmutation-doped silicon, thus allowing for the formation of a large area, uniform junction. Breakdown at the junction periphery is prevented, even with very high electric fields, by physically beveling the edges of the diode, and by specially treating the edge [13]. This technology now offers APDs with diameters much larger than 0.5 in. , capable of operating at voltages in excess of 2 kV . APDs of 200 mm^2 area have typical surface dark currents of 200 nA , and bulk dark currents of less than 0.5 nA . The large area APDs can operate with gains up to $1,000$. The parameter k_{eff} , which determines the noise performance at high gain [11], is approximately 0.0015 , compared to 0.0025 quoted for the best "reach-through" structures. The typical quantum efficiency of current devices is $70-85\%$ in the $550-1000 \text{ nm}$ range of photon wavelengths, falling to a few percent at 300 nm , although there is an extensive effort being pursued to improve the

sensitivity of APDs at short wavelengths to extend their response into the UV region. Such APDs offer an overall reduction in system size and complexity, compared with general purpose PMTs, as well as improved ruggedness, reliability and longevity. Additional advantages include a linear response over a 7 decade range of signal intensities. The new photodetector draws less power than an equivalent PMT, and operates from a single high voltage. Since it is immune to the effects of magnetic fields it requires no shielding.

Miniaturized Amplification and Processing Electronics:

The development of miniaturized, low noise, low power amplification and processing electronics allows one to take full advantage of the new sensors and to develop highly compact spectroscopy systems. HgI₂ systems benefit much more strongly by the use of hybridized electronics than do the bulky Si[Li] or Ge cryogenically cooled systems, which require liquid nitrogen and high vacuum operation. We have concentrated our efforts towards the development of high performance electronics for space applications and synchrotron radiation applications.

a) Preamplifiers

A pulsed-light feedback preamplifier has been constructed using hybrid techniques in a standard 24-pin, dual-in-line package (DIP). The preamplifier has been tested with HgI₂ x-ray detectors, and the electronic noise level of the system was measured at below 20 electrons rms [14] at 12 μs shaping time; power consumption was 220 mW. Recently, a new design was implemented which allows for the further reduction of power consumption down to about 85 mW, without any deterioration in noise characteristics. The circuit is prepared for hybridization in a 14 pin dual-in-line package (0.79" x 0.47") and will weigh about 4 grams.

b) Amplifiers

A triangular shaping amplifier, including a wrap-around baseline restorer, computer controlled fine and coarse gains, and computer selectable shaping times, has been developed and hybridized in a 50-pin DIP package (1.5"x2.6"). The total power consumption of the amplifier is about 2.6 W. The amplifier can work in conjunction with a recently developed pile-up rejector (PUR), which has also been hybridized in a separate 2.1"x0.9" package. These circuits were tested with HgI₂ detectors for count rates of up to 75 kcps, and showed no practical differences with full sized commercial spectroscopy amplifiers at the selected shaping times. The details of the design and testing procedures are given elsewhere [15].

For space applications, the amplification circuit can often be simplified by using only single settings for the gain and shaping time. Also, pile-up rejection electronics can be eliminated for low count-rate experiments. Our present effort in collaboration with the University of Chicago, for example, is concentrated on such a design, which besides the amplification and shaping circuitry involves a baseline restorer, a peak detector and a sample-and-hold circuit. The power consumption of this design is about 150 mW, and it can be hybridized in a 16-pin DIP (0.89"x0.47") package.

c) Processing electronics

A quad single-channel analyzer (q-SCA) that has four independent SCAs, each followed by 24 bit scalers, has been developed and hybridized in a 1.5"x3.0" package. The circuit is built to be interfaced with a computer that can be used to set the threshold levels of the SCAs and provide for the readout of scaler contents. Total power dissipation is only 0.8 W. A more detailed description of the design is given elsewhere [15].

For many applications, a miniaturized low power multichannel analyzer is much more desirable than a series of SCAs. There is an active effort involving the University of Chicago and the Max Planck Institute to construct such processing electronics, including the ADC and assorted memories, digital signal processors and interfaces. By using a low power, successive-approximation 12 bit ADC (Analog Devices AD7878), and by combining 3 channels (thus effectively reducing it to a 9 bit system), and finally by incorporating Gatti corrections [16], it was possible to obtain differential nonlinearities below 1%.

Experimental Results:

Figure 1 shows a characteristic x-ray spectrum for copper taken with an HgI₂ spectrometer operating as an integral part of the Scanning Electron Microscope and Particle Analyzer (SEMPA) prototype instrument. The characteristic x-rays were excited by electrons. The spectrum shows well-separated Cu-K_α and Cu-K_β lines at 8.0 and 8.9 keV, with an energy resolution of 218 eV (FWHM) (at the 8.0 keV peak). Also shown are Cu-L lines (L_α, L_β at 928, 948 eV, respectively) exhibiting 190 eV (FWHM) energy resolution. Figure 2 presents a Ni target fluorescence spectrum measured with the same instrument used to obtain the data in Figure 1. In addition to the Ni-K_α and -K_β lines at 7.5 and 8.3 keV, the combined Ni-L lines are clearly visible at 849 eV with an energy resolution of 182 eV (FWHM). The SEMPA instrument was developed for NASA's Mariner Mark II Comet Rendezvous/Asteroid Flyby Mission to analyze cometary dust, and was designed to provide the simultaneous information of both an SEM image and the elemental composition of dust grain specimens.

Figure 3 shows an x-ray spectrum of meteorite Murchison, taken with an HgI₂ spectrometer inserted into the Alpha-X Backscattering Instrument. A ²⁴⁴Cm alpha source was used to excite fluorescent x-rays from the sample. The Alpha-X Backscattering Instrument is under development in collaboration with the University of Chicago and the Max Planck Institute to analyze the composition of the Martian surface on the upcoming Mars'94 Mission.

Figure 4 presents a composite of x-ray spectra from different targets taken with an HgI₂ array. For relatively low count-rate conditions (10 kcps) the following FWHM energy resolutions were obtained: 252 eV at 5.9 keV (Mn-K_α), 380 eV at 17.44 keV (Mo-K_α), and 479 eV at 24.14 keV (In-K_α). The spectra shown here were measured using the Stanford Synchrotron Radiation Laboratory's (SSRL) intense SR beams to excite elemental targets. HgI₂ detector arrays are being developed to enhance the benefits of synchrotron radiation sources in several areas of advanced biological and materials science research. Recently, a two-dimensional array of twenty elements was fabricated, and construction of a 100-element detector array system has also begun.

Figures 5-9 report results obtained with a large area Avalanche Photodiode (APD). An avalanche photodiode was optically coupled to a CsI(Tl) scintillator (1.27 mm x 1.27 mm). The diameter of the APD was 15 mm. The APD/scintillator detector was tested by using different radiation sources. Figure 5 shows the gamma ray spectrum taken using a ¹³⁷Cs source. An energy resolution of 6.24% for the ¹³⁷Cs (662 keV) gamma line was obtained. Figure 6 shows an energy resolution of 7.7% for a 511 keV line (²²Na source) and Figure 7 shows an energy resolution of 23.1% for an 80 keV line (¹³³Ba source). The APD/scintillator combination was also tested with a 122 keV line (⁵⁷Co source) and the energy resolution was 16.3% (cf. figure 8). Another APD was also measured with a BGO scintillator irradiated with a ²²Na source (511 keV and 1275 keV gamma rays). Figure 9 shows the spectrum taken at 0°C. The FWHM at 511 keV is 11.2%. The same BGO crystal was measured with a PM tube, and the FWHM at 511 keV was 11.6%. In Figure 9, the bismuth escape peak (511 keV - 76 keV) was well distinguished on the left shoulder of the 511 keV peak, a feature which is not possible to observe with a PM tube.

Future Development:

The requirements for space instrumentation are in many aspects very similar to those for terrestrial field applications. The reduced weight, power and size of the spectrometer can lead to extremely attractive portable x-ray fluorescence instruments and gamma-ray spectrometers for environmental pollution monitoring, geological exploration, marine mineral analysis, archeometry, and industrial material quality assurance. One can foresee new generation, energy dispersive, detector-array gamma cameras which are able to efficiently reject Compton scatter, and thereby enhance medical or industrial images.

Our continuing effort is directed toward the improvement in HgI₂ crystal growth methods, the refinement of detector fabrication techniques, and to the development of new designs of the associated electronics. In

the area of APDs, we are putting an extensive effort into developing large scale, two dimensional detector arrays. The development of miniaturized, low noise, low-power processing electronics allows one to take full advantage of the favorable properties of these new sensors. Rapid progress in commercial operational amplifiers, and in CMOS microcomputers and other hardware logic elements with lower power consumption, reduced noise, and lower cost, strongly benefits the portable x-ray spectrometric instrumentation field. For large scale detector arrays, these advances can be translated into a possibility for constructing very powerful systems with affordable costs per electronics channel.

Acknowledgments:

The research work described in this paper was supported by the National Aeronautics and Space Administration, Contracts NASW-4492 and NAS5-33045; NIH Grant No. 5R01 GM37161. The work was carried out, in part, by the Jet Propulsion Laboratory, California Institute of Technology, under a contract with the National Aeronautics and Space Administration. In addition the authors wish to acknowledge the support and helpful assistance of Mr. Bart Dancy in the construction of the HgI₂ spectrometer probes, Ms. Fanny Riquelme for the fabrication of the HgI₂ detectors, Mr. Marek Szawlowski of Advanced Photonix, Inc. for the results of his measurements on APDs, and Mr. Wayne Schnepfle for assistance in preparation of this paper.

References:

- [1] M. Schieber, W.F. Schnepfle and L. Van den Berg, "Vapor Growth of HgI₂ by periodic Source or Crystal Temperature Oscillation," *J. Crystal Growth*, 33 (1976), 125.
- [2] Y.F. Nicolau, M. Dupuy and Z. Kabsch, "Differential Scanning Calorimetry and Scanning Cathodoluminescence Microscopy Study of Doped α -HgI₂ Crystals," *Nucl. Instr. and Meth.*, A283 (1989), 149-166.
- [3] A.J. Dabrowski, "Solid-State Room-Temperature Energy-Dispersive X-Ray Detectors," *Adv. X-ray Anal.*, 25 (1982), 1.
- [4] H. Scholtz, "On Crystallization by Temperature-Gradient Reversal," *Acta Electronics*, 17 (1974), 69.
- [5] H.A. Lamonds, "Review of Mercuric Iodide Development Program in Santa Barbara," *Nucl. Instr. and Meth.*, 213 (1983), 5-12.
- [6] S.P. Faile, A.J. Dabrowski, G.C. Huth and J.S. Iwanczyk, "Mercuric Iodide (HgI₂) Platelets for X-Ray Spectroscopy Produced by Polymer Controlled Growth," *J. Crystal Growth*, 50 (1980), 752.
- [7] J.B. Barton, A.J. Dabrowski, J.S. Iwanczyk, J.H. Kusmiss, G. Ricker, J. Vallerger, A. Warren, M.R. Squillante, S. Lis and G. Entine, "Performance of Room-Temperature X-ray Detectors Made from Mercuric Iodide (HgI₂) Platelets," *Advances in X-ray Analysis*, Vol. 25, Plenum Press, NY (1981), 31-37.
- [8] J.S. Iwanczyk, Y.J. Wang, J.G. Bradley, J.M. Conley, A.L. Albee and T.E. Economou, "Performance and Durability of HgI₂ X-Ray Detectors for Space Missions," *IEEE Trans. Nucl. Sci.*, 36, No. 1 (1989), 841-845.
- [9] T.E. Economou, J.S. Iwanczyk and A. Turkevich, "The X-Ray Mode of the Alpha Particle Analytical Instruments," proceedings of the Lunar and Planetary Sci. XXII Conf. (1990), 309-310.
- [10] B.E. Patt, R.C. Dolin, T.M. Devore, J.M. Markakis, J.S. Iwanczyk, N. Dorri and J. Trombka, "Radiation Damage Resistance in Mercuric Iodide X-Ray Detectors," *Nucl. Instr. and Meth.*, A299 (1990), 176-181.
- [11] P.P. Webb, R.J. McIntyre and J. Conradi, "Properties of Avalanche Photodiodes," *RCA Review*, June 1974, 234-278.

- [12] N. Gelazunas et al. "Uniform Large-Area High-Gain Silicon Avalanche Radiation Detectors from Transmutation Doped Silicon," Applied Physics Letters, Vol. 30, No. 2 (1977).
- [13] J. S. Iwaczyk, "Light Responsive Avalanche Diode," U.S. Patent 5,057,892 (1991).
- [14] J.S. Iwaczyk, A.J. Dabrowski, B.W. Dancy, B.E. Patt, T.M. Devore, A. Del Duca, C. Ortale, W.F. Schneppe, J.E. Barksdale and T.J. Thompson, "An Ultra Low Noise, Low Power Hybrid Preamplifier for X-ray Spectrometry," IEEE Trans. Nucl. Sci., NS-34 (1987), 124-126.
- [15] J.S. Iwaczyk, N. Dorri, M. Wang, R.W. Szczebiot, A.J. Dabrowski, B. Hedman, K.O. Hodgson, and B.E. Patt, "20-Element HgI₂ Energy Dispersive X-ray Array Detector System," IEEE Trans. Nucl. Sci., 39, No.5 (1992), 1275-1280.
- [16] C. Cottini, E. Gatti and V. Svelto, "A New Method for Analog-to-digital Conversion," Nucl. Instr. and Meth., 24 (1963), 241.

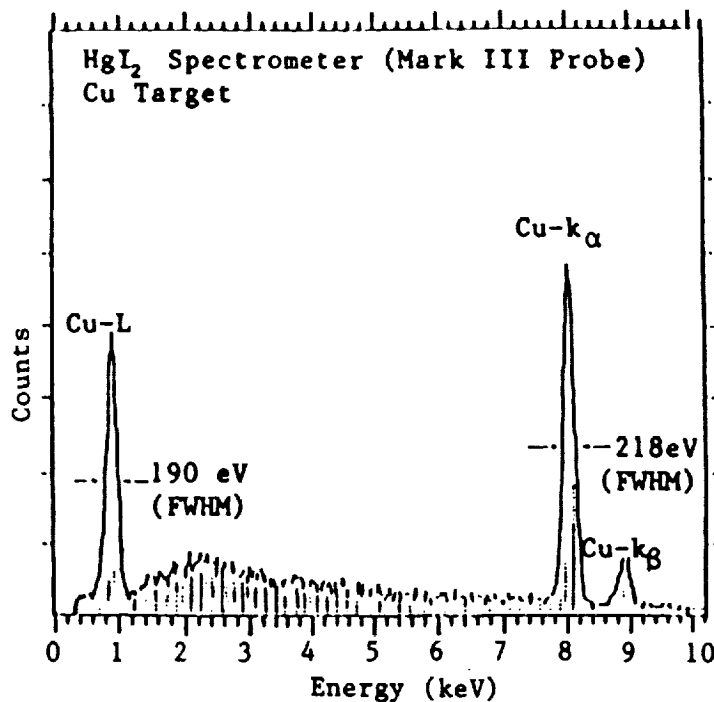


Figure 1. X-ray fluorescence spectrum for copper.

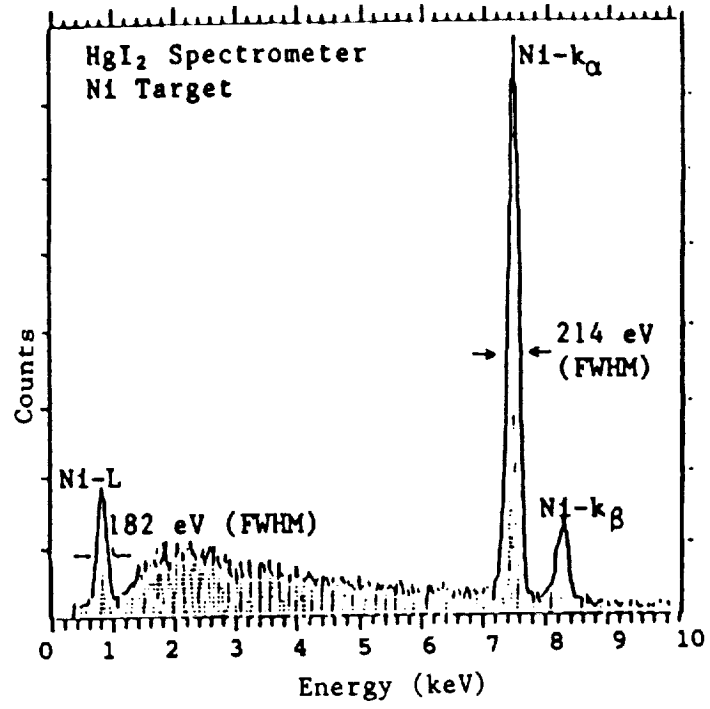


Figure 2. X-ray fluorescence spectrum for nickel.

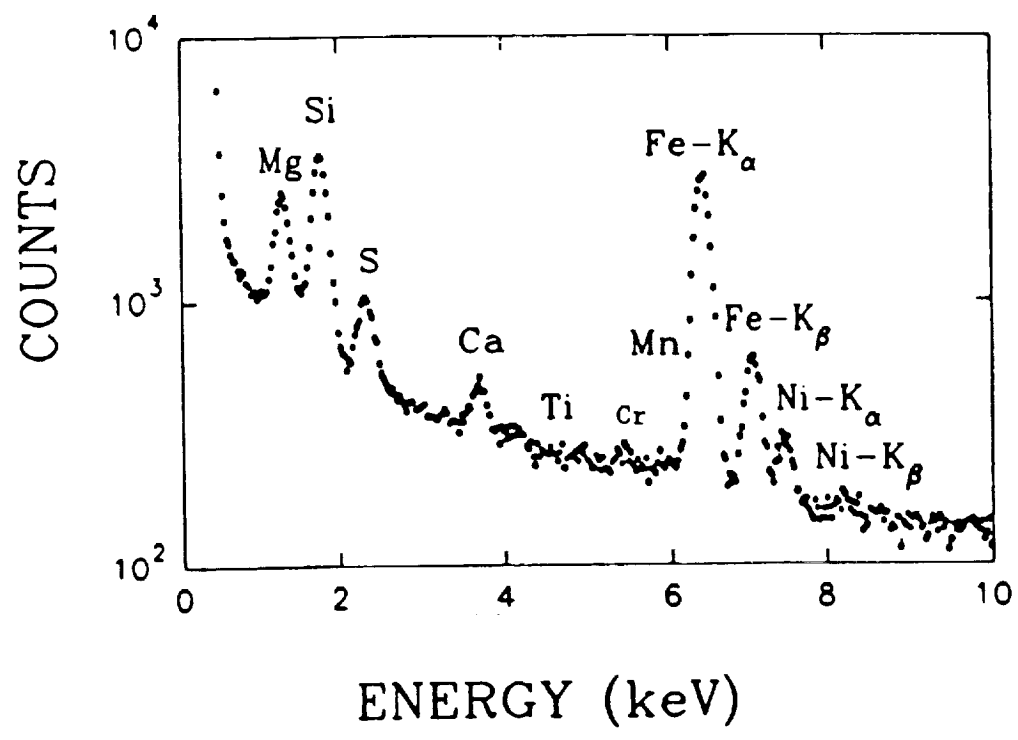


Figure 3. X-ray spectrum from a sample of meteorite Murchison taken with a HgI₂ detector probe (excited by a ²⁴⁴Cm source).

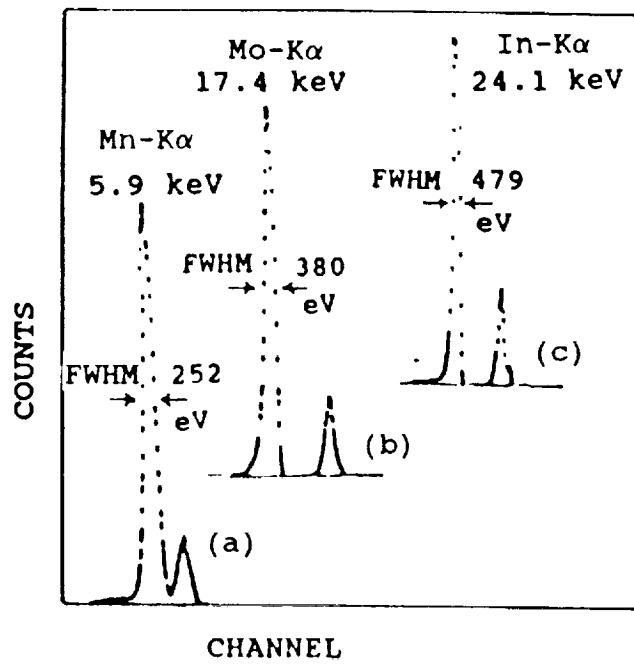


Figure 4. Spectra taken with HgI₂ array for: (a) Mn-K; (b) Mo-K; and (c) In-K fluorescent emission lines.

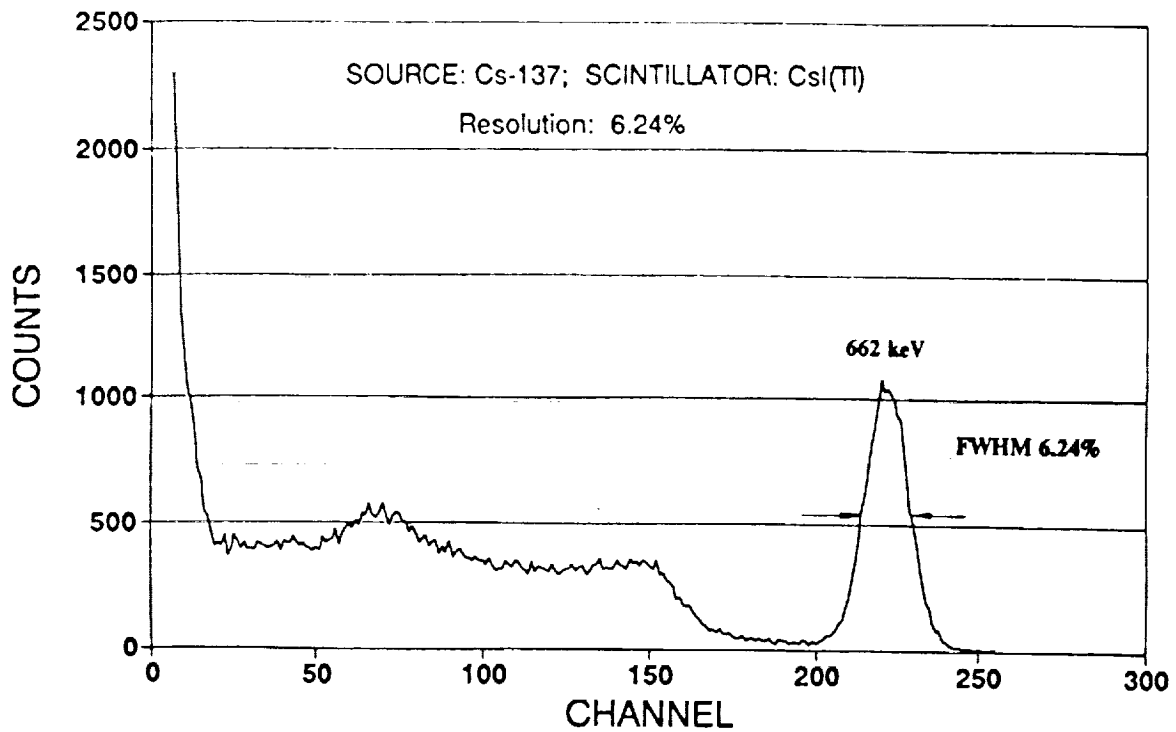


Figure 5. Spectrum from a ¹³⁷Cs source measured with an APD/CsI(Tl) detector.

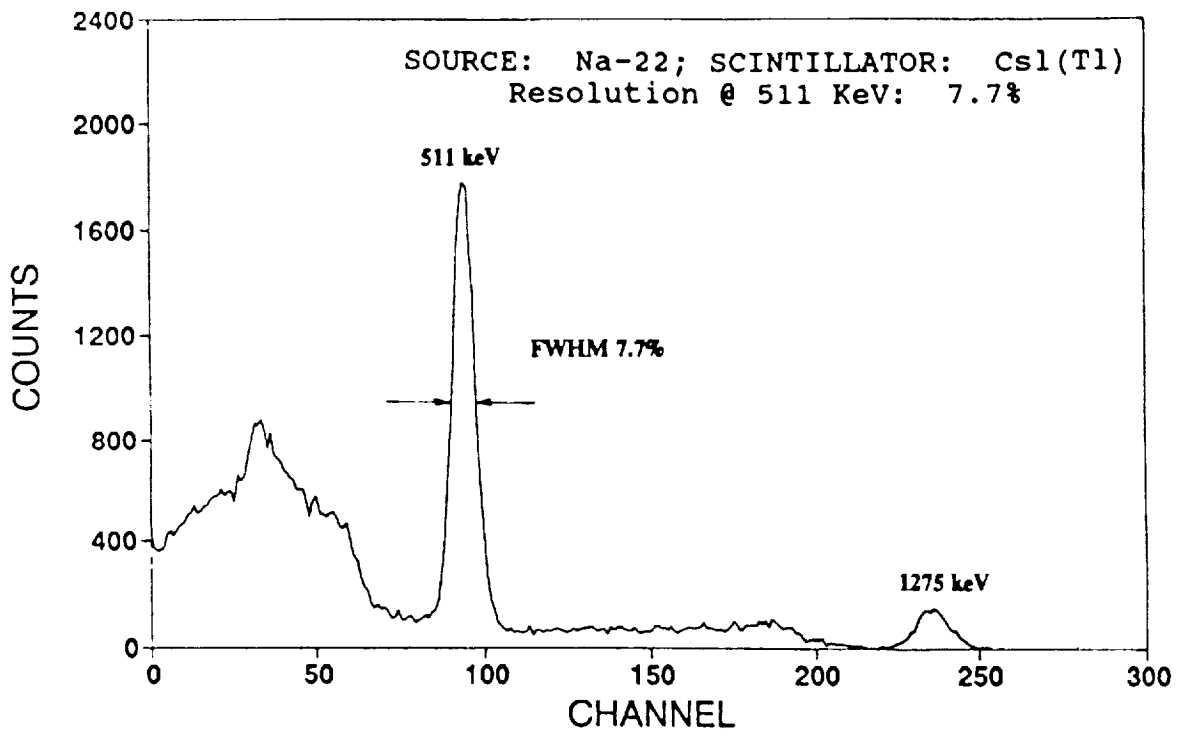


Figure 6. Spectrum from a ^{22}Na source measured with an APD/CsI(Tl) detector.

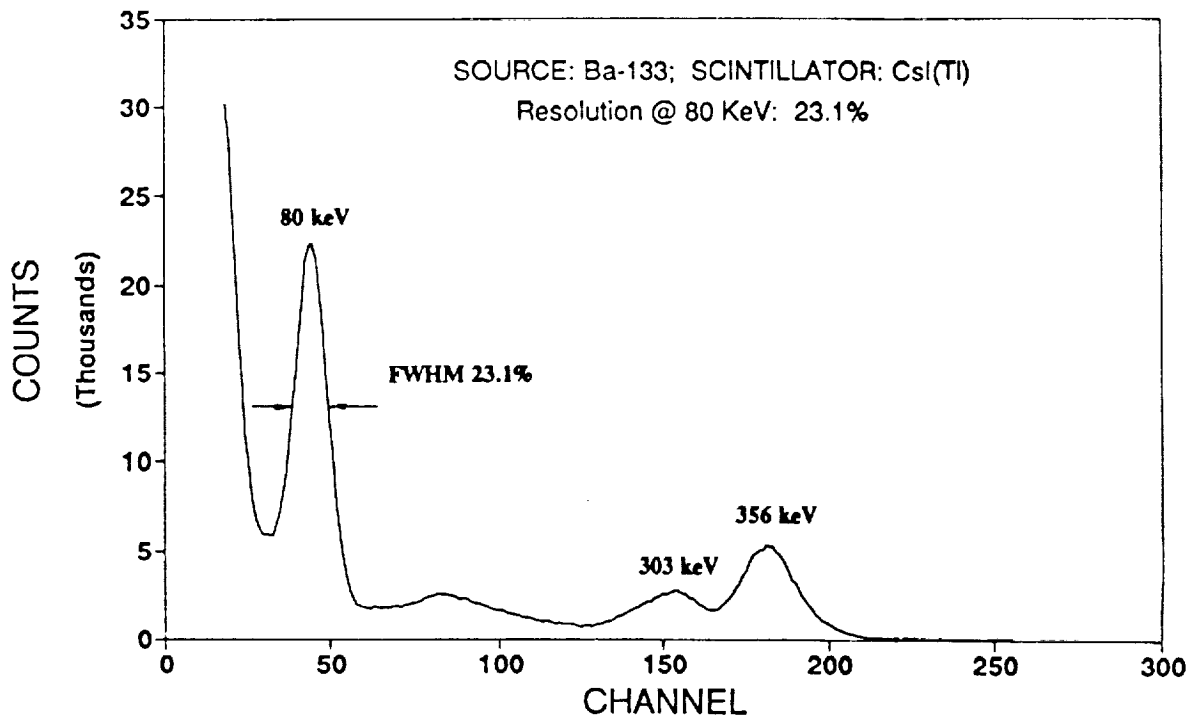


Figure 7. Spectrum from a ^{133}Ba source measured with an APD/CsI(Tl) detector.

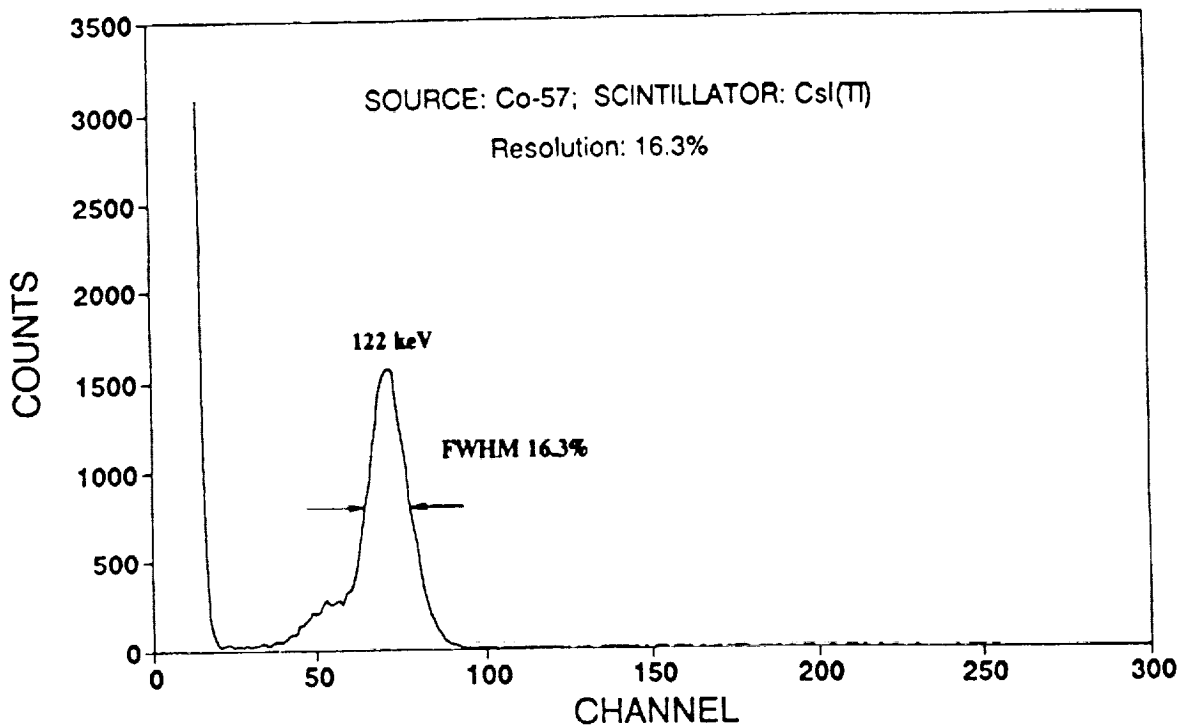


Figure 8. Spectrum from a ^{57}Co source measured with an APD/CsI(Tl) detector.

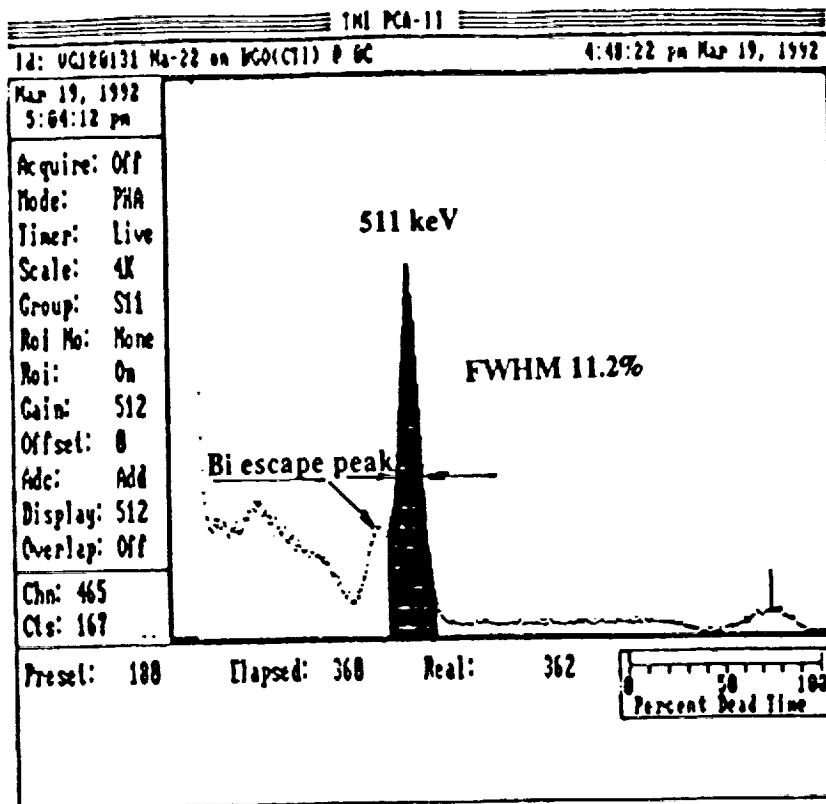


Figure 9. Spectrum from a ^{22}Na source measured with an APD/BGO detector.

Backscatter Mössbauer Spectrometer (BaMS) for Extraterrestrial Applications. D.G. AGRESTI, T.D. SHELFER, M.M. PIMPERL, E.L. WILLS, and M.H. SHEN, University of Alabama at Birmingham, and R.V. MORRIS, NASA-Johnson Space Center.

Mössbauer spectroscopy is a nuclear gamma resonance technique particularly well suited to the study of materials that contain iron (^{57}Fe). It can provide information on the oxidation state of iron as well as the type and proportion of iron-containing mineral species in a sample of interest. Iron Mössbauer spectroscopy (FeMS) has been applied to samples believed to have come from Mars (SNC meteorites) and has been helpful in refining the choice among putative Martian surface materials by suggesting a likely nanophase component of the Martian regolith [1]. Figure 1 shows a FeMS spectrum of a Martian analogue material (Hawaiian palagonite); it is dominated by ferric-bearing phases and shows evidence of a nanophase component. FeMS has also been applied to lunar materials, an example of which is shown in Figure 2. It can be used to measure the maturity of lunar surface material and has been proposed as a prospector for lunar ilmenite, an oxygen resource mineral [2].

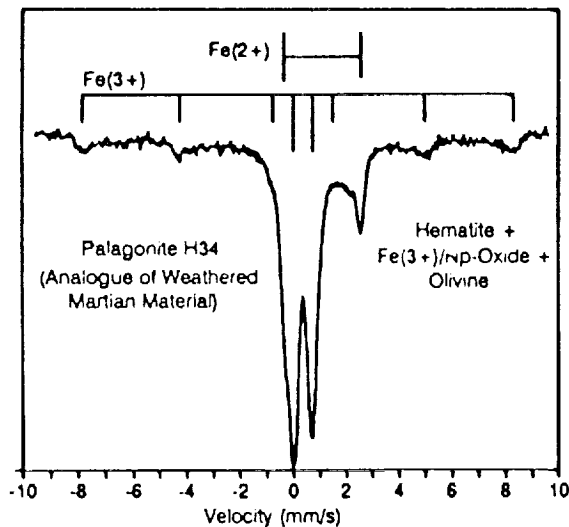


Fig. 1. Martian analogue.

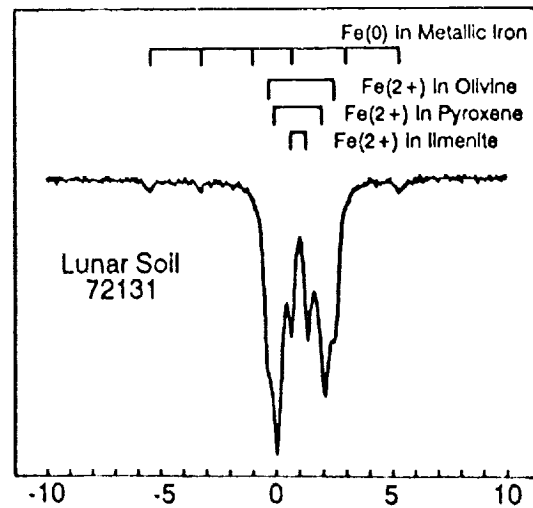


Fig. 2. Lunar sample.

Several years ago we suggested a backscatter Mössbauer spectrometer (BaMS) for a Mars rover mission [3]. Backscatter design was selected as most appropriate for *in-situ* application because no sample preparation is required. Since that time, we have continued to develop the BaMS instrument in anticipation that it would eventually find a home on a NASA planetary mission. Gooding proposed BaMS as a geochemistry instrument on MESUR [4]. More recently, an LPI workshop has recommended that BaMS be included in a three-instrument payload on the next (1996?) lunar lander [5].

The typical laboratory spectrometer contains as its principal elements a velocity transducer for modulating by Doppler effect the frequency of gamma rays emitted from a ^{57}Co source, a detector for recording the radiation transmitted through or scattered by the sample being studied, and electronics to control the velocity of the source and record the resulting spectrum. For planetary applications, each of these components must be miniaturized and integrated into a single package suitable for a space instrument.

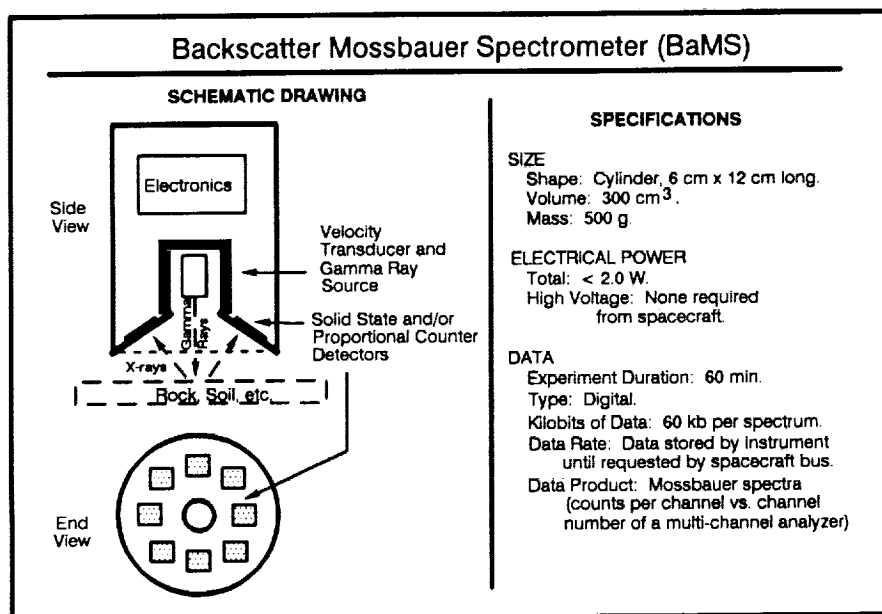


Figure 3. BaMS schematic.

We propose an instrument approximately the size and shape of a soft-drink can, as shown in Figure 3. For the velocity transducer we have constructed a version, shown in Figure 4, of the traditional two-coil (drive with feedback) design that operates with good linearity and is less than 1% the mass and volume of the typical laboratory transducer [6,7]. We have obtained Mössbauer spectra with room-temperature silicon-based PIN detectors, as have others [8]. The circuit design for a small electronics package including detector bias supply, analog pulse amplifier, pulse-height analyzer, drive control circuitry, and data storage has been completed. We are now assembling a prototype BaMS instrument of design appropriate for space applications that should be completed shortly. An instrument development program is also underway in Europe [8].

We have also tested piezoelectric and electrostrictive devices as velocity transducers as well as other solid-state detectors (HgI_2) and a gas-filled proportional counter designed for backscatter application. X-ray fluorescence (XRF) capability can readily be incorporated into BaMS, resulting in a BaMS/XRF instrument. We refer the reader to a more comprehensive discussion of applications, principles of operation, and alternate technologies [9].

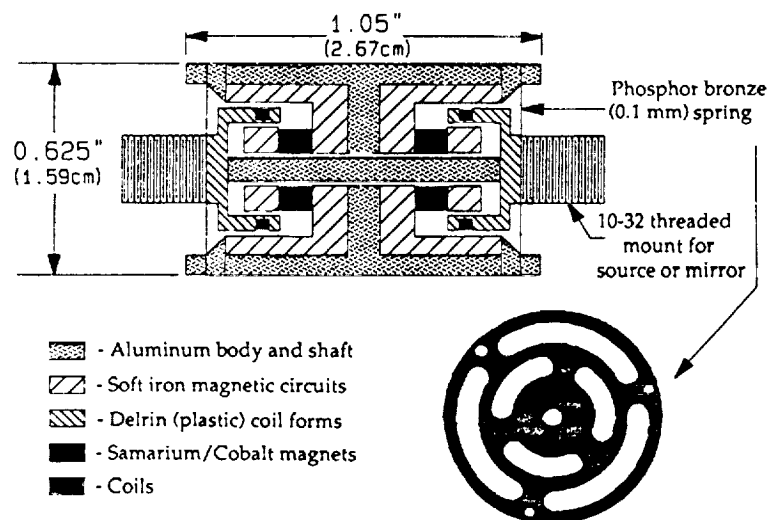


Fig. 4. Mini velocity transducer. Drive coil has 64 turns of 40-gauge magnet wire (11.4Ω). Pickup coil has 642 turns of 51-gauge wire (790Ω).

References

- [1] "Evidence for pigmentary hematite on Mars based on optical, magnetic, and Mössbauer studies of superparamagnetic (nanocrystalline) hematite." R.V. Morris, D.G. Agresti, H.V. Lauer, Jr., J.A. Newcomb, T.D. Shelfer, and A.V. Murali. *J. Geophys. Res.* **94** (1989) 2760-2778.
- [2] "Mössbauer spectroscopy for lunar resource assessment: Measurement of mineralogy and soil maturity." R.V. Morris, D.G. Agresti, E.L. Wills, T.D. Shelfer, M.M. Pimperl, M.-H. Shen, and M.A. Gibson. In *Joint Workshop on New Technologies for Lunar Resource Assessment* (Santa Fe, April, 1992, Lunar and Planetary Institute), pp. 45-46.
- [3] "Mössbauer spectroscopy for mineralogical analysis on planetary surfaces," R.V. Morris, D.G. Agresti, T.D. Shelfer, and T.J. Wdowiak. In *Proceedings, Pathfinder Sample Acquisition, Analysis, and Preservation Instrument Technology Workshop* (Houston, November, 1988, pub. by NASA HQ).
- [4] "Geochemistry on the Mars Environmental Survey (MESUR) mission." J.L. Gooding. In *First MESUR Science Definition Team Meeting, Notes and Handouts* (NASA Ames Research Center, February, 1991).
- [5] "Conclusions and Recommendations." *Workshop on Early Robotic Missions to the Moon* (Lunar and Planetary Institute, Houston, February 1992).
- [6] "Backscatter Mössbauer spectrometer (BaMS) for planetary applications: Transducer design considerations." T.D. Shelfer, M.M. Pimperl, D.G. Agresti, E.L. Wills, and R.V. Morris. *Lunar Planet. Sci.* **22** (1991) 1229-1230.
- [7] "Development of a backscatter Mössbauer spectrometer (BaMS) for planetary applications." T.D. Shelfer, M.M. Pimperl, E.L. Wills, D.G. Agresti, and R.V. Morris. *Lunar Planet. Sci.* **23** (1992) 1283-1284.
- [8] "Mössbauer backscattering spectrometer for mineralogical analysis of the Mars surface." G. Klingelhöfer, J. Foh, P. Held, H. Jäger, E. Kankeleit, and R. Teucher. *Hyperfine Interactions* (1992), in press.
- [9] "Extraterrestrial Mössbauer spectrometry." D.G. Agresti, R.V. Morris, E.L. Wills, T.D. Shelfer, M.M. Pimperl, M.H. Shen, B.C. Clark, and B.D. Ramsey, *Hyperfine Interactions* (1992), in press.

A Sub-cm Micromachined Electron Microscope

A.D. Feinerman, D.A. Crewe, D.C. Perng, and S.E. Shoaf

Microfabrication Applications Laboratory, Electrical Engineering and Computer Science Department (M/C 154), University of Illinois at Chicago, Box 4348, Chicago, IL 60607

A.V. Crewe

Enrico Fermi Institute and the Department of Physics, University of Chicago, 5640 S. Ellis Ave., Chicago, IL 60637

A new approach for fabricating macroscopic ($\sim 10 \times 10 \times 10 \text{mm}^3$) structures with micron accuracy has been developed. This approach combines the precision of semiconductor processing and fiber optic technologies. A (100) silicon wafer is anisotropically etched to create four orthogonal v-grooves and an aperture on each $10 \times 12 \text{mm}$ die. Precision $308 \mu\text{m}$ optical fibers are sandwiched between the die to align the v-grooves. The fiber is then anodically bonded to the die above and below it. This procedure is repeated to create thick structures and a stack of 5 or 6 die will be used to create a miniature scanning electron microscope (MSEM). See Figure 1. Two die in the structure will have a segmented electrode to deflect the beam and correct for astigmatism. The entire structure is UHV compatible.

The performance of an SEM improves as its length is reduced¹ and a sub-cm 2keV MSEM with a field emission source should have approximately 1nm resolution². A low voltage high resolution MSEM would be useful for the examination of biological specimens and semiconductors with a minimum of damage. The first MSEM will be tested with existing $6 \mu\text{m}$ thermionic sources.³

Reprinted with permission from the *Journal of Vacuum Science Technology A*, vol. 10, no. 4, part 1, July-August 1992, pp. 611-616.

In the future a micromachined field emission source will be used. The stacking technology presented in this paper can produce an array of MSEMs 1 to 30mm in length with a 1mm or larger period. A key question being addressed by this research is the optimum size for a low voltage MSEM which will be determined by the required spatial resolution, field of view, and working distance.

I. INTRODUCTION

An MSEM can operate in previously inaccessible locations. For example, an MSEM on a portable boom could inspect the deterioration of a fusion reactor's walls from plasma and radiation damage without disassembling the reactor to bring its sections to the microscopy laboratory. As a second example the scanning tunneling microscope (STM) has atomic resolution but the operator has difficulty locating interesting features on the specimen with a single choice of magnification. An MSEM with only 1000X magnification and a 100 μ m field of view observing the STM tip would alleviate this problem.

The technology used to make a single MSEM will also make an array of MSEMs for direct write lithography. Matching the MSEM array period with that of the substrate would simplify the drive electronics. This MSEM array would also be useful for a rapid inspection of specimens. Once a defect had been located similar spots on adjacent sections of the specimen could be quickly examined without a mechanical translation.

II. MICROSCOPE STRUCTURE

The silicon die used in this research are from 3-in. 3-5 ohm-cm (100) n-type silicon wafers 381 μ m thick (Figure 2). The structure is designed to have the fibers rest on the etched v-groove surface as opposed to resting on the

groove's edges (Figure 3). The relationship between groove width (W), fiber diameter (D), and gap between silicon die is given by the following equations⁴ where $\theta = \cos^{-1}(\sqrt{2/3}) = 35.26^\circ$.

$$\text{if } D \leq \frac{W}{\cos(\theta)} \quad \text{Gap} = \frac{D}{\sin(\theta)} - \frac{W}{\tan(\theta)} \quad (1)$$

$$\text{if } D \geq \frac{W}{\cos(\theta)} \quad \text{Gap} = \sqrt{D^2 - W^2} \quad (2)$$

The glass deforms up to $1.6\mu\text{m}$ during anodic bonding to silicon^{5,6}. This deformation will increase the fiber/silicon contact area and the increase will be larger if the contact point is below the silicon wafer surface⁷ (Figure 3a). The bond strength between the fiber and the silicon will increase as the contact area increases. Die have been stacked with 308 and $450\mu\text{m}$ diameter fibers in $270\mu\text{m}$ wide grooves yielding 152 and $360\mu\text{m}$ gaps between the silicon die respectively. Attempts to bond $510\mu\text{m}$ fibers into the $270\mu\text{m}$ grooves have not been successful, possibly due to the small fiber/silicon contact area.

The wafers were cleaned and then oxidized in steam at 900°C to grow 40nm of SiO_2 . A 200nm Si_3N_4 layer was then deposited over the SiO_2 in an LPCVD reactor. The top of the wafers were coated with HMDS primer and Shipley 813 photoresist. Rectangular $270 \times 7000\mu\text{m}^2$ and square $740\mu\text{m}$ windows were opened in the photoresist after aligning the pattern to the wafer flat. The Si_3N_4 was etched for 50 seconds in a Tegal 803 plasma etcher; then the photoresist was removed. The bottom surface of the wafer was aligned to the etched features on top of the wafer with an infrared aligner, then plasma etched. The exposed oxide was removed with a 2 minute immersion in buffered HF acid, the wafers were then immersed in a quartz reflux system containing an anisotropic etching solution (44% by weight KOH in H_2O at 82°C). This solution etches the

silicon (100) direction 400 times faster than the (111) direction⁸ and has a negligible etch rate for Si_3N_4 .⁹ The wafers were kept in this solution for 5.5 hours until the KOH solution etched through the wafer and a $740\mu\text{m}$ square opening formed a $200\mu\text{m}$ square aperture on the opposite side of the wafer. The $270 \times 7000\mu\text{m}^2$ openings formed v-grooves $191\mu\text{m}$ deep to hold 6mm long fibers. The Si_3N_4 etch mask was then removed with a 10 minute immersion in 50% HF acid followed by a 5 minute deionized H_2O rinse. In the future a boron etch stop will be used to create circular apertures using a process similar to that which creates micromachined ink jet nozzles.¹⁰ The wafers were then cut into $10 \times 12\text{mm}$ die using a MicroAutomation 1006A dicing saw and cleaned. The die were aligned and anodically bonded⁷ together with $308\mu\text{m}$ duran fibers as shown in (Figures 4 and 5). Duran or pyrex is chosen because their thermal expansion coefficients of $3.2 \times 10^{-6}/^\circ\text{C}$ closely match that of silicon at $2.6 \times 10^{-6}/^\circ\text{C}$. Both glasses have nearly identical chemical composition and are trademarks of Schott and Corning respectively. A second advantage is that the glasses can be attached to silicon at 250°C with a bond strength of 350psi ¹¹. The bond is strong enough (1.0 ± 0.5 pounds) to allow the die to be wire bonded. A stack of six die with $152\mu\text{m}$ gaps forms an electron optical column 3mm long. The column is mounted on an Airpax 1.1"x1.1" glass sealed 18 pin header which is attached to a standard vacuum flange (Figure 6).

The accuracy of the stacking technique is limited by the precision of the glass fibers, silicon die, and v-groove etching. Optical fibers drawn with laser micrometer control have a diameter tolerance of $\pm 0.1\%/ \text{km}$ of fiber¹² or $\pm 0.3\mu\text{m}/ \text{km}$ for a $308\mu\text{m}$ fiber. A kilometer of fiber would provide enough material for several thousand microscopes. The total indicated runout (TIR), which is defined as the maximum surface deviation, on a $10 \times 12\text{mm}^2$ double polished silicon die is much less than $1\mu\text{m}$. The etched v-groove (111)

surfaces also have less than $1\mu\text{m}$ of TIR. At present the overall accuracy of the column is limited by the $\pm 5\mu\text{m}$ infrared alignment of etched features in the top and bottom surfaces of the silicon die. This accuracy will be improved by initially etching a feature through the silicon wafer and aligning each surface to this feature. The stacking technique should achieve submicron accuracy.

The relationship between operating voltage and minimum column length is being explored assuming a maximum electric field of $10\text{kV}/\text{mm}^1$. Stacking with fibers $D \mu\text{m}$ in diameter, the maximum gap between the silicon die is $0.577xD$ if the fiber rests inside the v-groove and has a contact point at the silicon wafer surface. The silicon is etched at least $0.211xD$ to seat the fiber and $0.577xD$ if the v-groove completes. The die must be thicker than the etch depth for structural integrity and the minimum die thickness is assumed to be the fiber diameter. The length of a six layer column with the maximum gap between thin layers is $6xD + 5 \times 0.577xD$. A 1mm column with 640 volts between layers ($64\mu\text{m}$ gaps) can be fabricated from $110\mu\text{m}$ fibers and wafers.

III. ELECTRON SOURCE

The resolution of an electron microscope improves as the source brightness is increased. It has been predicted¹ that a micromachined field emission source can be 2 to 3 orders of magnitude brighter than a conventional field emission source. Micromachined and conventional field emission sources will be integrated into a stacked structure to verify their performance. Initial testing of the column will be carried out with a low brightness micromachined thermionic emitter. This will give a rough test of the column performance and measure the maximum electric field that can be sustained between silicon layers separated by 30 to $300\mu\text{m}$ gaps.

The micromachined thermionic emitters³ are fabricated on a silicon wafer (Figure 7). The wafers are oxidized in steam at 1100°C to grow 1 μ m of SiO₂. The SiO₂ layer electrically isolates the filament from the substrate. A 1 μ m tungsten layer is then sputtered on top of the SiO₂ and patterned with a wet etchant. The SiO₂ below the tungsten film is removed in buffered HF for 20 to 50 minutes depending on the filament width. The wafer is then immersed in KOH to etch 10 μ m of silicon to avoid any possible contact between the substrate and the heated filament. A filament that emitted 10amps for 60 minutes is shown in (Figure 8).

IV. ELECTRON OPTICAL CALCULATIONS OF EINZEL LENS AND DEFLECTOR

Preliminary electron optical calculations of the Einzel lenses in (Figure 9) were performed as follows. Previous experience indicated that the number of mesh points in the axial direction is more critical than in the radial direction and a grid (or mesh) was chosen with 701 lines along the optical axis and 50 lines in the radial direction. The electrodes themselves are defined in the grid as equipotential surfaces that will have fixed values during the calculation. The potential far from the optical axis is assumed to vary linearly between the electrodes. The calculation assumes cylindrical symmetry which will be justified if the circular apertures in the die are 10 times smaller than the square openings (Figure 2). The computational mesh is finer near the apertures where the potential is expected to vary faster. The next step is to solve Laplace's equation for the defined mesh using the finite difference method to obtain the potential on the axis. The rectangular grid is transformed to a triangular mesh by connecting the corners of the rectangles. The vertices of the triangles are the points that are assigned a potential each time through an iteration, with the final convergence solution

varying by no more than one part in 10^{-8} from the previous solution. Paraxial rays are traced with a fourth order Runge-Kutta routine after the axial potential is calculated. The input to the routine is simply the initial position and slope of the electron, so the position and size of the source and a beam defining aperture can be included in the calculation.

The following parameters can be changed in the design of our three element micromachined Einzel lens: thermionic electron source size, thickness and spacing of the electrodes, aperture size and thickness, and position of the aperture on the electrode (leading or trailing edge). See Figure 9. The first aperture size defines the maximum angle of accepted emission. The second aperture diameter defines the potential necessary to focus over a desired range. The third aperture has little effect as long as it is on the order of the first aperture size. The electrode spacing is given by equation (1).

The optical properties (aberration coefficients, potential range for desired focal points, etc.) of two lenses can be meaningfully compared only if their first order focal positions are identical. Two implementations of an electrode structure designed to give a good range of focal positions (from the exit of the gun out to infinity, for instance) were investigated as shown in Figure 9. The individual electrode contributions to the axial potential and a ray trace comparison between the two lenses are shown in (Figures 10 and 11). It appears that the more gradual focusing effect of the second electrode with the aperture on a trailing instead of a leading edge is the more desirable design.

The final two electrodes in Figure 9 are segmented to correct for astigmatism and to simulate a parallel plate deflector (Figure 12). The beam deflection angle is given by $\tan(\alpha) = (LE_{tr})/(2V)$, where L is the axial

length of the deflector (gap between silicon die), V is the beam energy as it enters the deflector and E_{tr} is the uniform transverse electric field created between the deflector plates. A field of view of $100\mu\text{m}$ requires a 0.57° deflection with a 5mm working distance. A 1kV beam is deflected 0.57° with a transverse field of 130V/mm and an L of 0.152mm.

V. CONCLUSIONS

A new technique has been developed for creating thick three dimensional structures with an accuracy approaching $1\mu\text{m}$ in three directions. The technique combines semiconductor processing and fiber optic technology. The method is being used to fabricate several versions of a miniature SEM (MSEM) 2.5 to 3mm thick from five or six silicon die. The entire structure is assembled by hand and is very rugged. The fabrication method presented in this paper can produce a six layer structure by using $110\mu\text{m}$ silicon wafers and glass fibers with 640 volts between layers (Figure 1b). The method could also fabricate arrays of MSEM's for direct write lithography and wafer inspection. Three advantages of an MSEM would be: reduction in column and vacuum hardware cost, ease of operation as all the critical components are permanently aligned to the electron optical axis, and, due to its small size, the ability to observe specimens in previously inaccessible locations.

ACKNOWLEDGMENTS

This research was supported by an NSF RIA 9009842 "Microfabrication of Electron Optical Components," a State of Illinois Technology Challenge Grant "Microfabrication Applications Laboratory," and Monolithic Sensors Inc. "Stacking of Pressure Transducers." The authors are indebted to Professor Max Epstein and Casey Cott of Northwestern University Electrical Engineering

Department for supplying the pyrex fiber and to Dr. Walter Siegmund of Schott Fiber Optic for supplying the duran fiber. Special thanks to Dr. Peter Loeppert and James Branthaver of Monolithic Sensors for guiding and assisting with the silicon processing, Mr. Wayne Ahlstrom of Mallinicrodt for chemical etching assistance, Mr. Bryan Maurantonio of MEMC for insights on silicon wafer technology, Mr. John Schnecker of Buchler for polishing assistance, and to Anthony Cocco for several helpful suggestions.

References

- 1 T.H.P.Chang, D.P. Kern, and D.P. Muray, J. Vac. Sci. Technol. B 8, 1698 (1990).
- 2 A.V. Crewe, University of Chicago, "A Sub-Miniature Integrated Electron Microscope," private communication (1990).
- 3 D.C. Perng, D.A. Crewe, and A.D. Feinerman, J. Micromech. Microeng. 2 no. 1, in press (1992).
- 4 M.A. Mentzer, in "Principles of Optical Circuit Engineering", Appendix IV, p301-307, M. Dekker, New York (1990).
- 5 D.E. Carlson, J. Amer. Ceram. Soc. 57, 291 (1974).
- 6 D.E. Carlson, K.W. Hang, and G.F. Stockdale, J. Amer. Ceram. Soc. 57, 295 (1974).
- 7 A.D. Feinerman, S.E. Shoaf, and D.A. Crewe, "Precision Aligning and Bonding of Silicon Die," Proceedings of the 180th ECS Conference, Phoenix, AZ, October, 1991.
- 8 K.E. Petersen, Proceedings of the IEEE 70, 422 (1982).
- 9 K.E. Bean, IEEE Trans. on Electron Devices ED-25, 1185 (1978).
- 10 E. Bassous, IEEE Trans. on Electron Devices ED-25, 1178 (1978).
- 11 G. Wallis, and D.I. Pomerantz, J. Appl. Phys. 40, 3946 (1969).
- 12 J. Gowar, in "Optical Communication systems," p99, Prentice Hall International, London (1984).

ORIGINAL PAGE IS
OF POOR QUALITY

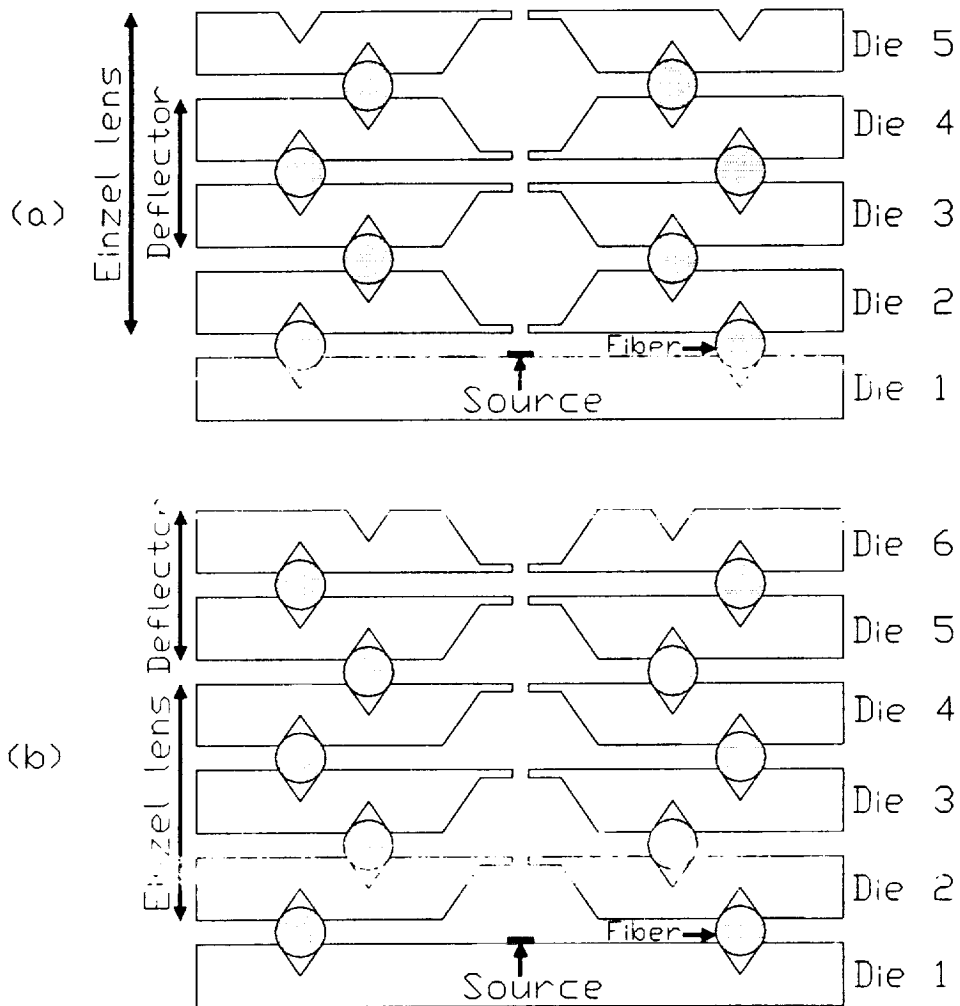


Figure 1

Silicon die are stacked with glass fibers that align and bond to the dies' v-grooves. The v-grooves are staggered to increase the die strength. The top and bottom surfaces of each die are optically aligned during fabrication. The stacking method is versatile and several electron optical columns will be fabricated and studied. Each column consists of a micromachined thermionic or field emission electron source, an Einzel lens that accelerates and focuses the emitted electrons, and two die with segmented electrodes to deflect the beam.

- a) Deflecting the electron beam inside a decelerating Einzel lens increases the field of view and working distance at the expense of circuit complexity.
- b) The beam is focused by a three electrode Einzel lens and then deflected.

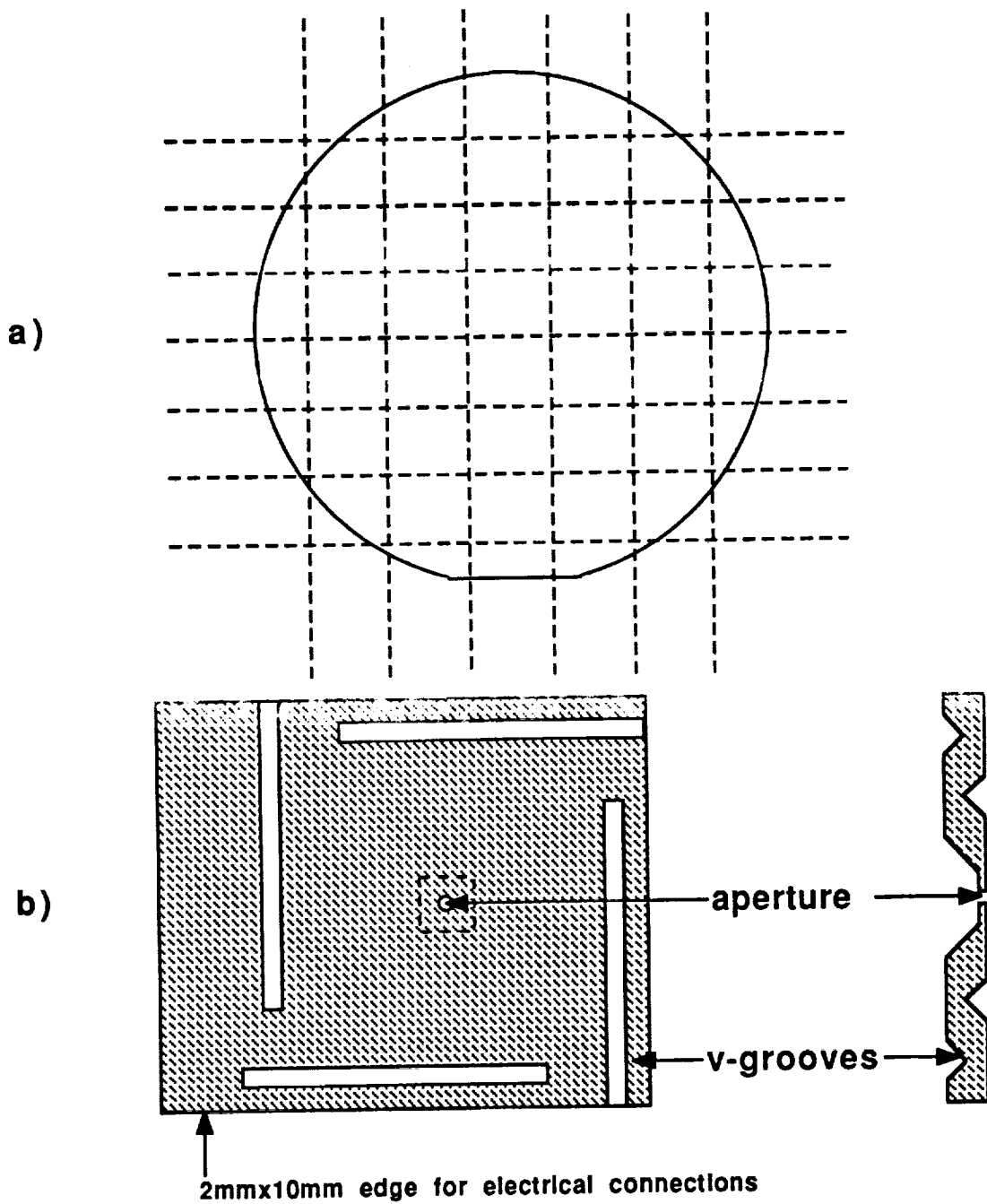


Figure 2

- a) A silicon wafer is processed to produce 26 10x12mm die.
 b) Each die contains 4 v-grooves and a membrane with a circular aperture. Entire wafers could be stacked with this technique by etching four v-grooves around the perimeter of the wafer. In this manner an array of MSEM's will be fabricated with a period of 1mm or larger.

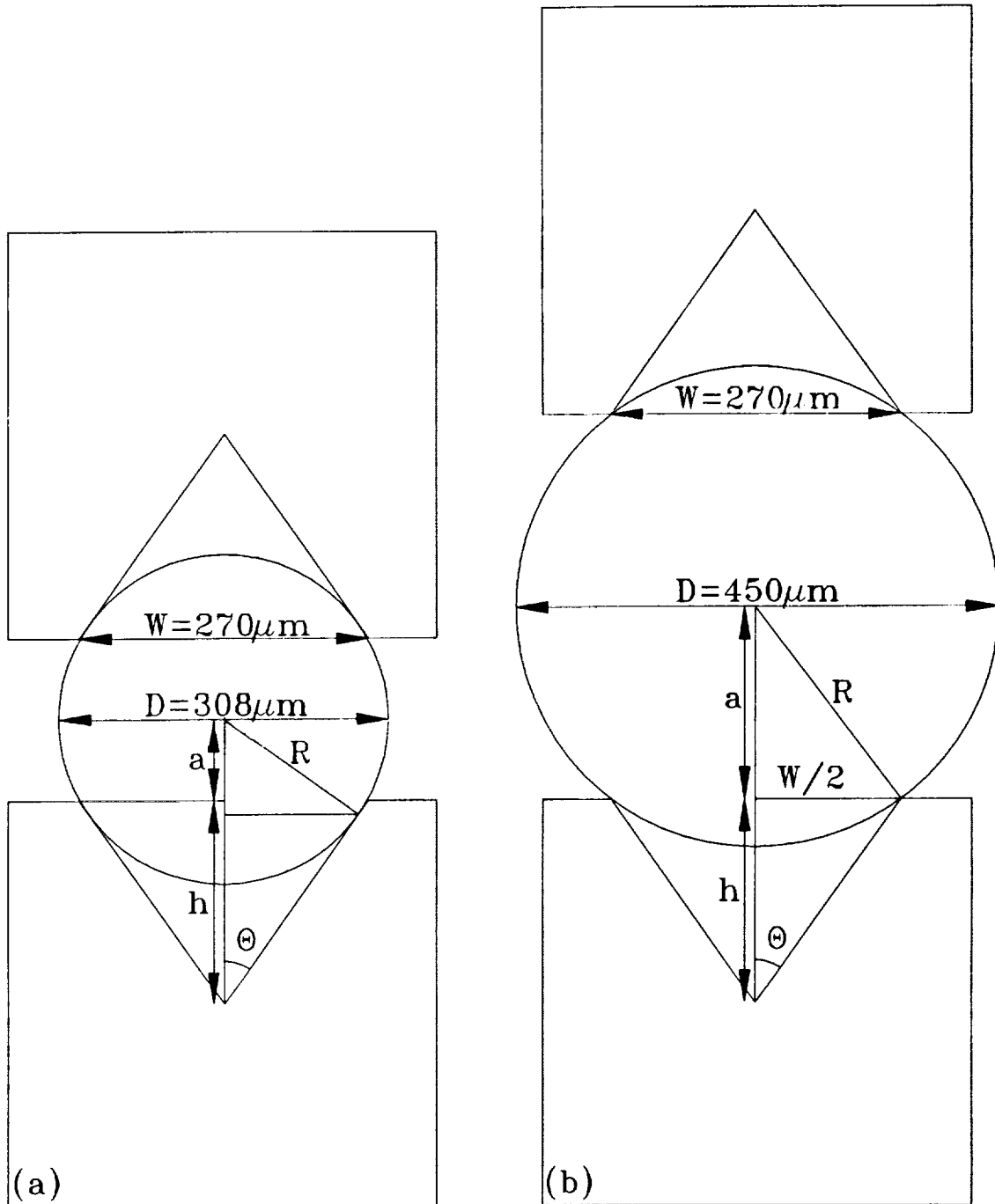


Figure 3

The gap between silicon die (2a) is determined by the v-groove width (W), and the fiber diameter ($D=2R$). The half angle of the v-groove is $\theta=35.26^\circ$, and the depth is $h=W/\sqrt{2}$.

- a) The center of a $308 \mu\text{m}$ fiber is positioned $76 \mu\text{m}$ above a $270 \mu\text{m}$ v-groove. The fiber contacts the silicon $13 \mu\text{m}$ below the silicon wafer surface.
- b) The center of a $450 \mu\text{m}$ fiber is positioned $180 \mu\text{m}$ above a $270 \mu\text{m}$ v-groove. The fiber contacts the silicon at the silicon wafer surface and rests on the groove's edges.

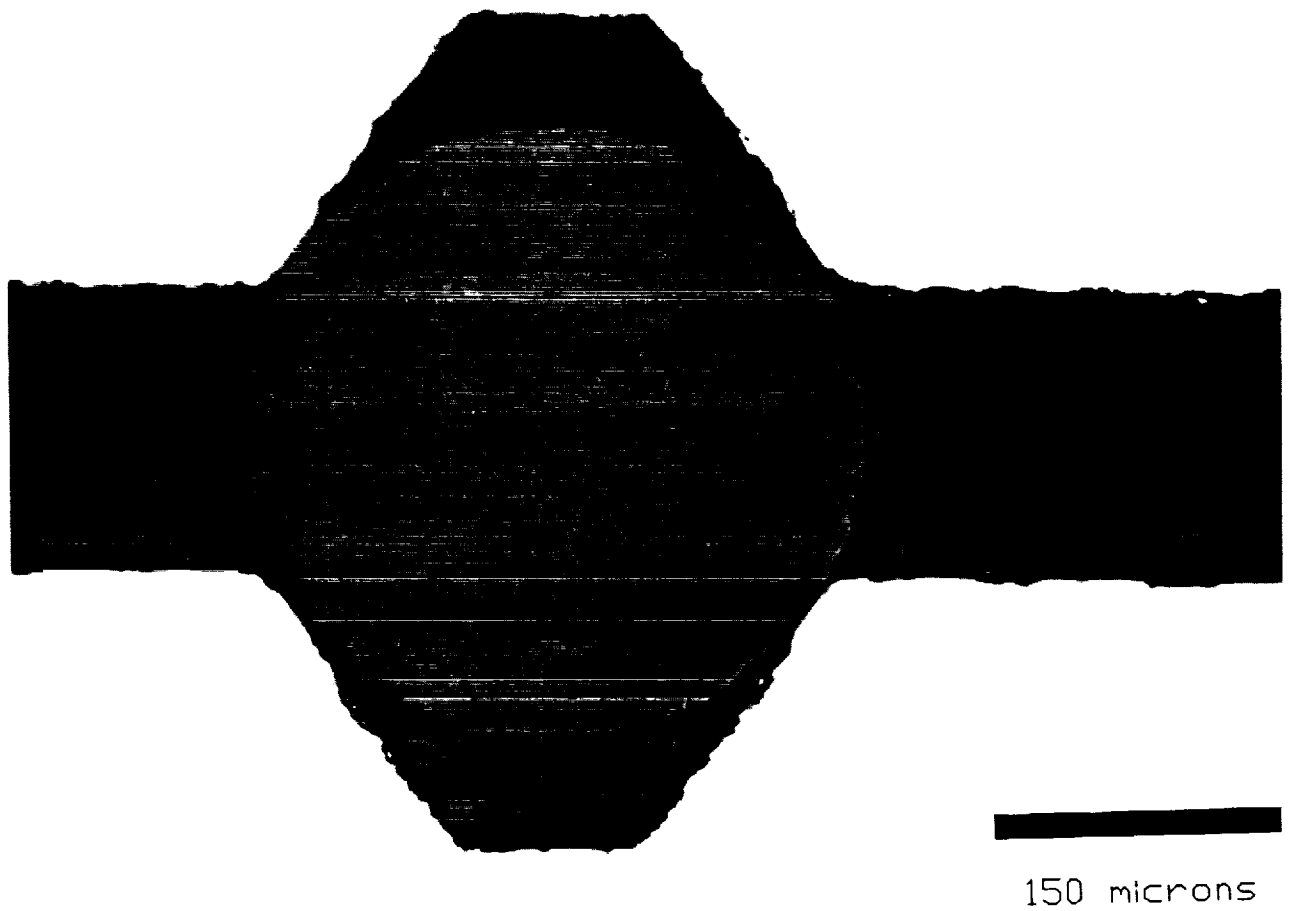


Figure 4

Two silicon die are aligned and anodically bonded to a $308\mu\text{m}$ diameter duran fiber. The die are aligned to within the accuracy of the optical micrograph $\sim\pm 2\mu\text{m}$. The separation between the die is $152\mu\text{m}$.

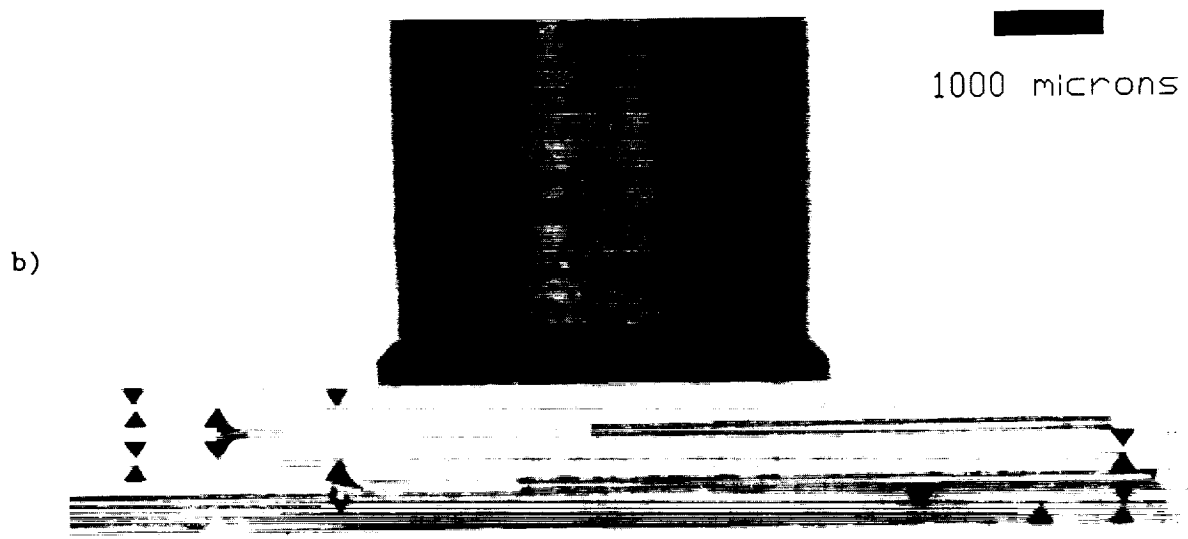


Figure 5

- a) Optical micrograph of three silicon die stacked with glass fibers. V-grooves on right are to check infrared alignment, while the rest are for fibers. At present the overall structure's accuracy is limited by a $\pm 5\mu\text{m}$ infrared alignment of the die's top surface to its bottom surface.
- b) Three silicon die will form an Einzel lens. The 0.16" vacuum pick up tool is visible in the micrograph showing the stack is self-supporting. The $2 \times 10\text{mm}^2$ overhang of the die (Figure 2b) is rotated 90° between layers to facilitate electrical connections.

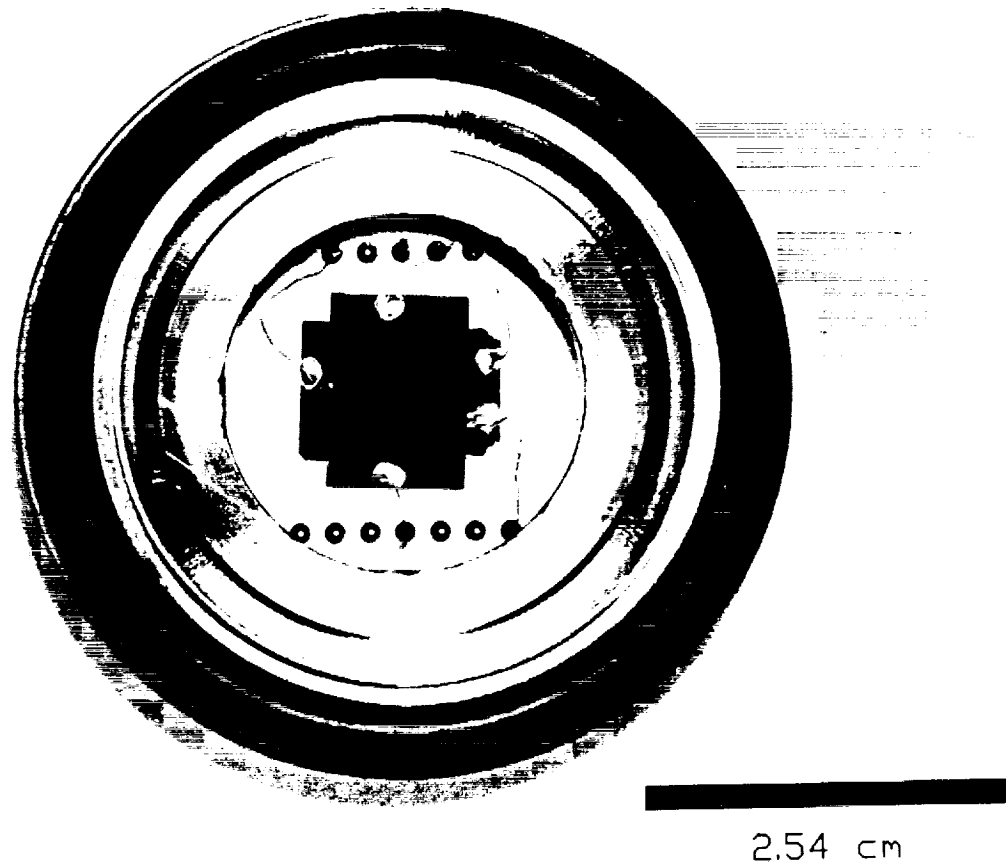


Figure 6

Four electrode stack mounted on an Airpax 1.1"x1.1" glass sealed 18 pin header. Two connections are made to the micromachined thermionic emitter on the bottom electrode. The header is seated into a 2.125" ISO quick-flange for mounting to vacuum test chamber. The structure is leak tight to 10^{-9} Torr.

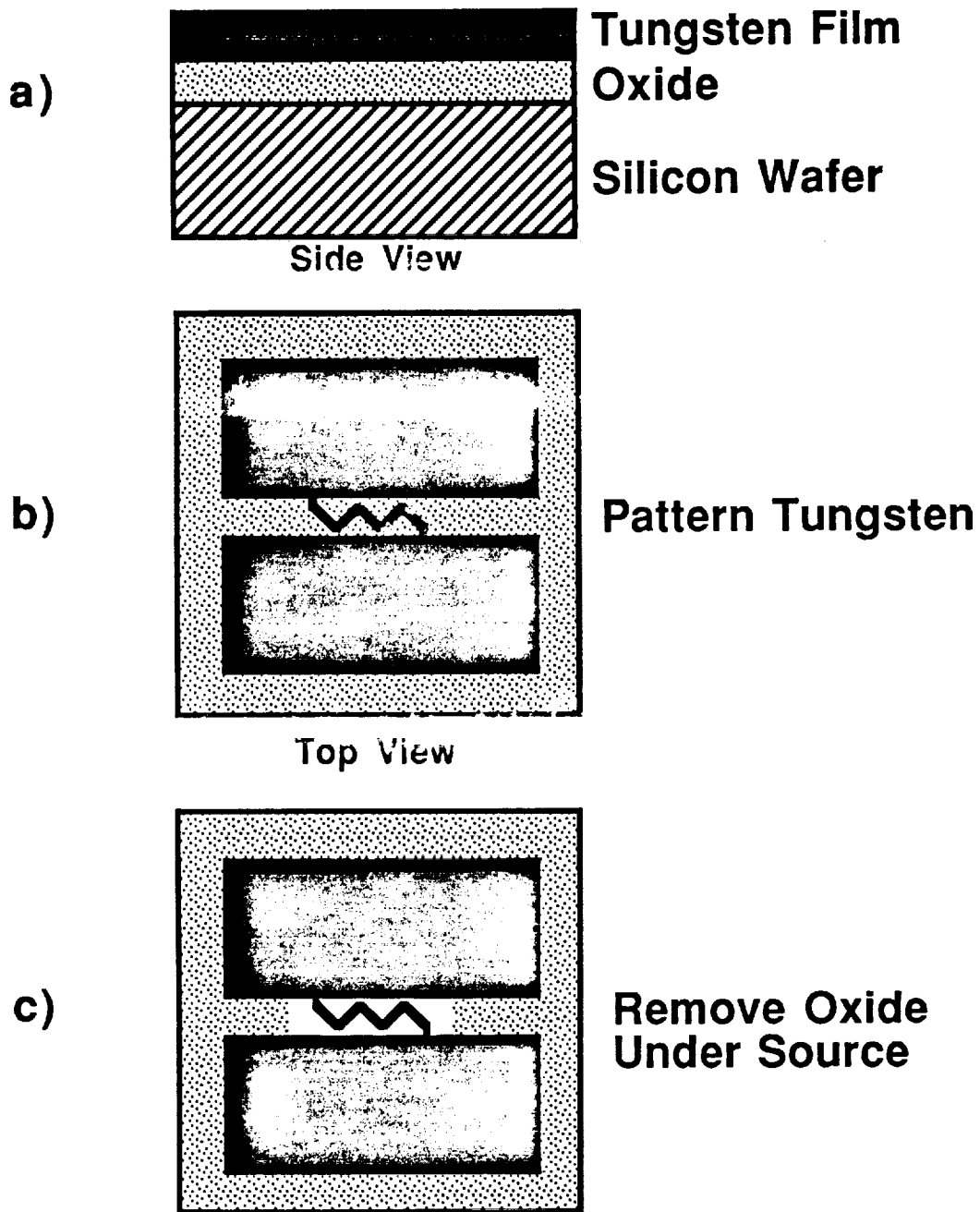


Figure 7

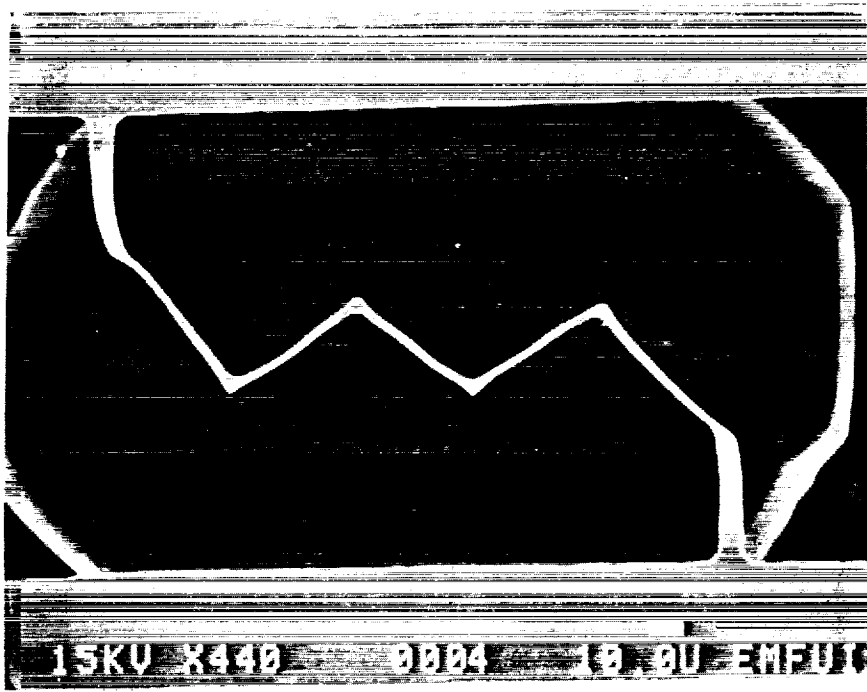
A Micromachined Thermionic Emitter.

a) A tungsten film is sputtered on an oxidized silicon wafer.

b) The tungsten film is photolithographically defined.

c) The oxide is removed from below the tungsten emitter and $10\mu\text{m}$ of exposed silicon is removed in KOH. The emitter can now be heated without interaction with the substrate.

a)



b)

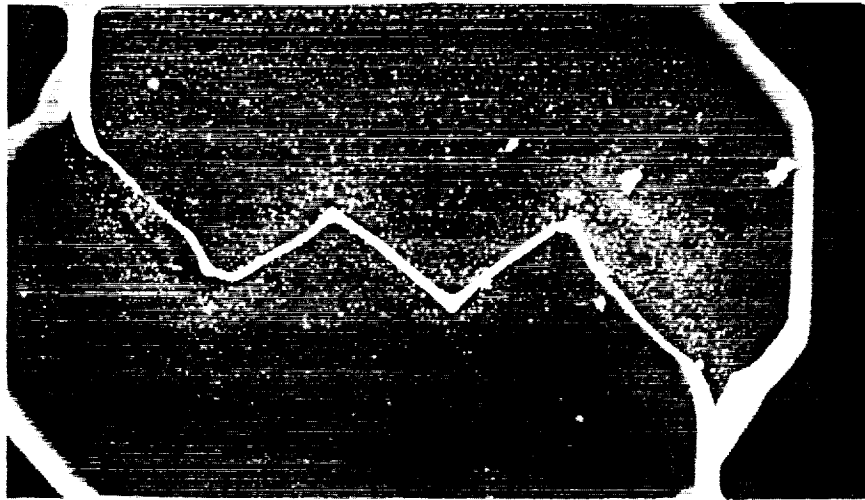


Figure 8

- a) Electron micrograph of zigzag thermionic emitter prior to operation. Each section is $6 \times 50 \mu\text{m}^2$.
- b) Electron micrograph of emitter after operation. The tungsten emitter is $.1 \mu\text{m}$ thick and emitted 10namps for 1 hour.

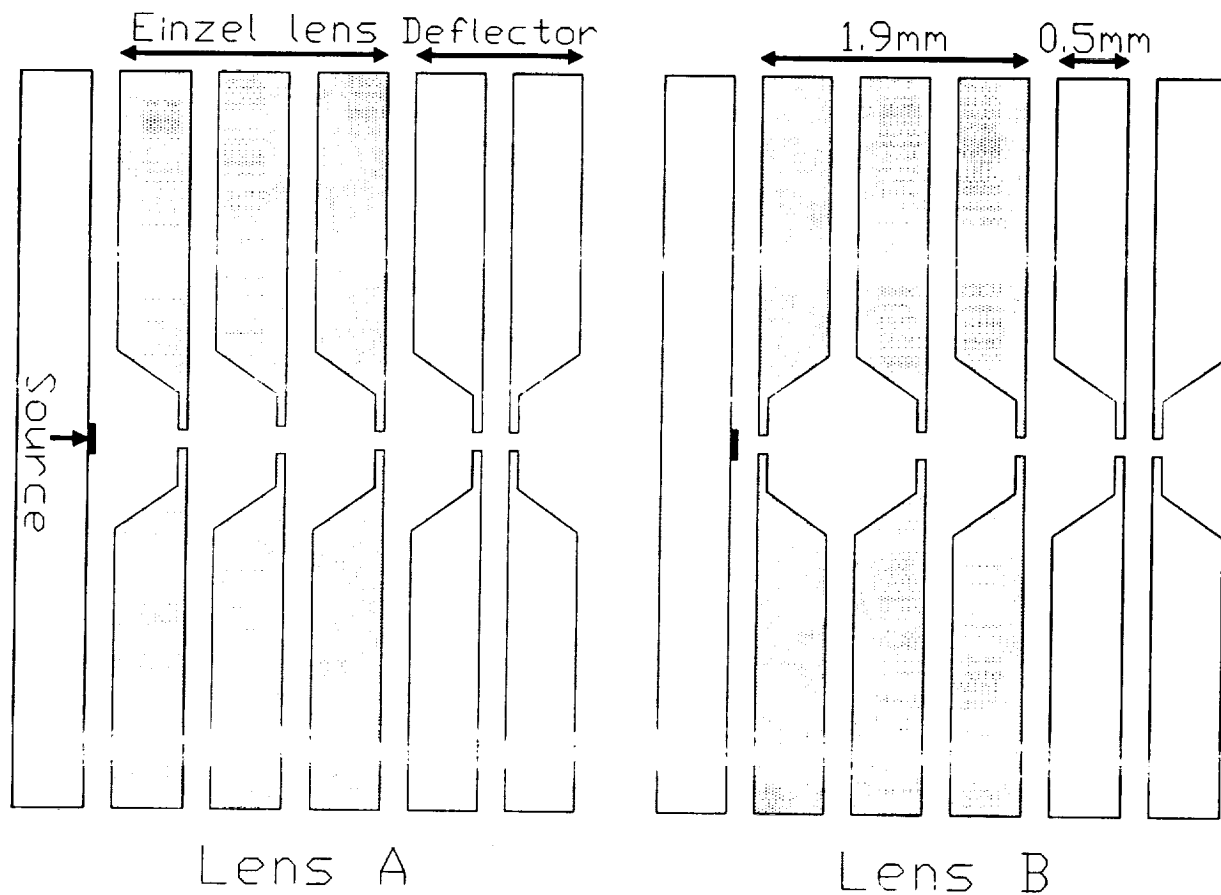


Figure 9

Two electron columns consisting of an electron source, Einzel lens, and deflectors were modeled. The Einzel lenses are shaded and the lenses differ only in the orientation of their first electrode. The first and third apertures are $100\mu\text{m}$ in diameter while the second aperture is $150\mu\text{m}$. The gaps between the silicon electrodes are approximately $200\mu\text{m}$. The focusing potential of the first electrode in the case of Lens B has an earlier and more gradual effect than in the case of Lens A.

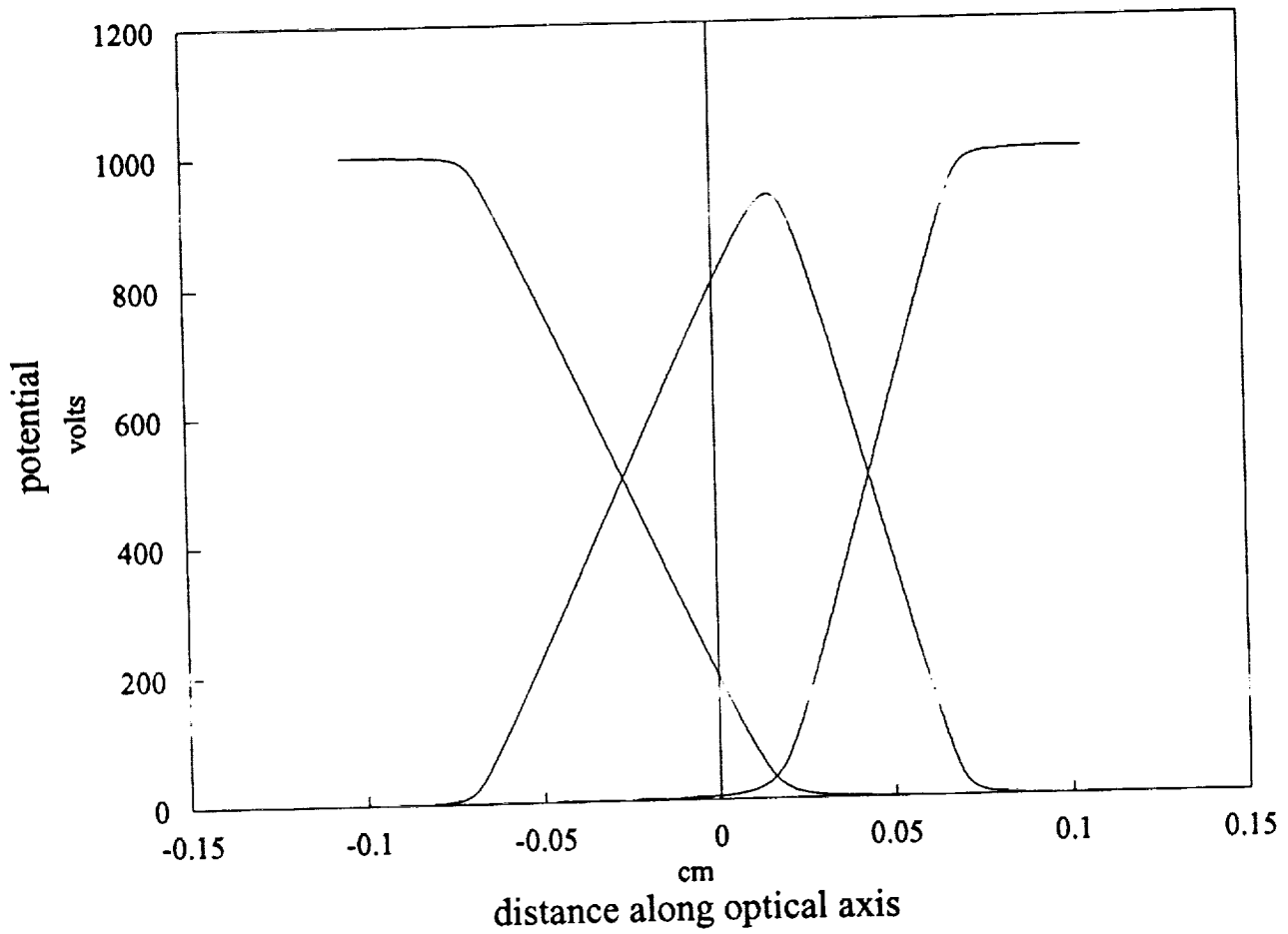
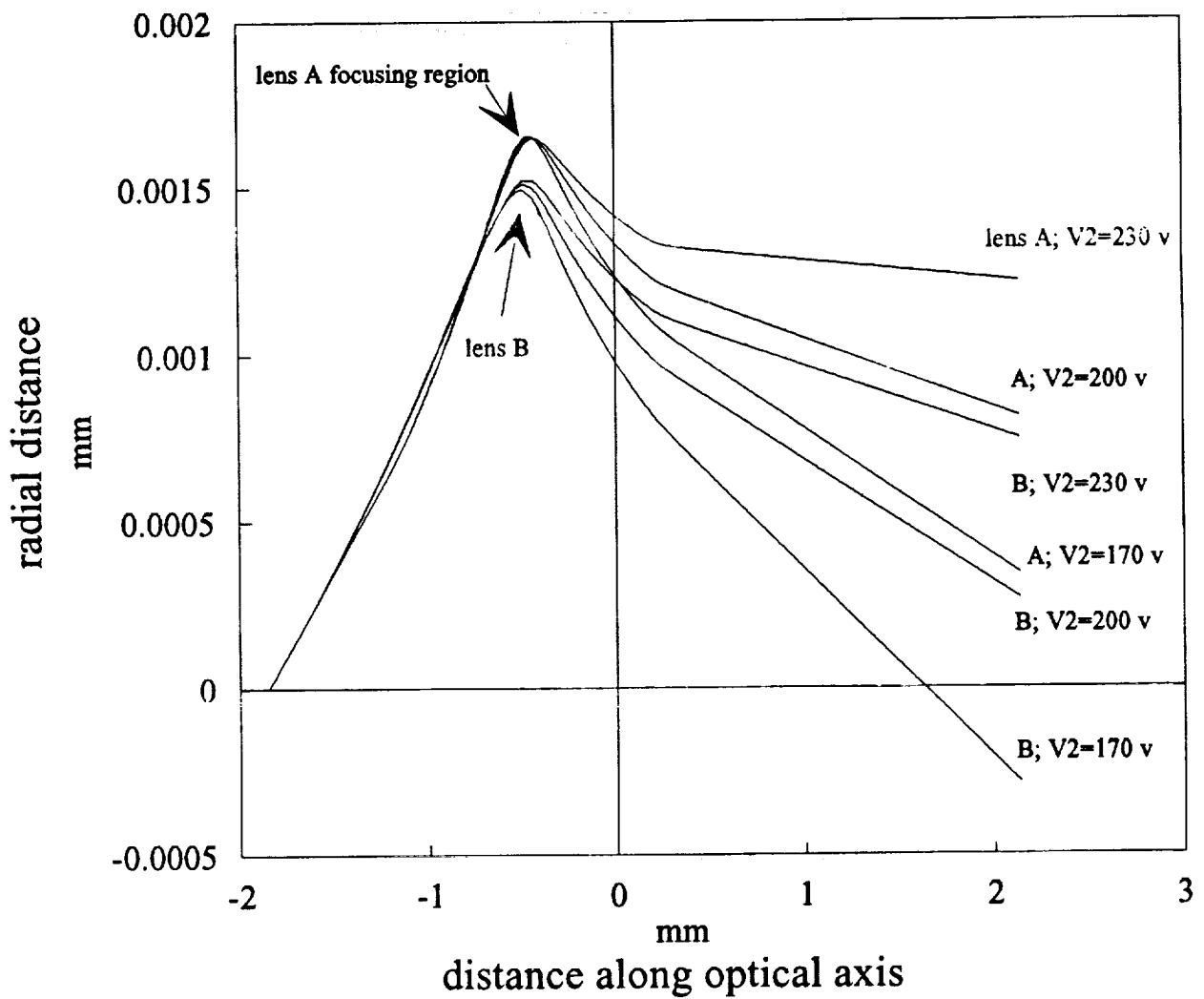


Figure 10

Individual electrode contributions to the axial potential for Lens B in Figure 9. The electrode potentials are normalized to 1 kV, a simple selectively scaled superposition of the individual contributions will provide the axial potential potential distribution for the lens.

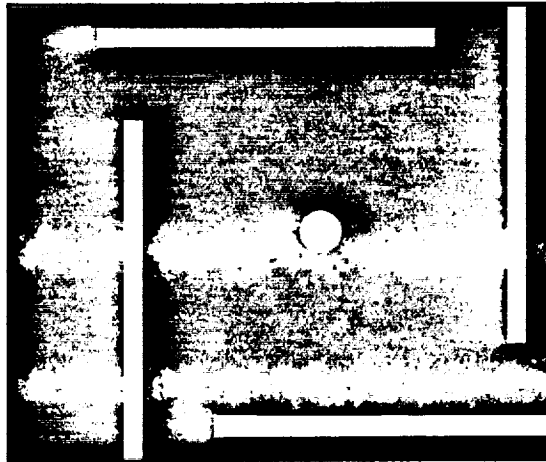


$V1 = V3 = 1000 \text{ v}$

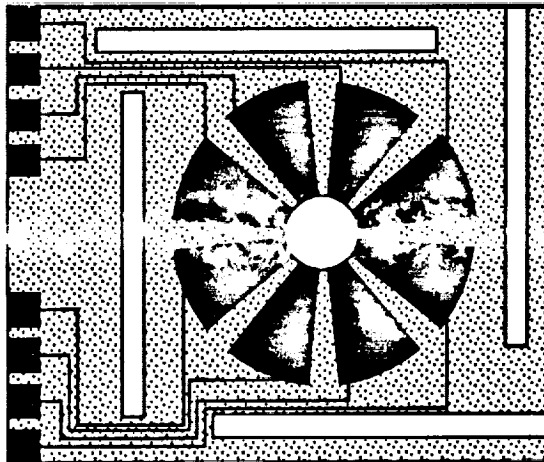
Figure 11

Ray trace comparison between the two micromachined three element Einzel lenses in Figure 9. The initial conditions for the fourth order Runge-Kutta ray trace routine are a point source on the axis with an initial angle of 1 mrad.

a)



b)



c)



Figure 12

- a) Both sides of each silicon die at a single potential will have a uniform coating of metal.
- b) One of the silicon die used to deflect the electron beam and correct for astigmatism. Die has eight independently controlled metal electrodes insulated from the silicon with a thick high quality SiO₂ layer.
- c) Cross-sectional view of deflector indicating the transverse electric field between the die.

**DIFFERENTIAL SCANNING CALORIMETRY (DSC)
FOR PLANETARY SURFACE EXPLORATION**

James L. Gooding and Douglas W. Ming
Code SN, NASA/Johnson Space Center, Houston, TX 77058-3696.

Principles of DSC. DSC is the quantitative measurement of the enthalpic response of a material to a systematic change in temperature [1]. In practice, the heat flow into or outward from a sample is measured as the sample is heated or cooled at a carefully controlled rate. DSC superficially resembles, but is not the same as, differential thermal analysis (DTA), which is the measurement of temperature differences between a sample and reference material as the pair is heated or cooled. The fundamental properties measured by DSC are enthalpies and temperatures of phase transitions and constant-pressure heat capacities. Depending on instrument design and the nature of the sample, high-quality DSC analyses can be obtained on only a few milligrams of solid materials. DSC requires direct contact with the sample and generally degrades, if not destroys, the sample as a consequence of heating. In laboratory applications, it is common to subject the gaseous effluent from the DSC to analysis by a separate evolved-gas analyzer (EGA).

Planetary Applications. In the planetary context, DSC can be used to identify minerals according to their heat-flow "fingerprints," using pattern-recognition strategies that are generally similar to those employed in spectrophotometry. The principal strength of DSC in the planetary context is identification of ices and volatile-bearing minerals, including clays, hydrous salts and oxides, and carbonates. Given the mineral identities, characteristic enthalpic peaks can be integrated to yield relative proportions of the minerals present. Unlike spectrophotometry, DSC results are relatively insensitive to particle coatings or other matrix effects. Although the appearance of a given heat-flow curve can depend on the physical characteristics of the sample, integrated ratios of enthalpic peaks change less severely with physical properties than do peaks in reflectance spectra.

Instrument Development History. DSC-based experiments have been previously designed but never flown on spacecraft. The Planetary Soil Water Analyzer (PSWA) experiment [2], which included a DSC backed by an electrolytic-cell detector for evolved water vapor, was developed in the early 1980s as a post-Viking follow-on experiment for Mars. However, no further Mars landing missions were flown and the PSWA project was discontinued. A preliminary design for a DSC experiment was included during the middle 1980s in plans for the Comet Rendezvous and Asteroid Flyby (CRAF) Penetrator-Lander but the instrument was never built and the CRAF mission has since been cancelled. Therefore, absence of planetary flight opportunities and the lack of sustained funding has seriously hindered development of flight-qualified DSC instruments.

In 1989, concepts for DSC-based planetary experiments were renewed as the Thermal Analyzer for Planetary Soils (TAPS) project at JSC (Fig. 1) [3,4]. Support for Phase A development of TAPS, with emphasis on applications to small Mars landers, was begun in mid-1992 through funding from the Planetary Instrument Definition and Development Program (PIDDP) at NASA Headquarters. The sample-acquisition function is being developed as an integral part of a self-contained experiment. Using 1980s technology, a version of TAPS packaged for

Mars applications is estimated to have the following characteristics: 1.2 kg mass, 850 cm³ volume, 5 W peak power, and 1.5-W hr per analysis.

Design Issues. The most important technological needs include small, reliable sample-delivery mechanisms and lightweight, energy-efficient electrical furnaces for the DSC. Miniaturization of electronic components is highly desirable but miniaturization of mechanical and sensor components faces natural limits set by the fundamental scale of the scientific problem. First, based on experience with lunar samples and with Viking results from Mars, the *minimum* size of a representative planetary soil sample (of about 2 g/cm³) is on the order of 10-100 mm³ (equivalent to a few tens of milligrams). Therefore, the sample-acquisition mechanisms and calorimetric sensors cannot be reduced below about the centimeter scale without substantial loss of scientific validity. Second, optimum operation of the DSC for analysis of volatile materials requires a continuous gas purge at ≥ 10 cm³ STP/min; the gas-purge system must be scaled for compatibility with the calorimetric sensors.

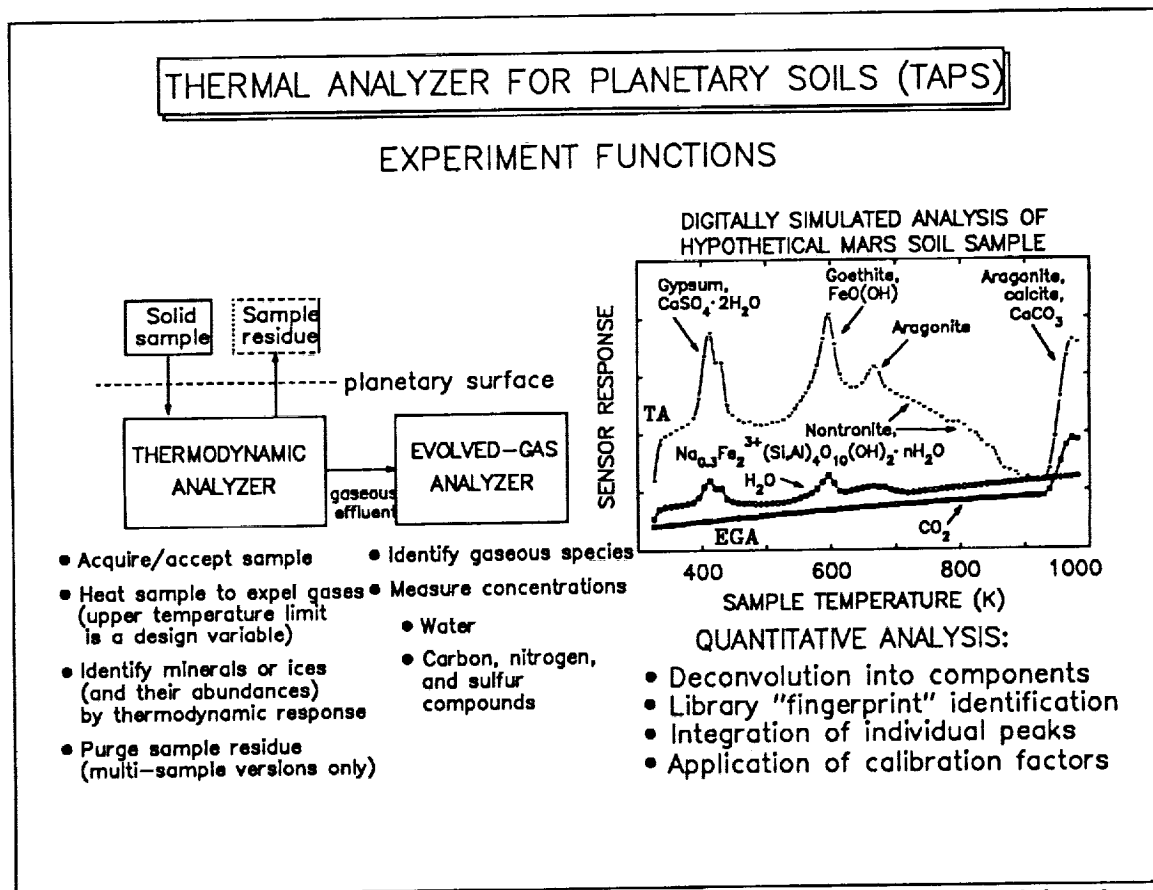


Figure 1. Functional diagram and simulated data for the TAPS experiment concept that is based on a DSC module backed by single-function gas sensors.

References: [1] Wendlandt, W. W. (1986) *Thermal Analysis* (third ed.), John Wiley and Sons, New York, 814 p. [2] Ball Aerospace Systems Division (1982) *Planetary Soil Water Analyzer Final Report*, Huntington Beach, CA, 54 p. [3] Gooding J. L. (1991) *Lunar Planet. Sci. XXII*, Lunar and Planetary Institute, Houston, TX, 457-458. [4] Gooding J. L. et al. (1992) *Lunar Planet. Sci. XXIII*, Lunar and Planetary Institute, Houston, TX, 427-428.

Micro-Sensors for in-situ Meteorological Measurements

David Crisp, William J. Kaiser, Thomas R. VanZandt,
Jet Propulsion Laboratory, California Institute of Technology,
and James E. Tillman, University of Washington

Abstract

Improved in-situ meteorological measurements are needed for monitoring the weather and climate of the terrestrial and martian atmospheres. We have initiated a program to assess the feasibility and utility of micro-sensors for precise in-situ meteorological measurements in these environments. Sensors are being developed for measuring pressure, temperature, wind velocity, humidity, and aerosol amounts. Silicon micro-machining and large scale integration technologies are being used to make sensors that are small, rugged, lightweight, and require very little power. Our long-term goal is to develop very accurate miniaturized sensors that can be incorporated into complete instrument packages or "micro weather stations," and deployed on a variety of platforms. If conventional commercially available silicon production techniques can be used to fabricate these sensor packages, it will eventually be possible to mass-produce them at low cost. For studies of the Earth's troposphere and stratosphere, they could be deployed on aircraft, dropsondes, radiosondes, or autonomous surface stations at remote sites. Improved sensor accuracy and reduced sensor cost are the primary challenges for these applications. For studies of the martian atmosphere, these sensor packages could be incorporated into the small entry probes and surface landers that are being planned for the Mars Environmental SURvey (MESUR) Mission. That decade-long program will deploy a global network of small stations on the Martian surface for monitoring meteorological and geological processes. Low mass, low power, durability, large dynamic range and calibration stability are the principal challenges for this application. Our progress on each of these sensor types is presented below:

a. Pressure: The first sensor to be developed was a silicon micro-machined capacitive aneroid barometer. This sensor determines atmospheric pressure by measuring the deflection of a thin silicon membrane that separates the atmosphere from a tiny evacuated chamber. Unlike commercially available micro-machined pressure sensors, the JPL barometer uses a high-frequency capacitive circuit rather than a piezo-resistive strain gauge to measure the deflection of the membrane. This technique not only provides vast improvements in positional sensitivity and dynamic range, it also overcomes serious temperature sensitivity problems that plague existing commercial devices. Our sensors use 1 to 5 mm square membranes that are 10 to 20 micrometers thick. Their mass is less than 0.1 gram. In spite of their small size, their dynamic range exceeds 5 orders of magnitude. More testing is needed to calibrate and fully characterize these devices, but our preliminary experiments indicate that they should meet all of our requirements. Recently, the Finnish meteorological instrument company, Vaisalla, has developed a similar device for use on the Mars 94/96 and MARSNET programs. We plan to obtain one or more of these devices for comparison with the JPL pressure sensor.

b. Temperature: A prototype thermo-couple based temperature sensor for Mars applications was fabricated several years ago by J. Tillman. It produced accuracies of 0.1 °C at temperatures between -70 and 70 °C. Even though the sensor circuit uses discrete components, it requires only 0.55 Watts for continuous operation. We are currently exploring a variety of options to reduce

the size and power requirements of this design, and to improve its survivability. We are also exploring other options, including all-silicon diode sensors.

c. Winds: We built a small pitot-static wind sensor from commercially available micro-machined pressure sensors. It determines wind speed by comparing the pressure exerted by the wind on the face of an exposed pressure sensor (pitot pressure) to that measured by a shielded sensor (static pressure). Our prototype pitot-static anemometer could detect winds as small as 0.1 m/s at the Earth's surface, but a much more sensitive device would be needed for wind measurements at high altitudes in the Earth's atmosphere, or in the thin Martian atmosphere. The sensitivity and dynamic range of this sensor could be improved dramatically by replacing the commercial pressure sensors with the JPL or Vaisalla micro-machined capacitive pressure sensors. Other measurement strategies that employ pitot-static measurements are also being studied, including the designs similar to the Orthogonal Windspeed Systems being marketed by Rosemont Inc. The advantage of this sensor is that it could be built into the mast of the MESUR landers, simplifying its deployment.

A third type of anemometer that is being considered for measuring the wind speed and direction in two dimensions is based on a mass-flow sensor. This sensor consists of a small heated element surrounded by a series of temperature sensors. The wind speed is estimated from the power needed to maintain the heated element at a constant temperature, while the wind direction is determined by comparing the temperatures measured by the surrounding temperature sensors. A silicon micro-machined 2-d mass flow sensor could be very small (0.5 sq. cm), and would consume very little power.

d. Humidity: Improved humidity sensors have been identified as the highest priority for both terrestrial and Martian meteorological applications. These sensors also pose the greatest technological challenges because they must provide accurate estimates of water vapor abundance for mixing ratios that vary from less than one part per million to greater than 1%. We are currently testing a prototype sensor that measures humidity by determining the dew-point temperature. Dew-point sensors are intrinsically accurate because the dew-point is a well-defined thermodynamic quantity. In conventional dew-point sensors, a small mirror is cycled through temperature, and the dew-point is detected by monitoring the intensity of a light beam reflected and scattered as liquid water or ice condenses on the mirror surface. Unfortunately, these sensors are usually relatively massive, complex, and consume excessive power, and their mirrors are easily contaminated by dust and salt spray. Our prototype humidity sensor has the advantages of the chilled-mirror dew-point hygrometer, but requires a much simpler configuration, and eliminates problems with contamination of the mirror. This device is a differential microbalance (DMB), which consists of shielded and unshielded quartz crystal oscillators that are attached to an 8 mm square thermoelectric cooler (TEC). The frequencies of the two crystals are monitored as the TEC is cycled through a range of temperatures. The frequency of the unshielded crystal changes almost continuously as it adsorbs water, and then changes abruptly at the dew-point, when liquid water or ice begins to condense on its surface. Our prototype device works well, but our initial tests have revealed a few shortcomings of this design. For example, the poor thermal coupling between the crystals and the thermoelectric cooler allows substantial temperature gradients to form across the crystal faces if they are scanned too rapidly through temperature. These gradients can compromise the accuracy of the dew-point temperature measurements. We are continuing to refine the DMB sensor design to address these problems. As a first step, we are replacing the crystal oscillator with a Surface Acoustic Wave (SAW) oscillator. Unlike the crystals that are currently being used, this type of oscillator operates by setting up a surface wave, rather than a body wave in the crystal. SAW's can therefore be attached directly to the TEC to provide a much better thermal contact. This should reduce the power consumption by allowing much faster scan rates. These oscillators also operate at much higher frequencies. This should improve their sensitivity to low water vapor amounts. A second class of DMB sensor, based on silicon micromachined cantilever oscillators is also being considered.

A Broad-Band Microseismometer for Planetary Applications

W. B. Banerdt, T. VanZandt, W. J. Kaiser, and T. W. Kenny
 Jet Propulsion Laboratory, California Institute of Technology
 Extended Abstract

There has recently been renewed interest in the development of instrumentation for making measurements on the surface of Mars. This is due to the Mars Environmental Survey (MESUR) Mission, for which ~16 small, long-lived (2–10 years), relatively inexpensive surface stations will be deployed in a planet-wide network. This will allow the investigation of processes (such as seismology and meteorology) which require the simultaneous measurement of phenomena at many widely spaced locations on the surface over a considerable length of time. Due to the large number of vehicles involved, the mass, power, and cost of the payload will be severely constrained. A seismometer has been identified as one of the highest priority instruments in the MESUR straw-man payload [1].

The requirements for an effective seismic experiment on Mars place a number of constraints on any viable sensor design. First, a large number of sensors must be deployed in a long-lived global network in order to be able to locate many events reliably, provide good spatial sampling of the interior, and increase the probability of seismic detection in the event of localized seismicity and/or high attenuation. From a practical standpoint, this means that individual surface stations will necessarily be constrained in terms of cost, mass, and power. Landing and thermal control systems will probably be simple, in order to minimize cost, resulting in large impact accelerations and wide daily and seasonal thermal swings.

The level of seismic noise will determine the maximum usable sensitivity for a seismometer. Unfortunately, the ambient seismic noise level for Mars is not well known. However lunar seismic noise levels are several orders of magnitude below that of the Earth. Sensitivities on the order of 10^{-11} g over a bandwidth of .04 to 20 Hz are thought to be necessary to fulfill the science objectives for a seismometer placed on the Martian surface [2].

Silicon micromachined sensor technology offers techniques for the fabrication of monolithic, robust, compact, low power and mass accelerometers. Conventional micromachined accelerometers have been developed and are commercially available for high frequency and large acceleration measurements [3]. The new seismometer we are developing incorporates certain principles of conventional silicon micromachined accelerometer technology. However, currently available silicon micromachined sensors offer inadequate sensitivity and bandwidth for the Mars seismometer application. Our implementation of an advanced silicon micromachined seismometer is based on principles recently developed at JPL for high-sensitivity position sensor technology. The implementation of currently available silicon micro-machining technology with these new principles should enable the fabrication of a 10^{-11} g sensitivity seismometer with a bandwidth of at least 0.01 to 20 Hz. The addition of force-rebalance feedback control to this device will enable the dynamic range to be extended by selecting sensitivity ranges over several orders of magnitude. The low Q properties of pure single-crystal silicon also allow the system to be designed with an extremely low mechanical damping coefficient, which is necessary in order to minimize the Brownian thermal noise limitations generally characteristic of seismometers with small proof masses [4]. The total volume of the seismometer is expected to be approximately 50 cm³ with a 50 gm total mass and power consumption of 20 mW. This will include both the sensor element and the sensor and feedback electronics.

A seismometer consists of a spring-supported proof mass (with damping) and a position sensor for measuring the displacement of the proof mass relative to the support structure. The spring-proof mass system is characterized by a natural frequency

$$\omega_0 = \sqrt{\frac{k}{m}} \quad (1)$$

where k is the spring constant and m is the magnitude of the proof mass. For frequencies below this natural frequency, the displacement of the proof mass, x_p , is given by

$$x_p = \frac{a_s}{\omega_0^2} \quad (2)$$

where a_s is the acceleration of the support structure. Thus in this frequency range the mechanical system acts as an acceleration-to-displacement transducer, with

$$a_s = x_p \omega_0^2 = \frac{x_p k}{m} \quad (3)$$

where a_s and x_p are now the acceleration and displacement sensitivity of the position sensor (i.e., the minimum resolvable acceleration and displacement). The output of the position sensor thus serves as a measure of the acceleration of the support structure. For a given sensitivity of the position sensor, (3) indicates that the acceleration sensitivity of the device can be improved by reducing ω_0 either by softening the support spring or by increasing the proof mass. Reducing the natural frequency, however, reduces the bandwidth of the seismometer. Thus, the increase in sensitivity is gained at the expense of frequency response. Another drawback of a low natural frequency is that it makes the system quite fragile and susceptible to damage from large accelerations. This adds considerable complexity to the mechanical system to improve its ability to withstand shocks during transport.

A more attractive method for improving the acceleration sensitivity of an instrument is to increase the sensitivity of the position sensor. In this case, a mechanical system with a higher resonant frequency (or stiffer suspension) can be used, leading to a wider operating bandwidth and insensitivity to physical shock. Thus the proof mass can be decreased, which will reduce the total instrument mass.

We have implemented this concept using a new type of high resolution capacitive position sensor and a single crystal silicon mechanical suspension. Our prototype sensor shows an acceleration sensitivity of approximately 10^{-9} g $\sqrt{\text{Hz}}$ over a bandwidth extending from 0.1 to 40 Hz. The device has a mass of under 120 gm and a volume of less than 100 cm³. It is well suited for measurement of local seismic events, as demonstrated through field testing.

We have developed an ultrasensitive capacitive position sensor for use in a small seismometer. The important characteristics of the position sensor are: 1) it provides a position sensitivity of better than 10^{-3} Å $\sqrt{\text{Hz}}$; 2) it has a wide operating bandwidth, including long term stability; 3) it has a small mass, volume, and power consumption; and 4) it is robust. In this position sensor, a grounded electrode of surface area of approximately 0.25 to 1.0 cm² is positioned near an electrode on the capacitance sensor. Variations in the relative spacing between these electrodes lead to changes in output from the high-frequency capacitance sensor.

A single-crystal silicon rectangular cantilever of dimensions $6 \times 30 \times 0.15$ mm is used as the spring for our seismometer. The silicon spring is cut from a larger wafer using a diamond saw. The cantilever is fixed at one end to the bottom of an aluminum support plate, using a 0.15 mm thick silicon spacer and an epoxy adhesive. A $10 \times 10 \times 3.8$ mm copper block is attached to the free end of the cantilever. This 3.4 gm block serves as both the proof mass and as one electrode for the capacitive position sensor. The static gap between the copper block and the electrode on the capacitive sensor can be adjusted sufficiently accurately using a fine-thread adjustment screw. The silicon spring has a spring constant of approximately 215 N/m in the vertical direction (force applied to the center of the proof mass and normal to its face). The large ratio of width to thickness of the spring gives a cross-axis sensitivity of less than 0.1%. The resonant frequency of the system in the vertical mode is approximately 40 Hz, and the mechanical Q is greater than 400 in air. This high Q value is essential for a low mass seismometer, as it reduces the thermal noise equivalent acceleration of the device, which for the present instrument is approximately 2.2×10^{-10} g $\sqrt{\text{Hz}}$.

Initial tests of the first microseismometer show that a very small, low-mass instrument using conceptually simple detection techniques can exhibit performance comparable to state-of-the-art instruments. This is an important result in the development of miniature seismic instrumentation for terrestrial, as well as planetary seismology.

- [1] Mars Science Working Group, *A Strategy for the Scientific Exploration of Mars*, JPL D-8211 (Internal Document), Jet Propulsion Laboratory, 1991.
- [2] Solomon, S.C., D.L. Anderson, W.B. Banerdt, R.G. Butler, P.M. Davis, F.K. Duennebie, Y. Nakamura, E.A. Okal, and R.J. Phillips, *Scientific Rationale and Requirements for a Mars Global Seismic Network*, LPI Tech. Rept. 91-02, Lunar and Planetary Inst., Houston, 1991.
- [3] Petersen, K.E., *Proc. IEEE*, **70**, 420, 1982.
- [4] Melton, B.S., *Rev. Geophys. and Space Phys.*, **14**, 93, 1976.

IMAGING SPECTROMETRY OF THE EARTH
AND OTHER SOLAR SYSTEM BODIES

Gregg Vane

Jet Propulsion Laboratory, California Institute of Technology
Pasadena, California 91109

ABSTRACT

Imaging spectrometry is a relatively new tool for remote sensing of the Earth and other bodies of the solar system, dating back to the late 1970s and early 1980s. It is a natural extension of the earlier multi-spectral imagers developed for remote sensing that acquire images in a few, usually broad spectral bands. Imaging spectrometers combine aspects of classical spectrometers and imaging systems, making it possible to acquire literally hundreds of images of an object, each image in a separate, narrow spectral band. It is thus possible to perform spectroscopy on a pixel-by-pixel basis with the data acquired with an imaging spectrometer.

Two imaging spectrometers have flown in space and several others are planned for future Earth and planetary missions. The French-built Phobos Infrared Spectrometer, ISM, was part of the payload of the Soviet Mars mission in 1988, and the JPL-built Near Infrared Mapping Spectrometer, NIMS, is currently en route to Jupiter aboard the Galileo spacecraft. Several airborne imaging spectrometers have been built in the past decade, including the JPL-built Airborne Visible/Infrared Imaging Spectrometer, AVIRIS, which is the only such sensor that covers the full solar reflected portion of the spectrum in narrow, contiguous spectral bands. NASA plans two imaging spectrometers for its Earth Observing System, the Moderate and the High Resolution Imaging Spectrometers, MODIS and HIRIS.

A brief overview of the applications of imaging spectrometry to Earth science will be presented to illustrate the value of the tool to remote sensing and indicate the types of measurements that are required. The system design for AVIRIS and a planetary imaging spectrometer will be presented to illustrate the engineering considerations and challenges that must be met in building such instruments. Several key sensor technology areas will be discussed in which miniaturization and/or enhanced performance through micromachining and nanofabrication may allow smaller, more robust and more capable imaging spectrometers to be built in the future.

Smart Focal-Plane Technology for Micro-Instruments and Micro-Rovers

Eric R. Fossum
 Jet Propulsion Laboratory
 California Institute of Technology

It is inevitable that micro-instruments and micro-rovers for space exploration will contain one or more focal-plane arrays for imaging, spectroscopy or navigation. In this paper, we explore the state-of-the-art in focal-plane technology for visible sensors. Also discussed is present research activity in advanced focal-plane technology with particular emphasis on the development of smart sensors. The paper concludes with a discussion of possible future directions for the advancement of the technology.

Visible focal-plane technology is currently dominated by charge-coupled devices (CCDs). The CCD can be used for both photon detection and as a readout multiplexer since its primary function is the shifting of charge packets. Scientific CCDs typically employ both modes of operation to utilize the maximum amount of chip area for the collection of photons and are routinely made in megapixel array sizes, with the largest demonstrated CCD size being 16 Mpixels.¹ Unfortunately, the electrodes which comprise the CCD and ensure high fidelity of the readout signal also block photons, particularly in the blue and ultraviolet (UV). Thus, separation of the sensor into a photoactive portion and a readout portion is often used to enhance the spectral response. The photoactive region may be a pinned photodiode² to obtain high blue response (or a platinum-silicide Schottky diode to obtain infrared response³). The readout CCD lies between photoactive regions and is typically covered by a metallic light shield. Thinning the chip to enable the back side of the chip to operate as the photoactive region has also been employed to enhance blue and UV (and infrared) response.⁴ Such a structure is mechanically fragile however.

There are major disadvantages to the CCD. In large array sizes, signal charge must be physically transported macroscopic distances (centimeters) without significant loss of fidelity, making CCD application in high radiation environments, low temperature environments, and high frame rate systems difficult to achieve. Additionally, voltages applied to the CCD are typically large (10-20 volts) and must drive high capacitance loads, making integration of timing and control signal generators and clock drivers with the image sensor nearly impossible.

The emergence of the high-definition television (HDTV) concept has driven commercial research and advanced development of image sensors away from the CCD and toward alternative approaches. The primary approach is the active pixel sensor⁵ because it avoids the physical transport of charge. The pixel is addressed for readout in random access fashion, i.e. by its X-Y address. The pixel consists of both the photoactive region and a readout transistor. The readout transistor senses the voltage developed in the photoactive region, and is read out in voltage-follower mode. The two components are often vertically integrated to maximize the size of the photoactive region. Transistor approaches to the active pixel sensor include MOSFETs,⁶ SITs,⁷ and BJTs.⁸ The active pixel sensor allows small, highly sensitive pixels, high readout rates, and, in principle, improved operation in high radiation environments and at low temperatures. The active pixel sensor also requires lower drive voltages and lower capacitance drivers thus permitting on-chip integration of both timing and drive electronics.

Integrability of drive electronics also implies the integrability of post-image-capture image and signal processing circuitry. The purpose of on-chip integration of signal processing in scientific instruments is to enhance the signal-to-noise ratio. Integration, in general, also decreases system size and weight and increases reliability - important issues for micro-instruments. For example, on-chip signal processing has been demonstrated for enhancing the compressibility of 256x256 images with negligible increase in system complexity.⁹ On-chip analog-to-digital conversion, presently under investigation at JPL for low-light-level imaging, enhances system dynamic range and eliminates all off-chip signal chain electronics. Multi-resolution image pyramid generation for rover vision is also being investigated at JPL for on-chip application. Significant power and weight savings can be achieved in this case as well.

There are many future directions for smart focal-plane technology.¹⁰ In the case of micro-instruments, increased signal processing to enhance science return has wide applicability. This processing can include noise reduction, electronic image stabilization,¹¹ non-uniformity correction, automatic focus, spatial oversampling for higher resolution imaging and on-chip analog-to-digital conversion. Other processing related to micro-instruments and micro-rovers includes windowed readout for region-of-interest, higher imaging rates, feature recognition (spatial and spectral) for autonomous mission replanning, stereo-vision processing for range information, and processing for active range sensing systems.

The low power, low weight and small size of future spacecraft and missions will require development of highly integrated, smart focal-plane technology. This area will require nurturing to ensure that anticipated future mission requirements can be met.

This work was supported by the National Aeronautics and Space Administration, Office of Aeronautics and Space Technology.

References

- ¹ R. Bredthauer, "The 4096x4096 CCD image sensor," in Proc. 1990 IEEE Workshop on Charge-Coupled Devices, Harriman, N.Y., May 18-20, 1990.
- ² N. Teranishi et al., "No image lag photodiode structure in the interline CCD image sensor," Proc. 1982 IEEE International Electron Devices Meeting.
- ³ See, for example, C.K. Chen, B. Nechay, B.Y. Tsaur, "Ultraviolet, visible and infrared response of PtSi Schottky-barrier detectors operated in the front-illuminated mode," IEEE Trans. Electron Devices, vol. 38(5), pp. 1094-1103 (1991).
- ⁴ C.-M. Huang, "Future development for thinned backside illuminated CCD imagers," Proc. 1991 IEEE Workshop on Charge-Coupled Devices, Ontario, Canada, June 7-9, 1991.
- ⁵ E.R. Fossum, "Active pixel sensors -- are CCD's dinosaurs?," Proc. SPIE vol. 1900, pp. 1-13 (1993).
- ⁶ See, for example, J. Hynccek, "BCMD-An improved photosite structure for high density image sensors," IEEE Trans. Electron Devices, vol. 38(5), pp. 1011-1020 (1991).
- ⁷ T. Mizoguchi et al., "A 250 k-pixel SIT image sensor operating in its high-sensitivity mode," IEEE Trans. Electron Devices, vol. 38(5), pp. 1021-1027 (1991).
- ⁸ Y. Nakamura et al., "Design of bipolar imaging device (BASIS)," IEEE Trans. Electron Devices, vol. 38(5), pp. 1028-1036 (1991).
- ⁹ S.E. Kemeny et al., "CCD Focal-plane image reorganization processors for lossless image compression," IEEE J. Solid-State Circuits, vol. 27(3), pp. 398-405 (1992).
- ¹⁰ E.R. Fossum, "Future directions in focal-plane signal processing for spaceborne scientific imagers," Proc. SPIE vol. 1541, pp. 62-67 (1991).
- ¹¹ T. Sakaguchi, "Electronic image stabilizer and digital feature of consumer video camera," Proc. International Symposium on Advanced Image-Acquisition Technology, Tokyo, Japan, Nov. 12-13, 1991.

EVOLUTION OF MINIATURE DETECTORS AND FOCAL PLANE ARRAYS FOR INFRARED SENSORS

by

Louis A. Watts

Science Applications International Corporation
Santa Barbara, California

1. INTRODUCTION

Sensors that are sensitive in the infrared spectral region have been under continuous development since the WW-II era. A quest for the military advantage of "seeing in the dark" has pushed thermal imaging technology toward high spatial and temporal resolution for night vision equipment, fire control, search track, and seeker "homing" guidance sensing devices. Similarly, scientific applications have pushed spectral resolution for chemical analysis, remote sensing of earth resources, and astronomical exploration applications.

As a result of these developments, focal plane arrays (FPA) are now available with sufficient sensitivity for both high spatial and narrow bandwidth spectral resolution imaging over large fields of view.¹ Such devices combined with emerging opto- electronic developments in integrated FPA data processing techniques can yield miniature sensors capable of imaging reflected sunlight in the near IR, and emitted thermal energy in the Mid-wave (MWIR) and longwave (LWIR) IR spectral regions. Robotic space sensors equipped with advanced versions of these FPAs will provide high resolution "pictures" of their surroundings, perform remote analysis of solid, liquid, and gas matter, or selectively look for "signatures" of specific objects. Evolutionary trends and projections of future low power micro detector FPA developments for day/night operation or use in adverse viewing conditions are presented in the following text.

2. DEVELOPMENT TIMELINE

Figure 2-1 shows a chronological progression of IR technology development in the U.S. spanning the technology from single element bolometer devices to large scale arrays of high performance MWIR and LWIR detectors having tens of thousands of elements. This chart shows the evolution of supporting semiconductor technology and materials processing techniques that enabled the development of various detector types of ever increasing performance at longer wavelengths. Shown on the upper part of the chart are those developments which ultimately led to FPAs with large numbers of micrometer sized detector elements processed with integrated circuit (IC) micro-electronic manufacturing processes. It is these arrays that have evolved over the past few decades that can provide the "smart eyes" for future space exploration equipment.

3. LIMITING TECHNOLOGIES

In projecting future trends for a specific field, it is often enlightening to review past limiting technologies as a function of time. The way in which seemingly impenetrable barriers have been broken-through by a new paradigm-shift can indicate potential means of overcoming current limitations to achieve even better future performance either in terms of sensitivity (SNR) or smaller lighter more capable systems. For example, early IR detectors (1940's) responded to thermal emissions from a scene by being heated and cooled by the incident energy, with variations in the detector material's physical properties (electrical resistance or capacitance,) being instrumented as a measure of the observed IR signal strength. These cyclic variations in the detector temperature were not sufficiently rapid for "raster scanning" of a scene to produce a usable image. Thus it appeared that the laws of physics limited the achievable detector speed or electrical bandwidth by the thermal mass of these bolometer

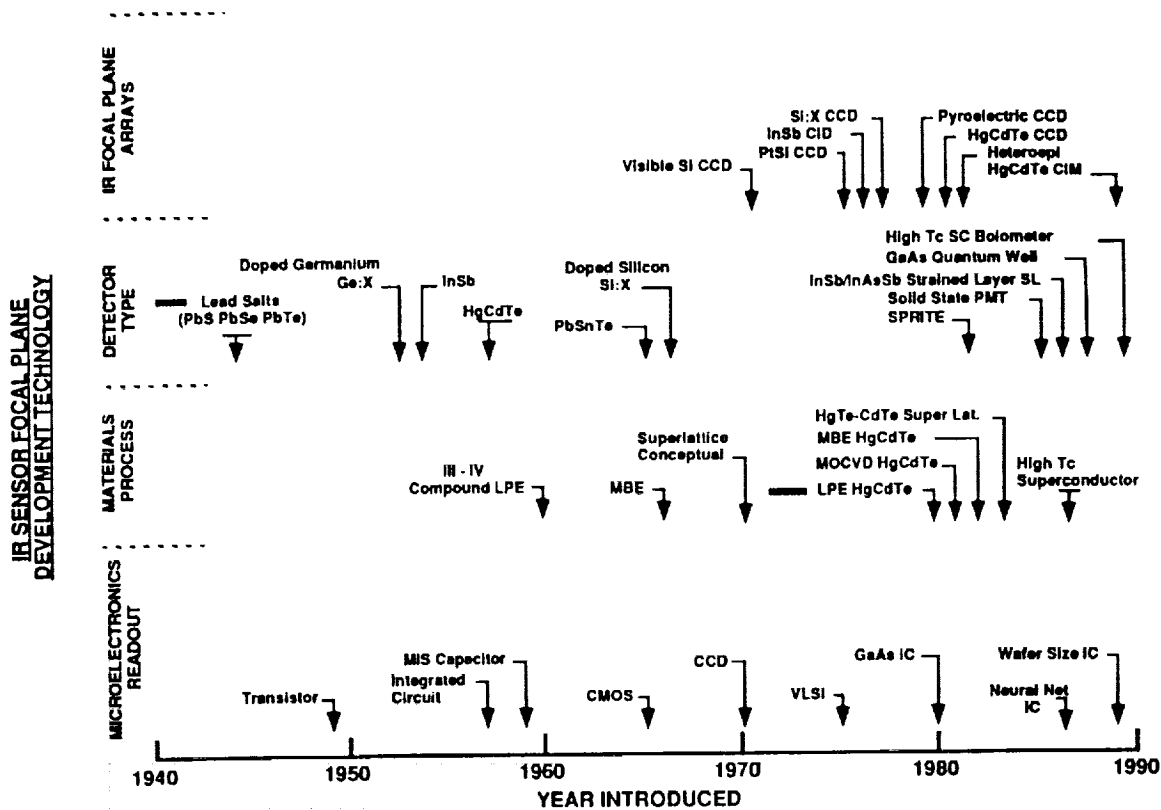


FIGURE 2-1 Infrared Detector and Focal plane array Development Timeline

devices, and by the attachment of electrical leads which in effect form a degrading heat-sink for the sensitive sensing element. The advent of semiconductor materials development in the 1950s and 1960s, however, provided the "break-through" that led to the development of quantum IR detectors capable of sensing photons with high electrical band-width. A host of military applications pushed the development of these IR sensing semiconductor photo conductors (PC), specifically for near IR (NIR), MWIR, and LWIR spectral regions.

Photo lithography, metalization, selective chemical etching, and micro wire bonding processes developed for the transistor and IC industry were applied to IR detector manufacture yielding arrays of PC detectors used for parallel-scanned imaging systems (FLIRS). The limiting technology thus shifted from the previous slow-responding detectors, to a detectability versus field of view/resolution limitation caused by the excessive bias power dissipation load from many PC detectors on a cooled FPA. Bias power and electrical lead heat-loading were the significant limitation problems for the LWIR applications where stable cryogenic cooling of the FPA is required for proper operation.

To circumvent this power load limitation and achieve even higher bandwidths, the new semiconductor technology was used to fabricate PN junction diode devices which act as photovoltaic (PV) IR detectors. This change in configuration results in high impedance detectors that need little bias current as do the previous PC devices.

Eliminating the bias power limitation through these PV diodes still left the electrical interconnection leads as the dominant limitation on the number of detector elements that could be used in linear or two-dimensional IR detector arrays within a cryo cooled Dewar package. A large number of leads presents a significant heat load on the FPA cooling, and requires a large physical package to support the large number of hermetically sealed low-noise vacuum

feedthroughs required to conduct the low-level detector signals out of the Dewar. The number of electrical leads or Dewar "real estate" needed for interconnections thus for several years became the limiting technology for PV detectors of InSb and HgCdTe arrays. The emergence of charge coupled devices (CCD) and charge Injection Devices (CID) provided a means of multiplexing the IR detector on the FPA and allow packaging large numbers of detectors in small practical sensors. Arrays of 1024 x 1024 are available for near IR sensing detectors, and 640 x 480 element arrays of In Sb & Hg Cd Te for the MWIR and LWIR regions.^{2,3} Figure 2-1 summarizes the described chronological development process and Figure 3-1 shows the number-of-detector elements and electrical-bandwidth tradeoffs required for various application requirements.

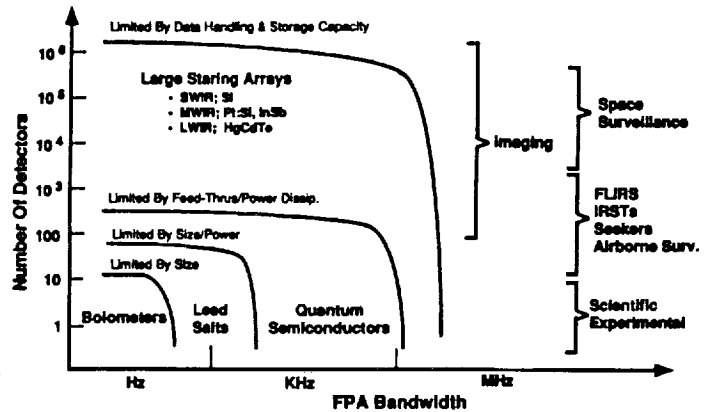


FIGURE 3-1
General Infrared Detector Requirements

4. CURRENT DETECTOR STATUS

Semiconductor quantum detectors are available to cover the IR spectrum; with silicon-based devices (Pt:Si) covering the near IR region, In Sb the MWIR (3-5 μ) region, and HgCdTe devices the LWIR (8-12 μ) region. Because HgCdTe is "tunable" with stoichiometric composition, one material can be used over the IR band to approximately 12 μ wavelength. For wavelengths beyond this 8-14 μ atmospheric window, extrinsic silicon and germanium devices cooled to approximately 20K are generally used.

Detector arrays from these materials are made with quantum efficiencies (Q_e) approaching the theoretical limit, element (pixel) sizes matching the diffraction limited optical spread function of reasonably fast ($f/2$) optical systems, and formats approximating standard television frame/display resolutions. These then are approaching the physical performance limits for semiconductor quantum photon detectors.

Readout devices using CCD and CID technologies are being superseded by integrating source-follower and capacitance transimpedance integrating amplifier (CTIA) integrated circuits that have ultra low-noise read rates of tens of megahertz. Thus, the capability of PC and PV semiconductor detector and silicon readout FPA combination is currently limited by the physics of the detection process and the interface electronic data handling capacity of the FPA. Clock signals, bias inputs, and non-uniformity correction circuitry add complexity to most FPAs, and thus tend to limit the miniaturization of sensors. On-chip processors are clearly needed.

Silicon based detector arrays used in the visible and near IR (or Pt:Si for MWIR) applications can be made in very large mega-pixel formats when used with silicon IC readout and data handling circuitry. Conversely, hybrid IR FPAs for the LWIR region using other detector materials bonded to silicon microelectronic devices are limited in physical size (number of pixels) to approximately 500-600 elements across because the differential thermal expansion properties of the dissimilar materials tends to stress and separate the hybridized assembly when repeatedly cycled to cryogenic operating temperatures. In spite of these limitations, current IR focal plane technology is clearly adequate for high reliability space applications

providing both high spatial and spectral resolution for imaging and scientific remote sensing spectral signature analysis in spectroscopy applications. But for micro-miniaturized sensors of comparable capability to current hardware, monolithic FPAs made with common detector/readout materials will be required to cover the spectrum in large formats, and these monolithic devices must include integral binary optical elements with on-FPA opto-electronic data processing for compactness.

Figure 4-1 presents a tabulation of some leading off-the-shelf large area imaging IR detector arrays along with their performance characteristics.

5. EMERGING TECHNOLOGIES FOR MINIATURE FPAs

Many new IR detector concepts are being reported in the literature including; quantum-well structures, superlattices, superconductor based detectors, and microstructures which act like tuned "antenna" arrays.⁴ Some of these concepts are variations on current technology, and some are truly new concepts that have the potential for significant improvements in covering larger spectrum regions more efficiently. It is beyond the scope of this paper to describe all of these new device concepts, but some clearly are applicable to effective miniaturization of sensors. Among the more promising new technologies that support a progressive stepwise "roadmap" from currently available technology to robust space sensors are the following:

1. Binary Optics
2. On-chip processing electronics
3. Un-cooled detectors
4. Pattern recognition (Neural Nets)
5. Spectrally selective detector assemblies

Binary Optical Elements For FPA Applications: The term binary or holographic optics refers to diffraction-based optical elements made with well developed silicon micro-electronic photo-etching processes. Etched patterns on transmitting or reflecting surfaces can be designed to perform the functions of traditional optical components; including anti-reflection (AR) coatings filters, lenses, prisms, and indeed other functions not feasible in conventional optical elements. These binary elements are designed with common electrical engineering calculations (Maxwell's equations) and manufactured by standard micro electronic IC fabrication processes to form unusually powerful FPA assemblies.

"Moth-eye" AR coatings and micro-lens arrays are the more common binary optics used for FPA performance enhancements. The moth-eye AR surface is a pattern that is etched into an optical element and thus is not subject to separation and peeling degradation as are conventional AR coatings of dissimilar materials. These diffractive optics AR surfaces are generally "tuned" to a desired passband where the performance can surpass even expensive multi-layer coatings. Figure 5-1 shows a typical moth-eye AR coating etched into a silicon surface. Micro-lens arrays are used in conjunction with detector arrays as proximal field lenses, one for each element in the detector array. In this configuration, the lenses condense each focal plane pixel onto a detector element which thus can be much smaller than the pixel by the magnification ratio of the lens. Thus the FPA retains a 100% fill-factor while the detectors are spaced to allow for processing electronics to be located between the elements. See figure 5-2.

Lenslet arrays sandwiched with spatial filter patterns are capable of on-FPA optical computing for pattern recognition and other pre-processing techniques intended to reduce the data handling loads. These and other binary optics and "retinal" FPA processing techniques are discussed in detail by W.Veldkamp in an other part of this workshop report, and hence will not be repeated here.

| | A | B | C | D | E | F | G | H | I | J |
|----|--------------------|---------------|----------------|---------------|--|--------------------|-----------------|--------------|-----------------|---------------|
| 1 | | Amber | Amber | Rockwell | Rockwell | Rockwell | SBRC | SBRC | Cincinnati E. | Cincinnati E. |
| 2 | Type | InSb | InSb | SWIR HCT | SWIR HCT | SWIR HCT | InSb | InSb | InSb | InSb |
| 3 | Format | 256x256 | 512x512 | 256x256 | 256x256 | 640x480 | 256x256 | 640x480 | 256x256 | 160x120 |
| 4 | Pitch (microns) | 38 | 25 | 40 | 40 | 27 | 30 | 20 | 30 | 50 |
| 5 | Readout Type | DI | DI | DI | CTIA | DI | Source Follower | DI | Source Follower | DI |
| 6 | Frame Rate | 250 Hz 4@4Mhz | 60Hz 4@4Mhz | 300+ 1@20Mhz | 300+ 1@20Mhz | 60+ 4@5.8Mhz | 60/(100 Hz?) | 4Hz | 4Hz | 100Hz |
| 7 | Dark Current | 1900 e/s @50K | 1.6E7e | 1200e @50K | 1200e @50K | <500e | <400e/s @50K | | 30e/s @40K | |
| 8 | Storage Capacity | 400e? | 400e? | 4E7e | 0.2-1.0E6e | 1.28E6e | 6E5e | | 3E5e | 3.50E+07 |
| 9 | Read Noise @60Hz | 400e? | 400e? | <400e | 10-50e (100eassy) | <500e | <300e/150typ | 1200e | 30e | 1500e |
| 10 | Quant Noise | 400e? | 400e? | approx = read | Included above | approx = read | | | | |
| 11 | Quantum Efficiency | 50-80%AR | 50-80%AR | 60-90% | 60-90% | 60-90% | >80% | >80% | 70% | 70% |
| 12 | Spectral | >1.0? | >1.0? | >0.8 micron | >0.8 micron | >0.8 micron | >0.3 microns | >0.3 microns | 1-5.4microns | 1-5.4microns |
| 13 | Operability | 98% spec | 95%? | 99% | 99% | 97% | >99% | >99% | >99% | >99% |
| 14 | How defined | 1/2 D* | 1/2 D* | 1/2 D* | 1/2 D* | 1/2 D* | 3*NEP | | | |
| 15 | Binning | Yes | No | No | No | No | No | No | | |
| 16 | Status | OTS | Fanout develop | OTS | Designed only | Imaged | OTS | Hybridized | Delivered | OTS |
| 17 | Comments | | | Reset ripple | Reset:global,ripple or non destructive | Designed shuttered | 5MHz bursting | | Crosstalk<.1% | Crosstalk<.1% |
| 18 | | | | | | | Reset,Ripple or | | | |
| 19 | | | | | | | Non Destructive | | | |

FIGURE 4-1 Currently Available Large Area Imaging IR Arrays

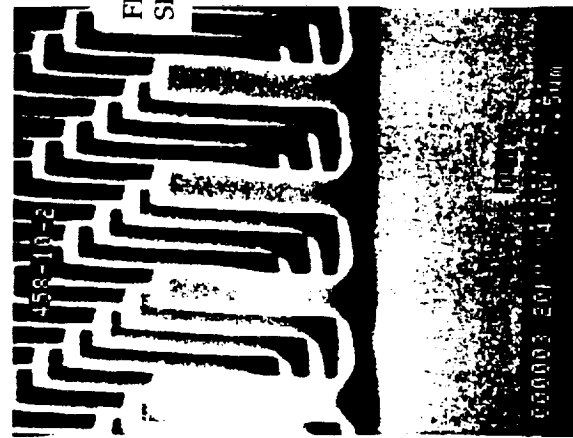


FIGURE 5-1 SEM Photo Of "Motheye" Microstructure

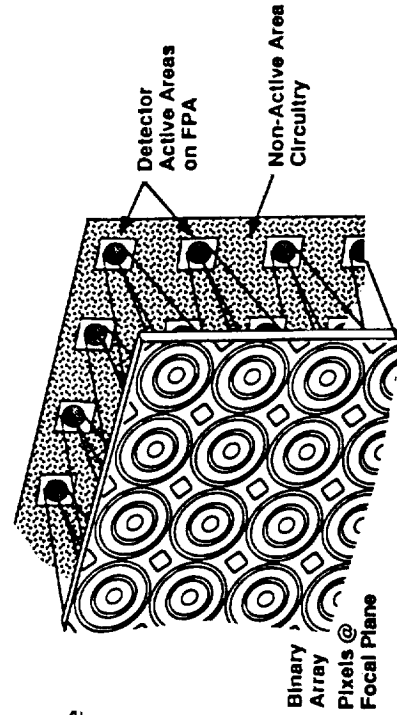


FIGURE 5-2 Binary Optics Lenslets Used To Correct "Fill-factor" And Allow Space For On-FPA Processing Electronic Circuitry

Other micro-structure devices, related to binary optics in terms of design and fabrication processes have been developed for sensor applications. Micro-bolometer IR detector arrays and "resonant structures" are examples of devices usable for robust IR detection. The bolometer arrays are described in a subsequent section. Resonant structure technology being developed by the Honeywell Sensor and Systems Development Center in Bloomington, Mn., represents an emerging trend in monolithic sensor fabrication for low power, rugged, and highly reliable sensor elements that clearly are applicable to space exploration applications, and warrants further description here.

Silicon-based resonant sensors (RS) are micron sized structures made with mature silicon processing technology. The principle of operation is to measure a shift in the resonant frequency of a microbeam as some force is applied to the structure thereby straining the beam. Equipped with integral monolithic silicon drive/sense and buffer circuitry, these devices are very small extremely robust self contained sensor elements providing digital output signals directly. Because the operating mechanism senses "time-base" variations (frequency) rather than electrical property changes, resonant structure sensors are inherently stable in operational calibration. The resonant micro-structure device is capable of sensitive wide dynamic range operation, and under adverse environmental conditions. Configured properly, these devices can be used for strain gages, pressure sensors, accelerometers, and sealed "Golay cell" thermal energy detectors. Figure 5-3 shows the RS principle of operation, and 5-4 diagrams a pressure sensor or accelerometer concept. Figure 5-5 shows an electron microscope view of an encapsulated micro-beam RS with the driver contact in place (light colored area)

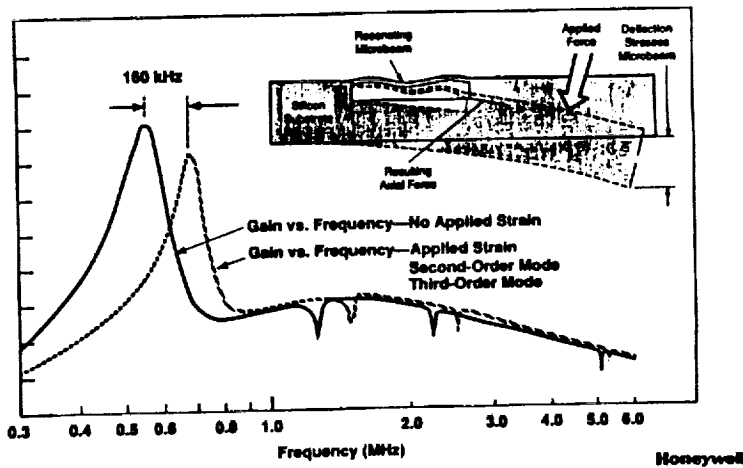


FIGURE 5-3
Resonant Structure;
Principle Of Operation

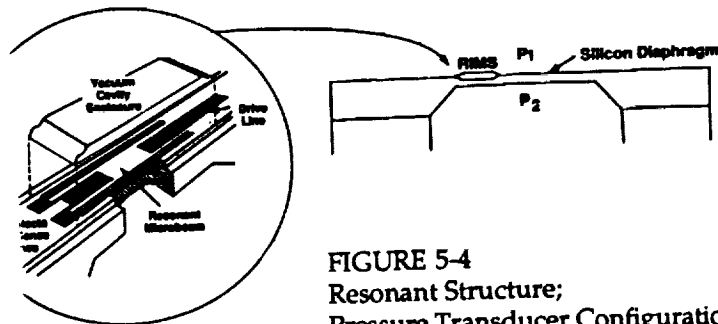


FIGURE 5-4
Resonant Structure;
Pressure Transducer Configuration

On FPA chip processing electronics: A practical "next step" toward miniaturization of sensors is to integrate onto the detector focal plane array sufficient electronic signal to provide ultra low-noise detection, internal clock generation, time delay integration of spectral analysis on two-dimensional arrays, and a robust simple interface to external electronics. Rockwell International has developed SWIR Hg Cd Te FPAs with these features⁵ and intends to exploit them for upcoming NASA space applications. R.I. also has extended their on-chip processing to include correlated double sampling, selectable integration capacitors, and externally selectable high pass filter banks all working in the "charge domain" within the FPA readout device. These semi-programmable SWIR devices operate with ultra-low noise (10s of electrons) at 90K operating temperature, and about 100 electrons at thermo electric cooling temperatures of 150-200K. An integrated chip/TE cooler assembly of this type forms a large part of a SWIR sensor, replacing large bulky electronics, cryo-coolers, and interconnection cabling.

Amber Engineering in Santa Barbara California has recently announced a 256x256 pixel detector of indium- Antimonide (In Sb) equipped with an integrated "massively parallel processed" signal processor chip.⁶ This device operates in the MWIR (3-5 μ) spectral region and forms the heart of an effective thermal imaging system.

Irvine Sensors in Irvine, California has pursued processing of FPA signals through "Z-plane" technology where electronic circuitry is stacked in the "z" dimension behind two dimensional staring mode X-Y detector arrays. A recent development involves a densely packed 3-dimensional computer-processor to perform processing algorithms from the IR array output data.⁷ Among the functions being performed by the Z-technology is "data extraction" via neural network type processing; a form of "smart" data compression to facilitate data flow from the FPA. This technology is exceptionally compatible with current detector arrays for near term miniaturization of Space Sensors Figure 5-6 shows a 128 X 128 element detector array packaged with electronics to perform all of the clocking and read-out functions, and additionally includes a neural net type computer and controllable filter bank to facilitate image processing functions. This assembly represents a significant step in miniaturization of smart sensors that can perform edge-enhancement, pattern recognition, motion detection trajectory prediction, and other such functions with minimal interface with external computer equipment.

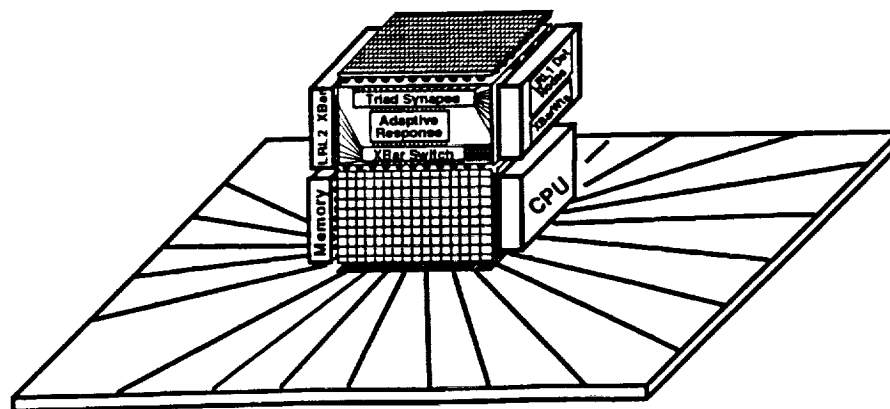


FIGURE 5-6 Irvine Sensors Integrated IR Detector/Processor Module

Uncooled Detector Development: There has been a large general effort to develop IR detectors that do not require cryogenic cooling because cryo-coolers are bulky, heavy and consume large amounts of power. Liquid cryogenics present a logistics problem for space applications, and radiative coolers are bulky and somewhat delicate. Thus, uncooled IR detectors are very desirable to avoid the cooling problem.

Classic lead-salt (PbS, PbSe) SWIR and MWIR detectors although somewhat slow electrically, when combined with modern read out devices and operating in a staring mod, have sufficient electrical bandwidth for imaging operation with high sensitivity in the 1-5 micron region. Several vendors including Optoelectronics Inc., Petaluma California provide such detector-readout combination devices.

Pyro-electric and ferro-electric detectors have been developed for imaging sensors by Texas Instruments in Dallas, Texas and others. These devices are essentially thermally modulated electrical capacitors, and can be operated uncooled or in a "temperature stabilized" mode with a single-stage TE cooler. Pyro/ferro electric devices offer a relatively near term potential for space sensors in specific applications where high sensitivity and electrical bandwidth are not necessary.

A relatively new non-cooled (but TE stabilized) detector technology consisting of arrays of microbolometers has been pursued by Honeywell for the U.S. Army CECOM for Night vision and electro-optics.⁷ These devices, developed under the High Density Array Development (HIDAD) program are thin-film micro bolometers made in 240x336 pixel arrays of 2-mil square elements. Operating in the LWIR (8-12 micron) spectral region, these devices are unique for uncooled detectors in that optical chopping or modulated IR radiation is not required for their detection mechanism. NEDT sensitivities of 0.09C and frame rates of 30Hz are reported for the 240-336 element arrays. Clearly this rugged detector technology made by conventional sequential metalization and etching processes on silicon material and which require no cryogenic-cooling is worthy of development for space sensor applications. Figure 5-7 shows a typical thin film HIDAD pixel element concept.

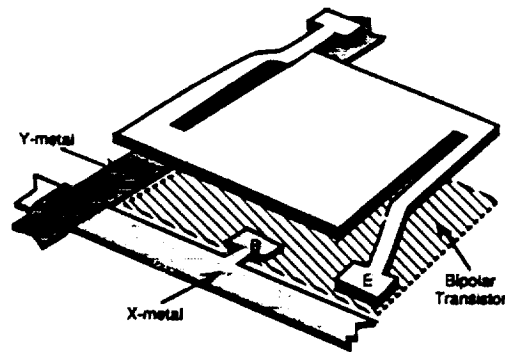


FIGURE 5-7
HIDAD Microbolometer IR
Detector Element Concept

On-FPA Pattern Recognition & Artificial Neural Networks (ANN) An electronic means of providing on-FPA signal processing by high density electronic packaging was discussed above in describing the Z-plane technology. A "next step" in developing "smart" focal planes is to build complex FPAs with layered structures of optical spatial filters, binary diffraction optical elements, and active silicon circuitry. Such opto-electronic FPAs can approximate trainable neural nets with the physical layers arranged as "layers" of neuron nodes in the ANN. These compact rugged low power detector/processor devices thus can become the "smart" building blocks for sensors intended to look for specific EOIR signatures, objects, events or other spatial/spectral patterns. For non-spectrographic applications the ANN can be used to pre-process the large volume of data from complex two dimensional FPAs sending only the pertinent information from the sensor for further processing. These devices thus perform a data-compaction function for applications interested only in thematic changes, moving objects, or transient events. Edge enhancement and 'nearest neighbor' pixel suppression for contrast

improvement and other SNR improvement processes significantly improve the performance of smart sensors which can be made in micro-miniature sizes.

Spectrally Selective Detectors. Quantum detectors of HgCdTe are being fabricated on graded electrical band-gap PN junctions where photo diodes implanted at various physical locations along this graded-gap region will respond to different wavelengths of incident IR flux. See figure 5-8. Because the graded gap crystal material is formed by varying the constituents of the $Hg_{(1-x)}Cd_xTe$ during the crystal growth process, the optical index of-refraction also varies with location across the gap. With proper geometry and material stoichiometry combined with etched binary optic diffractive patterns, a single chip self contained spectrometer for moderate spectral band-widths can be constructed. The bulk associated with optics, spectrographs, filters, etc. are thereby eliminated.

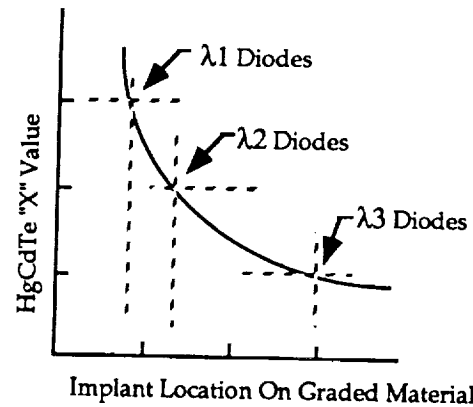


FIGURE 5-8 Graded Band-Gap HgCdTe Allows Monolithic Spectrally Selective Detectors

6. CONCLUSIONS AND RECOMMENDATIONS

Technology exists in varying degrees of development maturity from which to fabricate micro miniaturized IR sensors specifically designed for near automated space flight applications. Such "smart" sensors range from thermal imagers with low data rate interfaces to hyperspectral sensors capable of performance rivaling systems like the AVIRIS, but operating in the extended IR spectrum; and all contained on a micro-chip based focal plane assembly. Long term development of "virtual reality" human interface systems will then allow for man-in-the-loop operation of remote exploration tools (Moon, mars) in day/night conditions. The key to these useful virtual interfaces is to have sufficient "environmental" data to recreate the scene at a remote location so that the operator feels that he is actually "in" the real scene. Sensors can be available to accumulate such data for space exploration applications if certain technologies are developed in the proper sequence.

Figure 6-1 shows a time sequenced "road map" of IR FPA and processor/readout schemes that can lead to these advanced systems when the appropriate technology has been developed.

| | Detectors | Readouts | Applications |
|------------|--|---|--|
| 0-3 Years | <ul style="list-style-type: none"> • Si • PtSi • InSb • HgCdTe | <ul style="list-style-type: none"> • Direct Injection CCD • CTIA • SFD | <ul style="list-style-type: none"> • Thermal Imager • Spectrometer • Imagery Spectrometer |
| 3-5 Years | <ul style="list-style-type: none"> • Uncooled Tech. • On Chip Filter | <ul style="list-style-type: none"> • Parallel Processing • Neural Operator | <ul style="list-style-type: none"> • Smart Automated Sensors |
| 5-10 Years | <ul style="list-style-type: none"> • Spectral Detector | <ul style="list-style-type: none"> • Complex Integrator • Optronic Processor (Amichronic) | <ul style="list-style-type: none"> • Smart Sensors • Virtual Reality Output |

Earth Observation
Planetary Observation
Telescopes

Orbiting Telescopes

General Purpose
Remote Sensing

FIGURE 6-1 Progressive Development Of Increasingly More Complex IR Sensors

REFERENCES

1. D. A. Scribner, M. R. Kruer, and J. M. Killiani, "Infrared focal plane array technology," in Proc. IEEE 79, 66-82 (1991)
2. P. R. Norton, "Infrared Image Sensors", Optical Engineering, Vol. 30, No.11, (1991).
3. L. J. Kozlowski, et.al, "Large staring IRFPAs of Hg Cd Te on alternate substrates", Rockwell International Publication.
4. A. Tebo, "Infrared Imaging: Detector Arrays", Optical Engineering Reports, No. 101, (May, 1992).
5. L.J. Kozlowski, "Low noise 2-5 micron PACE-1 Hg Cd Te 10 x 132 FPA with 25 micron pitch and on-chip signal processing including CDS and TDI", Rockwell International Publication.
6. Private Communication with D. Smith, Amber Engineering, Santa Barbara, Ca., (1992)
7. Private Communication with J. Carson, Irvine Sensors, Irvine, CA., (1992).

Microtechnologies
and
Applications to Space Systems Workshop

MICROSPACECRAFT



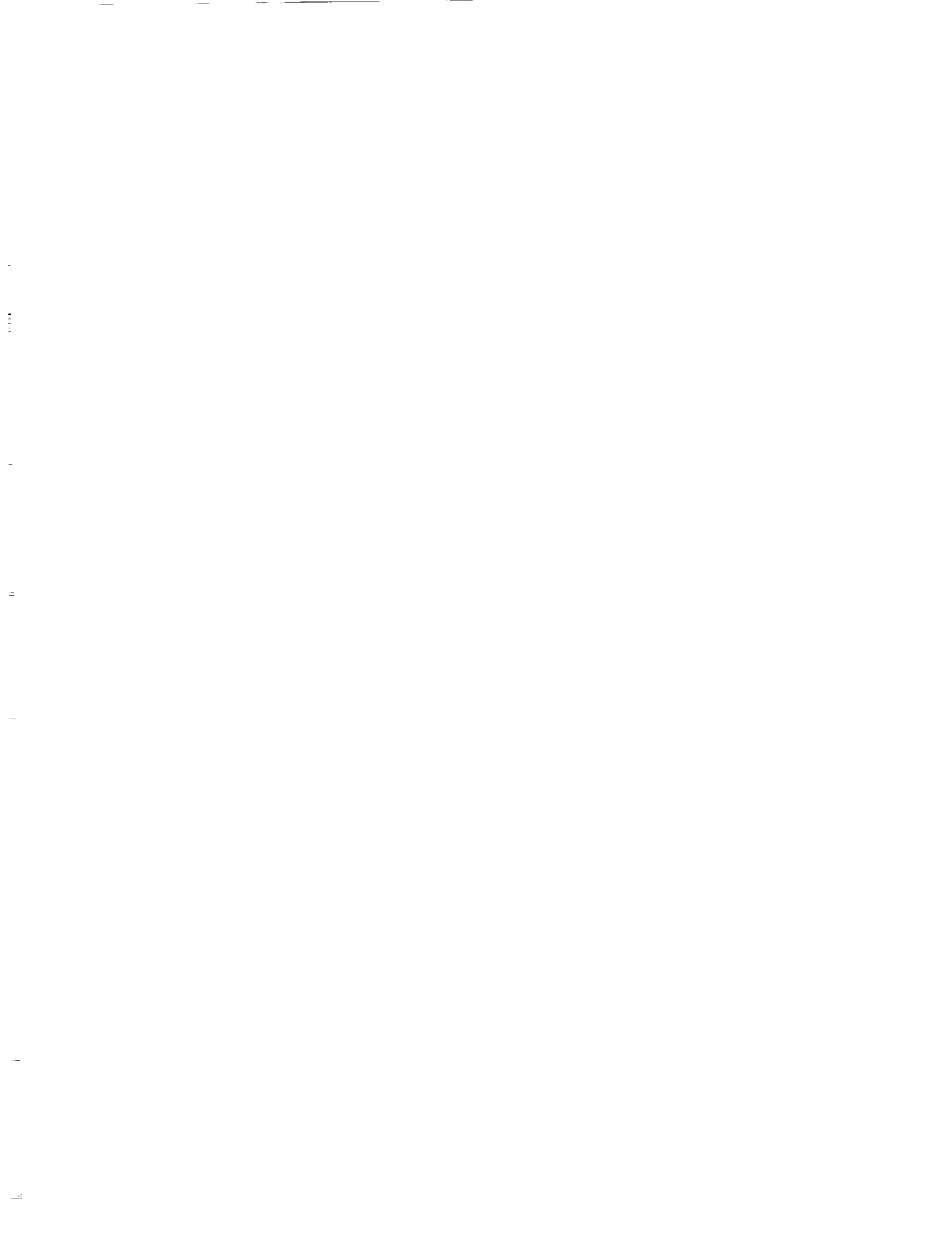
ASTEROID INVESTIGATION WITH MICROSPACECRAFT (AIM)

Christopher G. Salvo
Jet Propulsion Laboratory
California Institute of Technology
Pasadena, California 91109

ABSTRACT

Technology development by SDIO and other sources over the past several years has produced many high performance miniaturized spacecraft components. Although many of these components were designed for short operational lifetimes, some may be applicable to longer missions. The intent of the AIM design effort was to develop a conceptual microspacecraft system using SDIO-like technology to perform a near Earth asteroid (or comet) imaging science mission from a Pegasus launch vehicle. To achieve this, technology was deliberately pushed beyond state-of-the-art in all subsystem areas. Although the components and technologies used are based on the capabilities of current laboratory prototypes and technology demonstration devices, this conceptual spacecraft design will require some significant amount of development to be realized.

The AIM microspacecraft concept is envisioned as a ~ 25 kg, 0.5 m diameter by 0.6 m high hexagonal cylinder capable of conducting an imaging asteroid (or comet) flyby and returning the data to Earth. It is launched into low Earth orbit three to a Pegasus, each with its own solid propulsion stage for injection into an interplanetary intercept orbit with a different near Earth body. Mission durations range from as little as 4 - 6 months to about 2 years depending on the target, with launch opportunities occurring at least once per year.



Development of MMIC Technology
for SATCOM Applications

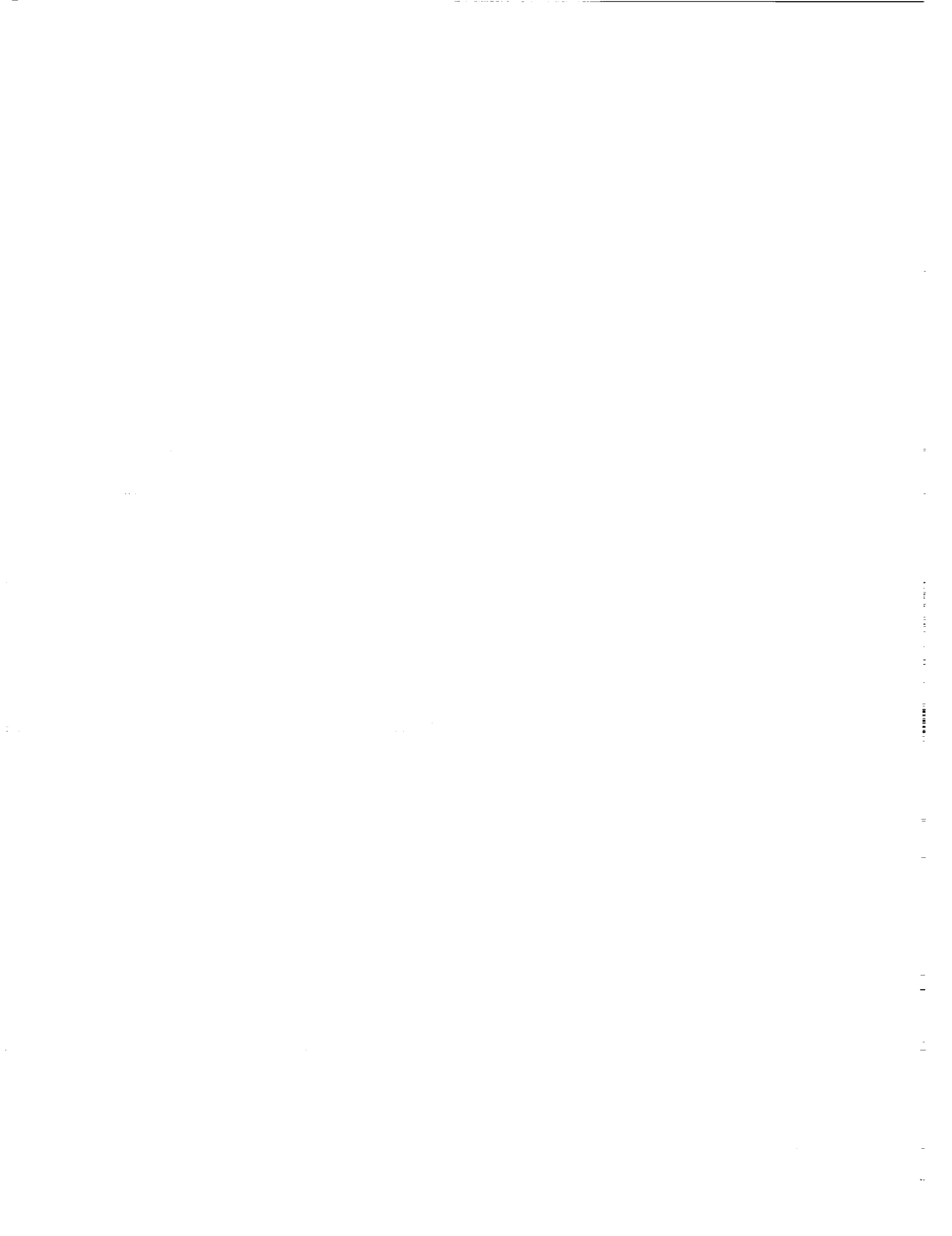
John J. Berenz

TRW

Electronic Systems Group
One Space Park
Redondo Beach, CA 90278

ABSTRACT

MMIC technology enables reduction of the size, weight, and cost of satellite systems. We have developed a family of Gallium Arsenide-based monolithic upconverters and downconverters for use in satellite systems such as ATDRSS, Milstar, and Brilliant Pebbles. The trend is toward the development of more complex multifunctional integrated circuits (MFICs) to reduce parts count, improve reliability, and reduce assembly and tune costs. We have demonstrated signal chip transceivers which integrate seven functions. More advanced heterojunction technologies are being developed to improve performance. Indium phosphide-based MMICs are being developed for NASA LeRC.



POWER SUBSYSTEM STATE-OF-THE-ART ASSESSMENT
AND MINIATURIZATION TECHNOLOGY NEEDS

R. C. Detwiler
Jet Propulsion Laboratory
California Institute of Technology
Pasadena, California 91109

ABSTRACT

This presentation provides an overview of the present status of power subsystem components. Performance predictions for power components (sources, storage and Power Management and Distribution (PMAD)), will also be shown. These predictions establish the near term, less than 10 year, limits to power subsystem miniaturization. Micropower component technology needs to enable a microspacecraft power subsystem are outlined.

Sources include mini Radioisotope Thermoelectric Generators (RTGs) and solar cell technologies including: silicon, gallium arsenide, germanium and band gap. Energy storage elements include embeddable microbatteries consisting of a limited number of cells. PMAD concepts address the single chip power system and single chip power converters.



THE APPLICATION OF MICROT TECHNOLOGY
TO SPACECRAFT ON-BOARD COMPUTING

Leon Alkalaj
Jet Propulsion Laboratory
California Institute of Technology
Pasadena, California 91109

ABSTRACT

The recent focus and concern for smaller, less costly missions, has given further impetus for the development of microspacecraft. Microtechnology advances in the areas of sensors, propulsion systems, and instruments, make the notion of a specialized miniature spacecraft feasible in the immediate future. However, all of the spacecraft subsystems have to rely on existing on-board computing and data processing technology which is still characterized by high mass, volume, and power consumption. Moreover, the performance of current on-board computers may also pose a constraint on mission capability and scientific return.

In this report, we will survey recent advances in chip packaging and stacking techniques that allow miniature computers to be developed for space applications. Several orders of magnitude in mass, volume and power consumption are possible using these techniques. Moreover, performance improvements can be achieved by increasing the scale of multiprocessing. Most importantly, long-term survivability can potentially be improved by increasing the level of redundancy and fault tolerance.



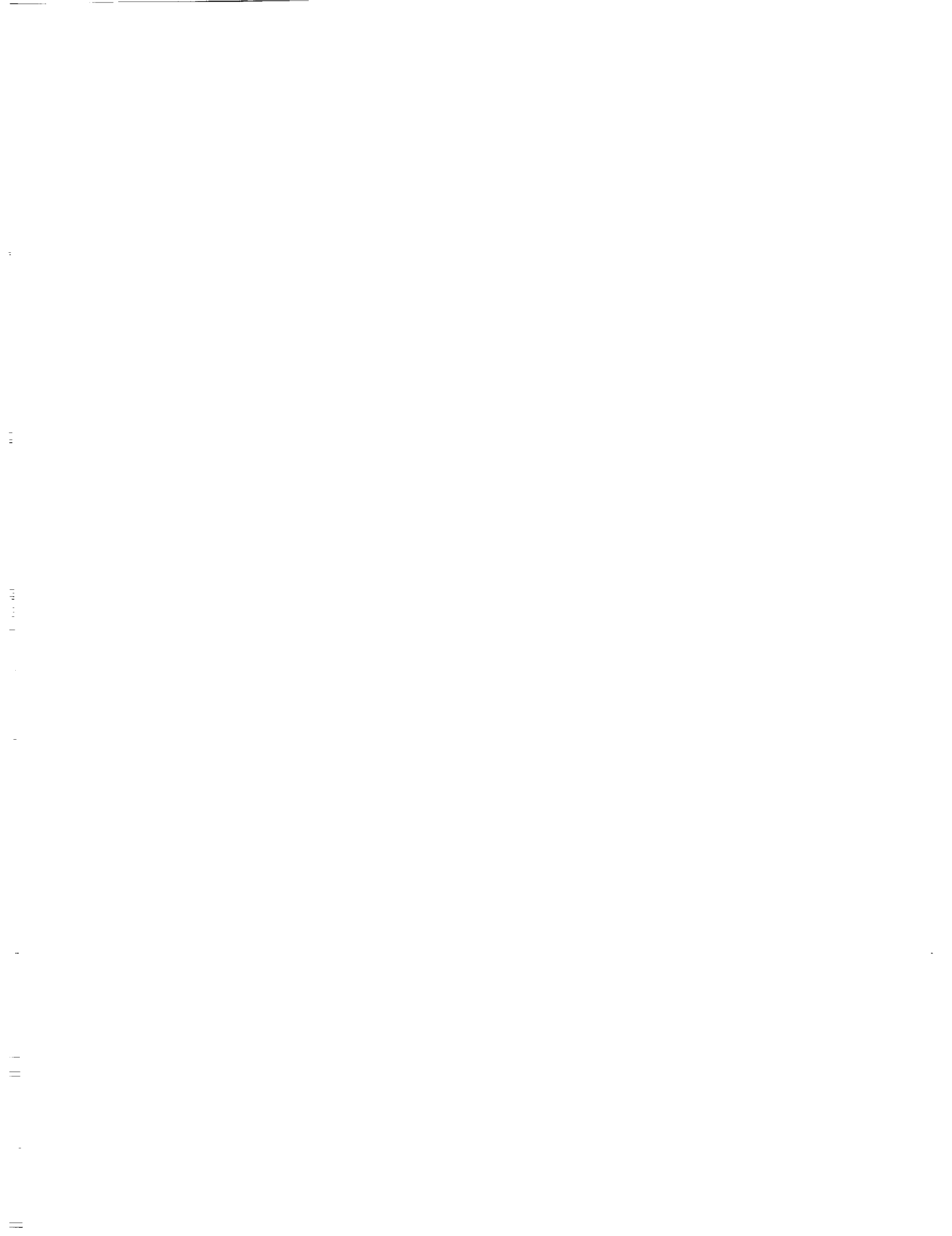
ELECTRONIC PACKAGING FOR MICROSPACECRAFT APPLICATIONS

David Wasler
Jet Propulsion Laboratory
California Institute of Technology
Pasadena, California 91109

ABSTRACT

The intent of this presentation is to give a brief look into the future of electronic packaging for microspacecraft applications. Advancements in electronic packaging technology areas have developed to the point where a system engineer's visions, concepts and requirements for a microspacecraft can now be a reality. These new developments are ideal candidates for microspacecraft applications. These technologies are capable of bringing about major changes in how we design future spacecraft while taking advantage of the benefits due to size, weight, power, performance, reliability and cost. This presentation will also cover some advantages and limitations of surface mount technology (SMT), multi-chip modules (MCM) and wafer scale integration (WSI), and what is needed to implement these technologies into microspacecraft.

PRECEDING PAGE BLANK NOT FILMED



Microspacecraft Attitude Control

George E. Sevaston

Jet Propulsion Laboratory
California Institute of Technology
Pasadena, CA 91109

ABSTRACT

The essential requirement on a microspacecraft attitude control subsystem (ACS) is that it must provide a means of affecting the orientation of the spacecraft bus. Thus, it must be capable of delivering adequate torque for some finite interval of time through appropriate actuators. This clearly limits the applicable technologies and the degree to which certain key components can be miniaturized. Beside actuators, other basic components include sensors, electronics and a command and data subsystem interface. Depending on the choice of realization and the desired level of onboard autonomy, a computer may also be included. In the case of the sensors, accuracy capabilities are governed by the allowable size and mass of the package. In the case of the computer, power, as well as size and mass are limiting. The expected ACS subsystem requirements of a generic microspacecraft will be examined. These will then be discussed in the context of what is both feasible and technologically achievable. Fundamental limits and major development needs will be identified.

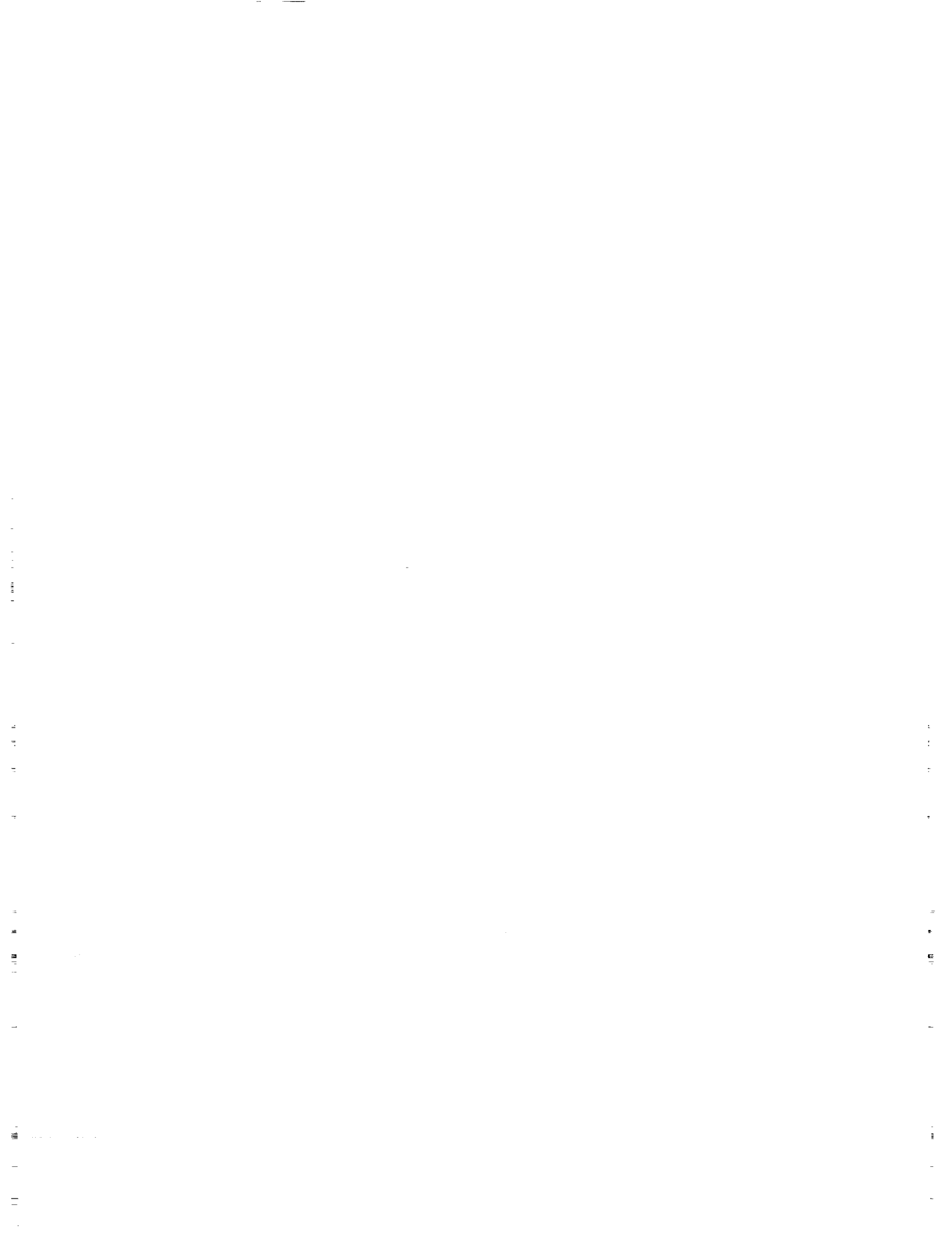
PRECEDING PAGE BLANK NOT FILMED

Lightweight Structures and Mechanisms for Microsatellites

Robert Wendt
Martin Marietta Civil Space and Communication
Denver, CO 80201

For small lightweight satellites, Martin Marietta is investigating several structure technologies including monocoque composite shell structures, high conductivity composite thermal management systems, thin film photovoltaic, and innovative mechanisms. Of particular importance are mechanisms because as the overall spacecraft size decreases, the size of the mechanisms remains constant. These mechanisms including door actuators, deployment devices, release devices and electrical connectors can constitute a major portion of the total spacecraft weight. Martin Marietta has developed and fabricated several innovative mechanisms using shape memory alloys (SMA). In many cases, complex gear/motor/cable actuation systems can be replaced with a single small diameter SMA wire. Thus, significant weight reductions and the space for the mechanism can be achieved using SMA. In addition, SMA mechanisms contain significantly less parts and should decrease touch labor and the associated cost while improving reliability by reducing the number of interaction parts which may fail. Technical issues under investigation are synchronization of the SMA devices and actuation frequency, which is dependent on the rate of heat application and removal.

PRECEDING PAGE BLANK NOT FILMED



Advanced Microfabrication Technologies for Microspacecraft

M. Ghezzi, B. Bagepalli, S. Kodiyalam, C. Korman, K. Browall
 GE Corporate Research and Development, Schenectady, NY 12301

Norman Alexander, GE Astro Space Division, Princeton, NJ 08543

ABSTRACT

Advanced microfabrication technologies offer the prospect of reducing the weight and size of spacecraft through the use of lighter and stronger materials in conjunction with new mechanical/ structural design concepts and design optimization methods. At the same time electronic components have been scaled down while increasing functional utility. A two-fold benefit is derived for space applications through the use of less expensive components and lower launch costs associated with lighter components. GE-CRD is actively pursuing research in these key technologies for a wide range of applications including satellites. These key technologies will be reviewed and an update on GE progress will be given.

The need to reduce weight and lower cost, while maintaining product quality and reliability are primary drivers in the design of satellites, in general, and microsattellites in particular. For the structural subsystem, these requirements pose a complex design problem unless new mechanical design concepts and computer-aided design optimization methods are employed. Several new concepts like battery pack doubling as panel reinforcements and fuel tanks as integral structural members need to be utilized. In addition, new viscoelastic material damping concepts for spacecraft components provide for lighter weight/lower cost designs, while satisfying the structural dynamics requirements.

High density interconnects (HDI) technology permits the use of bare ICs on a ceramic substrate with 90% active area utilization. A copper/polyimide multilayer structure is the backbone of the technology, which has demonstrated a size/weight reduction of >10x compared to printed circuit board with performance up to the GHz level. HDI modules have exceptional mechanical robustness as evidenced by survival of 180 Kg rapid acceleration tests.

Microelectromechanical systems (MEMS) are redefining sensors and actuators by miniaturization through micromachining techniques. Sharing many fabrication steps with HDI we have developed a new technique for surface micromachining of copper/polyimide structures using computer-aided laser patterning. Millimeter-size electromechanical switches have been made with dielectric isolation > 200 v, maximum current density of 10^5 amp/cm², contact resistance of 20 μ ohm cm² and interrupt time of a few milliseconds.

HDI technology leads to a significant reduction of power supply size, as demonstrated by the 5x5x.5 cm³ dimensions of a 1 MHz Dual Forward Resonant Power Supply. Integrated circuits, capacitors and transformers are either embedded in an HDI structure or made by a copper/polyimide process. Efficiencies > 80% have been predicted with a power density of 4W/cm³.

Inorganic coatings on polymers allow the surface properties of structural materials to be engineered for space applications, while achieving weight reduction commensurate with the substitution of polymers for metals. For example, metal coatings can increase resistance to oxygen plasma attack in LEO orbits, reduce EMI/RFI interference, or reduce thermal degradation.



MICROSPACECRAFT FOR SPACE SCIENCE
IN ISAS, JAPAN

by Hirobumi Saito
Institute of Space and Astronautical Science, Japan

ABSTRACT

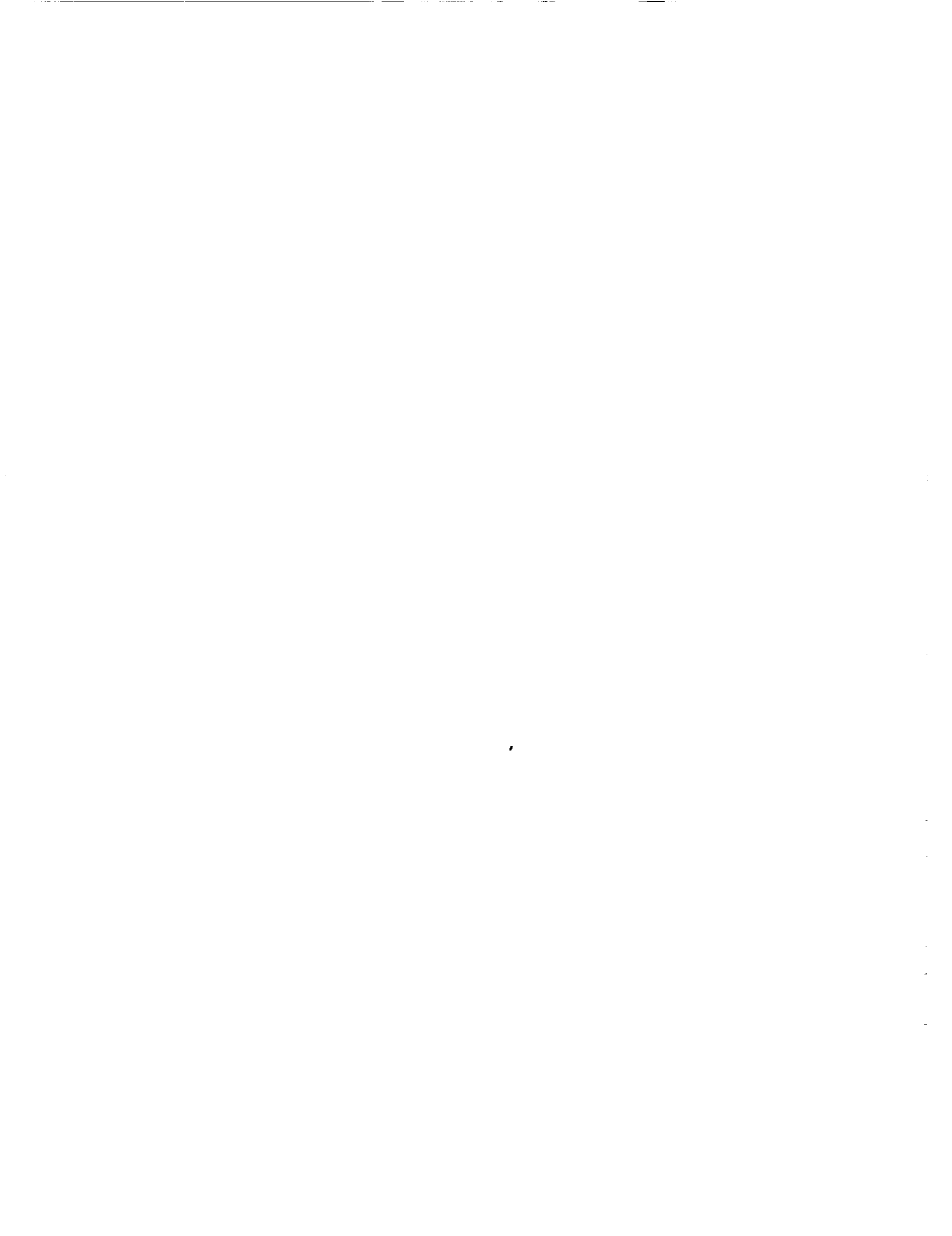
The Institute of Space and Astronautical Science (ISAS) in Japan has launched 21 spacecraft into orbit for since 1970, and has proceeded steadily in various fields of space research. The size and weight of the spacecraft developed have been selected to be small in order to keep their low cost and short development phase. This presentation shows the compact style to deal with space in ISAS. Also, the several microspacecraft for planetary missions are presented. The video film is performed to introduce the ISAS space activities.

PRECEDING PAGE BLANK NOT FILMED



Microtechnologies
and
Applications to Space Systems Workshop

**SPACE STATION, SHUTTLE
& PROPULSION**



Microfabricated silicon biosensors for microphysiometry

L.J. Bousse, J.M. Libby, and J.W. Parce
Molecular Devices Corp.
4700 Bohannon Drive
Menlo Park, CA 94025

Abstract

Microphysiometers are biosensor devices that measure the metabolic rate of living cells by detecting the rate of extracellular acidification caused by a small number of cells. The cells are entrapped in a microvolume chamber, whose bottom surface is a silicon sensor chip. In a further miniaturization step, we have recently fabricated multichannel flow-through chips that will allow greater throughput and multiplicity. Microphysiometer technology can be applied to the detection of microorganisms. We describe the sensitive detection of bacteria and yeast. Further applications of microphysiometry to the characterization of microorganisms can be anticipated.

Introduction

The first silicon sensors were essentially extensions of purely electronic components to transducing components. A good example is the ion-sensitive field-effect transistor, first described in 1970 [1]. This transistor is an active electronic device coupled to an insulator/electrolyte interface which gives it a chemically dependent threshold voltage. This represents the electronic component point of view. Soon afterwards, however, a mechanical point of view became prominent as well, and was summarized in a well-known review paper by Peterson [2]. This development was made possible by the rapid progress in micromachining, and the realization that silicon as a material has favorable mechanical properties for many applications.

One can thus conceive of two aspects to silicon sensor technology: using the electronic aspect of silicon (e.g. all FET-based chemical sensors; various types of magnetotransistors), and using the mechanical properties (e.g. pressure sensors and accelerometers). Much of the recent most impressive progress in microsensor technology comes from combining these two aspects. A recent example of a commercial device that does this is a surface micromachined accelerometer with integrated circuitry [3].

Our work concerns the application of a silicon sensor chip for bioassays [4-7] and immunoassays [8-10]. In this case, the silicon chip also fulfills two functions: it is the chemical sensor, but it is also an important mechanical part of the fluid path needed to operate the system. We have described applications of silicon micromachining for our sensors [11]. It is the combination of these two properties of silicon which make it the material of choice for our application.

We have called the bioassay application of the silicon sensor a microphysiometer, which is a device which allows the measurement of the metabolic rate of cells [4]. Most of the applications we have described up to now are intended for mammalian cells [4–7]. In this paper, we will present an example of detection of microorganisms, namely bacteria and yeast, using the microphysiometer. Our preliminary work in that area concentrated on detecting *Escherichia Coli*, and measuring the effect of antibiotics on these bacteria [12]. The methods described in this paper may prove useful in a number of fields in which sensitive microbial detection and identification are of significant importance. These include environmental, food, and industrial processes where small numbers of contaminating microorganisms may be difficult to detect with existing methods but, after being allowed a period of growth, may have a significant impact on the ecosystem, patient, or product. In many cases the identity of these organisms must be determined in order to establish the source of the contamination and the likelihood of problems occurring (e.g. pathogenic capability or production of a toxin that causes food toxicity).

LAPS devices in microvolume chambers

The sensor device we use is called a Light-Addressable Potentiometric Sensor (LAPS) [13] (see Figure 1). It consists of an MIS or EIS capacitor which is illuminated by an AC-modulated light source, at a wavelength short enough to generate carriers in silicon, but also long enough to penetrate sufficiently. The typical wavelength we use is 940 nm. The illumination typically occurs at the backside of the device, so that the frontside is free to form one surface of the sensing chamber. When the capacitor is biased in inversion, the depletion region at the frontside surface collects light-generated carriers, generating an AC photocurrent. When the capacitor is biased in accumulation, there is no photocurrent. The resulting AC photocurrent/bias curves show a steep transition between these two states. We use the position of the inflection point in these curves to track changes in the potential at the insulator surface. Depending on the material used as the outer gate material of the LAPS, it can be used to detect pH, redox potential, or cations using an ion-selective membrane [13]. In all the applications described in this paper, we use a Si_3N_4 surface to detect pH changes. The measurement of the photocurrent/bias curves, and the calculation of the inflection point voltage is done with custom hardware and software.

In all our work to date, we have not focused on the LAPS as a stand-alone sensor, but rather on the combination of LAPS with another concept, namely microvolume reaction chambers. This consists of using the LAPS as part of a chamber with volume in the order of a microliter. Using such a small volume allows sensitive detection of any pH-changing reaction. According to the analysis of pH changes in a microvolume reaction chamber [14], the measured signal is a rate of pH change given by:

$$\frac{dpH}{dt} = \frac{R}{V \beta_V + S \beta_S} \quad (1)$$

where R is the rate at which a reaction produces H^+ or OH^- ions (in moles/second), β_V and β_S represent the volume and surface buffering capacity, respectively, V is the chamber volume, and S the surface area present.

This equation shows that the two important factors in the sensitivity of the system are the chamber volume, and the solution buffer capacity. In most cases, the surface buffer capacity is not dominant and can be ignored. Surface buffering, however, becomes the limiting factor when the volume is reduced below a certain point.

In the case of an immunoassay, an enzyme label is used to detect the analyte of interest, and R comes from an enzyme-catalyzed reaction [9,13]. In the case of a bioassay, the metabolism of living cells in the chamber causes the pH changes.

Measurement of cellular metabolism

Living cells constantly consume energy for a variety of purposes, such as maintaining chemical concentration gradients, mechanical motion or deformation, and the synthesis of compounds. This energy is stored in the form of adenosine triphosphate (ATP), that must therefore constantly be replenished. A variety of catabolic pathways exist in which nutrient compounds are broken down to provide energy in the form of ATP. We have analyzed these in detail in Ref. [15]. The two most important ones are glycolysis, which is the conversion of glucose to lactic acid without requiring the presence of oxygen, and aerobic respiration, which requires the presence of oxygen that enables a more complete metabolic breakdown of glucose, with CO_2 as the ultimate product. This carbon dioxide dissolves in water, and some of it is hydrated into carbonic acid. Thus, in both cases the end result of an energy-yielding metabolic pathway is an acidic substance. The metabolism of living cells therefore tends to acidify the extracellular environment. Table 1 gives a more complete list of energy producing pathways, and the amount of ATP and protons they generate. The method we use to detect cellular metabolism is the measurement of the rate of acidification it induces in the extracellular environment.

There are some important differences between microorganisms and mammalian cells when placed in a microphysiometer. Many more energy-producing pathways are available to most microorganisms. This means that the results will depend strongly on the carbon source. For instance, certain microorganisms have the ability to use pathways that alkalize the environment rather than acidify it. Finally, microorganisms require less delicate treatment than mammalian cells, and can be entrapped with methods that would harm or kill mammalian cells.

In order to survive, cells must be bathed in a culture medium to supply them with nutrients, and keep the pH of the environment in a tolerable range. On average, a flow of this medium is needed to bring fresh nutrients and remove the acid byproducts of cellular metabolism. However, when there is a flow of medium in the microvolume chamber where the cells are, the chamber pH is determined by that of the medium. Thus, to measure the rate of extracellular acidification, the medium flow must be

periodically interrupted. In the absence of medium flow, the cells act as a source of protons, and Eq. (1) can be used to predict the resulting rate of pH change. It is seen that the measured signal is proportional to the acidification rate.

The measurement method consists of periodically turning the medium flow on and off, and measuring the acidification rate during the off periods. Figure 2 shows a diagram of the setup we use to carry out such a measurement, and Figure 3 shows an example of the result. The data are usually plotted as the acidification rate as a function of time. The main applications of this technique we have explored previously are the detection of receptor/ligand interactions [5], and in-vitro toxicology [16].

A multichannel, flow-through, microphysiometer chip

In all the embodiments of our technology which we have described previously, one silicon sensor chip is used in one flow chamber assembly, to constitute a single microphysiometer channel. Typically, eight channels are then combined in one table-top instrument.

Clearly, a silicon sensor chip with multichannel capability would be very desirable. However, as soon as several fluid streams are present in one chip, several new issues arise. There must be a separation between different flow channels, and a means to introduce cells into each chamber. This can be accomplished by etching channels into the surface of a silicon chip. Cells can then be introduced in all channels at once by coating a glass cover slip with a layer of adherent cells, and placing it over all the channels. This means, however, that entry and exit ports to these fluid channels cannot be at the top surface, since that is covered by the glass cover slip. The logical solution is to etch openings completely through the chip, with interfaces to the rest of the fluidics at the bottom of the chip.

Along these lines, we have designed and fabricated an eight-channel flow-through microphysiometer chip. Figure 4 shows the cross-section of one of the channels. The procedure to fabricate this chip starts with growing an oxide layer on a double-sided polished n-type silicon wafer, and patterning it to expose the frontside areas where the channels will be. The channel is then etched 100 μm deep in a wet anisotropic etchant solution. Next, openings are made on the backside for the flow-through holes, and anisotropically etched all the way through the wafer. The initial oxide layer is then stripped, leaving a bare patterned wafer. The process from then on is similar to the standard LAPS process described in [17]: essentially field oxidation, active area patterning, gate oxide, and LPCVD nitride deposition. One difference is that the backside now contains two gold electrodes: one makes contact to the silicon, and the other is on top of the field oxide, and is used as a controlling electrode.

Figure 5 shows the front and back sides of the completed 23 \times 23 mm chips. This chip combines in one unit all the chambers of a complete desktop microphysiometer. It could be used to make a much more compact eight-channel instrument, or several of these chips could be used to make an instrument with many more channels. This last option would be useful in applications such as drug discovery which require high throughput, and applications where redundancy is required to achieve very high reliability

performance. Another advantage of a multichannel micromachined chip is that many of the critical components of the system are combined in one chip, making the system easier and potentially cheaper to build.

Detection and characterization of microorganisms

Our initial experiments involving microbial cells used a chamber design which was different from that previously described [4,5] for eucaryotic cells. The metabolism of microbial cells was measured with a cell capsule which consisted of two fluid paths which passed through circular 0.45 μm pore polycarbonate membranes located above "reading areas" of a silicon chip (Fig. 6). The diameter of each of these membranes, and hence the boundaries of the cellular environment, was 700 μm . Before cells were introduced into one of these fluid paths (the other served as a negative control), a "background" acidification rate of 2.1 (SD of 2.8) $\mu\text{V/s}$ was observed. The liquid passing through the chamber was OF medium and flow was on for 100 sec at a rate of 75 $\mu\text{l/min}$ and off for 100 sec.

The bacterium *Escherichia coli* (ATCC 25922 cells) was grown at 37° C overnight in Trypticase soy broth, counted with a Petroff-Hauser direct cell counter, and then diluted into oxidation/fermentation (OF) medium (Difco Laboratories; Detroit, Michigan) at a concentration of 10^5 cells per ml. One tenth ml (10,000 cells) of this suspension was introduced into the cell chamber at 37° C. At this point the acidification rate was 3.1 (SD of 1.0) $\mu\text{V/s}$, which was not statistically different from the background acidification rate. However, when the fluid passing through the counting chamber was switched to a salts solution with very low buffering capacity, an acidification rate of 53.8 (SD of 2.6) was observed (Fig 7). The time from introduction of cells until the beginning of these rate determinations was approximately 29 min.

Similarly, the yeast *Saccharomyces cerevisiae* was grown overnight in Sabouraud dextrose medium (Difco) and diluted to 10^4 cells per ml in OF medium. One tenth ml of this suspension passing through the cell chamber at 25° C carried 1000 yeast cells into the chamber and yielded an acidification rate of 153 $\mu\text{V/s}$ (SD of 7.7), as shown in Fig. 8.

It should be noted that this particular cell chamber was designed to test the concept of microbial cell entrapment and was not specifically designed for optimum sensitivity. This design did demonstrate that a temporary substitution of one medium for another of lower buffering capacity (this switch was temporary because the latter was incapable of supporting growth) could greatly improve the ability to detect microbial metabolism. It is likely that a cell chamber constructed to take advantage of fluid switching capability but with a significantly lower cell chamber volume would represent a design with the capability for a sizable improvement in sensitivity.

In addition to detection, the microphysiometer has the possibility of characterizing the nature of the entrapped microorganisms. The response of different organisms to changes in the carbon source varies. The doubling time of an organism in a given growth medium can be measured in the microphysiometer, and is characteristic for that organism. Also, certain antibiotics are selective in inhibiting the growth of certain types of

microorganisms. It is possible to expose organisms to a sequence of different growth media, with and without antibiotics, to gain information about their nature, as we showed in [12].

Design of a micromachined, multichannel, microorganism-sensing chip

Given the flow-through chip for adherent eucaryotic cells we describe above, a design for a similar device for the entrapment and detection of microorganisms can be suggested easily. The key requirement is a flow channel that goes through a microorganism-entrapping membrane. In contrast to the chip of Fig. 4, this means a different chip must contain the inlet and outlet flow channel. Thus we suggest the concept shown in Fig. 9: two silicon chips, separated by a membrane. The lower chip contains the LAPS sensors, and has fluid inlets in the bottom. The function of the upper chip is to form the top of the microvolume chamber, collect the flow through the membrane, and guide it to an outlet. As before, a mechanical fixture applies enough pressure to hold these three components in place, and contains the fittings to interface the fluid connections with external pumps and valves.

One important issue in this design is to ensure that the flow in each channel goes as we expect, and does not leak underneath or through the membrane from one channel to the next. This potential problem can be handled in several ways. First, the membrane that we intend to use has directional openings which only go through, and not sideways (e.g., a track-etched 0.45 μm pore size polycarbonate membrane). Thus, the lateral flow resistance between neighboring channels is very high. To avoid lateral flow underneath the membrane, if pressure is not sufficient, a thin hydrophobic gasket material (silicone rubber, for instance) may be added.

Conclusions

We believe the microphysiometer is a powerful and general tool for detecting how living cells react to their environment, and for detecting components in the environment that affect living cells. We have only begun to explore these applications. In addition, there are many possibilities in applying this technology to the identification and characterization of microorganisms.

The advantages of integrating the silicon sensor with silicon micromachining technology are clear: integration allows multichannel sensors to be made, and miniaturization of the instrumentation. The direction of further developments will probably be the further integration of all critical components of the fluid path shown in Fig. 2 on the chip or close to it. The first candidate for further integration will be the valve which allows switching between two fluid streams, so that we can minimize the dead volume between the valve and the chamber.

Acknowledgments

This work was supported in part by DARPA contract number MDA972-92-C-0005.

References

- [1] P. Bergveld, Development of an ion-sensitive solid-state device for neurophysiological measurements, *IEEE Trans. Biomedical Eng.*, BME-17 (1970) pp. 70-71.
- [2] K.E. Peterson, Silicon as a mechanical material, *Proc. of the IEEE* 70 (1982) pp. 420-457.
- [3] H. Steele and L. May, Attributes of surface micromachining as shown by a monolithic accelerometer, *Sensors Expo West Proceedings*, 1992.
- [4] J.W. Parce, J.C. Owicki, K.M. Kercso, G.B. Sigal, H.G. Wada, V.C. Muir, L.J. Bousse, K.L. Ross, B.I. Sikic, and H.M. McConnell, Detection of cell affecting agents with a silicon biosensor, *Science*, 246 (1989) pp. 243-247.
- [5] J.C. Owicki, J.W. Parce, K.M. Kercso, G.B. Sigal, V.C. Muir, J.C. Venter, C.M. Fraser, and H.M. McConnell, Continuous monitoring of receptor-mediated changes in the metabolic rates of living cells, *Proc. Natl. Acad. Sci. U.S.A.*, 87 (1990) pp. 4007-4011.
- [6] K.M. Raley-Susman, K.M. Kercso, J.W. Parce, J.C. Owicki, and R.M. Sapolsky, Direct measurement of neurotransmitter activation of cellular metabolism in cultured hippocampal neurons. *J. Cell. Biol.* 111 (1990) 339a.
- [7] L.J. Bousse, D.L. Miller, J.C. Owicki, and J.W. Parce, Rapid determination of cellular metabolic rates with a silicon microphysiometer, *Technical Digest Transducers '91*, San Francisco, June 1991, pp. 74-77.
- [8] J.D. Olson, P.R. Panfili, R. Armenta, M. Femmel, H. Merrick, J. Gumperz, M. Goltz, and R.F. Zuk, A silicon sensor-based filtration immunoassay using biotin-mediated capture, *J. Immunological Methods*, 134 (1990) 71-79.
- [9] L. Bousse, G. Kirk, and G. Sigal, Biosensors for detection of enzymes immobilized in microvolume reaction chambers, *Sensors and Actuators*, B1 (1990) 555-560.
- [10] V.T. Kung, P.R. Panfili, E.L. Sheldon, R.S. King, P.A. Nagainis, B. Gomez, D.A. Ross, J. Briggs, and R.F. Zuk, Picogram quantitation of total DNA using DNA-binding proteins in a silicon sensor-based system. *Anal. Biochem.* 187 (1990) 220-227.
- [11] L.J. Bousse, J.W. Parce, J.C. Owicki, and K.M. Kercso, Silicon micromachining in the fabrication of biosensors using living cells. *Technical Digest IEEE Solid State Sensor and Actuator Workshop* (Hilton Head, 1990) pp. 173-176.
- [12] J.M. Libby, D.L. Miller, and G. Humphries, Determination of metabolic activity and antibiotic sensitivity of *Escherichia Coli* with a silicon-based biosensor, *Abstracts of the 89th annual meeting of the American Society for Microbiology*, New Orleans, 1989, p. 457.
- [13] D. G. Hafeman, J. W. Parce and H. M. McConnell, Light-addressable potentiometric sensor for biochemical systems, *Science*, 240 (1988) 1182.

- [14] L. Bousse, J. C. Owicki and J. W. Parce, Biosensors with microvolume reaction chambers, in: S. Yamauchi, Ed., *Chemical Sensor Technology*, Tokyo and Amsterdam: Kodansha/Elsevier, 1992; Vol. 4: pp. 145-166.
- [15] J.C. Owicki and J.W. Parce, Biosensors Based on the Energy Metabolism of Living Cells: The Physical Chemistry and Cell Biology of Extracellular Acidification. *Biosensors and Bioelectronics* 7: 255-272 (1992).
- [16] L.H. Bruner, K.R. Miller, J.C. Owicki, J.W. Parce, and V.C. Muir, Testing Ocular Irritancy In Vitro with the Silicon Microphysiometer. *Toxicology In Vitro* 5: 277-284 (1991).
- [17] L.J. Bousse, D. Hafeman, and N. Tran, Time dependence of the chemical response of silicon nitride surfaces, *Sensors and Actuators B1* (1990) pp. 361-367.

| Carbon Source | Pathway | Reaction | ATP Yield | H ⁺ per ATP |
|---------------|-------------|--|-----------|------------------------|
| Glucose | Glycolysis | glucose --> 2 lactate ⁻ + 2 H ⁺ | 2 | 1.000 |
| Glucose | Respiration | glucose + 6 O ₂ --> 6 HCO ₃ ⁻ + 6 H ⁺ | 36 | 0.167 |
| Glutamine | Respiration | glutamine + 9/2 O ₂ + 3 H ₂ O --> 5 HCO ₃ ⁻ + 2 NH ₄ ⁺ + 3 H ⁺ | 27 | 0.111 |
| Pyruvate | Respiration | pyruvate ⁻ + 5/2 O ₂ + H ₂ O --> 3 HCO ₃ ⁻ + 2 H ⁺ | 15 | 0.333 |

Table 1

Figure Captions

- Figure 1.** Diagram of basic LAPS setup. The electronics makes three analog connections to the sensor, beyond those to the LED: one to the bulk silicon, one to a controlling electrode, and one to the reference electrode.
- Figure 2.** Instrumentation schematic. Culture medium is pumped from a reservoir by a peristaltic pump, and passes through a debubbler/degasser, a selection valve, the flow chamber, the reference electrode, and finally goes to a waste receptacle. The valve controls which of two pumped streams of medium enters the flow chamber (not shown). A personal computer controls the LAPS electronics, the pump, and the valve; it also manages data acquisition, analysis, and storage.
- Figure 3.** Example of a metabolic rate measurement. (A) pH vs. time. (B) The acidification rates resulting from the data in (A). Receptors on the cells were activated with an agonist midway through the period shown, causing a strong increase in acidification rate.
- Figure 4.** Cross-sectional diagram of one channel of a multichannel flow-through microphysiometer chip.
- Figure 5.** (A) Diagram of the frontside of the multichannel flow-through microphysiometer chip. (B) Photograph of the backside of the same chip, showing separate gold leads for backside contact and controlling electrode.
- Figure 6.** Diagram of cell chamber and flow path for bacterial detection
- Figure 7.** Acidification rates of *E. coli* in OF (low buffered) and salts solution (very low buffered) media
- Figure 8.** Acidification rates of yeast in OF medium (low buffered) and salts solution (very low buffered) media
- Figure 9.** Cross-sectional diagram of one channel of a conceptual flow-through microphysiometer chip for the entrapment and detection of bacteria.

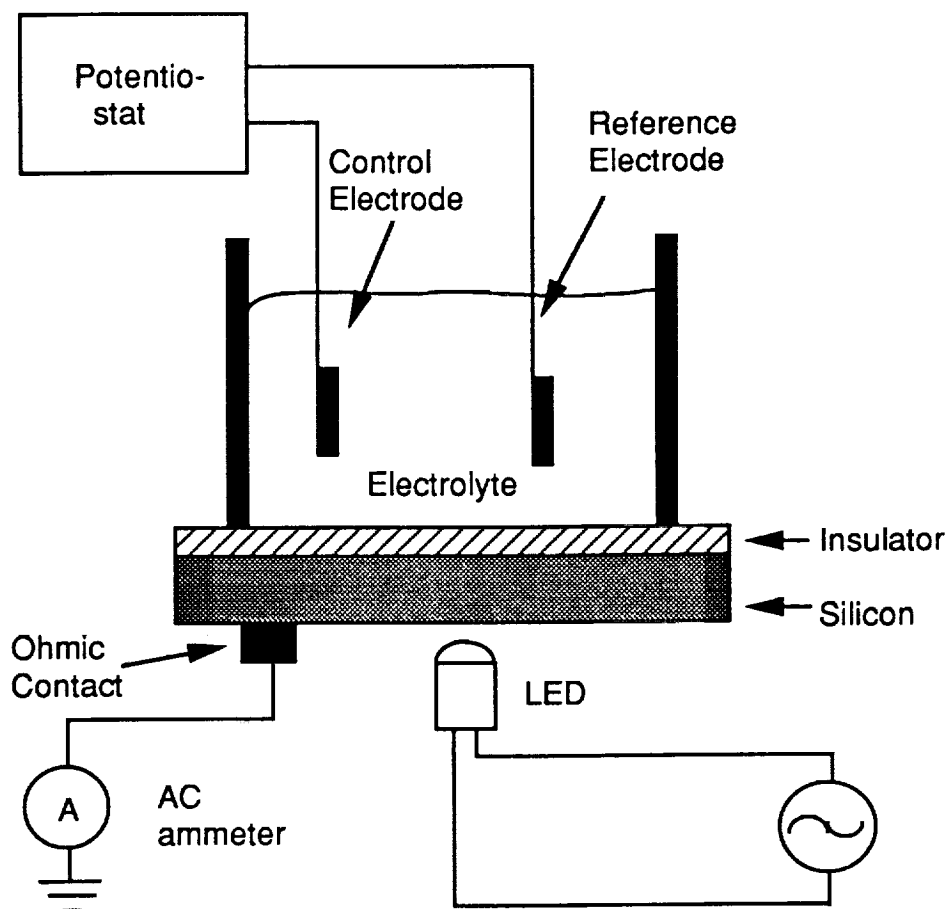


Figure 1.

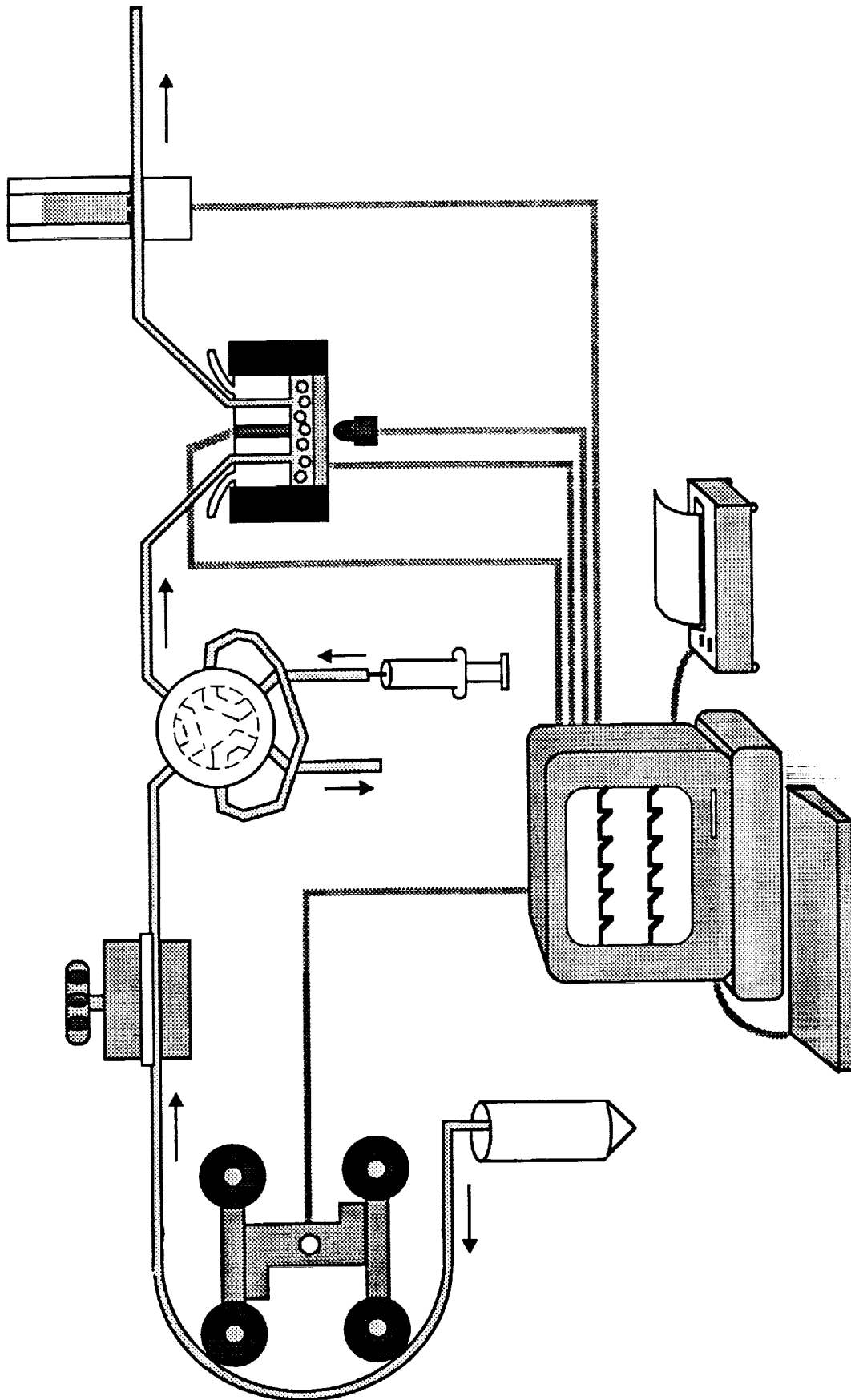


Figure 2.

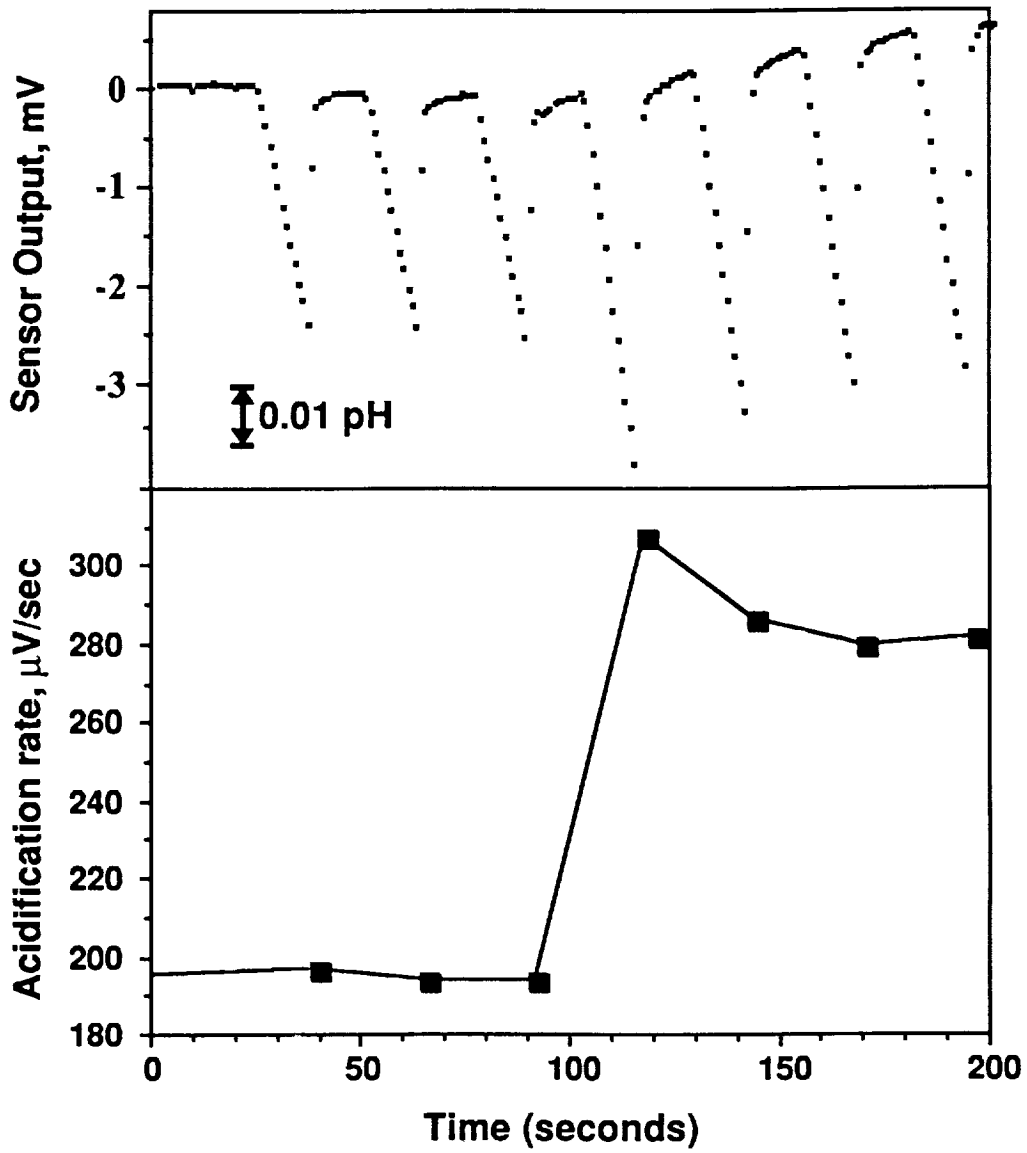


Figure 3.

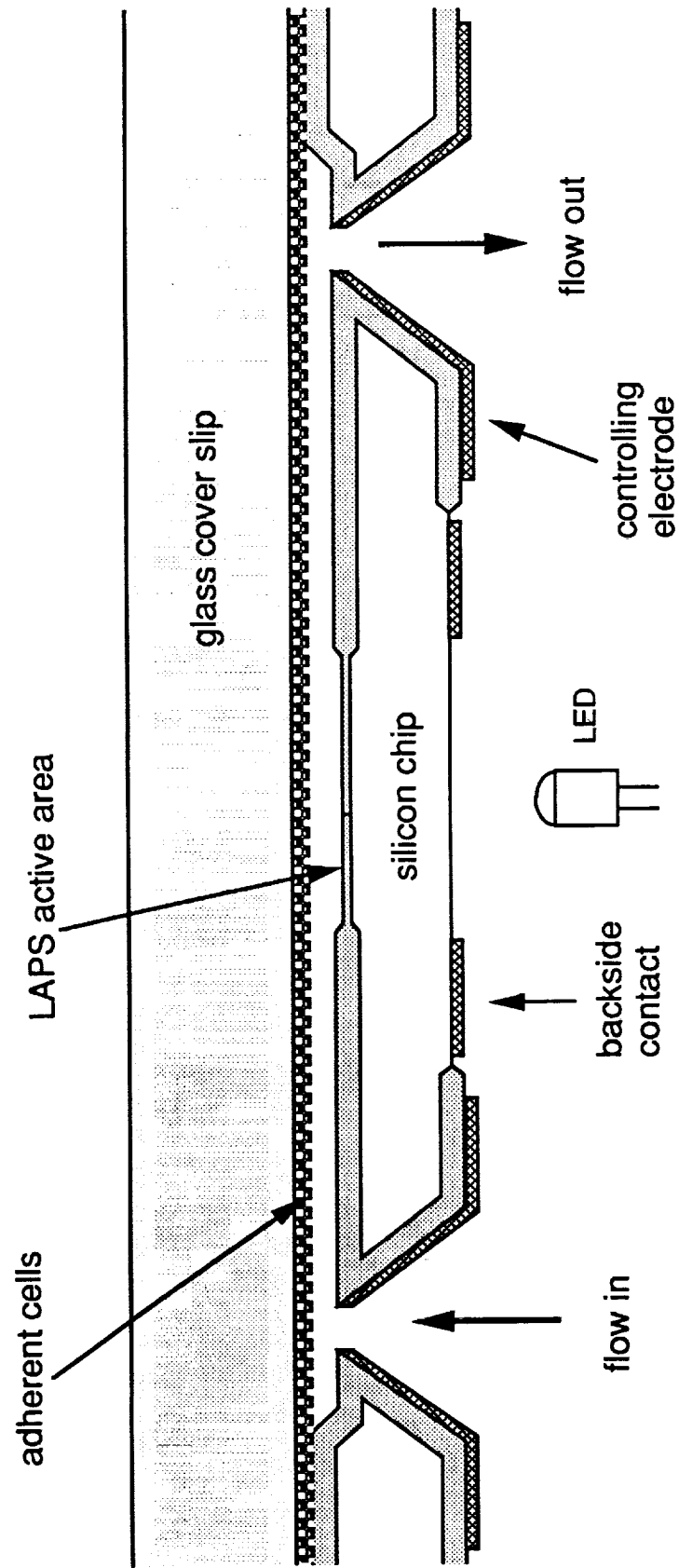


Figure 4.

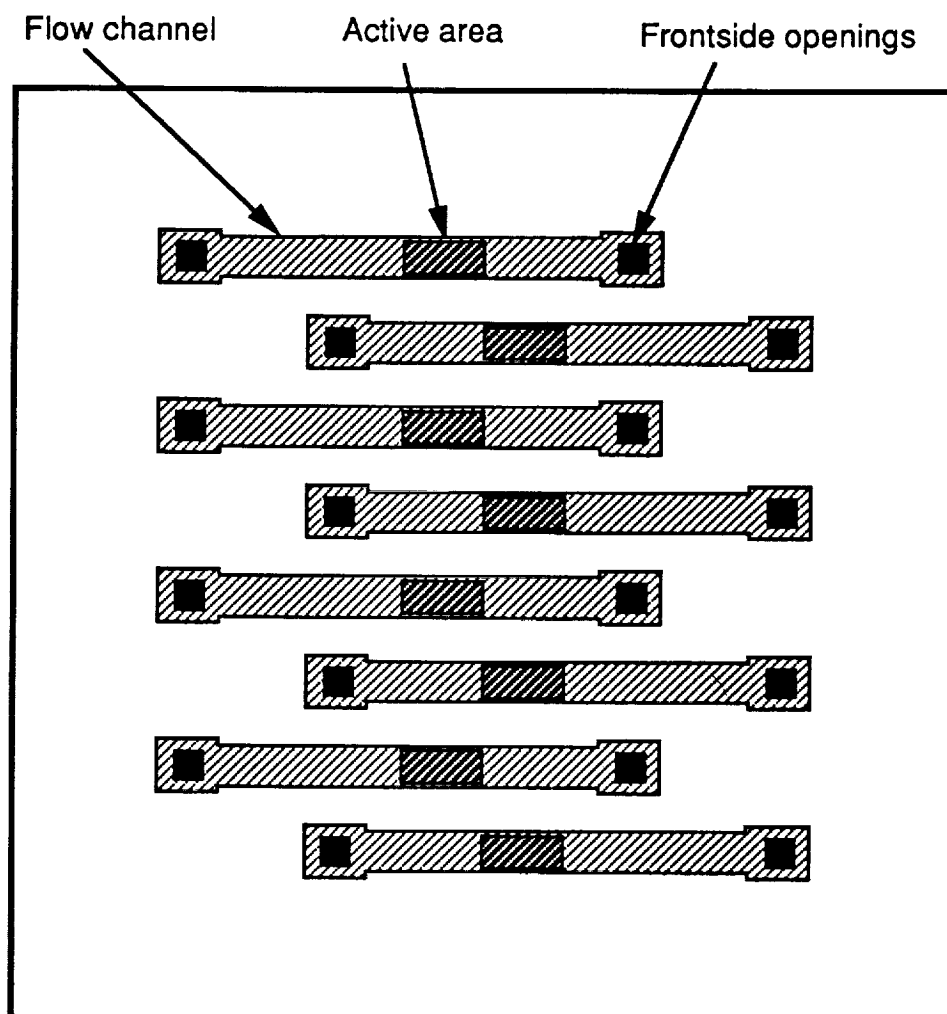


Figure 5 A.

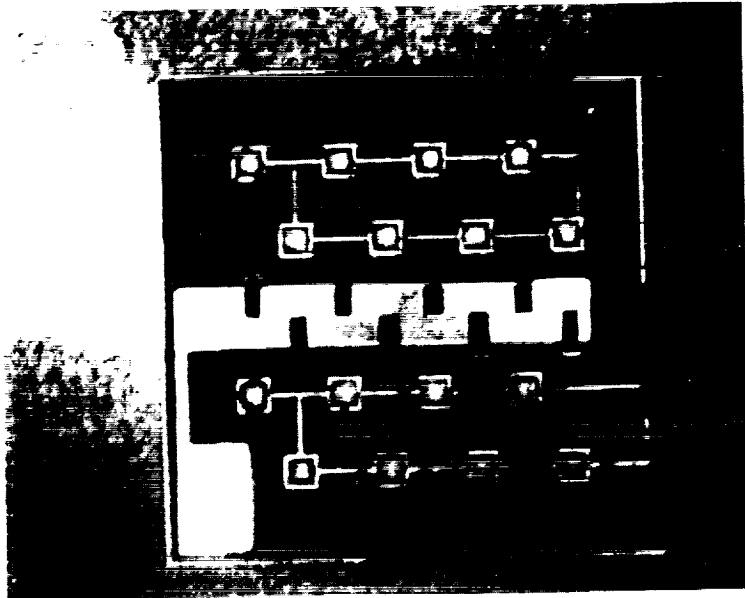


Figure 5B.

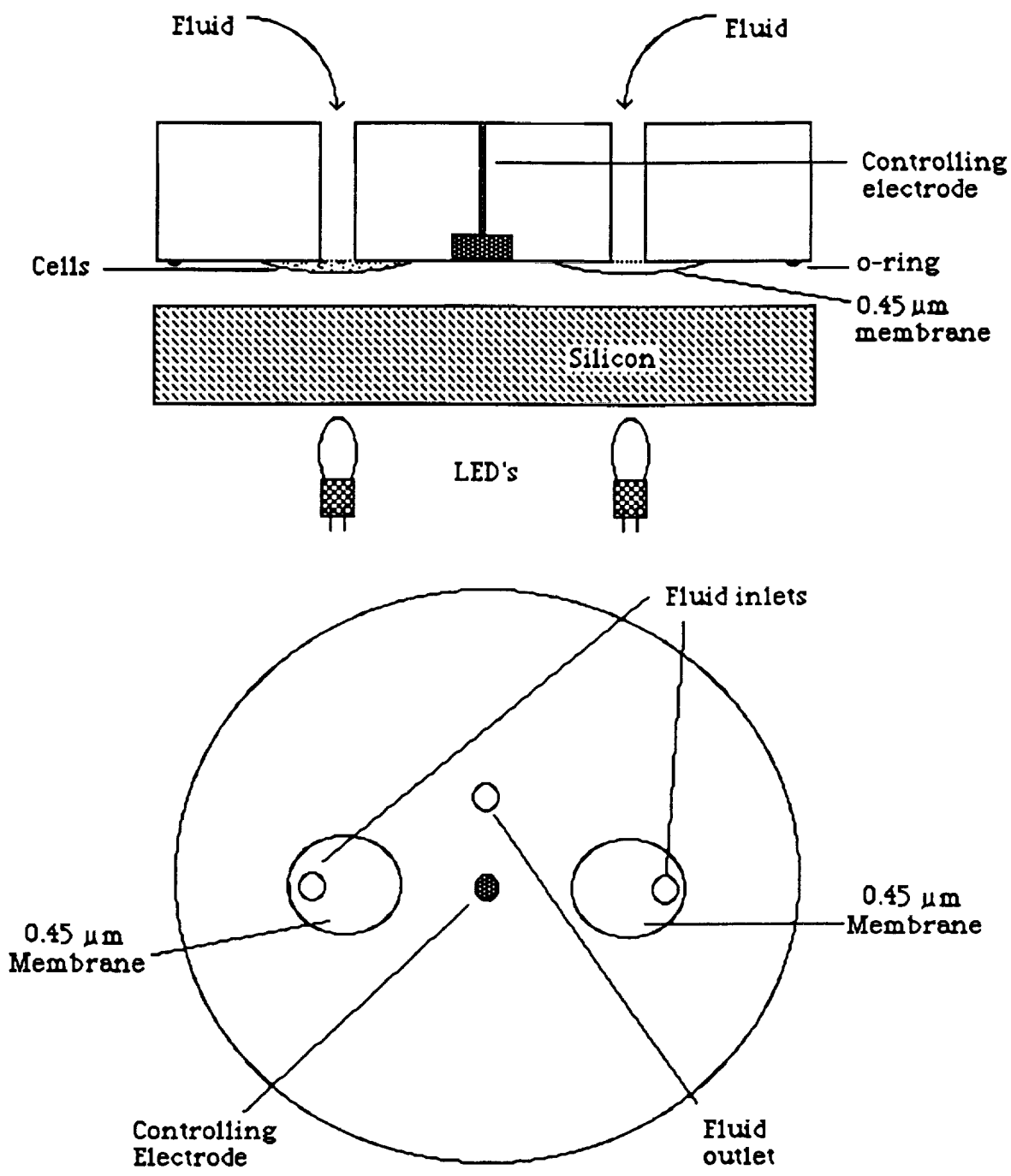


Figure 6.

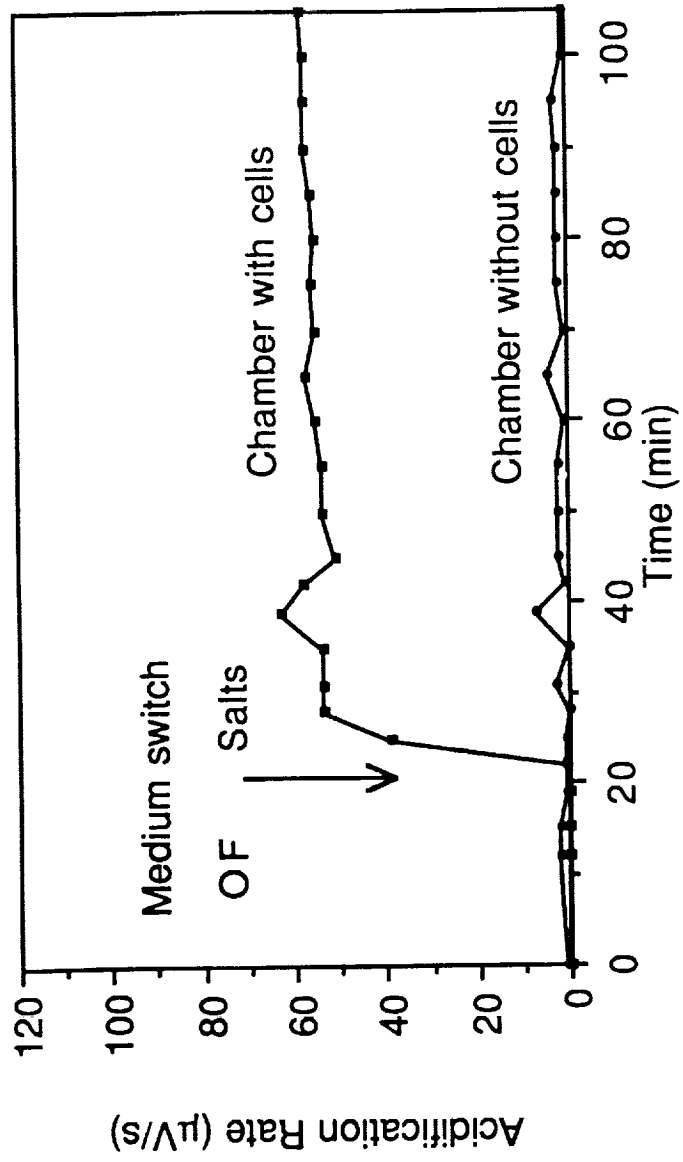


Figure 7.

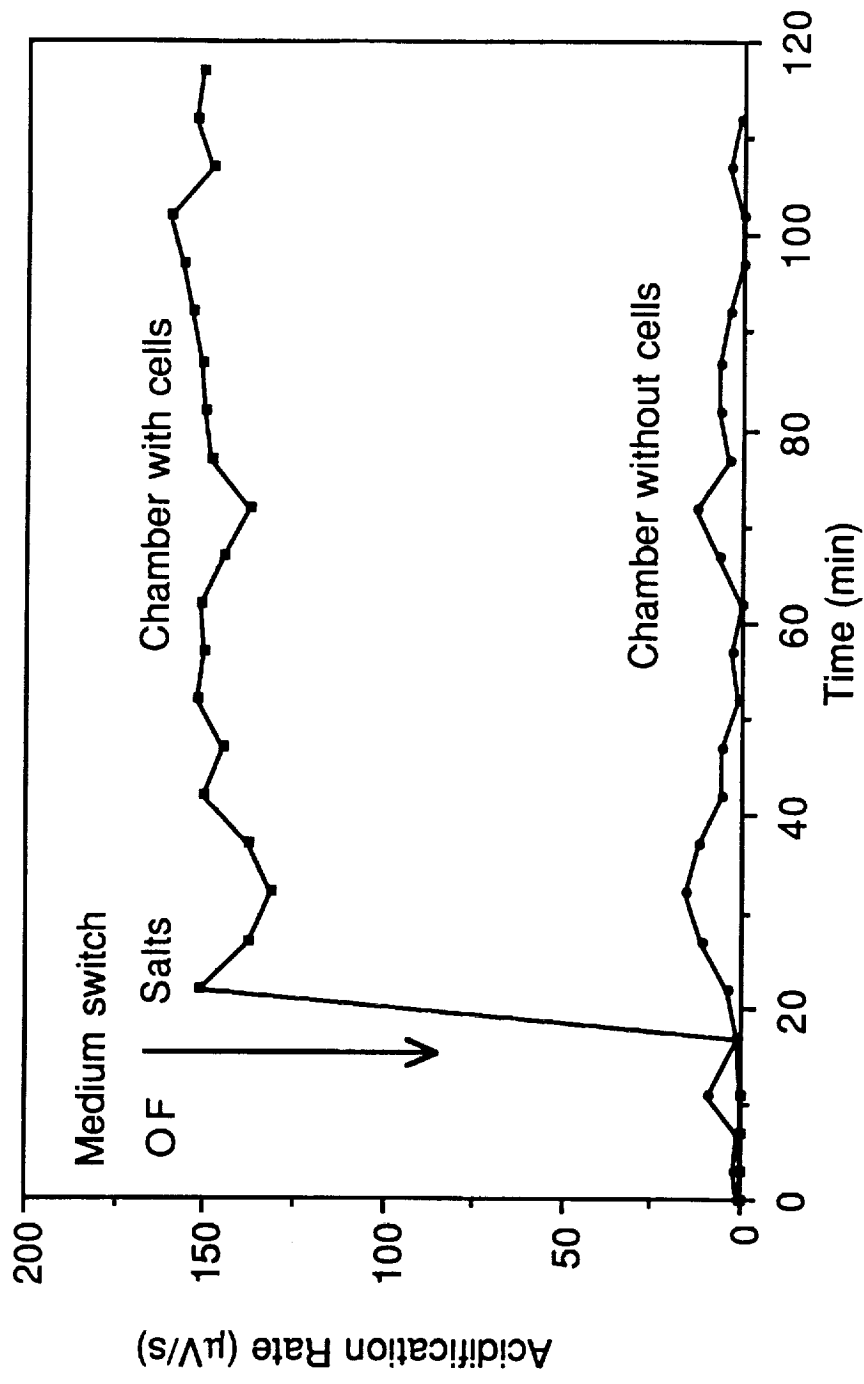


Figure 8.

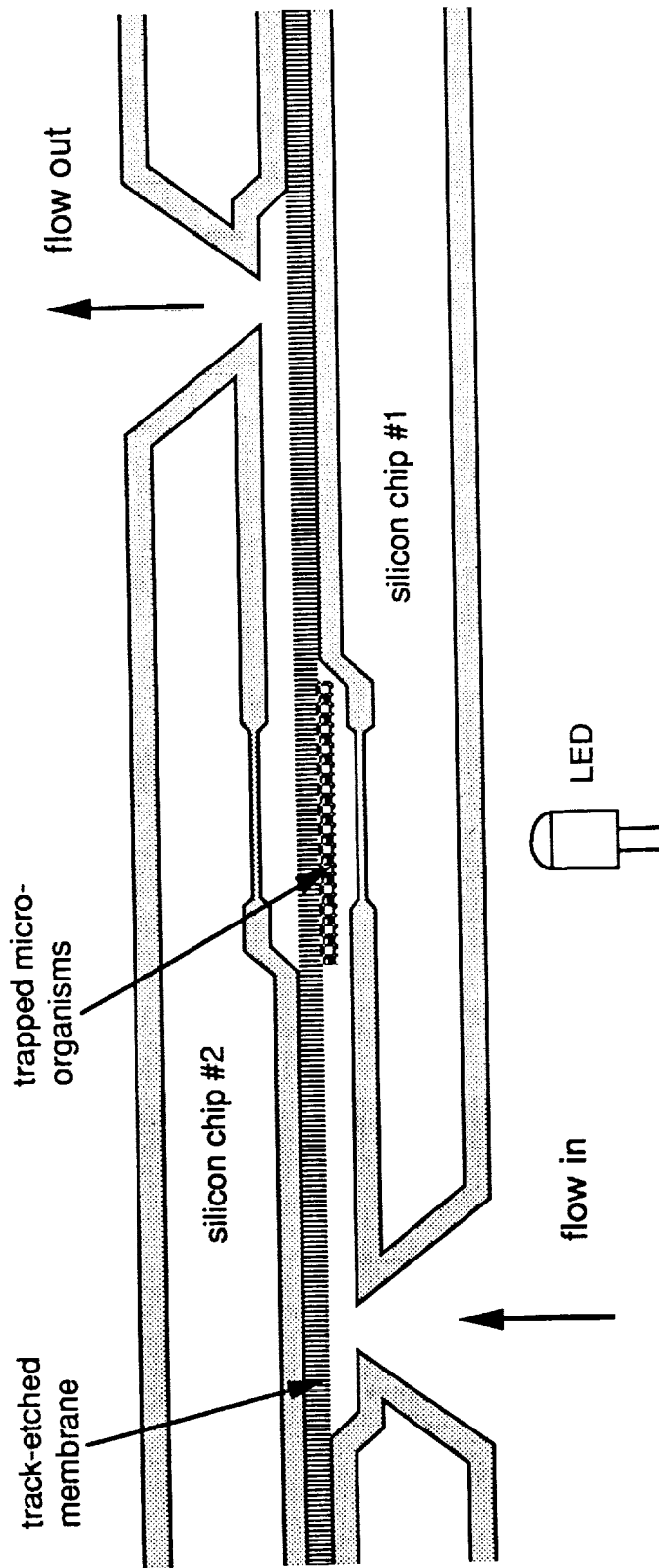


Figure 9.

Microtechnologies
and
Applications to Space Systems Workshop

MICROROVERS

ROBOTIC VEHICLES FOR PLANETARY EXPLORATION

Brian H. Wilcox
Jet Propulsion Laboratory
California Institute of Technology
Pasadena, California 91109

ABSTRACT

Future missions to the Moon, Mars, or other planetary surfaces will use planetary rovers for exploration or other tasks. Operation of these rovers as unmanned robotic vehicles with some form of remote or semi-autonomous control is desirable to reduce the cost and increase the capability and safety of many types of missions. However, the long time delays and relatively low bandwidths associated with radio communications between planets precludes a total "telepresence" approach to controlling the vehicle. A program to develop planetary rover technology has been initiated at the Jet Propulsion Laboratory (JPL) under sponsorship of the National Aeronautics and Space Administration (NASA). Prototype systems with the necessary sensing, computing, power and mobility resources to demonstrate realistic forms of control for various missions have been developed and initial testing has been completed. These testbed systems, the associated navigation techniques currently used and planned for implementation, and long-term mission strategies employing them are all described in this talk.

Difficulties Inherent in Miniaturizing
Current Rover Technologies for
Use as Planetary Explorers

Gerald P. Roston
Carnegie Mellon University

Technologies currently under consideration for planetary rovers are intended for vehicles of a certain size. As the size of the rover decreases, certain difficulties arise, including:

- The locomotion characteristics change
- Some subsystems scale non-linearly
- Some subsystems don't scale
- Certain mission objectives are unachievable

The talk will focus on how these difficulties can arise. Not being aware of these difficulties can lead to improper designs based on the false assumption that the designs scale in some linear fashion.

?



MICROMACHINING TECHNOLOGIES FOR AUTOMOTIVE APPLICATIONS

William C. Tang, Ph.D.
Senior Research Engineer
Micro-Sensors & Actuators Department
Scientific Research Laboratories
Ford Motor Company

Abstract

The rapid advancement of micromachined mechanical devices is a direct result of innovative adaptations of the well-established integrated-circuit technology. The major motivation for research in this field is the potential applications in batch-fabricated integrated sensors and silicon-based microactuators. These devices promise new capabilities and improved performance-to-cost ratio over conventional hybrid-manufactured devices. Micromachined transducers that can be fabricated compatibly with an integrated circuit process are the building blocks for integrated microsystems with added functionality, such as closed-loop control and signal conditioning. These advantages are especially attractive in the highly cost- and quality-competitive automotive industry.

In advanced vehicle design, increase in sophisticated electronic controls is inevitable. Various automotive sensors and actuators are identified to be critical to future vehicle development. Bulk- and surface-micromachining based on single-crystal and polycrystalline silicon have demonstrated great potential for satisfying automotive demands for low-cost, high-quality, and high-reliability microsensors and actuators. Several microfabricated sensors are described as examples to illustrate the applicability of micromechanics in the automotive industry.



Toward Milli-Newton Electro-and Magneto-Static Microactuators

Long-Sheng Fan

IBM research Division/ Almaden Research Center
650 Harry Road, K66/803, San Jose, CA 95120-6099

Abstract

Microtechnologies can potentially push integrated electro-and magneto-static actuators toward the regime where constant forces in the order of milli-Newton (or torques in the order of micro-Newton Meter) can be generated with constant inputs within a volume of $1.0 \times 1.0 \times 0.02 \text{ mm}$ with "conventional" technology. "Micro" actuators are, by definition, actuators with dimensions confined within a millimeter cube. Integrated microactuators based on electrostatics [2]-[5] typically have force/torque in the order of sub-micro-Newton (sub-nano-Newton-Meter). These devices are capable of moving small objects at MHz frequencies [5]. On the other hand, suppose we want to move some one cubic millimeter object around with 100G acceleration, a few milli-Newton force will be required. Thus, milli-Newton microactuators are very desirable for some immediate applications, and it challenges micromechanical researchers to develop new process technologies, designs, and materials toward this goal.

Technologies for High-Aspect-Ratio Microstructures Most of the surface-micromachined microtransducers are polysilicon-based microstructures [1]. These structures, being IC-processed flatlanders, have small vertical stiffness and, in the case of lateral gap actuators, small in-plane force/torque and relatively large fringe field components in the vertical direction [2]-[5]. Together, these cause large vertical movements which are not always desirable. Fortunately, stiffness goes as cube of the thickness, and usable force/torque go linearly with the thickness while keeping those undesirable vertical fringe fields nearly unchanged. Thus, alternative material/process for thick-structure micromachining, techniques that increase structural thickness without sacrificing the minimum in-plane features, are developed to overcome the inherent planar IC process and thickness limitations of thin film deposition techniques [6]-[11]. Among these, plated material can have some desirable properties such as ferromagnetism and lower stress as compare to as-deposited CVD or sputtered thin films. To make these metal structures, a photoresist material is deposited on a seed layer and patterned into a "stencil" through which structures are electroplated before removing the resist stencil and the seed layer underneath. The plated metals conform to the photoresist profile and form smooth sidewalls, and typical plating rates are large enough to make hundred micrometer thick structures feasible. Although synchrotron light sources preferably with storage rings are required in the deep x-ray technology [6][7], many efforts [8]-[11] have been on fine tuning some more "conventional" lithography techniques to achieve an aspect ratio toward 10:1 with less perfect resist sidewall profiles. In the following, we will call a technique fine tuned from conventional technology and produce $20 \mu\text{m}$ thick structures with $2 \mu\text{m}$ gaps an "advanced" lithography technique.

Area Efficient Approach to Milli-Newton Actuators One should fully exploit the two planar dimensions before pushing the third (out of plane) dimension further from those advanced lithography techniques. This can be achieved in an electrode tree structure with interleaved branches which connected to interdigitated fingers. In this approach, each pair of fingers form an energy storage cell, which popularizes the whole area and efficiently convert electrical field energy into force or torque, and maintain a constant output vs. input relation within a small operation range. In the case of electrostatics with advanced lithography process, one can estimate that in a 1 mm by 1 mm area, with $20 \mu\text{m}$ thick structures, $6 \mu\text{m}$ wide electrodes, $2 \mu\text{m}$ air gaps, (smaller gap is achievable with specific process [12], but a conservative value is taken here), $10 \mu\text{m}$ branch width, branch separation of $25 \mu\text{m}$ for the interdigitated fingers and $5 \mu\text{m}$ otherwise, and a maximum voltage of 100 V one can get a lateral force of 1.1 mN . The device has a top plate to hold all the mover electrode branches together. The plate could be either metal or process-compatible dielectric material. Assuming a $5 \mu\text{m}$ separation between the plate and stator electrode branches, the vertical force is 0.3 mN . The vertical stiffness, being at least three order of magnitude larger than their polysilicon version, should be able to take the load without much difficulties. Also, ground plane might not be necessary in these thick structures as observed in [11] again because of the stiffness in the vertical direction.

Magnetic Pole Finger Device Comparing magnetic actuators to electrostatic actuators with similar dimensions, the force ratio is equal to energy density ratio $[cB/E]^2$, where c is the velocity of light, B and E are the maximum magnetic and electrical field. In the sub-millimeter region, some practical values are $B=1.1T$ (B_s of Permalloy 22 wt. % Fe, 78 wt. % Ni) and $E=50$ volts across $1\ \mu\text{m}$. Here, magnetic actuators have a typical force advantage of 10 times over electrostatic ones. Isotropic magnetic materials with low H_c , low B_r and high B_s should be used for an ideal linear relation between the B and H , and for a maximum force before magnetic saturation. The proposed magnetic pole finger device is a "quasi dual" to interdigitated electrodes, and can achieve the magnetic saturation limit on the pole faces and have high linearity for fine lateral movements. Assuming the same technology as used in the electrostatic actuators described in the last paragraph except with single-branch one-mm-long Permalloy, the lateral force will be 1.6mN , and the saturation field B_s is achieved in the air gap with 70mA current through a 50 turns coil. Thus, a single magnetic branch of the tree generates more force than electric tree described in the last paragraph, and a lateral force of 16mN can be generated if deep x-ray process is used. The $2\ \mu\text{m}$ gap used in this case is more for the purpose of reducing the magnetode pitch than increasing the magnetic field in the air gap which can be achieved by increasing current in the coil. It seems to be superior to electrostatic actuators except an area efficient design is hardly feasible without field saturations. Besides, the coil structures, needed to generate mmf, will either take large area or complicate the fabrication process. Thus, the trade off is between high voltage vs. high DC power, high area efficiency vs. high energy density, and conducting material vs. soft magnetic material. In either case, by using area efficient designs, or magnetic pole finger devices, microfabricated actuators will be able to move one-cubic-millimeter objects around with an acceleration approaching 100G.

REFERENCES

- [1]. R.S.Muller,R.T.Howe,S.D.Senturia,R.L.Smith,R.M.White, Microsensors, IEEE Press, 1990.
- [2]. L.S.Fan,Y.C.Tai,R.S.Muller,"IC-processed electrostatic micromotors", Technical Digest, IEEE Int. Electron Device Meeting, San Francisco, CA, (1988) 666-669.
- [3]. M.Merengany,P.Nagarkar,S.D.Senturia,J.H.Lang,"Operation of microfabricated harmonic and ordinary side-drive motors", Proc. IEEE MEMS'90 workshop, Nappa Valley, CA, (1990) 1-8.
- [4]. W.C.Tang,T.C.H.Nguyen,R.T.Howe,"Laterally driven polysilicon resonant microstructures", Sensors and Actuators, vol. 20 (1989)25-32.
- [5]. J.J.Yao,S.C.Arney,N.C.MacDonald,J.Microelectromech. Systems 1, 14 (1992).
- [6]. E.W.Becker, W.Ehrfeld,P.Hagmann,A.Maner and D.Munchmeyer,"Fabrication of microstructures with high aspect ratios and great structural heights by synchrotron radiation lithography, galvanofarming, and plastic moulding (LIGA process)", Microelectronic Engineering 4 (1986) 35-56.
- [7]. H.Guckel,T.R.Christenson,K.J.Skrobis,D.D.Denton, B. Choi,E.G.Lovell, J.W.Lee,S.S.Bajikar and T.W.Chapman, "Deep X-Ray and UV lithographies for micromechanics", Proc. of the IEEE Solid-State Sensor and Actuator Workshop, Hilton Head, SC, (1990) 118-122.
- [8]. A.B.Frazier,M.G.Allen,"High aspect ratio electroplated microstructures using a photosensitive polyimide process", Proc. IEEE MEMS'92 workshop, Travemunde, Germany (1992) 97-102.
- [9]. G.Engelmann,O.Ehrmann,J.Simon,H.Reichl, "Fabrication of high depth-to-width aspect ratio microstructures",Proc. IEEE MEMS '92 workshop, Travemunde, Germany (1992).
- [10]. F.Shimokawa,A.Furuya, and S.Matsui, "Fast and extremely selective polyimide etching with a magnetically controlled reactive ion etching system", Proc. IEEE MEMS '91 workshop, Nara, Japan (1991) 192-197.
- [11]. Y.Gianchandani,K.Najafi,"Micron-sized, high aspect ratio bulk silicon micromechanical devices" Proc.IEEE MEMS '92 workshop, Travemunde, Germany (1992) 208-213.
- [12]. T.Furuhata,T.Hirano,K.J.Gabriel,H.Fujita, "Sub-micron gaps without sub-micron etching", Proc. IEEE MEMS '91, Nara, Japan (1991) 57-62.

Micro Structures and Micro Actuators for Implementing Sub-millimeter Robots

R.S. Fearing
Dept. of EE&CS
Univ. of California
Berkeley, CA 94720

Abstract

There are many advantages to shrinking robots and mechanical actuators to the same size as the parts to be manipulated. Extremely delicate forces can be applied, robots can be readily parallelizable, and the relative accuracy required can be markedly reduced. This talk considers some initial ideas towards implementing practical sub-millimeter robotic systems, in particular, fabrication of multi-degree-of freedom silicon actuators. The micro-robot will use silicon structures that can be folded out of the plane of the wafer. One of the major difficulties in building millimeter scale micro-robots is overcoming forces due to friction and wiring. Friction forces can be reduced by using flexures instead of rotary or linear sliding joints, and using fluid lubrication, such as an air-bearing. Mobile devices on a sub-millimeter scale working in a fluid medium could be useful for manipulation and testing of small material samples. The power requirements for such robots working at low speeds are very favorable.

1. Introduction

In the not too distant future, mobile micro-robots, such as depicted in Fig. 1, may be batch fabricated using silicon and photo-lithographic techniques. The silicon may be used for on-board intelligence, and in addition for electro-mechanical sensor and actuator systems. This micro-robot-on-a-chip has been popularized by Brooks and Flynn [1989]. These robots may see wide application in micro-tele-operation for very small inaccessible areas, and in the massively parallel handling of small biological or electromechanical elements.

An integrated system for manipulating dry parts in the plane using multiple mobile manipulation units was proposed by Pister et al [1990]. This device consists of a 1 cm^2 substrate with an air bearing to support individual 1 mm^2 platforms (see Fig. 2). The individual platforms are driven in the plane by electrostatic forces, and could carry grippers, probes for sensing, or tools for processing. By incorporating capacitive position sensing of the platforms, an integrated micro system for parts handling could be made on a single chip.

2. Three Dimensional Micro-Mechanical Structures

To be useful, silicon micro-robots will need tools to interact above the plane of the wafer, not just in it. One promising approach, called "silicon origami" [Shimoyama, 1992] or micro-hinges [Pister, et al 1991] allows planar fabrication, followed by 3 dimensional assembly of structures. This paper examines some of the new tool making capabilities obtainable with this process.

Current integrated micro systems are limited by the mostly planar micro-machining techniques available. For some applications, it will be necessary to have sensors and actuators that extend far beyond the surface of the device, e.g. micro-robots. For example, a sensor or probe may need to be sufficiently far from the sensor surface to avoid boundary layer effects.

One way to build three dimensional devices is to use new fabrication techniques, for example, Laser-assisted Chemical Vapor Deposition (LCVD). In LCVD, a focussed laser beam activates chemical species which can either locally deposit or etch a structure depending on the

gas medium used in the reaction chamber. Complicated structures such as a boron spring [Westberg et al, 1991] and stepped pits with controlled slopes [Bloomstein and Ehrlich, 1991] have been demonstrated with LCVD. Volume resolution of $1\mu m^3$ has been obtained.

While LCVD is very flexible for machining three dimensional structures, it is inherently a serial process, and hence much slower than photo-lithographic fabrication. An alternative approach is to perform conventional two dimensional processing, and then to assemble (post-process) three dimensional structures from planar components. These components could be bonded to each other using, for example, welding techniques [Fedder and Howe, 1991].

One method to simplify three dimensional assembly is to fabricate components that can be constrained to rotate or slide into place. Pister et al [1991] have shown hinged structures that can be rotated out of the plane to build three dimensional structures. (A similar method was independently developed by Shimoyama [1992]). A simple example is shown in Figure 3, with a $2\mu m$ thick plate rotated out of the plane, and held in place by friction in the hinge. A typical sensing application which requires sensors away from the surface is a hot-wire anemometer for measuring air flow. Figure 4 shows a 3 axis hot-wire anemometer, assembled by folding 3 orthogonal hinge structures out of the plane. (The anemometer structure extends approximately $200\mu m$ above the substrate). One advantage to the hinged 3 dimensional structures, compared with LCVD, is that all the planar lithographic resolution is maintained.

Standard surface micromachining, has high planar resolution, low vertical resolution, and limited vertical range (typically less than $5\mu m$). These characteristics make surface micromachining an excellent choice for planar applications, but have limited utility for three dimensional designs. We present a process in which structures are fabricated using surface micromachining, and then rotated out of the plane of the wafer on integrally fabricated hinges. The resulting structures have high resolution in both the planar and vertical directions, and have a vertical range from $10\mu m$ to more than a millimeter. This hinge-based method allows the benefits of high resolution surface lithography while providing access to the third dimension with higher vertical resolution than previously possible. Drawbacks of hinge-based designs include the need for post-process assembly, and incompatibility with typical MOS processes.

2.1. Process

The simplest version of the hinge fabrication process is a three mask, double layer polysilicon process with oxide sacrificial layers (Figure 5). A sacrificial phosphosilicate glass (PSG) layer is deposited on a bare substrate, followed by an undoped polysilicon layer (*poly1*), and a doping PSG layer. All depositions are by low pressure chemical vapor deposition (LPCVD). The polysilicon is patterned in a plasma etcher. This polysilicon etch defines the majority of the structural components, including the hinge 'pins', about which most structures will rotate. A second sacrificial PSG is deposited and both the first and second sacrificial oxides are patterned in a plasma etcher. This etch defines contacts between the second polysilicon layer and the substrate, as well as contacts between the two polysilicon layers. A second layer of polysilicon (*poly2*) is deposited and patterned. This second polysilicon etch defines the 'staples' which tie the first polysilicon layer to the substrate, as well as forming additional structural components. Finally, the sacrificial layers are removed in a concentrated HF etch, the wafers are rinsed in deionized water, and air dried at room temperature. Perforations are used in the larger structures to allow complete release in the 1 minute release etch.

Typical film thicknesses for the sacrificial and doping PSG layers are between 0.5 and $2.5\mu m$. Polysilicon layers are typically between 1 and $2\mu m$ thick. If the structures are intended to be electrically active (e.g. the anemometers discussed below), the substrate is passivated with a $0.5\mu m$ thermal oxide and $0.1\mu m$ LPCVD nitride before the first sacrificial oxide is deposited.

Dimples can be added to the polysilicon layers by patterning part way through the sacrificial layers with BHF. These dimples are not strictly necessary, but help prevent the polysilicon layers from adhering to the substrate and to each other after release. Portions of *poly1* can be anchored to the substrate, if desired, by etching contacts in the first sacrificial PSG before the *poly1* deposition.

If the total thickness of the two sacrificial oxide layers is greater than the thickness of the first polysilicon layer, then the pin of the hinge will be able to slide between the two legs of the *poly2* staple. This sort of 'play' in the hinge is not generally desirable, and can be eliminated by using a timed BHF etch immediately following the patterning of *poly1*. This timed etch undercuts the sacrificial oxide under the hinge pin, and due to the poor step coverage of low temperature LPCVD oxide, indirectly reduces the second sacrificial oxide thickness near the pin as well. This results in a partially encased *poly1* pin, under (and almost inside) a *poly2* staple. Since the hinge location is now determined by the *poly1* pin rather than the *poly2* staple contacts, we refer to this as a 'self-aligned' pin.

2.2. Design

Given the three mask process above, it is possible to make several different types of hinges, as illustrated in Figure 6. The simplest of these is the 'substrate hinge', which consists of a *poly1* plate and hinge pin constrained by a *poly2* staple. The staple is attached to the substrate at two contact points, and the plate is free to rotate a full 180 degrees off of the substrate. Note that the freedom of the plate to rotate may be limited by the geometry of the pin and staple. If the width of the pin is greater than the sum of the thicknesses of the *poly1* and sacrificial oxide layers, then the pin will be unable to rotate a full 90 degrees without contacting the substrate and staple.

The substrate hinge is used to hinge *poly1* plates to the substrate. To hinge plates to each other requires a different type of hinge. Two *poly1* plates can be hinged together using a 'scissor hinge'. *poly2* strips are attached between interdigitated *poly1* fingers, preventing the two *poly1* plates from pulling apart, and allowing the plates a relative rotation of roughly 180 degrees. This type of hinge can only fold 'concave-down'. A similar scissor hinge, illustrated in the figure, hinges two *poly2* plates together and folds 'concave-up'.

Unlike substrate hinges, there is no 'pin' in a scissor hinge. Given the typical film thicknesses used, a substrate hinge which is intended to rotate 90 degrees must have a pin which is no more than 2 μm wide. Scissor hinge geometries are not constrained by the film thickness of the structural or sacrificial layers. As a result, scissor hinges can be made with all geometries much wider than 2 μm , making them much stronger than substrate hinges.

2.3. Assembly

After the release etch, the structures are rotated into their final positions. This is currently accomplished at a probe station using standard electrical probing equipment to rotate the structures into position. A sharp probe tip is slid under a released structure and raised to lift the structure off of the surface of the wafer, and rotate it into the desired position. By inter-locking two hinged structures, the final position of the structures can be accurately controlled.

Assembly is a labor intensive process (e.g. the gripper requires roughly 10 minutes for assembly), however we are working on designs which require no manual assembly. Hydrodynamic forces may prove to be very useful in automating the assembly process. We have observed that many structures rotate 90 degrees or more during the post release rinse, and a directed stream of air from a capillary tube has a similar effect on released structures.

2.3.1. Micro Probe

Another out of plane sensing capability provided by the hinge structure is shown in Figure 7. A probe for electrical testing can be made with an intrinsic spring, and electrical contact to substrate through hinges. This structure has not been tested.

2.3.2. Parallel-Plate Gripper

Recently, planar (roughly 2 μm thick) micro-grippers have been fabricated with a gripping range on the order of 10 μm , [Kim, Pisano, Muller, 1991]. The hinge technology offers the opportunity to produce micro-grippers of a scale difficult to obtain with previous micro-machining processes. Grip surface dimensions and gripper openings measured in hundreds of microns are possible, while actuating resolution is on the order of microns. The structure in Figure 8 is a parallel-plate gripper consisting of four separate pieces. The two jaws of the gripper are folded up separately and locked in place at one end by another plate with two slots in it. The jaws are suspended at the end of 400 μm -long beams, each of which is 20 μm -wide. A 1 mm-long tendon travels from each jaw and locks into the vertical handle. When the handle is pulled back, the tendons pull the jaws open. When the handle is released, the spring force of the support beams closes the jaws. In the 'closed' (rest) position the jaws are actually 100 μm apart. Over 100 cycles of up to 0.5 mm opening have caused no damage to the gripper.

2.4. Actuation of Hinge Structures

The rotary hinge joints have very high friction, and elastic joints, such as a cantilever beam, will be much easier to drive. There are several options for actuating these elastic joints, including shape-memory-alloy [Ikuta, 1990], electromagnetic [Wagner and Benecke, 1991], and electrostatic drives. Although the forces are very small, low voltage electrostatics is perhaps the easiest to implement on the hinge process with few additional masks. Figure 9 shows a single degree-of-freedom actuator, which consists of a movable plate supported cantilever beam, and a fixed plate.

A useful range of motion for this actuator is 0° to 10° . (Assume that the hinge joint is locked in place). When a potential difference is applied between the fixed and moving plate, the plates are attracted to each other. To estimate the order of magnitude of this force, we can assume that the plates are approximately parallel with a gap of 10 μm . A typical plate size would be 200 μm ($= a$) square, with plate thickness 2 μm ($= h$). Then the electrostatic force normal to the plate (F_z) for 10 volts applied between the plates, is given by

$$F_z = \frac{\partial}{\partial z} \frac{1}{2} CV^2 = \frac{V^2 \epsilon_0 a^2}{2 h^2} = 2 \times 10^{-7} N . \quad (1)$$

The actuator is unidirectional without the restoring force of the cantilever. The cantilever spring should be soft for the plate to be "pulled-in", yet strong enough to support the weight of the plate. Using a 2 μm thick polysilicon layer, a 200 μm long beam of square cross section will have appropriate compliance. The approximate spring constant for such a polysilicon beam will be about $4 \times 10^{-2} \text{Nm}^{-1}$ [Lin et al, 1991]. The mass of the plate is $m_{plate} = \rho_{Si} l \times w \times d$, where ρ_{Si} is the density of silicon, $2.3 \times 10^3 \text{Kg m}^{-3}$. For a square plate, 200 μm on each edge, 2 μm thick, the mass of the plate is approximately $2 \times 10^{-10} \text{Kg}$, with weight of $2 \times 10^{-9} \text{N}$. The displacement of the cantilever beam due to the weight of one plate is:

$$\delta = \frac{K_{beam}}{m_{plate} g} = \frac{2 \times 10^{-9} N}{4 \times 10^{-2} \text{Nm}^{-1}} = 5 \times 10^{-8} m , \quad (2)$$

which is negligible, only 0.1% of the unactuated gap. Because of the inverse square relationship

between F_z and the gap, the 10 V potential will be sufficient to drive the plates together.

To build multi-degree of freedom robots, a network of these single degree-of-freedom actuators and elastic joints needs to be interconnected, for example, as proposed by Shimoyama et al [1991]. A possible interconnection scheme for these actuators is shown in Figure 10, where the left figure shows a stack unactuated, and the right figure shows an actuated stack. The plates are supported by cantilever beams that connect to scissor hinges on each side of the plate. Although the figure shows a planar manipulator, alternate plates could be orthogonally stacked in the plane, to give a 3 dimensional manipulator. For 200 μm plates, the gravitational force for even a stack of 20 plates would cause only a 10% deflection of the bottom plate in the stack.

There are many problems to building this type of stacked structure using the hinge process. A recent paper by Pister [1992] provides some strategies for building this device. Thin and flexible polysilicon ribbon cable can be fabricated to wire up all the plates to external connections. These connections would loop around the scissor hinge and not exert any force when operation. Self-assembly catches can be added so that structures fold up and latch into place during sufficient excitation, for example, by a rinsing step. Polysilicon piezo-resistive strain gauges can be used to measure force or position of the joints (the bending of the cantilever), and thin film transistors can be added to the plates to control plate addressing. Many problems remain to be worked out, but there is hope for an implementable stacked actuator design.

3. Summary

A new surface micromachining process has been developed which allows the fabrication of a wide variety of three dimensional structures. The three mask process allows structures to be hinged to the substrate as well as to each other. By fabricating the structures in the plane of the wafer, conventional lithographic techniques can be used to define features with high resolution. These structures can then be rotated out of the plane of the wafer and assembled into three dimensional designs with detailed features in three dimensions. Several structures have been fabricated and tested, including a hot wire anemometer and a gripper. Given the variety of electrical and mechanical devices which can be integrated with this relatively simple process, the outlook for sophisticated electromechanical systems, including micro-robotics, seems promising.

Acknowledgments

Partial funding for this research was provided by the Semiconductor Research Corporation under grant 91-DC-008, the Berkeley Sensor and Actuator Center, and the National Science Foundation under grants NSF-IRI-9157051. The author thanks K.S.J. Pister for his valuable contributions and collaboration.

References

- [1] T.M. Bloomstein and D.J. Ehrlich, "Laser Deposition and Etching of Three Dimensional Microstructures" *1991 Int. Conf. on Solid-State Sensors and Actuators (Transducers '91)*, June 1991, San Francisco, CA, pp. 507-511.
- [2] R.A. Brooks and A.M. Flynn, "Rover on a Chip", *Aerospace America*, October 1989, pp 22-26.
- [3] G.K. Fedder and R.T. Howe, "Thermal Assembly of Polysilicon Microstructures", *IEEE Micro Electro Mechanical Systems*', pp. 63-68, Nara, Japan, Feb. 1991

- [4] C.J. Kim, A.P. Pisano, and R.S. Muller, "Overhung Electrostatic Microgripper" *1991 Int. Conf. on Solid-State Sensors and Actuators (Transducers '91)*, June 1991, San Francisco, CA, pp. 610-613.
- [5] L. Lin, A.P. Pisano, and A.P. Lee, "Microbubble Powered Actuator", *1991 Int. Conf. on Solid-State Sensors and Actuators (Transducers '91)*, June 1991, San Francisco, CA, pp. 1041-1044.
- [6] K.S.J. Pister, R.S. Fearing, and R.T. Howe, "A Planar Air Levitated Electrostatic Actuator System", *IEEE Workshop on Micro Electro Mechanical Systems*, Napa Valley, CA Feb. 12-14 1990.
- [7] K.S.J. Pister, M.W. Judy, S.R. Burgett, and R.S. Fearing, "Microfabricated Hinges: 1 mm Vertical Features with Surface Micromachining", *IEEE Transducers '91*, San Francisco, CA June 1991.
- [8] K.S.J. Pister, "Hinged Polysilicon Structures with integrated CMOS TFTs", to appear, Hilton Head 92, Solid State Sensor and Actuator Workshop.
- [9] I. Shimoyama, H. Miura, K. Suzuki, and T. Yasuda, "Artificial Insects (Silicon Micro-Robots)", 6th Int. Conf. on CAD/CAM, Robotics, and Factories of the Future, London 1991.
- [10] H. Westberg, M. Bowman, S. Johansson, and J. Schweitz, "Truly 3 dimensional Structures Microfabricated by Laser Chemical Processing", *1991 Int. Conf. on Solid-State Sensors and Actuators (Transducers '91)*, June 1991, San Francisco, CA, pp. 516-519.

Figure 1. Idealized Micro-Robot Operating in Fluid Medium

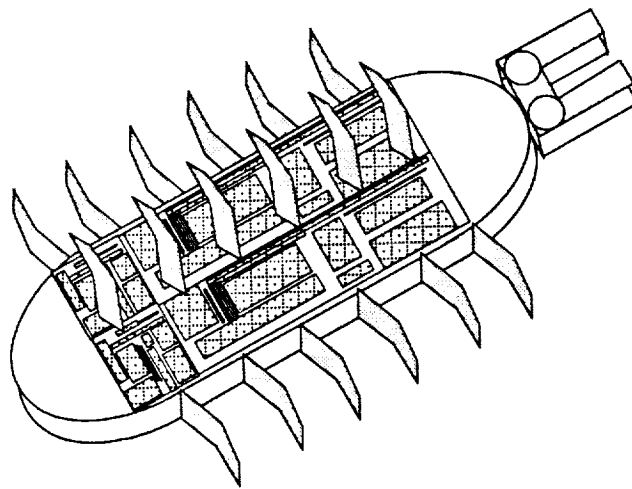


Figure 2. Probing platforms floating on air bearing

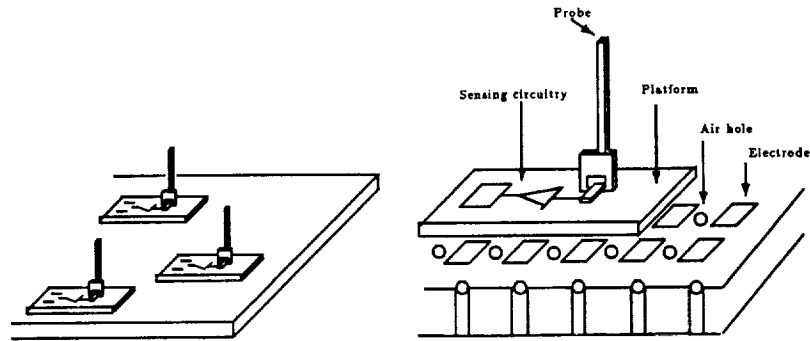


Figure 3. Polysilicon beam with polysilicon staple-type hinge folded out of plane.

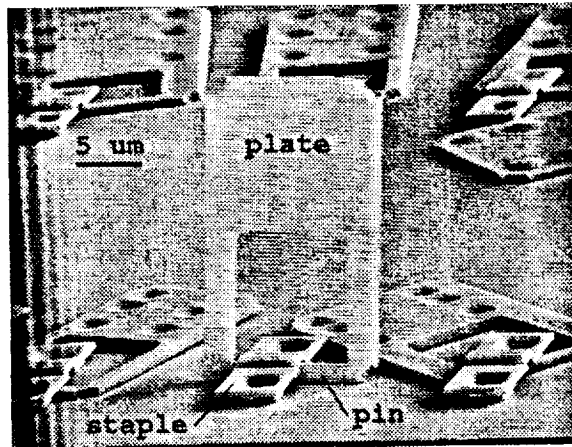


Figure 4. Three axis hot-wire anemometer constructed from 3 hinged sections

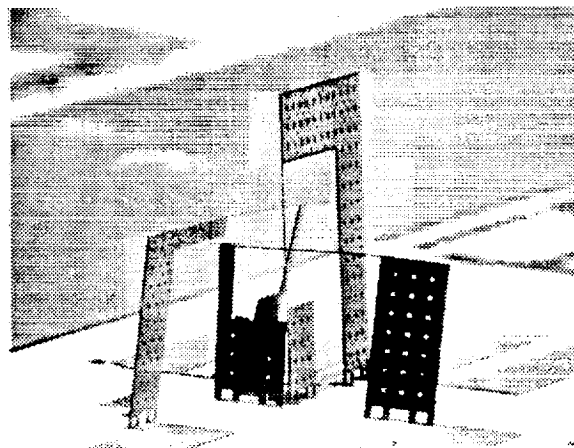


Figure 5. The hinge process sequence. At top is shown a cross section after poly 1 has been patterned and the second layer of PSG deposited. Following this, contacts are etched through both layers of PSG. Next, poly-2 is deposited and patterned. Finally, the oxide is removed in a sacrificial etch, and the poly-1 layer is free to rotate out of the plane of the wafer.

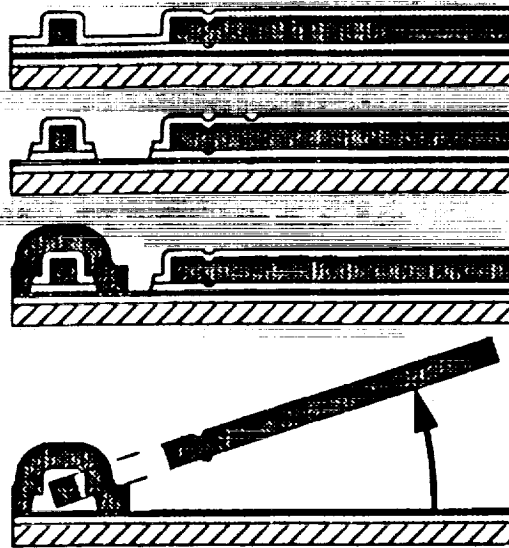


Figure 6. Three basic hinge types (A) A substrate hinge, which is used to hinge released structures to the substrate. (B) A 'concave down' scissor hinge, used to hinge released structures to each other. (C) A 'concave up' scissor hinge.

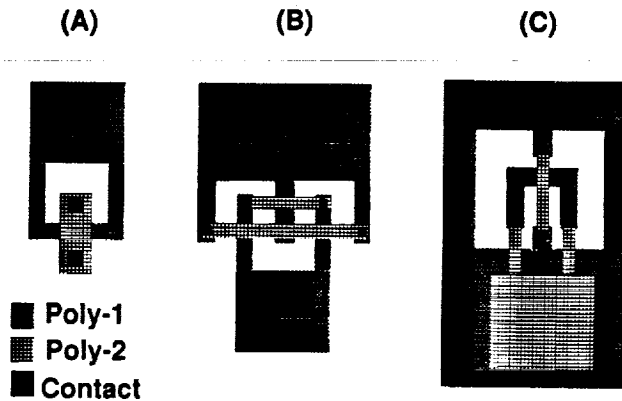


Figure 7. A Compliant microprobe. The total length of the spring is 3 mm.

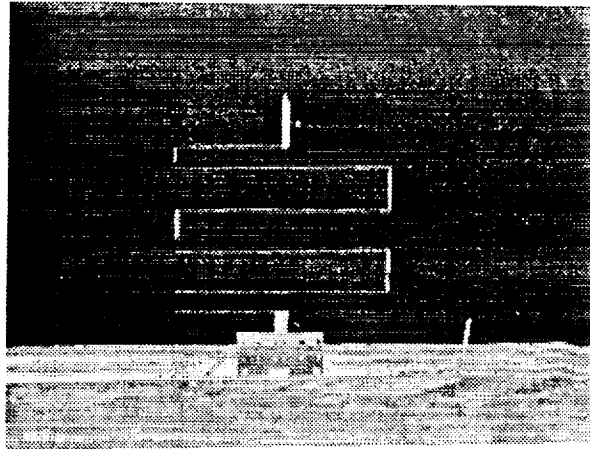


Figure 8. A parallel plate gripper. The gripper is normally closed, with a gap of 100 μm between the plates. Pulling the vertical bar (left side) causes the jaws to open. Opening of 0.5 millimeter is possible with no damage to the device.

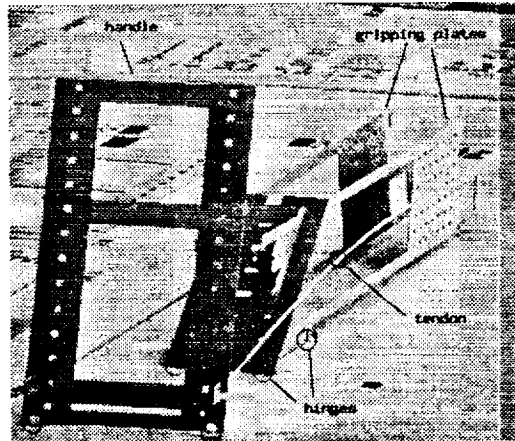


Figure 9. Single hinge type actuator (1 DOF)

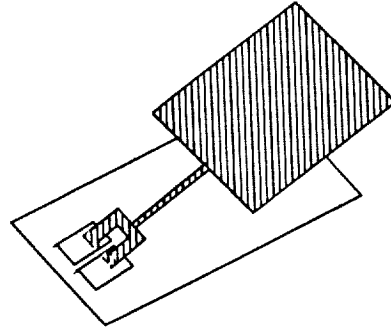
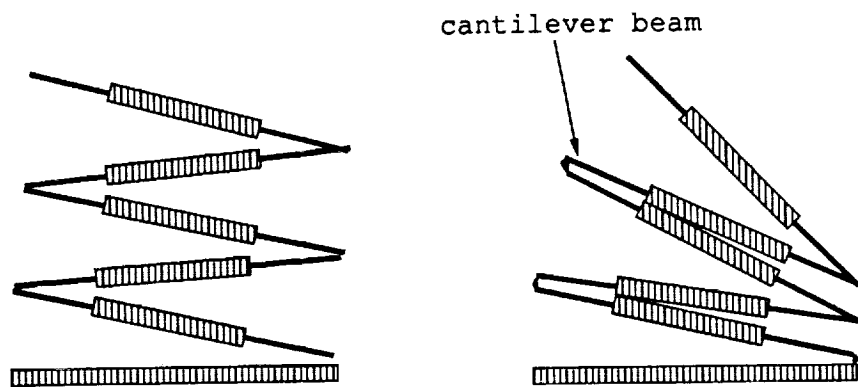


Figure 10. Stacked hinge type actuators



Microtechnologies
and
Applications to Space Systems Workshop

**MICROTECHNOLOGIES
OF THE FUTURE**

THE UNIVERSITY OF CHICAGO

1964

THE UNIVERSITY OF CHICAGO LIBRARY

100 EAST EAST

CHICAGO, ILL.

THE UNIVERSITY OF CHICAGO LIBRARY

100 EAST EAST

CHICAGO, ILL.

Micromachined Electron Tunneling Infrared Sensors

T.W. Kenny, W.J. Kaiser, J.A. Podosek, H.K. Rockstad, and J.K. Reynolds

Center for Space Microelectronics Technology

Jet Propulsion Laboratory, California Institute of Technology, Pasadena, CA 91109

Introduction

Many infrared detectors have been developed over the last 40 years.¹⁻³ In most cases, they may be classified as either quantum or thermal detectors, depending upon whether the incoming radiation is converted to excitations which are collected, or is converted to heat and detected through changes in temperature.⁴ Quantum detectors must separate optically generated excitations from thermally generated excitations, and therefore require cooling for detection of infrared photons ($\lambda > 5 \mu\text{m}$). In contrast, thermal detectors which operate at room temperature can be very sensitive to infrared radiation. Because of restrictions on power consumption or the availability of cryogenics, many applications are driven towards the use of uncooled thermal infrared detectors.

The development of thermal infrared detectors is limited by the availability of sensitive, low-mass thermometers. Phase transitions in solid state materials provide the sensitive thermometer for detectors such as pyroelectrics and HiTc bolometers. Other thermal infrared detectors have been based on thermocouple thermometers, or in the case of the Golay Cell, the thermal expansion of a small volume of trapped gas. In general, the thermodynamical optimization of these detectors has been carried out for many years and is nearly complete.

All thermal infrared detectors may be parameterized by the heat capacity of the active element, the thermal conductance between the active element and the surroundings, the response coefficient of the thermometer, and the noise spectra which arise from the anticipated noise sources. Using these parameters, it is straightforward to predict performance of any infrared sensor. It is possible, for example, to calculate the responsivity of a thermal infrared detector from these parameters. The user community is most interested in calculations of the Noise Equivalent Power (NEP), which is used to evaluate the utility of the proposed detector.

New thermal infrared detectors may be developed whenever a new solid-state thermometer, or a new fabrication technology becomes available. Recent examples include the use of silicon micromachining to construct miniature infrared detectors based on thermal isolation of pyroelectric materials, metal-film thermometers, high-temperature superconducting oxide films, and thermocouples. In some cases, these devices offer performance characteristics that approach fundamental limitations to the sensitivity of infrared detectors.

The Golay Cell consisted of a small cavity filled with gas at room temperature. The cavity is separated from the surroundings by a window and a thin, flexible membrane.⁵⁻⁷ The membrane was coated on one side with a thin metallic film, which has significant absorption throughout the infrared whenever the sheet resistance of the film is approximately half of the impedance of free space.⁸⁻¹⁰ The trapped gas in the Golay cell was heated by contact with the membrane, and expanded thermally, which forced the membrane to deflect outward. This deflection is usually detected with optical or capacitive displacement transducers.¹¹ At present, these detectors are bulky, fragile, difficult to fabricate, and expensive. Nevertheless, they have been widely used, primarily because of their improvement in NEP over all other uncooled detectors in the mid to far infrared.

The advantage to operation of an infrared detector in this manner may be described as follows. All thermal infrared detectors benefit from reduction in the heat capacity of the thermometer. In the Golay cell, the gas coupled to the membrane displacement represents an easily manufactured, very low heat capacity thermometer. In addition, this thermometer is very sensitive, in that the volume of an ideal gas at room temperature changes by 0.3% for each 1K change in temperature. The low heat capacity and high sensitivity combine to make the Golay cell infrared detector as much as 5-10 times more sensitive than typical pyroelectric detectors.

Attempts to miniaturize the Golay cell for incorporation into focal plane arrays have been unsuccessful because of scaling laws which relate the sensitivity of conventional miniature displacement transducers and their active area. The resulting detectors were interesting, but not as useful as arrays of pyroelectric or bolometric detectors.

Prototype Tunneling Infrared Sensor Theory

With the above considerations in mind, we have begun the development of an improved Golay cell. This new sensor is constructed entirely from micromachined silicon components. In this device, a silicon oxynitride (SiO_xN_y) membrane is deflected by the thermal expansion of a small volume of trapped gas. To detect the motion of the membrane, we use an electron tunneling displacement transducer.^{12,13} This sensor, like the assemblies used in Scanning Tunneling Microscopy (STM),^{14,15} detects electrons which tunnel through the classically forbidden barrier between a tip and a surface. As in the STM, the electron current is exponentially dependent on the separation between the tip and the surface. The sensitivity of tunneling transducers constructed and operated by our group is typically better than $10^{-3} \text{ \AA}/\sqrt{\text{Hz}}$. Through use of the electron tunneling transducer, the scaling laws which have prevented the miniaturization of the Golay cell are avoided. This detector potentially offers low-cost fabrication, compatibility with silicon readout electronics, and operation without cooling. Most importantly, this detector may offer better sensitivity than any other uncooled infrared sensor, with the exception of the original Golay Cell.

The responsivity and noise of the electron tunneling infrared detector may be calculated as for any thermal detector. It is important to note that this particular prototype was not optimized to achieve the best possible sensitivity.

A cavity of area $(0.1 \text{ cm})^2$ and thickness 0.015 cm, filled with air at atmospheric pressure is trapped between a pair of silicon wafers, one of which has been etched through to a 0.5- μm thick silicon oxynitride membrane as shown in Fig 1. The outer surface of the membrane is coated with $\sim 70 \text{ \AA}$ of gold to serve as an electrode for tunneling as well as an efficient absorber of infrared radiation. The heat capacities of the gas, membrane, and gold films sum to $C = 7.9 \times 10^{-7} \text{ J/K}$, and the thermal conductances between these elements and the surroundings sum to $G = 1.9 \times 10^{-4} \text{ W/K}$. In this case, the heat capacity is dominated by the membrane, while the thermal conductance is dominated by conduction through the trapped gas to the window. The mechanical properties of the membrane may be calculated, given its dimensions.¹⁶ The coefficient of motion (change in position per unit change in temperature) of the center of the membrane is approximately $1 \times 10^{-4} \text{ cm/K}$, assuming that air is an ideal gas at room temperature and pressure.

A tunneling transducer is used to measure the deflection of the membrane. When biased at fixed voltage, the tunneling current has the following dependence¹⁷ on tip-substrate separation:

$$I = I_0 \exp(-\beta \sqrt{\Phi} s), \quad (1)$$

where Φ is the tunnel barrier height in eV, s is the tip-membrane separation in Å, and β is a conversion factor with a value of $1.025 \text{ eV}^{-1/2} \text{ \AA}^{-1}$. The temperature coefficient (fractional change in current per unit change in temperature) of the trapped gas and tunnel sensor is $\alpha = (1/I)(\partial I/\partial T) = 2.3 \times 10^4/\text{K}$, for $\Phi = 5 \text{ eV}$. This large temperature coefficient is a product of the large thermal expansion of gases at room temperature, and the extreme sensitivity of vacuum tunneling to changes in relative position. For comparison, α for a good resistance bolometer is of order unity.

With this information, it is possible to calculate the response of the sensor per unit input power. The responsivity of the electron tunneling infrared detector is given by :

$$S = \frac{I \alpha}{(G^2 + (\omega C)^2)^{1/2}} = 1.2 \times 10^{-1} \text{ A/W} \quad (\omega=0). \quad (2)$$

It is important to remember that the responsivity is not in itself a useful figure of merit for comparisons between infrared sensors because it contains no information about the noise of the sensor.

We shall consider the contributions of several kinds of noise. For each source, an expression for the square of the Noise Equivalent Power, $(\text{NEP})^2$, appears. The NEP is defined as the signal power that would be detected with a unity signal-to-noise ratio in the presence of a given source of noise. The expression for the NEP refers to a bandwidth of 1 Hz. Since the noise sources being considered are broadband, reducing the bandwidth of the measurement (increasing the integration time) is expected to improve the sensitivity. An absorber efficiency of 100% is assumed in this expression.

The NEP of a thermal infrared detector is given by: ¹⁸

$$(\text{NEP})^2 = 4k_B T^2 G + \frac{2e(G^2 + (\omega C)^2)}{I \alpha^2} + 16A\sigma k_B T^5. \quad (3)$$

The first term arises due to temperature fluctuations in the trapped gas, and is common to all thermodynamic objects which are isolated from a temperature reference by a fixed thermal conductance. The second term is due to shot noise in the tunnel current, and is equivalent to a Johnson noise term which is commonly found when analyzing resistance bolometers. The third term is due to statistical fluctuations in the arrival of photons, and is the fundamental limit to the sensitivity of all thermal infrared sensors. In

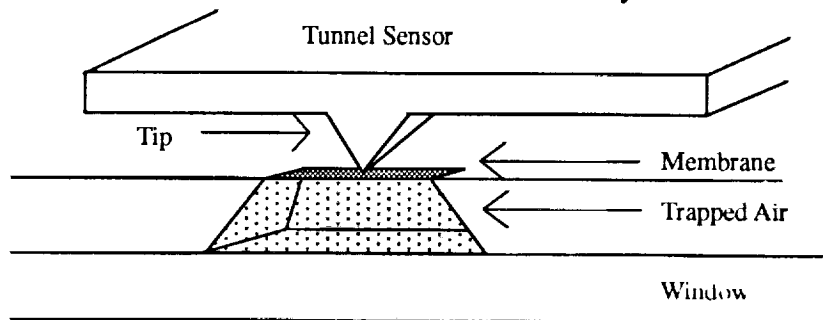


Fig. 1 This drawing shows the design of the prototype tunneling infrared sensor. Infrared radiation, incident from the bottom of the figure, is absorbed in a thin metal film deposited on the membrane and induces thermal expansion in the trapped gas. The deflection of the membrane is monitored by the tunneling transducer.

this expression, $k_B = 1.38 \times 10^{-23}$ W/K is Boltzmann's constant, T is the operating temperature, ω is the modulation frequency, A is the absorbing area of the detector, and $\sigma = 5.67 \times 10^{-12}$ W/(cm² K⁴) is the Stefan-Boltzmann constant.

It is important to note the role played by the large response coefficient, α , in this expression. Since α is larger than 10^4 K⁻¹, the shot noise term in (3) is greatly reduced until ωC becomes much larger than G .

For the dimensions and operating parameters of this infrared sensor, the NEP associated with thermal noise, shot noise, and photon noise is 3.0×10^{-11} W/ $\sqrt{\text{Hz}}$, 1.4×10^{-13} W/ $\sqrt{\text{Hz}}$, and 5.2×10^{-12} W/ $\sqrt{\text{Hz}}$, respectively, at $\omega \ll G/C$. The thermal noise dominates the NEP for all modulation frequencies below 10 kHz.

Noise in amplifiers should not play an important role due to the large transducer sensitivity. Commercial operational amplifiers are readily available that contribute less than shot noise to the NEP.

If we sum these contributions to the noise, and consider the 50% efficiency of the absorber, the predicted NEP of the prototype is 7×10^{-11} W/ $\sqrt{\text{Hz}}$ at chopping frequencies below 10 kHz. At frequencies below 10 kHz, the NEP is dominated by thermal fluctuations. At frequencies above 10 kHz, the contribution from shot noise dominates the other sources of noise and degrades the NEP of the detector. The calculated contributions to the NEP of the prototype are plotted as a function of frequency in Fig. 2. For comparison, the NEP of a commercially available pyroelectric infrared sensor is shown as well.

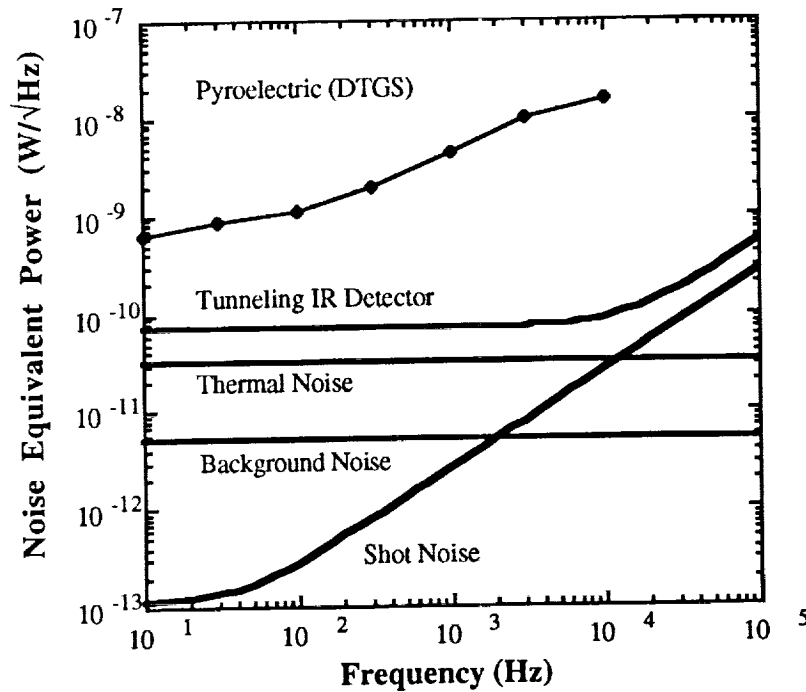


Fig. 2 This graph shows the contributions to the NEP of the tunneling infrared detector. The NEP of a typical pyroelectric infrared detector is shown for comparison

Prototype Tunneling Infrared Sensor

We have designed and constructed a prototype electron tunneling infrared sensor based on an early version of our tunneling transducer. Micromachining has been used in this case to produce cm-scale components with μm -scale precision. In contrast to conventional tunneling devices, the relative position of the electrodes is controlled through use of electrostatic forces applied between the elements. The electrostatic forces induce deflection of a micromachined silicon cantilever spring. Use of the electrostatic actuator is important because of insensitivity to thermal drifts and immunity to creep. Also the response of the electrostatic actuator is a function only of the geometry and mechanical properties of the device, whereas the response of piezoelectric actuators is also dependent on the characteristics of the material, which may not be reproducible between devices or over time. Finally, the electrostatic actuator may be miniaturized more easily because the scaling laws are known exactly, and the fabrication is less complex than for the piezoelectric actuator. Figure 3 shows a sketch of the micromachined infrared sensor components. The components are approximately 4 cm^2 in area. The inner rectangular area of the folded cantilever spring can be deflected upward or downward relative to the outer segments by application of a voltage between the large electrode and a corresponding deflection counter-electrode which is deposited on another component of the sensor. Given the mechanical properties of the silicon as well as the dimensions of the spring structure, we can calculate the properties of the spring. Because the spring constant scales rapidly with the dimensions of the legs of the folded cantilever, its characteristics can easily be tailored to meet the needs of a specific application. Various methods for manufacturing a suitable tunneling tip are available.^{8,19} We have formed silicon tips directly from the substrate by undercutting a $60\text{ mm} \times 60\text{ mm}$ square of SiO_2 with EDP. The active surfaces of all electrodes are prepared by evaporation of 3000 \AA thick Au films through a micromachined shadow mask.

Once the device is assembled, a voltage is applied to the electrostatic deflection electrodes. This deflection voltage produces an attractive force between the electrodes, which reduces the electrode separation. When the tip is within several \AA of the membrane, a tunnel current is established. Active regulation of the tip-electrode separation using feedback control of the tunneling current is carried out as

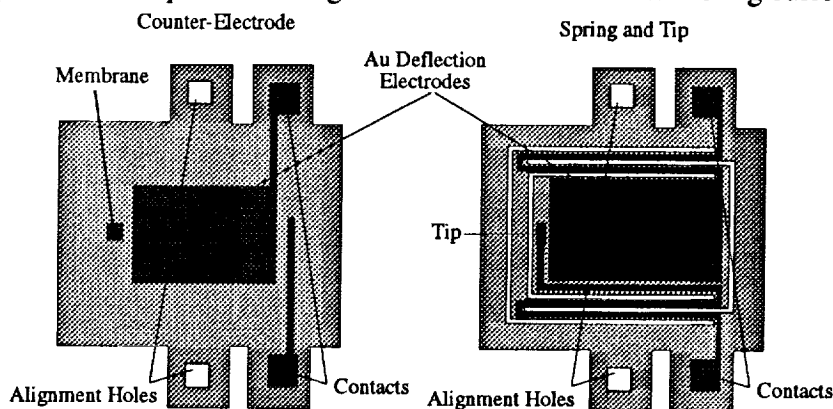


Fig. 3 This drawing shows the design of the micromachined silicon tunneling transducer. A folded cantilever spring, which supports a micromachined tip and a deflection electrode, is suspended over the micromachined counterelectrodes. Electrostatic forces between the deflection electrodes are used by a feedback loop to control the tunneling current. Variations in the deflection voltage occur with the absorption of IR radiation.

for STM. The absorption of infrared radiation causes thermal expansion of the trapped gas, and a resulting change in the tunneling current. The feedback circuit responds by reducing the deflection voltage, thereby forcing the cantilever to track the motion of the membrane. Infrared signals are monitored by recording the variations in deflection voltage.

The micromachined tunneling transducer was operated and characterized. While operating in the laboratory, displacement sensitivities of $10^{-3} \text{ \AA}/\sqrt{\text{Hz}}$ at 10 Hz and $10^{-4} \text{ \AA}/\sqrt{\text{Hz}}$ at 1 kHz were measured.

The prototype infrared sensor was made operational, and infrared response was observed with a variety of laboratory blackbody sources. A careful calibration was carried out by chopping between 300 K and 77 K blackbodies with area 1 cm^2 located 10 cm from the sensor. Considering the geometric factors and allowing for atmospheric transmittance from source to sensor, the average modulated signal power at the sensor was $1.6 \times 10^{-7} \text{ W}$. The signal to noise ratio at the chopping frequency of 10 Hz and bandwidth of 1 Hz was measured to be 200, so the experimental NEP of the prototype infrared sensor is $8 \times 10^{-10} \text{ W}/\sqrt{\text{Hz}}$. Noise in this prototype was dominated by the sensitivity of the transducer to mechanical vibration.

In the case of the prototype infrared sensor, the resonant frequency of the large cantilever that was used to track the displacement of the membrane was too small. As a result, the separation between the tunneling contacts was not well controlled, and true tunneling only occurred during a small fraction of the operating time. In addition, the transducer was sensitive to vibration, and the vibration signals increased the total noise during measurements.

Improved Tunneling Infrared Sensor

To construct an improved infrared sensor, we have chosen to dispense with the cantilever altogether, and apply the rebalance force from the feedback circuit to the membrane directly. A drawing of the improved infrared sensor is shown in Fig. 4. The device is operated by applying a deflection voltage to the membrane to pull it to within tunneling distance of the tip. A standard wide-bandwidth STM feedback loop is used to control the deflection voltage so as to maintain the tunneling current at a constant value. Upon the absorption of infrared radiation, the pressure in the trapped gas will change, affecting the force applied to the membrane by the gas. The feedback circuit will respond to this by adjusting the rebalance force so as to keep the membrane in the same position.

We have built and operated an infrared sensor based on this improved design. A preliminary calibration was carried out, giving an NEP of at least $2\text{-}4 \times 10^{-10} \text{ W}/\sqrt{\text{Hz}}$. The absorber used in this particular sensor was not well optimized; further reductions in NEP by as much as a factor of 3 may occur with an optimized absorber. A complete characterization of this sensor is presently under way.

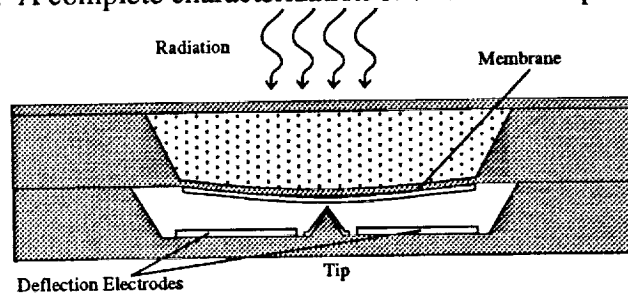


Fig. 4 This drawing shows the design of the improved tunneling infrared sensor. Electrostatic deflection is used by a feedback loop to control the position of a silicon nitride membrane. Variations in this deflection voltage are required to compensate for IR-induced variations in the pressure of the trapped gas.

The performance of this improved sensor exceeds that of the prototype in several important respects. First, the sensitivity to vibration is reduced because the mass of the moving transducer element is reduced by 5 orders of magnitude and the resonant frequency is increased by 3 orders of magnitude. Second, the bandwidth of the feedback loop that controls the transducer may now be increased by more than two orders of magnitude. Finally, the elimination of the folded cantilever allows the design of a simpler structure; this structure may be more easily fabricated and miniaturized. The improved sensor occupies only as much real estate on the focal plane as the absorber, and may be more easily arrayed.

The measured sensitivity of the tunneling infrared sensor is already competitive with the best commercial pyroelectric sensors. The NEP of this detector may be further improved by reducing G . Techniques for reducing G include using xenon for the gas, reducing the area of the membrane, and increasing the thickness of the cavity to reduce the surface area-to-volume ratio. These straightforward modifications will allow reductions in the NEP by an additional factor greater than 5. With these modifications, the first uncooled infrared detector with performance approaching background limits may be realized.

This detector can be made to operate at lower temperatures through the use of a more ideal gas, such as helium. The contribution to the NEP from thermal fluctuations should decrease linearly with temperature. Below 100 K, other technologies, particularly HiTc bolometers, HgCdTe, and InSb, should still be superior to this detector.

The tunneling infrared sensor, being assembled entirely from micromachined silicon, can be miniaturized and batch-fabricated or integrated into arrays. Individual detectors of diameter less than 100 μm can be assembled without development of additional technology by scaling the design of the improved infrared sensor. Each element would require a tunneling transducer with its own feedback circuit; therefore, integration of sensor and control electronics is necessary.

There are many potential applications of this detector since it is sensitive to radiation throughout the infrared. However, it appears ideally suited to applications that benefit from or require the use of an uncooled detector in measurement of radiation in the mid and far infrared, such as NASA planetary missions.

Tunneling Accelerometer

The tunneling transducer has also been investigated for application to measurement of acceleration. For example, the prototype micromachined tunneling transducer featured acceleration sensitivity of approximately $10^{-7} \text{ g}/\sqrt{\text{Hz}}$ at 10 Hz.

We have begun the development of an improved tunneling accelerometer which is intended to offer sensitivity of $10^{-8} \text{ g}/\sqrt{\text{Hz}}$ at all frequencies between 5 Hz and 1 kHz. This improved accelerometer features a lightweight, wide-bandwidth cantilever that is used to follow the motion of a suspended 1 mg proof mass. In this device, the feedback forces are applied to the cantilever instead of the proof mass. Since the feedback loop does not attempt to control the position of the proof mass, the loop may be operated both below and above the resonance of the proof mass. The bandwidth of the feedback loop is limited by the resonance of the cantilever, which is expected to exceed 10 kHz.

As for the infrared detector, it is important to consider not only the responsivity, but also the noise associated with this accelerometer. The performance of this miniature accelerometer is limited by thermal noise-induced vibrations in both the proof mass and the cantilever. We have carried out a thorough

analysis of the contributions of thermal noise to the sensitivity of the tunneling accelerometer. By separating the functions of cantilever and proof mass, the physical parameters of these components may be independently optimized to reduce thermal noise while preserving acceleration sensitivity. The details of this analysis are planned to be published elsewhere.

We thank J. Maserjian, and P.J. Grunthner for their encouragement and support. We are indebted to K. Potter and D. Rutledge for assistance with the development of the oxynitride membranes.

The work described in this paper was performed by the Center for Space Microelectronics Technology, Jet Propulsion Laboratory, California Institute of Technology and was jointly sponsored by the Defense Advanced Research Projects Agency, the Strategic Defense Initiative Organization/ Innovative Science and Technology Office, and the National Aeronautics and Space Administration, Office of Aeronautics, Exploration, and Technology.

-
- ¹ F. Sibille, *Re. Prog. Phys.* 49, 1197 (1986).
 - ² E.H. Putley, in *Optical and Infrared Detectors*, ed. R.J. Keyes (Springer, Berlin, 1977), pp. 71-98.
 - ³ T. Limperis, J. Mudar, in *The Infrared Handbook*, eds. W.L. Wolfe and G.J. Zeiss (Environmental Research Institute of Michigan, Ann Arbor, 1978), Ch. 11.
 - ⁴ T.G. Blaney, in *Infrared and Millimeter Waves Vol. 3*, ed. K.J. Button (Academic Press, New York, 1980) pp. 1-75.
 - ⁵ M.J.E. Golay, *Rev. Sci. Inst.* 18, 347 (1947).
 - ⁶ M.J.E. Golay, *Rev. Sci. Inst.* 20, 816 (1949).
 - ⁷ A. Hadni, *Essentials of Modern Physics Applied to the Study of the Infrared* (Pergamon, Oxford, 1967), pp. 269-283.
 - ⁸ L.N. Hadley, D.M. Dennison, *J. Opt. Sci. Am.* 37, 451 (1947).
 - ⁹ C. Hilsum, *J. Opt. Sci. Am.* 44, 188 (1954).
 - ¹⁰ A. Hadni, *Essentials of Modern Physics Applied to the Study of the Infrared* (Pergamon, Oxford, 1967), pp. 252-7.
 - ¹¹ M.J.S. Smith, L. Bowman, J.D. Meindel, *IEEE Trans. Biomed. Eng.*, BME-33, 163 (1986).
 - ¹² S.B. Waltman and W.J. Kaiser, *Sensors and Actuators* 19, 201 (1989).
 - ¹³ T.W. Kenny, S.B. Waltman, J.K. Reynolds, and W.J. Kaiser, *Appl. Phys. Lett.* 58, 100 (1991).
 - ¹⁴ G. Binnig, H. Rohrer, Ch. Gerber, and E. Weibel, *Phys. Rev. Lett.* 49, 57 (1982).
 - ¹⁵ G. Binnig, H. Rohrer, Ch. Gerber, and E. Weibel, *Phys. Rev. Lett.* 50, 120 (1983).
 - ¹⁶ W.C. Young, *Roark's Formulas for Stress and Strain*, 6th Ed. (McGraw-Hill Book Company, New York, 1989).
 - ¹⁷ G. Binnig and H. Rohrer, *IBM J. Res. Develop.* 30, 355 (1986).
 - ¹⁸ F.J. Low and A.R Hoffman, *Appl. Opt.* 2, 649 (1963).
 - ¹⁹ R.B. Marcus, T.S. Ravi, T. Gmitter, K. Chin, D. Liu, W.J. Orvis, D.R. Ciarlo, C.E. Hunt and J. Trujillo, *Appl. Phys. Lett.* 56, 236 (1990).

Macro, Mini, Micro and Nano (M³N) Technologies for the Future

Craig R. Friedrich, Associate Professor
Robert X. Gao, Research Associate

Robert O. Warrington, Director
Gang Lin, Visiting Assistant Professor

**Institute for Micromanufacturing
Louisiana Tech University
Ruston, Louisiana 71272
(318) 257-2357**

Microelectromechanical Systems (MEMS), Micro Systems Technologies (MST) and Micromanufacturing are relatively recent phrases or acronyms that have become synonymous with the design, development, and manufacture of "micro" devices and systems. Micromanufacturing encompasses MEMS or MST and, in addition, includes all of the processes involved in the production of micro things. Integration of mechanical and electrical components, including built-in computers, can be formed into systems which must be connected to the macroworld. Macro, mini, micro, and nano technologies are all a part of MEMS or micromanufacturing. At this point in the development of the technology, it is becoming apparent that mini systems, with micro components, could very well be the economic drivers of the technology for the foreseeable future.

Initial research in the fabrication of microdevices using IC processing technology took place over thirty years ago [1]. Anisotropic etching of silicon was used to produce piezoresistive diaphragms. Since the early 60's, there has been gradual progress in MEMS until the early 1980's when worldwide interest in the technology really started to develop. During this time high aspect ratio micromachining using X-rays was started in Germany [2]. In 1987 the concept of a "Silicon Micromechanics Foundry" was proposed [3]. Since then the interest in the U.S., Germany and Japan has increased to the point where hundreds of millions of dollars of research monies are being funneled into the technology (at least in Germany and Japan) and the technology has been classified as critical or as a technology of national importance by the U.S. government.

Projects Utilizing M³N Technologies

Four areas of concentration will be developed within the Institute for Micromanufacturing at Louisiana Tech University. They are:

- * The design and fabrication of microdevices, such as micro-motors, actuators, sensors, pumps, valves, and connectors.
- * The design and fabrication of microstructures, such as micro-heat exchangers, filters, distillation columns and supports for micro-devices and systems.
- * Research related directly to the manufacturing processes, including fabrication, metrology assembly and testing of the microproducts mentioned above.

- * Microsystem research involving the integration of these microdevices/structures and interfacing of these systems with the macroworld.

Several technologies will be developed and used for the fabrication of these micro devices and structures. First, the existing capabilities in diamond bit machining at Louisiana Tech University will be enhanced. Second, conventional photo lithography and chemical etch will be developed and used for the fabrication of low aspect ratio devices and structures. Third, as X-ray lithography technology becomes available at the Center for Advanced Microstructures and Devices (CAMD) in Baton Rouge, Louisiana Tech and LSU researchers will utilize a dedicated beam line to fabricate high aspect ratio devices and structures. Finally, research and development will be performed on small machines that can build these microproducts.

The Institute for Micromanufacturing is currently involved in the integration of different technologies with direct applications. Several examples of this will be detailed. These applications include micro heat exchangers and heat and mass transport at the micro level, smart bearings with self-diagnostic capabilities, advanced ultra-precision air bearings, surface-driven electrostatic micro positioners and shape memory alloy propulsion for micro robots.

Micro Heat Exchangers

There are applications of micromanufacturing where the final device is in the "mini" region but has elements in the micro domain. Such a device is a micro heat exchanger. A micro heat exchanger is hereby defined as a device with a heat transfer surface density (heat transfer surface area divided by active heat transfer volume) above 5000. Typical compact heat exchangers have a surface density of only 1000 to 3000. With such a high surface density, micro heat exchangers have a very high volumetric heat transfer coefficient.

The micro heat exchangers currently under development are based on high conductivity copper and precision diamond machining. For the plate-type cross flow heat exchanger, thin foils of oxygen free (SAE alloy CA122) or electronic grade (SAE alloy CA110) are used to form the plates. These foils are typically 125 micrometers thick. In the surface of these foils, micro flow channels are machined with specially contoured diamond tools. This machining is performed on an air bearing spindle to reduce vibration and improve channel surface finish. The size of the channels can be variable but are typically 85 micrometers deep and 100 micrometers wide at the bottom [4]. A machined foil is shown in Figure 1 and a single flow channel is shown in Figure 2. After machining, the foils are stacked such that each layer has its channels running perpendicular to the adjacent layers, thus forming the cross flow device. The stack is then vacuum diffusion bonded and the faces are diamond machined flat. The device is then ready for use.

The current design is very conservative so that the fabrication and operating variables may be more easily identified. Current testing is with a device composed of a

total of 80 layers. Thus each fluid side has 1440 flow passages and the total active volume is 1.64 square centimeters. The surface density for this particular device is 6876 square meters/cubic meter. Filtered water at 20° C and 70° C were used as the working fluids. The mass flow rate was typically 0.02 to 0.04 kilograms/second. These operating parameters gave a 2 to 5 atmosphere pressure drop through the core and a volumetric heat transfer coefficient of 45 megawatts/cubic meter-K (log-mean temperature difference). A design model predicts that a device with a volumetric coefficient over 300 mega-watts/cubic meter-K is easily attainable [5].

Smart Bearings with Self-diagnostic Capabilities

Bearings are the fundamental mechanical components widely used in manufacturing and other industrial branches. Though small in volume, they are highly complex in construction, featuring different parts like rolling-elements, raceways and cages. Depending on the type of applications, bearings are mostly sealed up after machine assembly and often used under extreme conditions such as in cryogenic regions or high temperature, corrosive media or ultra high speeds. In case of overloading or overheating, bearing failure will occur and manufacturing precision will suffer greatly or a critical component may fail endangering human life.

An effective way of preventing such critical situations and thus helping to maintain the manufacturing precision and improve the machine operation security is the on-line, real time supervision of bearing operating environment [6]. The environment mainly consists of the bearing load and operating temperature. This can be achieved by equipping the bearings with self-checking and error reporting functions through integration of sensors and microelectronics into the bearing environment. This concept is shown in Figure 3.

The sensors embedded in the "smart bearings" generate real time electronic signals which correspond to the force and temperature variations in the bearing components. The operating signals will be continuously monitored by microelectronic circuitry located in the bearing housing. The operating signals will be compared with pre-determined "threshold" values which represent a critical loading or temperature condition. Should a critical condition exist, a signal indicating potential damage will be sent from an embedded high frequency data transmitter to the machine control system which then can make corresponding adjustments. In using only an overload signal, the control system is not burdened with a continual stream of data. However, to generate critical "signatures", the real-time data can be monitored and stored for subsequent evaluation which will also be beneficial to improving the existing machine control algorithm. A novel feature of the smart bearing is that for data transmission, no direct cable connection will be needed. This wireless method is especially suitable for applications where the accessibility of the measurand is not easily available. Similarly, the power supply for the embedded transducer will be provided through non-contact voltage induction.

In contrast to traditional methods of manufacturing precision controls which focus

on post-error adjustment and compensation, instrumented smart bearings will allow on-line error source location and pre-failure adjustment. This method can be very well applied to the high-tech areas like aerospace and the military or automotive industry, where high precision, reliability and accuracy of manufacturing and operation are required.

Herring Bone Air Bearings for Ultra-Precision Spindles

Air bearings of all types (including linear guides, x-y tables, and spindles) have been widely employed in the ultra-precision engineering field to ensure the extremely high precision requirements of machinery such as in diamond-tool machining. The design optimization of the journal air bearing for precision and high performance applications is currently in progress. Among various self-acting air bearings, the herring bone type shown in Figure 4 has been considered as one of the best bearings for high speed spindles due to its high efficiency and high stability. For the best possible bearing design, the relationship between the design specifications and the bearing characteristics, such as load capacity and stability, must be known. However, the design information available in the literature only give a limited number of design specification sets. This information is, in most cases, insufficient for design optimization. Therefore, the design of herring bone bearings, especially when high speed and stability are required, still depends mainly on testing and the experience of the designer. Because of this, the design of herring bone air bearings is still very challenging.

The Reynolds equation, which governs the performance of the air bearing, has been numerically solved by specially developed finite element method programs. Once the solution, that is the pressure distribution over the bearing surface, is obtained, the bearing performance may be simulated in the computer.

The groove pump-in angle β affects the bearing load capacity W , as well as the stability indirectly through the bearing attitude angle Θ , (which is a divergent angle between the eccentricity and the direction of load), as shown in Figure 5. The eccentricity ratio in the figure is defined as a ratio of eccentricity to average bearing clearance ($\epsilon = e/h_0$), while Λ is a nondimensional parameter used to express the rotational speed and n is the number of grooves. Through such figures, the influence of the design specifications on the performance of the herring bone bearing over the most common ranges have been discussed. Consequently, the design optimization of the bearing has been made possible [7].

Surface-driven Micro Electrostatic Positioner

In the past several years, there has become a growing need for micro-sized motors and actuators for applications in micromanufacturing and other microelectromechanical systems domain (MEMS). Among other topics, the design and fabrication of micro electrostatic motors have found widespread interests. Compared to conventional electromagnetic motors commonly used in the large-scale motion world, electrostatic equivalents promise numerous advantages like simple structure, small size, high force-to-

-volume ratio and fine motion/step control.

Among different types of electrostatic motors (side-driven, surface-driven and cylindrical harmonic or wobble), the surface-driven version effectively utilizes the whole stator/slider overlapping area so that its force density is the highest. The basic motion principle is that a sequence controlled multiphase excitation voltage pattern (positive, negative and ground) is applied on the electrodes which are either evenly or unevenly pitched on the stator board. This voltage pattern will induce electrical charges in the slider film which is laid on the top of the stator surface. The interaction between the induced electrical charges in the slider film and the applied charges on the stator electrodes results in three types of forces: an upward levitational force which reduces the contact friction between the slider and the stator, a repulsive force between electrical charges of the same polarity and an attractive force between opposite charges. The combined effects of these forces is that each time the voltage pattern is applied, the slider will move a certain length (step), which corresponds to the electrode pitch width, in a certain direction and at a certain speed, depending on the configuration of the excitation voltage pattern. The slider motion will continue when the voltage pattern cycle applied on the electrodes is shifted and repeated. To enable easy modifications and flexible changes of the excitation voltage pattern for any desired slider motion behavior, the electronic circuits are software controlled by a computer. The excitation voltage generation part of the circuits was built with power bipolar and MOSFET transistors. For control unit protection and isolation, opto-couplers were used. In Figure 6, the principle of an electrostatic motor is schematically shown.

The arrangement of the stator electrodes (linear or radial) determines, whether the slider will perform a linear or a rotary motion. The resolution of the motion steps is mainly dependent on the dimensions and manufacturing precision of the electrodes. By appropriate connection of the slider to further mechanism, it can be well expected that high precision positioners, micro conveyors, micro feeders or micro drive systems can be realized which will find wide applications in conventional and micro manufacturing, medical, biochemical, aerospace or other relevant fields.

Biomechanical Micro Swimming Robots Using Smart Materials

The objective of this research is to design and fabricate microrobots with a simple method of propulsion using smart materials instead of electric motors. Such devices can be fabricated at a very small scale and will have a high strength to weight ratio for special applications.

In this study, two types of micro robots will be designed and fabricated with smart materials based on biomechanical similarity principles. The first type, as shown in Figure 7a, is a jellyfish-like robot with an umbrella made of shape memory alloy (SMA) which has the capability of remembering and reproducing its original shape when exposed to a change in temperature. The second type, as shown in Figure 7b, is a tadpole-like device with muscles made of either SMA or piezoelectric materials, which can change dimensions upon electrical stimulation.

The muscles within the umbrella of the jellyfish will be activated by heat generated from an electric current flowing in the SMA, while cooling will come from the liquid through which the robot is swimming. As the umbrella is heated, it will contract and will result in forward movement of the device. As the umbrella cools, it will return to its original position. With proper design, this impulse will provide a forward propulsion. The muscles on the sides of the tadpole will differentially expand and contract causing the tail to move in a sidewise direction. This reversing process will cause the tail to provide a forward propulsion similar to a fish. The main advantage of this robot is that it is easy to fabricate at small dimensions due to its simplicity of design, it should have high reliability due to the simple movement, and it has high efficiency because no mechanical mechanisms are used.

Designs using SMA materials, and the control systems required for the robots, are often complex and difficult to perform because of the lack of appropriate models. In addition, the hysteresis of the material causes added complexity to the design and fabrication and the hysteresis is not properly understood. A dynamic model of the SMA material has been developed to aid the design and control of the robots. The shape memory effect is the result of a crystalline transformation between two phases of the material and so the model is based upon that phenomenon. From this, the physical properties and behavior of the SMA may be computed for a specific configuration and set of parameters. The SMA is divided into the martensitic and austenitic phases, and the behavior of each is computed for variations in the stress and temperature fields.

To confirm the applicability of the model, a comparison between the model and experimentation was made. In the experiment, TiNi50 wire of 0.1mm diameter and 20mm length was loaded with a 360g mass, and then heated. The heating power was supplied as a square pulse and the wire was allowed to cool by natural convection and radiation into the room at 18 °C. Using heat transfer theory for the heating and cooling process, the simulation was developed for the two phase material. Excellent agreement was found between the simulation and experimental results.

Future Directions

The key to future technological applications will be the ability to rapidly and effectively integrate, as necessary, the macro-, mini-, micro-, and nano-world. Basic science is driving the scale down to, and beyond, the nano-domain. These investigations are necessary to understand material properties and behavior at the fundamental level. These studies are also necessary to understand the fundamental interactions between materials and outside influences such as electrical and magnetic fields, gravity, light, and electromechanical driving forces. Although the science learned at this level will greatly aid in the design and control of micro and nano devices, these devices must still adapt to the macro world.

The Institute for Micromanufacturing is dedicated to the integration of these various domains. Total integration will not be possible at the process level because of the

large difference in the dimensional orders of magnitude within the domain. Therefore it is necessary to design and fabricate assist-devices so that either humans or their kinematic extensions can grasp, manipulate, position, adjust, and assemble nano-components or attach/integrate nano-components into a macro- or mini-device. In addition, it will be necessary to develop the speed, sensitivity, reliability, and inspection aspects of micromanufacturing so that these curiosities may move from the laboratory to a production environment.

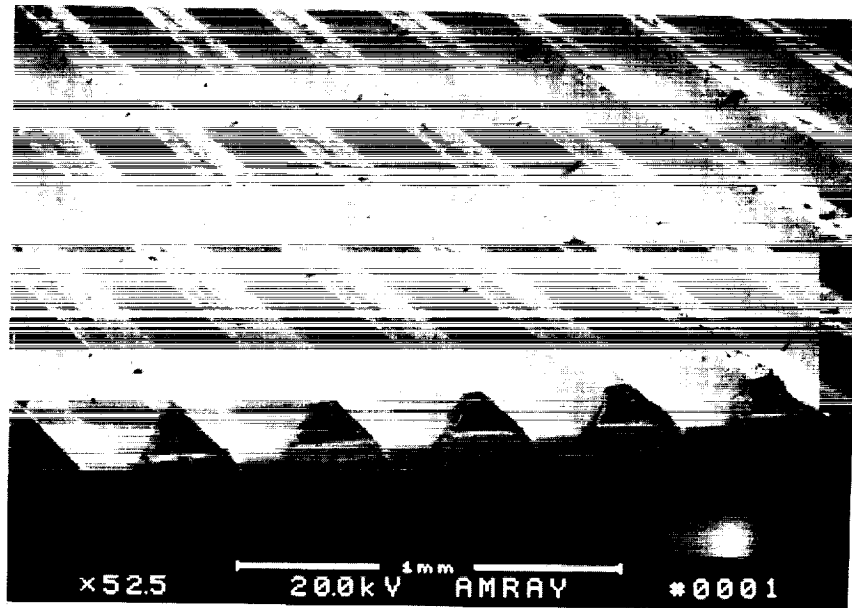


Figure 1. Micrograph of machined flow channels

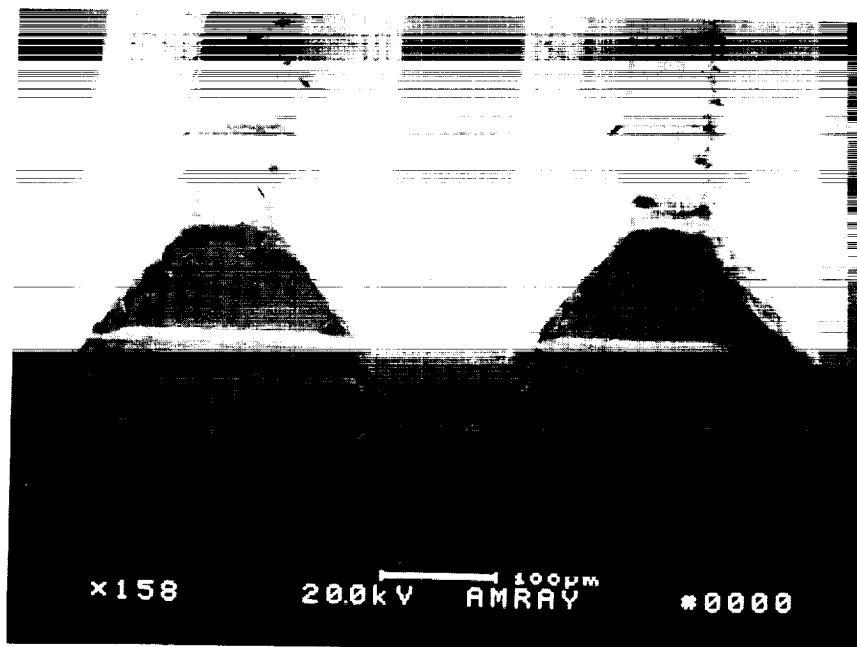


Figure 2. Micrograph of single flow channel (rms roughness 39 nm)

- Sensitive to force and temperature variations;
- Micro size, able to be implanted into bearings environment;
- Robust in mechanical construction;
- Minimal repercussion on bearings dynamics.

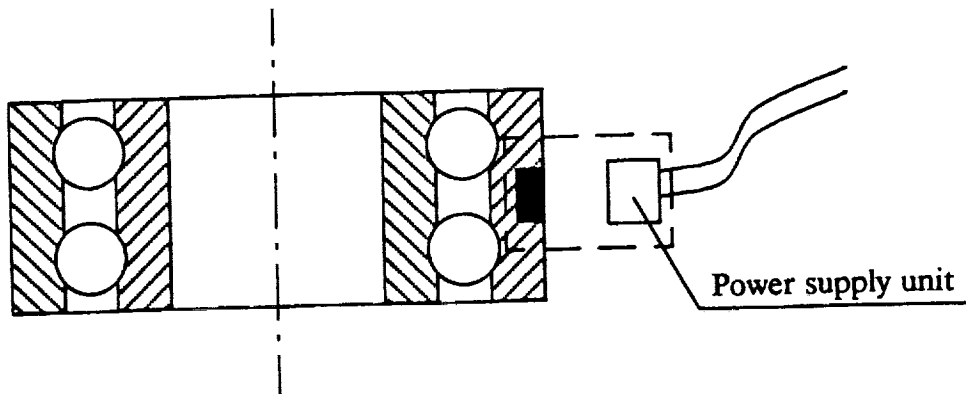


Figure 3. Sensor located in smart bearing

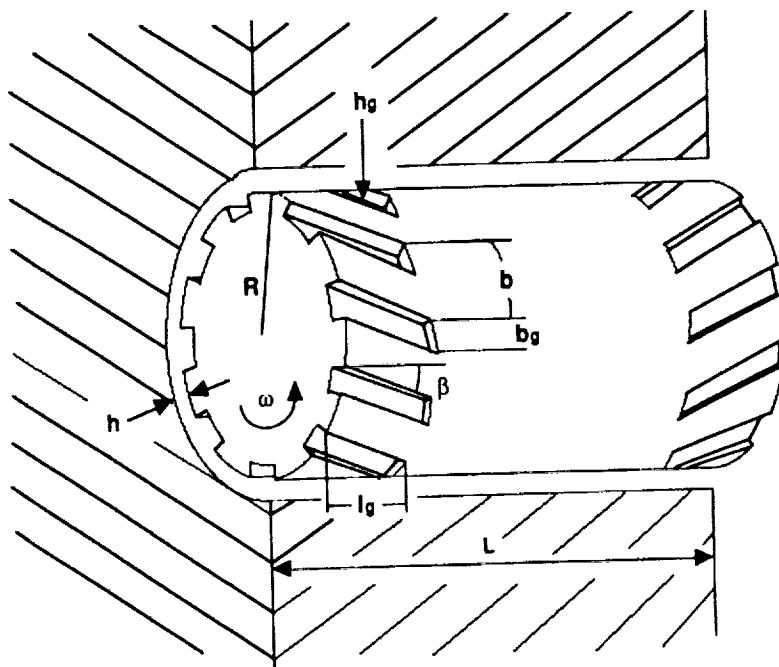


Figure 4. Configuration of a herring bone air bearing

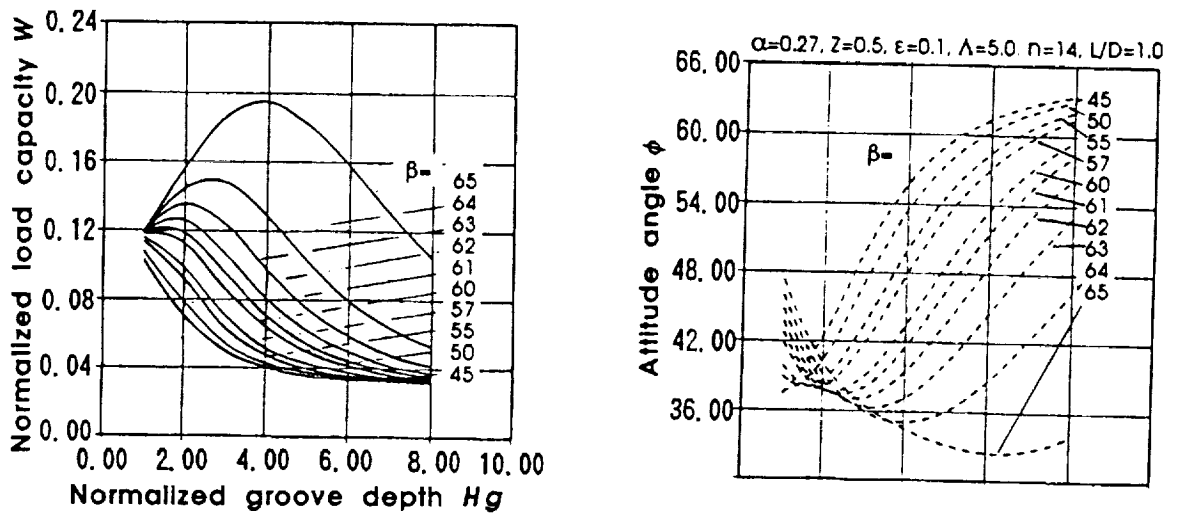


Figure 5. Influence of the groove pump-in angle

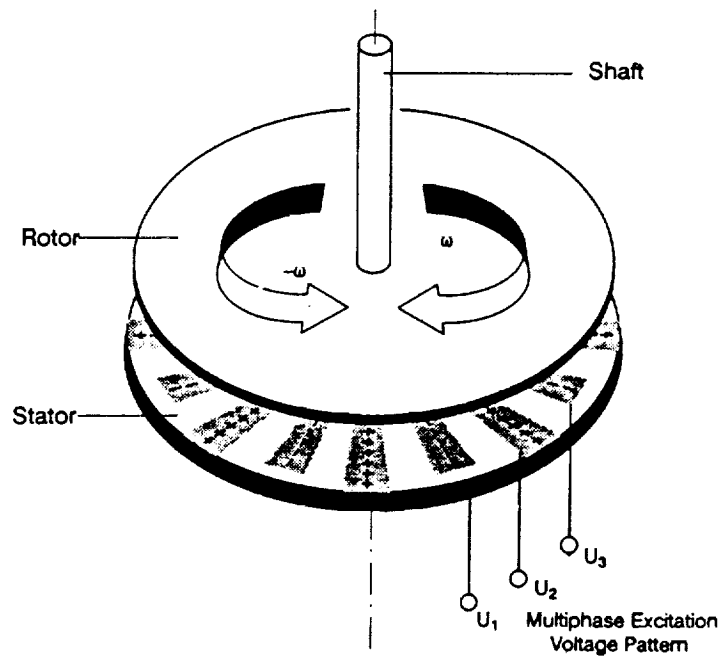
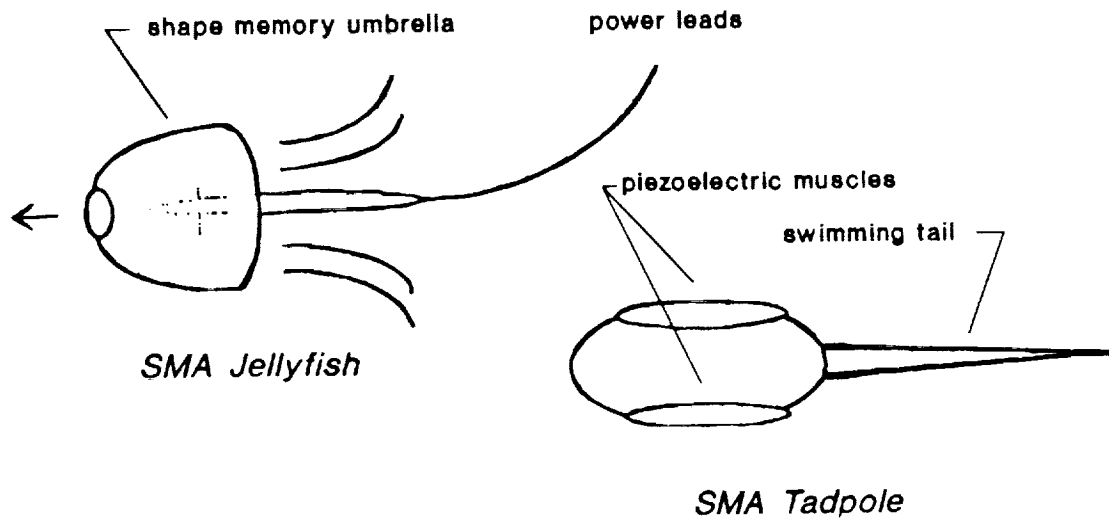


Figure 6. Layout of electrostatic motor



7a. Jelly-fish like robot

7b. Tadpole-like robot

Figure 7. Shape memory alloy robots

References

1. O.N. Tufte, P.W. Chapman and D. Long, "Silicon Diffused-Element Piezoresistive Diaphragms", *J. Appl. Physics*, 33, 3322-3329, 1962.
2. E.W. Becker, H. Betz, W. Ehrfeld, W. Glashauser, A. Heuberger, H.J. Michael, D. Münchmeyer, S. Pongratz and R.v. Siemens, "Production of Separation Nozzle Systems for Uranium Enrichment by a Combination of X-Ray Lithography and Galvano-plastics", *Naturwissenschaften*, 69, 520-523, 1982.
3. K. Petersen, "The Silicon Micromechanics Foundry", *IEEE*, 87TH0204-8, 1987.
4. C.R. Friedrich and R.O. Warrington, "Machining Metal Foils for Use in Microcompact Heat Exchangers", *Micro System Technologies '90*, Springer-Verlag, pp. 509-514, Berlin, 1990,
5. C.R. Friedrich and S.W. Kang, "Performance of High Flux Heat Exchangers Fabricated by Diamond Machining", submitted to *Precision Engineering*, 1992.
6. R.X. Gao, M. Bhandiwad and R.O. Warrington, "Smart Grinding Balls and Smart Bearings for On-line Process Supervision", to be presented at *7th ASPE Annual Meeting* in Orlando, Fl, October 1992.
7. G. Lin and T. Satomi, "Characteristics and Optimization of the Spiral Grooved Thrust Air Bearings", *Trans. JSME*, Ser. C, No. 541, vol. 57, pp. 2971-2977, (in Japanese), 1991.

Microtechnologies
and
Applications to Space Systems Workshop

GUIDANCE & CONTROL

CONTROL OF MICROMACHINED DEFORMABLE MIRRORS

M.L. Agronin, R. Bartman, F.Y. Hadaegh, W. Kaiser
Jet Propulsion Laboratory
California Institute of Technology
Pasadena, CA 91109-8099

P.K.C. Wang
Department of Electrical Engineering
University of California
Los Angeles, CA 90024

Abstract:

A micromachined deformable mirror with pixelated electrostatic actuators is proposed. The paper begins with a physical description of the proposed mirror. Then a mathematical model in the form of a nonlinear partial differential equation describing the mirror surface deformations is derived. This model is used to derive the required voltages for the actuators to achieve a specified static deformation of the mirror surface. This is followed by the derivation of a static nonlinear feedback controller for achieving noninteracting actuation. Then the structure for a complete control system for wavefront correction is proposed. The paper concludes with a discussion of the physical implementation of the proposed control system.

1. INTRODUCTION

In the development of large space interferometers and multi-aperture reflectors, deformable mirrors are used to compensate for distortions in elements of the optical train and/or in the instrument's field of view. Such mirrors should be small and lightweight. Moreover, they should be highly pixelated so that the deformations can be controlled with high lateral resolution.

The first actively controlled deformable mirrors were developed by NASA in the 1960's for use as solar collectors or as ground-based telescopes [1]. Since then, there has been extensive development in this area. Comprehensive surveys of works on actively controlled deformable mirrors were given by Ealey [2] and Tyson [3]. In 1977, Grosso and Yellin [4] developed a membrane mirror whose deformations are controlled by means of discrete electrostatic actuators. Subsequently, various forms of deformable mirrors with discrete piezoelectric and magnetostrictive actuators were also developed [5]-[9]. The advent of silicon VLSI technology has made possible the integration of deformable mirrors with microelectronic circuitry. In 1983, Hornbeck [10] perfected a deformable mirror device with pixelated mirror elements whose size is 51 μm square. The mirror deformations are controlled by electrostatic actuators driven by microelectronic circuits which are integrated with the mirror assembly. His mirror was used primarily as a light modulator. Later, in 1989, a wavefront control device with a deformable mirror integrated with control and sensor units was introduced by Ealey and Wheeler [11]. In their device, the actuators are spaced 1.0 mm apart. The voltages applied to the actuators are on the order of 200 volts. Recently, efforts have been initiated at the Jet Propulsion Laboratory in exploiting micromachining technology to develop deformable mirrors with the aforementioned characteristics and with pixelated electrostatic actuators which are spaced less than 25 microns apart. In this paper, attention is focused on the analytical design of control systems for such deformable

mirrors.

The paper begins with a physical description of the proposed mirror. Then a mathematical model in the form of a nonlinear partial differential equation describing the mirror surface deformations is derived. This equation is used to derive the required actuator voltages to achieve a specified static deformation of the mirror surface. This is followed by the derivation of a static nonlinear feedback controller for achieving noninteracting actuation. Then the structure for a complete control system for wavefront correction is proposed. The paper concludes with a discussion of the physical implementation of the proposed control system.

2. PHYSICAL DESCRIPTION OF DEFORMABLE MIRROR

Figures 1 and 2 show respectively the sketches of the top and side views of the proposed deformable mirror with pixelated capacitive actuators. The mirror may be realized as "flip chip"-type assemblies consisting of two matched micromachined silicon structures mounted face-to-face and fused together along their peripheries. The key elements of the mirror consist of simple, easily replicated, electrostatic linear actuators, each responsible for pulling on a small portion of a thin flexible silicon membrane which is the substrate for the deformable mirror. The mirror surface is formed by depositing a metallic or multi-layer dielectric film on the membrane. The membrane with posts (See Fig.2) is micromachined from a silicon sheet. The posts serve as supports for the membrane and also as halves of the electrostatic actuators. The bottom half of the mirror assembly consists of a set of posts with four silicon blades attached to each post. These blades serve as leaf springs for supporting the posts of the upper mirror assembly, and for providing a restoring force for the actuation system. This bottom assembly is micromachined from a silicon wafer. The electrostatic actuators are formed by attaching conductive pads to the upper posts and the bottom half of the mirror assembly. The electronic element access, electronic actuator drivers, and possibly the feedback controller circuitry may be monolithically integrated into the mirror assembly.

We note that the geometric structure of the deformable mirror proposed here differs from that of Hornbeck [10]. In his mirror, each actuator, when activated, produces a concave deformation of the mirror surface over the entire pixel. This causes focusing of the incoming light beam in front of the pixel. Here, each actuator pulls down on the mirror surface at a post area and thereby induces deformation over adjacent portions of the mirror surface. Except for the flat spots over the post areas, the overall shape of the mirror surface is determined by the displacements of all the actuators.

The initial performance goals for the proposed mirror will be the control of a 32×32 pixel flat mirror with 10 nm accuracy. Once these goals have been achieved, efforts will be directed at extending the number of pixels/control elements until 10 nm accuracy can be achieved over a 1024×1024 pixel surface.

3. MATHEMATICAL MODEL

Let Ω be an open connected subset of the Euclidean plane R^2 with a piecewise smooth boundary $\partial\Omega$ representing the spatial domain of the mirror. We introduce a mesh on Ω whose mesh points are denoted by $\mathbf{x}_{mn} = (x_{1m}, x_{2n})$, $m = 1, \dots, M$; $n = 1, \dots, N$. For a rectangular mirror, Ω is

specified by $\Omega_R = \{(x_1, x_2) \in R^2: |x_1| \leq \ell_1, |x_2| \leq \ell_2\}$, where the ℓ_i 's are specified lengths. For a circular mirror, Ω is specified by the disk $\Omega_C = \{(r, \theta), 0 \leq r \leq r_0, 0 \leq \theta \leq 2\pi\}$. At each mesh point \mathbf{x}_{mn} , we introduce a patch Ω_{mn} , a bounded open subset of Ω representing the effective spatial domain of the (m,n)-th actuator force containing \mathbf{x}_{mn} as an interior point. Typical meshes and patches for the rectangular and circular mirrors are shown in Fig. 3.

Let the mirror surface be a thin membrane with density $\rho = \rho(\mathbf{x})$ being a specified positive piecewise smooth function satisfying the following bounds:

$$0 < \rho_{\min} \leq \rho(\mathbf{x}) \leq \rho_{\max} < +\infty \text{ for all } \mathbf{x} \in \Omega. \quad (1)$$

The variation of the mass density due to the supporting posts can be included in ρ by setting $\rho(\mathbf{x}) = \rho_{mn}$ (a known constant) for $\mathbf{x} \in \Omega_{mn}$.

Let σ_{ij} , $i, j = 1, 2$ denote the components of the symmetric stress tensor in the mirror surface satisfying the positivity condition

$$c_1 \|\zeta\|^2 \leq \sum_{i=1}^2 \sum_{j=1}^2 \sigma_{ij} \xi_i \xi_j \leq c_2 \|\xi\|^2 \text{ for all } \xi = (\xi_1, \xi_2) \in R^2, \quad (2)$$

where c_1 and c_2 are known positive constants. In the special case with uniform tension T , we have $\sigma_{ij} = T\delta_{ij}$, where δ_{ij} denotes the Kronecker delta.

The downward displacement $u(t, \mathbf{x})$ normal to the mirror surface at a point $\mathbf{x} \in \Omega$ and time $t \geq 0$ can be described by the following equation:

$$\rho(\mathbf{x}) \frac{\partial^2 u}{\partial t^2} - \sum_{i=1}^2 \sum_{j=1}^2 \frac{\partial}{\partial x_i} \left(\sigma_{ij}(\mathbf{x}) \frac{\partial u}{\partial x_j} \right) = f, \quad (3)$$

where $f = f(t, \mathbf{x})$ is the surface force density whose explicit form will be derived later. Assuming that the mirror is rigidly attached to its boundary $\partial\Omega$, u must satisfy the boundary condition

$$u(t, \mathbf{x}) = 0 \text{ for } \mathbf{x} \in \partial\Omega \text{ and } t \geq 0. \quad (4)$$

Finally, the initial conditions for u are specified by

$$u(0, \mathbf{x}) = u_0(\mathbf{x}), \quad \frac{\partial u}{\partial t}(0, \mathbf{x}) = u'_0(\mathbf{x}) \text{ for } \mathbf{x} \in \Omega. \quad (5)$$

To derive an explicit expression for the surface force density f , we first consider the electrostatic force density over a patch Ω_{mn} due to a specified voltage $V_{mn}(t)$ applied to the (m,n)-th actuator. We assume that the mirror surface curvature is small so that each patch Ω_{mn} is essentially parallel to the bottom assembly. Thus each actuator's conductive surfaces can be regarded as making up a parallel-plate capacitor. Neglecting fringing effects of the electric field at the boundary of Ω_{mn} , the electrostatic force density is given by

$$f_e(t, \mathbf{x}) = \frac{1}{2} \epsilon_0 \left(\frac{V_{mn}(t)}{D - u(t, \mathbf{x}_{mn})} \right)^2 \quad \text{for all } \mathbf{x} \in \Omega_{mn}, \quad (6)$$

where D is the distance between the undeformed mirror surface and the bottom plane and ϵ_0 is the permittivity of free space. When $D \gg |u(t, \mathbf{x}_{mn})|$, (6) can be approximated by

$$f_e(t, \mathbf{x}) = \frac{1}{2} \epsilon_0 V_{mn}^2(t) / D^2 \quad \text{for all } \mathbf{x} \in \Omega_{mn}. \quad (6')$$

Considering each leaf spring as a small cantilever beam having uniform cross section with moment of inertia I and Young's modulus E , the force density f_s due to four leaf springs over the patch Ω_{mn} is given by

$$f_s(t, \mathbf{x}) = \frac{12EI}{\ell_{mn}^3 A_{mn}} u(t, \mathbf{x}_{mn}) \quad \text{for all } \mathbf{x} \in \Omega_{mn}, \quad (7)$$

where A_{mn} denotes the area of the patch Ω_{mn} . Here, we have neglected the inertial effects of the leaf springs.

Let ϕ_{mn} denote the spatial weighting function associated with the (m, n) -th actuator such that $\phi_{mn}(\mathbf{x}) = 0$ for $\mathbf{x} \in \Omega - (\Omega_{mn} \cup \partial\Omega_{mn})$. Combining (6) and (7), equation (3) becomes a nonlinear partial differential equation given by

$$\begin{aligned} \rho(\mathbf{x}) \frac{\partial^2 u}{\partial t^2} - \sum_{i=1}^2 \sum_{j=1}^2 \frac{\partial}{\partial x_i} \left(\sigma_{ij}(\mathbf{x}) \frac{\partial u}{\partial x_j} \right) \\ = \sum_{m=1}^M \sum_{n=1}^N \left\{ \frac{1}{2} \epsilon_0 \left(\frac{V_{mn}(t)}{D - u(t, \mathbf{x}_{mn})} \right)^2 - \frac{12EI}{\ell_{mn}^3 A_{mn}} u(t, \mathbf{x}_{mn}) \right\} \phi_{mn}(\mathbf{x}). \end{aligned} \quad (8)$$

Let $K(\mathbf{x}, \mathbf{x}', t, \tau)$ denote the Green's function corresponding to the solution of the linear equation:

$$\rho(\mathbf{x}) \frac{\partial^2 u}{\partial t^2} - \sum_{i=1}^2 \sum_{j=1}^2 \frac{\partial}{\partial x_i} \left(\sigma_{ij}(\mathbf{x}) \frac{\partial u}{\partial x_j} \right) = \delta(t - \tau, \mathbf{x} - \mathbf{x}'), \quad (9)$$

with boundary and initial conditions given by (4) and (5), where δ denotes the Dirac delta function at $t = \tau$ and $\mathbf{x} = \mathbf{x}'$. Equation (8) can be reformulated as a nonlinear integral equation:

$$\begin{aligned} u(t, \mathbf{x}) = \int_{\Omega} K(\mathbf{x}, \mathbf{x}', t, 0) u_0(\mathbf{x}') \, d\mathbf{x}' + \int_{\Omega} \frac{\partial K}{\partial t}(\mathbf{x}, \mathbf{x}', t, 0) u_0'(\mathbf{x}') \, d\mathbf{x}' \\ + \int_0^t \int_{\Omega} K(\mathbf{x}, \mathbf{x}', t, \tau) \sum_{m=1}^M \sum_{n=1}^N \left\{ \frac{1}{2} \epsilon_0 \left(\frac{V_{mn}(t)}{D - u(t, \mathbf{x}_{mn})} \right)^2 - \frac{12EI}{\ell_{mn}^3 A_{mn}} u(t, \mathbf{x}_{mn}) \right\} \phi_{mn}(\mathbf{x}') \, d\mathbf{x}' \end{aligned} \quad (10)$$

Under the assumption that the mirror deformations over Ω_{mn} are sufficiently small compared to D so that (6) may be approximated by (6'), equations (8) and (10) become linear. This assumption may not be justified when D is made small so as to reduce the operating voltage

levels of the actuators. For example, in Hornbeck's deformable mirror, D is 620 nm, and the peak mirror deformation for normal operation is around 100 nm. Evidently, (6') is not a good approximation for this case.

4. STATIC SHAPE CONTROL

Let $u_d = u_d(\mathbf{x})$ be the desired static shape of the mirror surface defined over the entire spatial domain Ω . It is required to determine the static voltages V_{mn} for each actuator to achieve the desired shape u_d . Let $K_s = K_s(\mathbf{x}, \mathbf{x}')$ denote the Green's function associated with the boundary-value problem:

$$\sum_{i=1}^2 \sum_{j=1}^2 \frac{\partial}{\partial x_i} \left(\sigma_{ij}(\mathbf{x}) \frac{\partial u}{\partial x_j} \right) = \delta(\mathbf{x} - \mathbf{x}'), \quad \mathbf{x} \in \Omega, \quad (11)$$

with boundary condition

$$u(\mathbf{x}) = 0 \quad \text{for } \mathbf{x} \in \partial\Omega. \quad (12)$$

Then, the static equation corresponding to (8) can be reformulated as an integral equation for the mirror displacement u corresponding to given static actuator voltages \bar{V}_{mn} :

$$u(\mathbf{x}) = \int_{\Omega} K_s(\mathbf{x}, \mathbf{x}') \sum_{m=1}^M \sum_{n=1}^N \left\{ \frac{1}{2} \varepsilon_0 \left(\frac{\bar{V}_{mn}}{D - u(\mathbf{x}_{mn})} \right)^2 - \frac{12EI}{\ell_{mn}^3 A_{mn}} u(\mathbf{x}_{mn}) \right\} \phi_{mn}(\mathbf{x}') d\mathbf{x}',$$

for $\mathbf{x} \in \Omega$. (13)

Let $\mathbf{u} = (u(\mathbf{x}_{11}), \dots, u(\mathbf{x}_{1N}), \dots, u(\mathbf{x}_{M1}), \dots, u(\mathbf{x}_{MN}))^T$ and $\bar{\mathbf{V}}^k = (\bar{V}_{11}^k, \dots, \bar{V}_{1N}^k, \dots, \bar{V}_{M1}^k, \dots, \bar{V}_{MN}^k)^T$, $k = 1, 2$. Setting $\mathbf{x} = \mathbf{x}_{ij}$ in (13) leads to a set of $M \times N$ algebraic equations relating \mathbf{u} and $\bar{\mathbf{V}}^2$. These equations can be written as

$$(\mathbf{I} + \mathbf{K})\mathbf{u} = \mathbf{P}(\mathbf{u})\bar{\mathbf{V}}^2, \quad (14)$$

where \mathbf{I} denotes the $MN \times MN$ identity matrix; \mathbf{K} is the $MN \times MN$ matrix whose k -th row \mathbf{K}_k is given by

$$\mathbf{K}_k = (K_{11}^{ij}, \dots, K_{1N}^{ij}, \dots, K_{M1}^{ij}, \dots, K_{MN}^{ij}), \quad i = \text{integer}(k/M), \quad j = k \text{ Mod}(M), \quad (15)$$

where

$$K_{mn}^{ij} = \left\{ \int_{\Omega} K_s(\mathbf{x}_{ij}, \mathbf{x}') \phi_{mn}(\mathbf{x}') d\mathbf{x}' \right\} \frac{12EI}{\ell_{mn}^3 A_{mn}}. \quad (16)$$

$\mathbf{P}(\mathbf{u})$ is the $MN \times MN$ matrix whose k -th row is $(p_{11}^{ij}(\mathbf{u}), \dots, p_{1N}^{ij}(\mathbf{u}), \dots, p_{M1}^{ij}(\mathbf{u}), \dots, p_{MN}^{ij}(\mathbf{u}))$, where

$$p_{mn}^{ij}(\mathbf{u}) = \frac{\varepsilon_0}{2(D - u(\mathbf{x}_{mn}))^2} \left\{ \int_{\Omega} K_s(\mathbf{x}_{ij}, \mathbf{x}') \phi_{mn}(\mathbf{x}') d\mathbf{x}' \right\},$$

$i = \text{integer}(k/M), \quad j = k \text{ Mod}(M). \quad (17)$

Explicit expressions for K_s and p_{mn}^{ij} corresponding to rectangular and circular mirrors are given in the Appendix.

If we set $\mathbf{u} = \mathbf{u}_d \triangleq (u_d(\mathbf{x}_{11}), \dots, u_d(\mathbf{x}_{1N}), \dots, u_d(\mathbf{x}_{M1}), \dots, u_d(\mathbf{x}_{MN}))^T$, then (14) becomes a set of $M \times N$ linear algebraic equations for the unknown actuator voltages $\bar{\mathbf{V}}$. Evidently, if $P(\mathbf{u}_d)$ is nonsingular, then $\bar{\mathbf{V}}^2$ is uniquely determined by

$$\bar{\mathbf{V}}^2 = P(\mathbf{u}_d)^{-1}(\mathbf{I} + \mathbf{K})\mathbf{u}_d. \quad (18)$$

The matrix $P(\mathbf{u}_d)$ is nonsingular if and only if its rows are linearly independent, or equivalently the $M \times N$ matrices given by

$$P_{ij}(\mathbf{u}_d) \triangleq \begin{bmatrix} p_{11}^{ij}(\mathbf{u}_d) & \dots & p_{1N}^{ij}(\mathbf{u}_d) \\ \vdots & & \vdots \\ p_{M1}^{ij}(\mathbf{u}_d) & \dots & p_{MN}^{ij}(\mathbf{u}_d) \end{bmatrix}, \quad i = 1, \dots, M; \quad j = 1, \dots, N, \quad (19)$$

are linearly independent. Since p_{mn}^{ij} depends on the desired mirror surface displacement \mathbf{u}_d , the set \mathcal{D} of all displacements \mathbf{u}_d such that $P(\mathbf{u}_d)$ is nonsingular corresponds to the set of all mirror surface displacements which have one-to-one correspondence with the actuator voltages $\bar{\mathbf{V}}_{mn}$. In fact, if we define the nonlinear mapping $\mathbf{u} = N(\mathbf{u})$ by $N(\mathbf{u}) = P(\mathbf{u})^{-1}(\mathbf{I} + \mathbf{K})\mathbf{u}$, then N is an invertible mapping with domain \mathcal{D} . In the case where the desired mirror surface deformation $\mathbf{u}_d = \mathbf{u}_d(\mathbf{x})$ has spatial symmetry, the number of equations in (14) can be reduced accordingly.

Now, given a set of actuator voltages $\bar{\mathbf{V}}$, the corresponding mirror surface displacements at the mesh points \mathbf{x}_{mn} can be determined by solving the nonlinear equation (14) for \mathbf{u} . If we define the nonlinear mapping $\mathbf{u} = N(\bar{\mathbf{V}}^2)\mathbf{u}$ by $N(\bar{\mathbf{V}}^2)\mathbf{u} = P(\mathbf{u})\bar{\mathbf{V}}^2 - \mathbf{K}\mathbf{u}$, then the solutions correspond to the fixed points of $N(\bar{\mathbf{V}})$. In physical situations where the actuator voltages satisfy a magnitude constraint of the form $\bar{V}_{mn}^2 \leq \bar{V}_{mn}^2 < \infty$, the set of all admissible $\bar{\mathbf{V}}$'s is given by $\mathcal{V} = \{\bar{\mathbf{V}} \in \mathbb{R}^{MN} : \bar{V}_{mn}^2 \leq \bar{V}_{mn}^2_{\max}, m = 1, \dots, M, n = 1, \dots, N\}$ (a hypercube in \mathbb{R}^{MN}). Then the set of all admissible \mathbf{u}_d 's is given by $N^{-1}(\mathcal{V})$.

Remarks:

(R-1) Once the required actuator voltages $\bar{\mathbf{V}}_{mn}$ for achieving the desired static mirror surface displacements at the mesh points are determined, the mirror surface displacements at other points in the spatial domain Ω can be found using (13) with $\mathbf{u}(\mathbf{x}_{mn})$ set to $\mathbf{u}_d(\mathbf{x}_{mn})$.

(R-2) In all the existing works on deformable mirrors, it is assumed that the static mirror surface displacements at the mesh points \mathbf{x}_{mn} are related to the actuator inputs by a linear transformation commonly called the influence function matrix which is valid for small

displacements. For large mirror displacements, the relation between $u(\mathbf{x}_{ij})$ and the actuator voltages \bar{V}_{mn} is given by (13) with \mathbf{x} set to \mathbf{x}_{ij} . This relation is implicit and nonlinear. In the special case of small displacements such that approximation (6') holds, this relation becomes linear. Using (13) with a single actuator at Ω_{mn} to obtain $u(\mathbf{x})$ in terms of \bar{V}_{mn} gives the usual influence function.

(R-3) If the number of actuators is less than the number of mesh points at which the desired mirror displacements are specified, then, under the linear approximation (6'), (14) consists of a set of overdetermined linear algebraic equations for the unknown variables \bar{V}_{mn}^2 . We may use the least-squares solution, which corresponds to obtaining the pseudo-inverse of the influence function matrix [3].

Noninteracting Actuation:

Due to stress in the membrane, the voltage \bar{V}_{mn} applied to the (m,n)-th actuator will influence the membrane displacements at all the patch locations. To simplify the mirror deformation control, it is desirable to introduce appropriate feedback and new control variables c_{mn} such that c_{mn} only influences the mirror displacement u at the mesh point \mathbf{x}_{mn} , and $u(\mathbf{x}_{mn})$ only depends on c_{mn} . Thus, the new controls c_{mn} produce noninteracting actuation of the mirror surface displacements at the mesh points. To achieve noninteraction, we introduce a static feedback control of the form $\bar{V}^2 = F(c - u)$, where F is a feedback gain matrix which may depend on u . Thus, in view of (14), we have

$$(I + K)u = P(u)F(c - u), \quad (20)$$

or

$$[I + (I + K)^{-1}P(u)F]u = (I + K)^{-1}P(u)Fc, \quad (21)$$

where $c = (c_{11}, \dots, c_{1N}, \dots, c_{M1}, \dots, c_{MN})^T$. To achieve noninteracting actuation, we seek an $MN \times MN$ matrix F such that $(I + K)^{-1}P(u)F = \Lambda$, a specified constant diagonal matrix with nonzero diagonal elements λ_{11} . Thus, u and c are related by a diagonal matrix operator given by

$$u = [I + \Lambda]^{-1}\Lambda c, \quad (22)$$

and the required feedback gain matrix F is given by

$$F = P(u)^{-1}(I + K)\Lambda. \quad (23)$$

In physical terms, the static feedback control in effect cancels the spring coupling forces to produce noninteracting actuation with respect to the new control c . In the special case where the mirror displacements are small as compared to the actuator gap D so that approximation (6') is valid, P becomes a constant matrix. Consequently, F is also a constant matrix and the noninteracting controller is linear. We note that $P(u)$ and K depend on the parameters E , I , D , and l_{mn} whose values can be accurately estimated. Therefore F can be determined with good accuracy. Finally, the foregoing noninteracting controller is also valid for the

dynamic case, since the couplings between the mirror displacements at the mesh points involve elastic forces only.

5. DYNAMIC SHAPE CONTROL

Assuming that the desired nominal static-shape u_d for the mirror is attainable by appropriate choices of the actuator voltages \bar{V}_{mn} , it is of interest to control the deviations of the mirror shape about u_d for wavefront correction. We propose to achieve this objective in three steps. Figure 4 shows the proposed structure of the overall control system for wavefront correction. First, a static feedback controller for achieving the desired nominal static mirror-shape and noninteracting actuation of the deformable mirror is introduced. The function of the minor-loop feedback controller is to modify the dynamic response of the actuators. This modification can also be performed ahead of the static feedback controller depending on the method of implementation. Finally, a global feedback controller which makes use of the output of the wavefront estimator to generate the appropriate actuating signals for wavefront correction is introduced. The static feedback controller has already been discussed in Sec.4. In what follows, the discussion will be devoted to the modification of the dynamic response of the actuator, and the global shape controller for wavefront correction.

5.1 Actuator Dynamics Modification

The main objective here is to modify the dynamics of the actuator to ensure satisfactory response to input commands. Since this controller is to be integrated with the mirror assembly, the control law should have the following properties:

- (i) It should be sufficiently simple so that it can be realized by microelectronic circuitry which can be integrated monolithically with the mirror microstructure.
- (ii) It should be model independent so that it is unnecessary to identify the system parameters for their implementation.
- (iii) Its performance should be sufficiently robust with respect to system parameter variations.

Since the mirror surface has very little internal damping, the actuator forces may induce undesirable surface vibrations. Therefore, it is necessary to introduce damping externally. A possible approach is to introduce external passive damping. This may be achieved by housing the bottom mirror assembly in an enclosure which contains air, and has minute holes for air passage. Alternatively, damping can be achieved by means of active feedback controls.

To derive appropriate forms for the active feedback controls, we make use of the partial differential equation (8) linearized about the nominal mirror surface deformation $\hat{u}_d = \hat{u}_d(\mathbf{x})$ produced by the static actuator voltage \bar{V} which produces the desired u_d . Note that $\hat{u}_d(\mathbf{x}) = u_d(\mathbf{x})$ only at the mesh points $\mathbf{x} = \mathbf{x}_{mn}$. Let $\delta u = u - \hat{u}_d$, and $\delta V = V - \bar{V}$. The linearized equation (8) is given by

$$\rho(\mathbf{x}) \frac{\partial^2 \delta u}{\partial t^2} - \sum_{i=1}^2 \sum_{j=1}^2 \frac{\partial}{\partial x_i} \left(\sigma_{ij}(\mathbf{x}) \frac{\partial \delta u}{\partial x_j} \right)$$

$$= \sum_{m=1}^M \sum_{n=1}^N \left\{ \left(\frac{\varepsilon_o \bar{V}_{mn}^2}{(D - u_d(\mathbf{x}_{mn}))^3} - \frac{12EI}{\ell^3 A_{mn}} \right) \delta u(t, \mathbf{x}_{mn}) + \frac{\varepsilon_o \bar{V}_{mn} \delta V_{mn}(t)}{(D - u_d(\mathbf{x}_{mn}))^2} \right\} \phi_{mn}(\mathbf{x}), \quad (24)$$

with boundary condition

$$\delta u(t, \mathbf{x}) = 0 \text{ for } \mathbf{x} \in \partial\Omega \text{ and } t \geq 0, \quad (25)$$

and initial conditions:

$$\delta u(0, \mathbf{x}) = u_o(\mathbf{x}) - u_d(\mathbf{x}), \quad \frac{\partial \delta u}{\partial t}(0, \mathbf{x}) = u'_o(\mathbf{x}) \text{ for } \mathbf{x} \in \Omega. \quad (26)$$

Consider the total energy functional of the perturbed mirror surface about u_d given by

$$\begin{aligned} \mathcal{E} = & \frac{1}{2} \int_{\Omega} \left\{ \rho(\mathbf{x}) \left(\frac{\partial \delta u}{\partial t} \right)^2 + T \left[\left(\frac{\partial \delta u}{\partial x_1} \right)^2 + \left(\frac{\partial \delta u}{\partial x_2} \right)^2 \right] \right\} d\mathbf{x} \\ & - \frac{1}{2} \int_{\Omega} \sum_{m=1}^M \sum_{n=1}^N \left(\frac{\varepsilon_o \bar{V}_{mn}^2}{(D - u_d(\mathbf{x}_{mn}))^3} - \frac{12EI}{\ell^3 A_{mn}} \right) (\delta u(t, \mathbf{x}))^2 \phi_{mn}(\mathbf{x}) d\mathbf{x}. \end{aligned} \quad (27)$$

This energy functional is nonnegative for all δu and $\partial \delta u / \partial t$ in the Sobolev space $H_0^1(\Omega)$ (i.e. the Hilbert space of all real-valued square integrable functions defined on Ω and vanishing on $\partial\Omega$ such that their first-order partial derivatives are also square integrable), if

$$\frac{\varepsilon_o \bar{V}_{mn}^2}{(D - u_d(\mathbf{x}_{mn}))^3} < \frac{12EI}{\ell^3 A_{mn}} \text{ for } m = 1, \dots, M, n = 1, \dots, N. \quad (28)$$

The time rate-of-change of \mathcal{E} , after integration by parts, and making use of (24) and boundary condition (25), is given by

$$\begin{aligned} d\mathcal{E}/dt = & \int_{\Omega} \frac{\partial \delta u}{\partial t} \left(\sum_{m=1}^M \sum_{n=1}^N \left\{ \left(\frac{\varepsilon_o \bar{V}_{mn}^2}{(D - u_d(\mathbf{x}_{mn}))^3} - \frac{12EI}{\ell^3 A_{mn}} \right) [\delta u(t, \mathbf{x}_{mn}) - \delta u(t, \mathbf{x})] \right. \right. \\ & \left. \left. + \frac{\varepsilon_o \bar{V}_{mn} \delta V_{mn}(t)}{(D - u_d(\mathbf{x}_{mn}))^2} \right\} \phi_{mn}(\mathbf{x}) \right) d\mathbf{x} \end{aligned} \quad (29)$$

By requiring that $\delta u(t, \mathbf{x}) = \delta u(t, \mathbf{x}_{mn})$ and $\partial \delta u(t, \mathbf{x}) / \partial t = \partial \delta u(t, \mathbf{x}_{mn}) / \partial t$ for all $\mathbf{x} \in \Omega_{mn}$, (29) reduces to

$$d\mathcal{E}/dt = \sum_{m=1}^M \sum_{n=1}^N \frac{\varepsilon_o \bar{V}_{mn} \delta V_{mn}(t)}{(D - u_d(\mathbf{x}_{mn}))^2} \left\{ \int_{\Omega_{mn}} \phi_{mn}(\mathbf{x}) d\mathbf{x} \right\} \frac{\partial \delta u(t, \mathbf{x}_{mn})}{\partial t}. \quad (30)$$

If we set

$$\delta V_{mn}(t) = -\gamma_{mn} \frac{\partial \delta u}{\partial t}(t, \mathbf{x}_{mn}) \phi_{mn}(\mathbf{x}), \quad \gamma_{mn} > 0, \quad (31)$$

then

$$d\mathcal{E}/dt = - \sum_{m=1}^M \sum_{n=1}^N \frac{\varepsilon_0 \bar{V}_{mn} \gamma_{mn}}{(D - u_d(\mathbf{x}_{mn}))^2} \left\{ \int_{\Omega_{mn}} \phi_{mn}(\mathbf{x}) d\mathbf{x} \right\} (\partial \delta u(t, \mathbf{x}_{mn}) / \partial t)^2 \leq 0. \quad (32)$$

The control law (31) implies local rate-feedback at each actuator location with feedback gain $-\gamma_{mn}$ only.

Incorporating the foregoing local rate-feedback with the noninteracting controller, the transfer function between u and c is a diagonal matrix $H(s)$ whose diagonal elements have the form:

$$h_{11}(s) = \frac{g_i}{(s^2 + 2\zeta_i \omega_i s + \omega_i^2)}, \quad i = 1, \dots, NM. \quad (33)$$

To achieve zero steady-state error for step actuator commands, a proportional-plus-integral minor-loop controller is introduced. The parameters of the controller and the gain g_i are chosen to ensure stability and satisfactory transient response to step-input commands. When the noninteracting controls are implemented by means of a digital computer, processing delays are introduced. These time-delays may be incorporated in $h_{11}(s)$.

5.2 Global Controller for Wavefront Correction

The initial step in wavefront correction is to estimate the wavefront of the incoming light wave reflected from the deformable mirror based on the output of the wavefront sensor. In physical situations, a wavefront sensor such as the Hartmann-Shack wavefront sensor uses an array of micro-lenses, each of which samples a portion of the incoming beam and focuses light onto a detector consisting of a CCD camera or a lateral field-effect photodiode array.

Let Ω_s be a bounded open connected subset of R^2 corresponding to the effective spatial domain of the wavefront sensor. We introduce a mesh on Ω_s whose mesh points are denoted by $\hat{\mathbf{x}}_{mn} = (\hat{x}_{1m}, \hat{x}_{2n})$, $m = 1, \dots, \hat{M}$; $n = 1, \dots, \hat{N}$. At each mesh point $\hat{\mathbf{x}}_{mn}$, we introduce a patch Ω_s^{mn} , a bounded open subset of Ω_s , representing the effective aperture of the (m,n) -th lenslet containing $\hat{\mathbf{x}}_{mn}$ as an interior point. Let $\Psi = \Psi(t, \hat{\mathbf{x}})$ denote the wavefront of the incoming wave reflected from the deformable mirror and impinging onto the wavefront sensor. The local gradient or angular tilt in the wavefront averaged over the aperture of the (m,n) -th lenslet is given by

$$\overline{\nabla \Psi(t, \cdot)} \Big|_{\mathbf{x}_{mn}} \triangleq \int_{\Omega_s^{mn}} \psi_{mn}(\mathbf{x}) \nabla \Psi(t, \mathbf{x}) d\mathbf{x} = f^{-1}(\hat{\mathbf{x}} - \hat{\mathbf{x}}_{mn}^0), \quad (34)$$

where ψ_{mn} is a given spatial weighting function associated with the (m,n) -th lenslet; f is the focal length of the lenslet; $\hat{\mathbf{x}}_{mn}^0$ is the nominal position of the focal spot for a collimated beam, and \mathbf{x} is the position of the focal spot for the incoming beam. Thus, the angular tilt in the wavefront can be estimated by measuring the deviations $(\hat{\mathbf{x}} - \hat{\mathbf{x}}_{mn}^0)$. From the local gradient data, it is possible to obtain an estimate of the

wavefront $\Psi = \Psi(t, \hat{\mathbf{x}})$ [12]. For wavefront sensors with circular apertures, it is advantageous to express Ψ in terms of Zernike polynomials. By comparing Ψ with a reference wavefront Ψ_R , we obtain the wavefront error $\delta\Psi = \Psi_R - \Psi$. In order to generate the mirror shape correction command from $\delta\Psi$, it is necessary to map the wavefront sensor domain Ω_s onto the mirror domain Ω . Let this mapping be a diffeomorphism S from Ω_s onto Ω . Then the mirror shape correction command δc is obtained by evaluating $\delta C(t, \mathbf{x}) \triangleq \delta\Psi(t, S^{-1}\mathbf{x})$ at all the actuator locations \mathbf{x}_{mn} in Ω . Again, due to the presence of processing delays in the wavefront estimator, a dynamic compensator may be incorporated in the global shape controller to ensure overall system stability.

6. PHYSICAL IMPLEMENTATION

In the physical implementation of the proposed control system, it is desirable to integrate as much as possible the electronic circuitry of the controllers with the mirror assembly. Due to the minute capacitances associated with the actuators, it is clear that the actuator drivers consisting of operational amplifiers must be located in the immediate vicinities of the actuators.

To implement the rate-feedback control given by (31) for damping, consider a parallel-plate capacitor driven by an operational amplifier as shown in Fig.5. Assume that the distance Δ between the capacitor plates is time varying so that the capacitance $C(t) = \epsilon_0 A / \Delta(t)$, where A is the area of each plate. Thus, we have

$$C(t) \frac{dv(t)}{dt} + v(t) \frac{dC(t)}{dt} = i(t), \quad (35)$$

where i is the current flowing to the capacitor. Using the expression for $C(t)$, (35) can be rewritten as

$$\frac{\epsilon_0 A}{\Delta(t)} \frac{dv}{dt} - \frac{\epsilon_0 A}{\Delta(t)^2} v \frac{d\Delta(t)}{dt} = i(t). \quad (36)$$

Now, if the voltage $v(t)$ is held at a constant value v_0 , then the plate velocity is related to $i(t)$ by

$$\frac{d\Delta(t)}{dt} = - \frac{i(t)\Delta(t)^2}{\epsilon_0 A v_0}. \quad (37)$$

Thus, rate-feedback can be introduced by sensing the current $i(t)$ through a resistor in series with the capacitor as shown in Fig.5. The current-sensing resistor can be attached directly to the bottom plate.

The proportional-plus-integral minor-loop controller can also be realized using operational amplifiers which can be integrated with the mirror assembly. Since the noninteracting controller requires algebraic manipulations, an external digital computer is needed for its implementation. However, it is possible to integrate this controller with the mirror assembly when single-chip specialized computers become available.

Finally, the wavefront estimator and the global mirror shape

controller require a digital computer with sufficiently high speed so that the processing time delay will not be detrimental to the performance of the overall system. Most likely, these components cannot be integrated with the mirror assembly.

To obtain some information on the orders of magnitude of various system parameters and variables, we consider a 1.7 mm square rectangular mirror with 15×15 actuator patches. Each patch is a $25 \mu\text{m}$ square pixel. The mirror membrane, leaf springs, and supporting posts are micromachined from single-crystal silicon sheets. Each leaf spring is a $45\text{-}\mu\text{m}$ long, $1\text{-}\mu\text{m}$ thick cantilever beam with rectangular cross-section (width = $4 \mu\text{m}$). Using known data for single-crystal silicon [13] (Young's modulus $E = 1.9 \times 10^7 \text{ N/cm}^2$, and mass density $\rho = 2.3 \text{ gm/cm}^3$), the electrostatic and spring forces associated with a single actuator can be computed from (6) and (7):

$$F_e \stackrel{\Delta}{=} f_e A = 2.7669 \times 10^{-21} [V/(D - u)]^2 \text{ N} \quad (38)$$

$$F_s \stackrel{\Delta}{=} f_s A = 8.340 \times 10^{-4} u \text{ N} \quad (39)$$

where V is the actuator voltage, D is in meters, and u is the tip displacement of the leaf spring in meters. For a square membrane with width L under uniform tension T , the upward restoring force on a square pixel with width ℓ located at the center of the membrane with a downward displacement u is given approximately by

$$F_T = 8T\ell u/L \text{ N.} \quad (40)$$

For $T = 1 \text{ N/m}$, and the given dimensions for the membrane and pixels, (40) becomes

$$F_T = 0.11765u \text{ N.} \quad (40')$$

For a typical membrane displacement $u = 0.1 \mu\text{m}$, and $D = 0.5 \mu\text{m}$, the required actuator voltage V can be computed by balancing the upward restoring forces F_s and F_T with the downward force F_e . The resulting V is equal to 0.8248 volt which is within the operating range of typical operational amplifiers.

Using the foregoing mirror parameters, the static actuator voltages V_{mn} for attaining a bi-parabolic mirror deformation are given by

$$u_d(x_1, x_2) = 1.9156 \times 10^{-13} (850^2 - x_1^2)(850^2 - x_2^2) \mu\text{m.} \quad (41)$$

The results are shown in Fig. 6.

7. CONCLUDING REMARKS

In this paper, we have only considered the analytical design of a control system for a micromachined deformable mirror. The approach is to introduce first appropriate static feedback controls for noninteracting actuation. Both local rate-feedback and a minor-loop controller are introduced for modifying the dynamics of the actuators. Then a global controller is introduced for wavefront correction. Special consideration is taken to integrate the controllers with the mirror assembly. Other important factors such as thermal effects on the performance of the controlled deformable mirror are not studied here. The results pertaining to the fabrication of the proposed deformable mirror, and the actual

performance of the proposed control system are planned to be reported in the near future.

Acknowledgments

This work was performed at the Jet Propulsion Laboratory, California Institute of Technology, under contract with the National Aeronautics and Space Administration. The work of P.K.C. Wang was also supported in part by NSF Grant ECS 87-18473.

References

- [1] J. Hecht, *Beam Weapons*, Plenum Press, New York, 1984.
- [2] M.A. Ealey, "Active and Adaptive Optical Components: The Technology and Future Trends," *Adaptive Optics and Optical Structures*, R.K. Tyson and J. Schulte in den Bäumen, Editors, *Proc.SPIE*, Vol.1271, pp.2-34, 1990.
- [3] R.K. Tyson, *Principles of Adaptive Optics*, Academic Press, 1991.
- [4] R.P. Grosso and M. Yellin, "The Membrane Mirror as an Adaptive Optical Element," *J.Opt.Soc. Am.*, Vol.67, No.3, 1977, pp.399-406.
- [5] J. Feinleib, S.G. Lipson, and P.F. Cone, "Monolithic Piezoelectric Mirror for Wavefront Correction," *Appl.Phys.Lett.*, Vol.25, pp.311-313, 1974.
- [6] V.V. Apollonov *et al.*, "Magnetostrictive Actuators in Optical Design," *Active and Adaptive Optical Components*, M.A. Ealey, Editor, *Proc.SPIE*, Vol.1543, pp.313-324, 1991.
- [7] W.G. Thorburn and L. Kaplan, "A Low Voltage Electrodistortive Mirror System for Wavefront Control," *Active and Adaptive Optical Components*, M.A. Ealey, Editor, *Proc.SPIE*, Vol.1543, pp.52-63, 1991.
- [8] M.A. Ealey, "Precision Electrodisplacive Microactuators," *Precision Engineering and Optomechanics*, D. Vukobratovich, Editor, *Proc.SPIE*, Vol.1167, pp.85-102, 1989.
- [9] M.A. Ealey and J.F. Washeba, "Continuous Facesheet Low Voltage Deformable Mirrors," *Opt.Engr.*, Vol.29, No.10, 1990, pp.1191-1198.
- [10] L.J. Hornbeck, "128 x 128 Deformable Mirror Device," *IEEE Trans. Electron Devices*, Vol.ED-30, No.5, pp.539-545, 1983.
- [11] M.A. Ealey and C.E. Wheeler, "Integrated Wavefront Corrector," *Adaptive Optics and Optical Structures*, R.K. Tyson and J. Schulte in den Bäumen, Editors, *Proc.SPIE*, Vol.1271, pp.254-264, 1990.
- [12] D.L. Fried, "Least Square Fitting a Wavefront Distortion Estimate to an Array of Phase Difference Measurements," *J.Opt.Soc. Am.*, Vol.67, pp.370-375, 1977.
- [13] K.E. Petersen, "Silicon as a Mechanical Material," *Proc. IEEE*, Vol.70, No.5, pp.420-457, 1982.

APPENDIX

Explicit expressions for K_s and p_{mn}^{ij} corresponding to rectangular and circular mirrors are given below.

For a rectangular mirror with spatial domain $\Omega = \Omega_R \stackrel{\Delta}{=} \{(x_1, x_2) \in R^2: |x_i| < l_i, i = 1, 2\}$ and uniform tension T , the Green's function K_s is given by

$$K_s(x_1, x_2, x'_1, x'_2) = \sum_{k=1}^{\infty} \sum_{k'=1}^{\infty} \frac{4l_1 l_2}{\pi T(k^2 l_1^2 + k'^2 l_2^2)} \sin\left(\frac{k\pi(x_1 + l_1)}{2l_1}\right) \sin\left(\frac{k'\pi(x_2 + l_2)}{2l_2}\right) \times \sin\left(\frac{k'\pi(x'_1 + l_1)}{2l_1}\right) \sin\left(\frac{k\pi(x'_2 + l_2)}{2l_2}\right). \quad (A1)$$

Let the actuator patches Ω_{mn} be square pixels with width Δ . Thus $\Omega_{mn} = \{(x_1, x_2) \in R^2: |x_1 - x_{1m}| < \Delta/2, |x_2 - x_{2n}| < \Delta/2\}$. Assuming that the actuator weighting function ϕ_{mn} corresponds to the characteristic function of Ω_{mn} (i.e. $\phi_{mn}(\mathbf{x}) = 1$ if $\mathbf{x} \in \Omega_{mn}$, and $\phi_{mn}(\mathbf{x}) = 0$ otherwise), the coefficients p_{mn}^{ij} defined by (17) are given by

$$p_{mn}^{ij} = \frac{\epsilon_0}{2(D - u_d(\mathbf{x}_{mn}))^2} \sum_{k=1}^{\infty} \sum_{k'=1}^{\infty} \frac{4l_1 l_2 \alpha_{mk'} \beta_{nk'}}{\pi T(k^2 l_1^2 + k'^2 l_2^2)} \times \sin\left(\frac{k\pi(x_{1i} + l_1)}{2l_1}\right) \sin\left(\frac{k'\pi(x_{2j} + l_2)}{2l_2}\right), \quad (A2)$$

where $\mathbf{x}_{ij} = (x_{1i}, x_{2j})$, and

$$\alpha_{mk'} = \int_{x_{1m} - \Delta/2}^{x_{1m} + \Delta/2} \sin\left(\frac{k'\pi(x'_1 + l_1)}{2l_1}\right) dx'_1 = \frac{2l_1}{k'\pi} \left\{ \cos\left(k'\pi\left(x_{1m} - \frac{\Delta}{2} + l_1\right)\right) - \cos\left(k'\pi\left(x_{1m} + \frac{\Delta}{2} + l_1\right)\right) \right\}, \quad (A3)$$

$$\beta_{nk'} = \int_{x_{2n} - \Delta/2}^{x_{2n} + \Delta/2} \sin\left(\frac{k\pi(x'_2 + l_2)}{2l_2}\right) dx'_2 = \frac{2l_2}{k\pi} \left\{ \cos\left(k\pi\left(x_{2n} - \frac{\Delta}{2} + l_2\right)\right) - \cos\left(k\pi\left(x_{2n} + \frac{\Delta}{2} + l_2\right)\right) \right\}. \quad (A4)$$

The Green's function K_s for a circular mirror with spatial domain $\Omega_c = \{(r, \theta), 0 \leq r \leq r_0, 0 \leq \theta \leq 2\pi\}$ and uniform tension T is given by

$$K_s(\theta, r, \theta', r') = \sum_{k=1}^{\infty} \sum_{k'=1}^{\infty} \frac{2}{\pi T r_o^2 [J_{k+1}(\lambda_{kk}, r_o)]^2} J_k(\lambda_{kk}, r) [J_{kk'}(\lambda_{kk}, r') \cos(k\theta) \times \cos(k\theta') + J_{kk'}(\lambda_{kk}, r') \sin(k\theta) \sin(k\theta')], \quad (A5)$$

where J_k denotes the Bessel function of the first kind of order k , and (λ_{kk}, r_o) is k' -th zero of J_k .

Let the actuator patches Ω_{mn} be fan-shaped pixels with radial length Δ and aperture angle θ_p as shown in Fig.3. Thus $\Omega_{mn} = \{(\theta, r): |\theta - \theta_m| < \theta_p/2, |r - r_n| < \Delta/2\}$. In this case, the coefficients p_{mn}^{1j} defined by (17) with ϕ_{mn} being the characteristic function of Ω_{mn} are given by

$$p_{mn}^{1j} = \frac{\epsilon_o}{2(D - u_d(\mathbf{x}_{mn}))^2} \sum_{k=1}^{\infty} \sum_{k'=1}^{\infty} \frac{2}{\pi T r_o^2 [J_{k+1}(\lambda_{kk}, r_o)]^2} J_k(\lambda_{kk}, r_j) \times [\hat{\alpha}_{mk'} \cos(k\theta_1) + \hat{\beta}_{nk'} \sin(k\theta_1)], \quad (A6)$$

where

$$\hat{\alpha}_{mk'} = \left\{ \int_{\theta_{mk'} - \theta_p/2}^{\theta_{mk'} + \theta_p/2} \cos(k'\theta') d\theta' \right\} \left\{ \int_{r_n - \Delta/2}^{r_m + \Delta/2} J_{kk'}(\lambda_{kk}, r') r' dr' \right\}, \quad (A7)$$

$$\hat{\beta}_{nk'} = \left\{ \int_{\theta_{nk'} - \theta_p/2}^{\theta_{nk'} + \theta_p/2} \sin(k'\theta') d\theta' \right\} \left\{ \int_{r_n - \Delta/2}^{r_n + \Delta/2} J_{kk'}(\lambda_{kk}, r') r' dr' \right\}. \quad (A8)$$

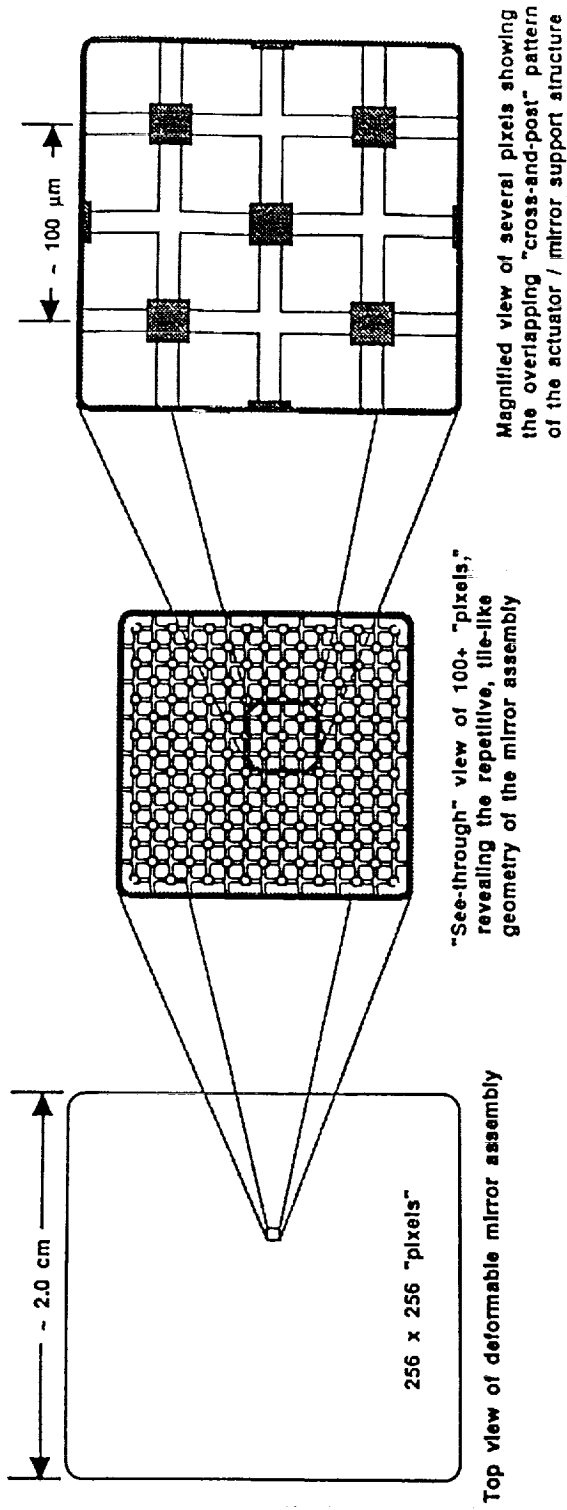
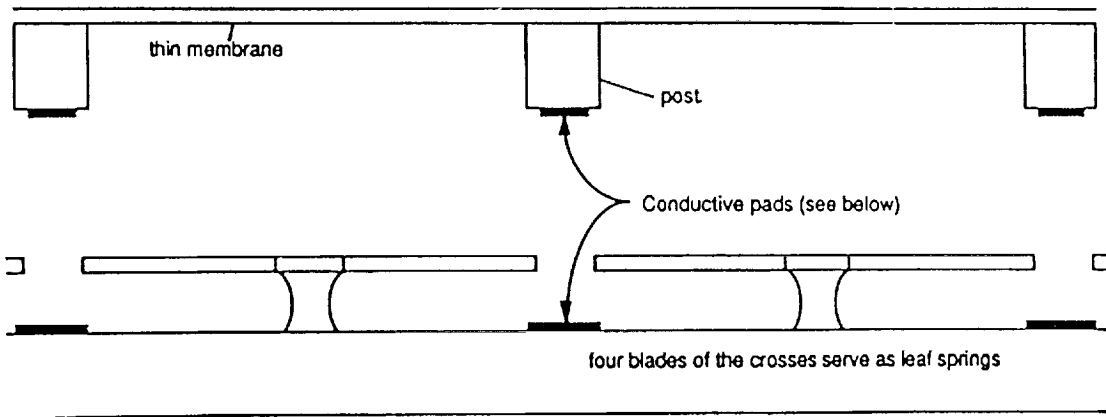


Fig.1 Top view of the deformable mirror.

Side view of upper wafer



Side view of the lower wafer

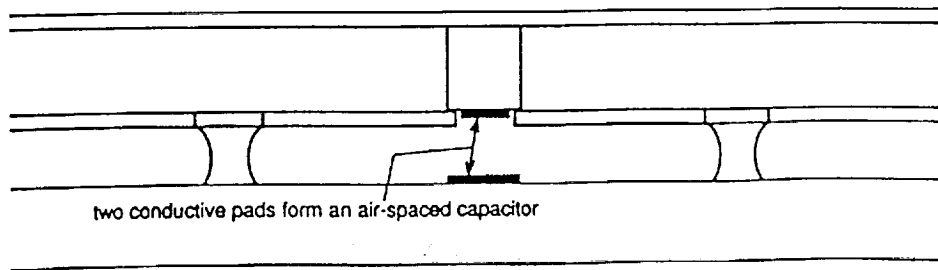
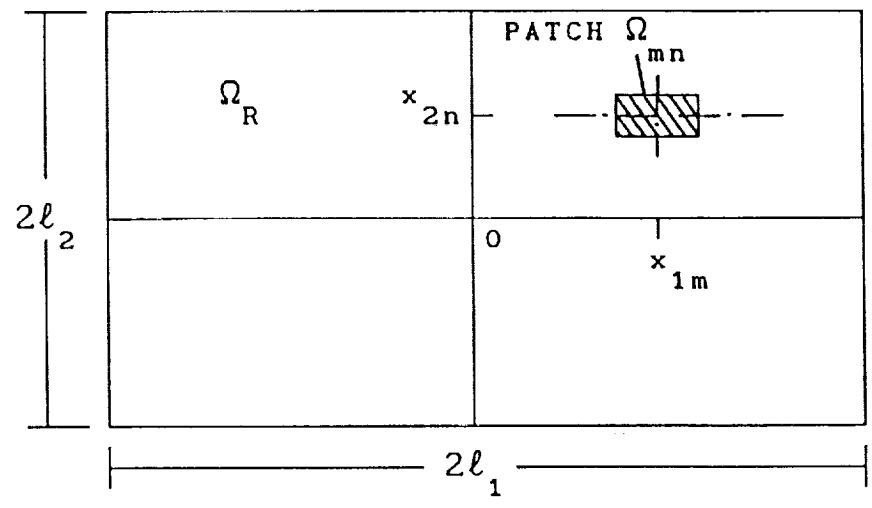


Fig.2 Side view of the deformable mirror.

RECTANGULAR MIRROR: $\Omega_R \triangleq \{(x_1, x_2) \in \mathbb{R}^2: |x_1| \leq l_1, |x_2| \leq l_2\}$,



CIRCULAR MIRROR: $\Omega_c \triangleq \{(r, \theta), 0 \leq r \leq r_o, 0 \leq \theta \leq 2\pi\}$.

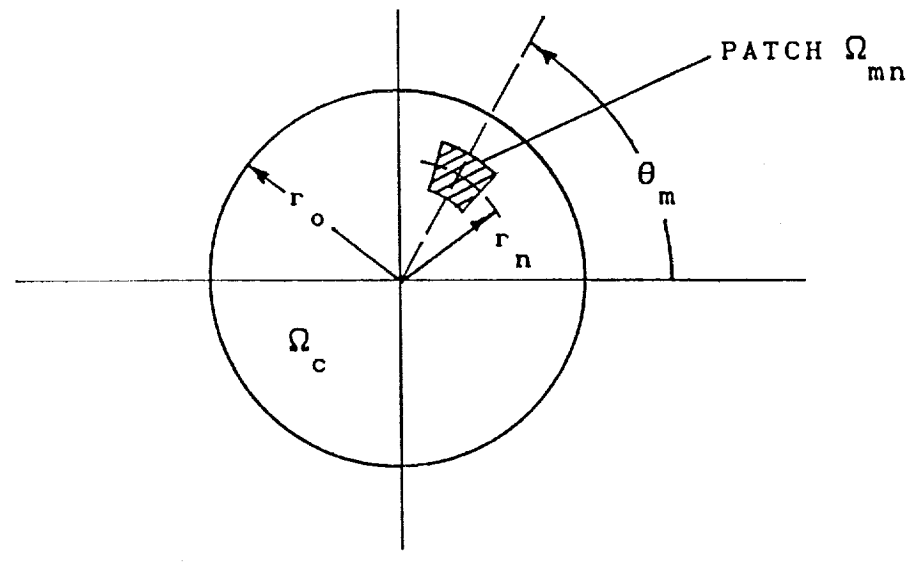


Fig.3 Typical meshes and patches for rectangular and circular Mirrors.

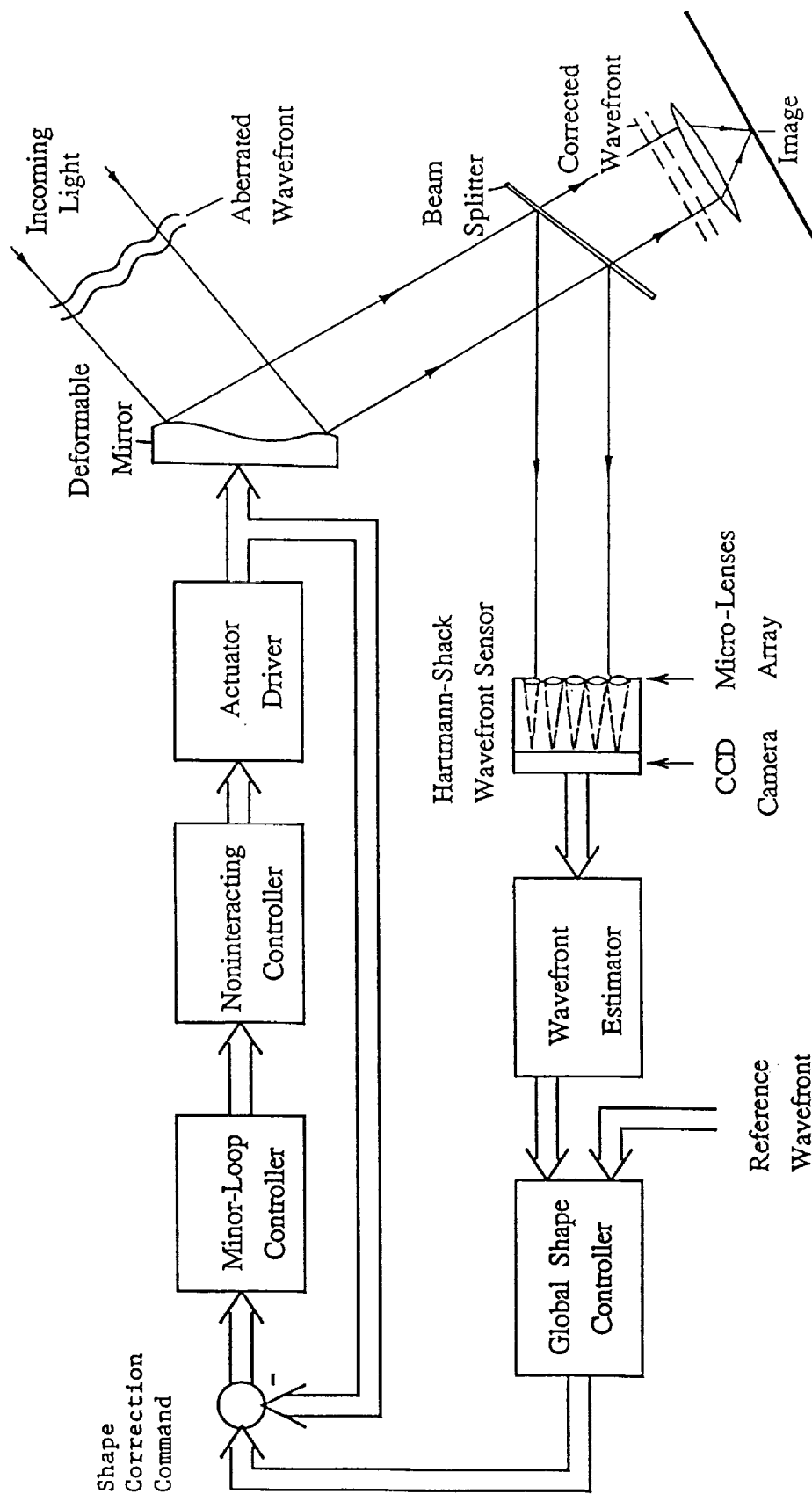


Fig. 4 Structure of the overall control system for wavefront correction.

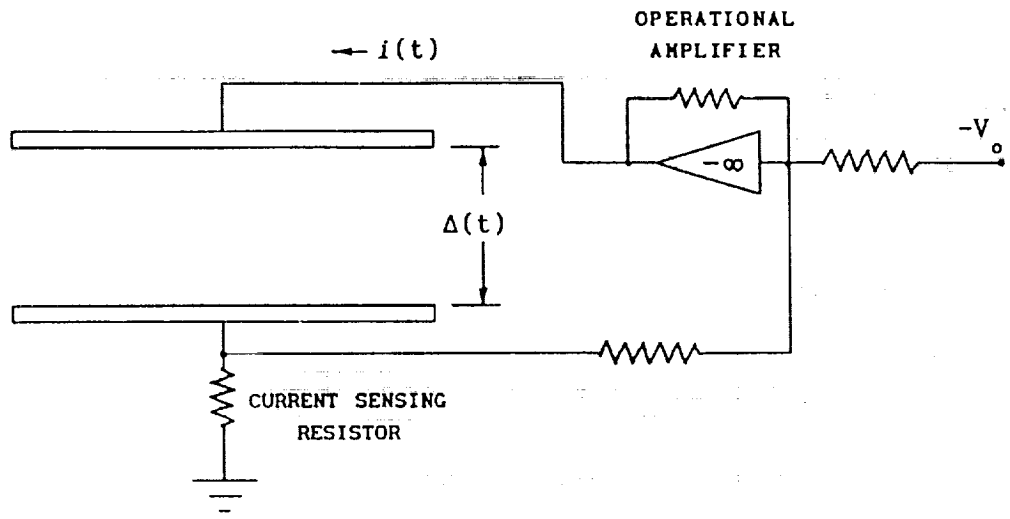


Fig.5 Implementation of local rate-feedback control.

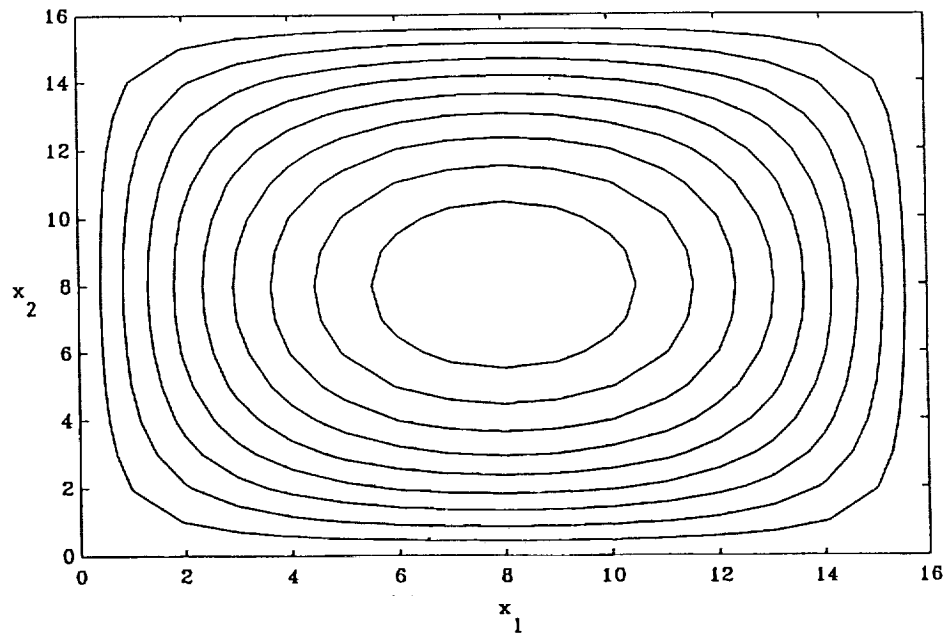
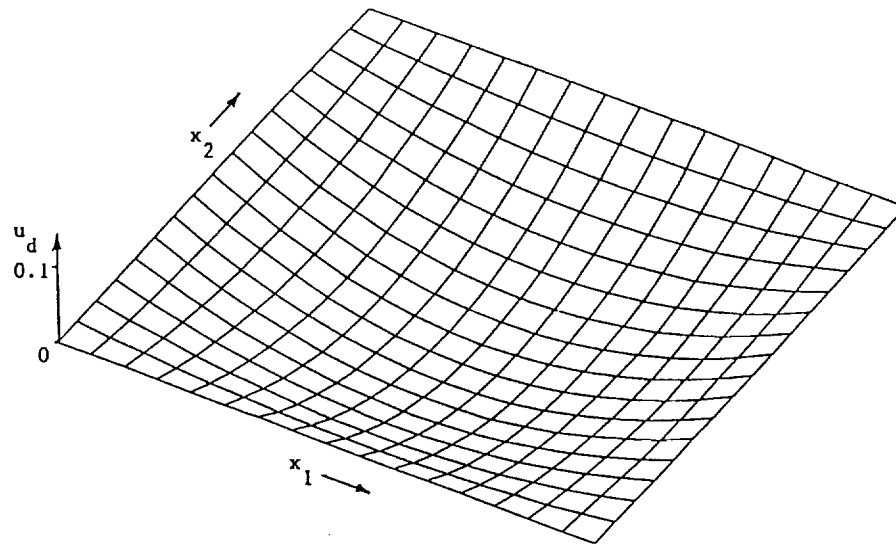


Fig.6a Desired bi-parabolic deformation u_d for a 1.7 mm square mirror with 15×15 actuators. (Minimum deformation at mirror center = $0.1 \mu\text{m}$.)

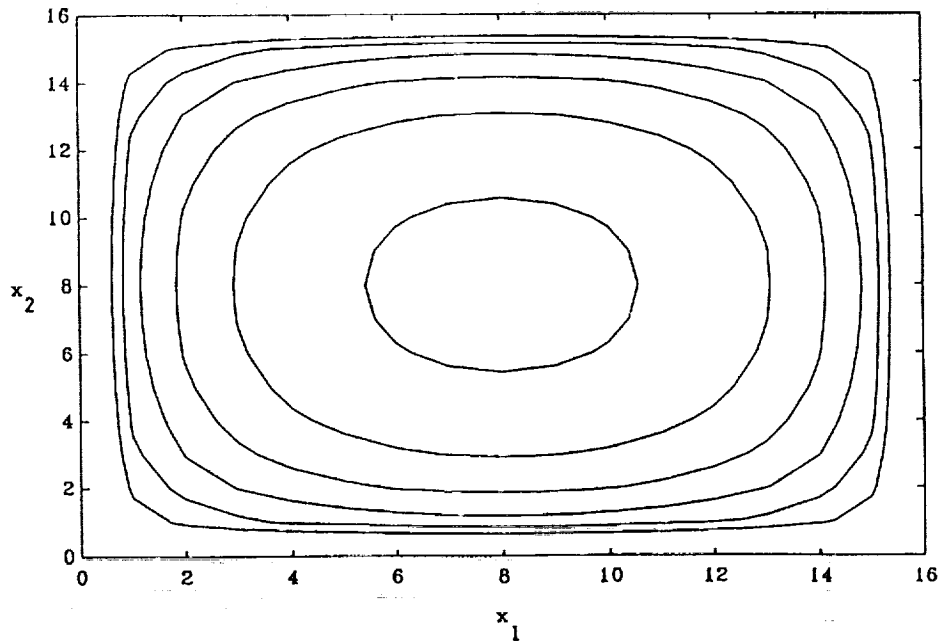
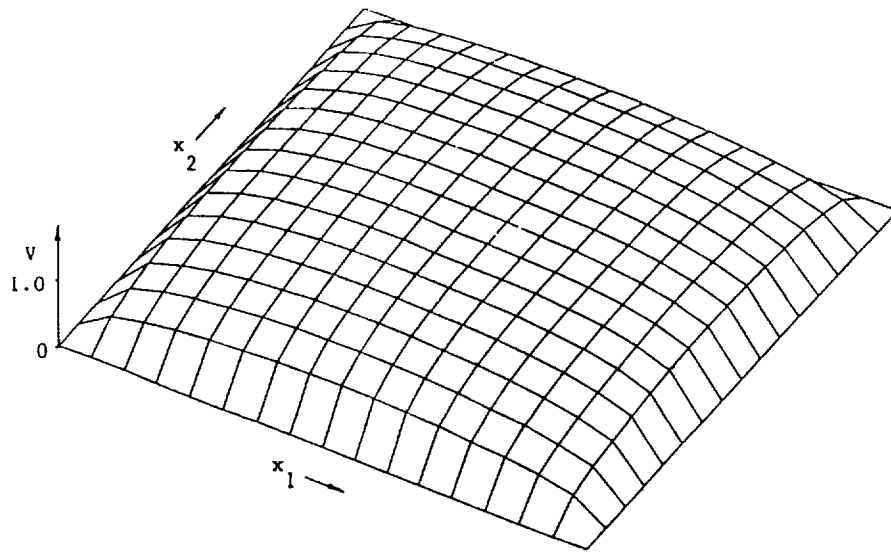


Fig.6b Required static actuator voltages V_{mn} for bi-parabolic mirror deformation given in Fig.6a. (Maximum voltage at mirror center = 0.8248 volt.)

Emerging Technologies in Microguidance and Control

Presented at Workshop on
Microtechnologies and Applications to Space Systems

at Jet Propulsion Laboratory
May 27 and 28, 1992

sponsored by NASA Office of Aeronautics and Space Technology

Dr. Marc S. Weinberg
The Charles Stark Draper Laboratory
Cambridge, MA 02139

Abstract

The Charles Stark Draper Laboratory has invented and developed inertial guidance systems for earth and space applications for over 50 years. Employing recent advances in microfabrication, Draper has developed inertial instruments of very small size and low cost. Microfabrication employs the batch processing techniques of solid-state electronics, such as photolithography, diffusion, and etching to carve mechanical parts. Within a few years, microfabricated gyroscopes should perform in the 10 to 100 deg/h range. Microfabricated accelerometers have demonstrated performance in the 50 to 500 microgravity range. These instruments will result in not only the redesign of conventional military products, but also new applications that could not exist without small, inexpensive sensors and computing.

Draper's microfabricated accelerometers and gyroscopes will be described and test results summarized. Associated electronics and control issues will also be addressed. Gimballed, vibrating gyroscopes and force rebalance accelerometers constructed from bulk silicon, polysilicon surface-machined tuning fork gyroscopes, and quartz resonant accelerometers and gyroscopes will be examined. Draper is pursuing several types of devices for the following reasons: (1) to address wide ranges of performance; (2) to realize construction in a flat pack; and (3) to lessen the risks associated with emerging technologies.

Introduction

The Charles Stark Draper Laboratory has invented and developed inertial guidance systems for earth and space applications for over 50 years. Recent advances in microfabrication have resulted in inertial instruments of very small size and low cost. Microfabrication employs the batch processing techniques of solid-state electronics, such as photolithography, diffusion, and etching to carve mechanical parts. These instruments and digital computing will result in not only the redesign of conventional military products, but also new applications which could not exist without small, inexpensive sensors, inertial measurement units (IMU), and computing.

Draper's microfabricated accelerometers and gyroscopes will be described and test results summarized. Associated electronics and control issues will also be addressed briefly. Gimballed, vibrating gyroscopes and force rebalance accelerometers constructed from bulk silicon, polysilicon surface-machined tuning fork gyroscopes, and quartz resonant accelerometers and gyroscopes will be examined. Draper is pursuing several types of devices for the following reasons: (1) to address wide ranges of performance; (2) to realize construction in a flat pack; and (3) to lessen the risks associated with emerging technologies.

Silicon Instruments

Gimballed Gyroscope

The silicon gimballed gyro was the first micromachined instrument which Draper has designed and built. A photograph of a gimballed gyro is shown in Figure 1. The gyro's operation is shown schematically in Figure 2. The gyro does not rotate continuously. The outer gimbal is driven at the resonance of the inner, sense gimbal resulting in a sinusoidal velocity of the effective masses along the X axis (defined by the inner flexures). Coriolis acceleration induced by a rate applied about the perpendicular Z axis causes a torque about the inner flexures, the sense axis.

Open loop, the amplitude of the inner gimbal position signal at drive frequency is proportional to the substrate angular rate about the vertical axis. The inner gimbal is operated closed loop with quadrature and in-phase loops with demodulation of gyro position output and remodulation of torques. Other possible loops include a frequency control loop, motor amplitude control, and two low frequency tilt control loops.

For optimal performance, on-chip preamplifiers are constructed using passive and active elements compatible with the gyro machining. To minimize the size and power of associated electronics, which can dwarf the

actual instrument requirements, it is desirable to select configurations that simplify the electronic requirements and minimize the number of control loops.

The torsional flexures define a well modeled spring inertia system. As shown in Figure 1, units have been constructed and tested with bridge and buried electrodes. The active area of current units is $350 \times 580 \mu\text{m}^2$.

In 12 hour drift runs with temperature control, drift stability of $300 \text{ }^\circ/\text{h}$ has been measured. Performance objectives for gyros are 10 (navigation) to $500 \text{ }^\circ/\text{h}$ (missile control).

Micromachining

The silicon gimballed gyro and accelerometer are etched from single crystal silicon using EDP anisotropic etching and a highly doped boron etch stop. The process is outlined in Figure 3. If a rectangular window is aligned with the $\langle 100 \rangle$ axes of the silicon crystal, the EDP etches undoped or lightly doped silicon so that $\langle 111 \rangle$ planes remain; that is, inside the window, a pit with sloped walls is dug and inside corners are sharply defined. The highly doped boron material resists the etch and is not removed.

Boron electrodes are first diffused into the silicon substrate (Figure 3). Photolithography defines the shapes of the electrodes. An epitaxial layer is then grown. Boron diffusion defines the gimbals and flexures. A silicon oxide window defines the outer geometry of the pit. Metal is deposited for electrical connections or for bridge electrodes. The EDP etches the silicon material inside the oxide window and beneath the gimbals to free up the gyro.

In-Plane Tuning Fork Gyroscope

Within the past year, in-plane gyro designs have been developed. The gyro's operation is shown schematically in Figure 2 and photograph, in Figure 4. The combs are excited so that electrostatic forces are generated which do not depend on the lateral position of the masses. The flexures are sized to insure that the tuning fork antiparallel mode is excited and that the translational modes are attenuated. The comb drives large amplitude vibrations in opposite directions by a self-excited oscillator loop so that linear acceleration is rejected. Angular rate in the plane of the substrate lifts one mass up and the other down through Coriolis acceleration; thus, the sense and input axis are identical (Figure 2).

Capacitors below the proof masses are used for gyro sense and, perhaps, force although open loop operation may be feasible. The fabrication may be done by bulk micromachining, as described above, or by

polysilicon surface micromachining, a process developed at the University of California, Berkeley, (Ref. 3) and the University of Wisconsin. The fabrication allows for gaps of a few microns.

Thus far, a pathfinder was constructed of nickel to demonstrate that the antiparallel mode could be excited and that the tuning fork configuration did indeed sense rate. Possible benefits of the tuning fork approach include: (1) simpler fabrication and better performance than gimballed; (2) compatibility with CMOS, which enables easy integration with on-chip electronics; (3) with the gimballed gyro, a complete inertial measurement unit (IMU) on a chip; and (4) static balance and stiffer springs that reduce sticking.

Force Rebalance Accelerometer

The Draper micromechanical accelerometer, which is shown in Figure 5, is constructed similarly to and is compatible with the gimballed gyro. The $300 \times 600 \mu\text{m}^2$ silicon proof is supported by torsional flexures. The location of gold mass determines whether the pendulum will sense accelerations parallel or perpendicular to the substrate; thus, one basic design enables the IMU on a chip. The angular rotation of the gimbal is sensed electrostatically by capacitors buried below the gimbal (Figure 5). Closed loop electronics generate a rebalance voltage proportional to acceleration that is applied electrostatically.

Mechanical stops are seen in Figure 3. Because of the small dimensions, molecular forces can become important. Mechanical stops reduce the surface area and lever arms and offer alternate materials so that sticking is avoided.

The measured performance of the photographed unit is $250 \mu\text{g}$ (overnight drift stability and residual of 1 g tumbles). As for the gyros, better performance requires larger gimbals.

Quartz Instruments

Resonant Accelerometer

The Draper quartz resonant accelerometer (QRA) is displayed in Figure 6. The accelerometer is constructed by simply stacking quartz pieces. Others have used sensitivity of resonant frequency to force to realize accelerometers. Draper's unique contribution is low cost fabrication where the frame, two pairs of tuning forks, and the proof mass base are photolithographically etched. Masses are attached to the proof mass base. Bonded to the active layer, frames restrain the proof mass against accelerations normal to the plane. Quartz tuning forks and proof are 1.5 cm long. The tuning forks are collinear, connected to opposite ends of the proof mass base. Active elements and frames are purchased from Statek, Orange, CA, manufacturer of tuning forks for time-keeping applications.

The QRA sensitive axis is parallel to the tuning forks. Tension in the tines increases lateral stiffness; hence, the resonant frequency is increased. Compression decreases the natural frequency. Each tuning fork is constructed into an oscillator circuit, seen in Figure 6, which interfaces easily with digital electronics.

Measured performance, overnight drift stability and residual of 1 g tumbles, is 50 to 100 μg in units sized for 130 g (crossing of the individual tuning fork resonant frequencies) with break acceleration of 800 g. Uncompensated thermal sensitivity after common mode rejection by the opposing tuning forks is less than 100 $\mu\text{g}/^\circ\text{C}$.

Larger in size than the silicon accelerometers, the QRA was developed earlier because its stiff suspension enables solid-state processing developed for time-keeping while avoiding sticking issues.

Tuning Fork Gyroscope

With parts manufactured by Statek, a quartz resonant gyroscope (QRG) is being assembled. The QRG is a single ended tuning fork, 5 mm long, with drive and sense electrodes on each tine. Operation is similar to the silicon tuning fork gyro; however, the electrostatic drive and sense are replaced by piezoelectric effects.

Summary

Draper has been developing silicon and quartz gyros and accelerometers for several years. The Draper gyros were the first, and, perhaps, the only, silicon gyros to have been demonstrated and tested.

The silicon micromechanical instruments are being constructed for very small inertial measurement units designed to fit into a flat pack (Figure 7). The illustration contains three gyros and accelerometers, vacuum packaging for the gyros, and custom digital electronics. Performance objectives for the silicon gyros are 10 (navigation) to 500 $^\circ/\text{h}$ (missile control). A relatively low marginal per silicon gyro projected cost of \$500 is based on production orders of 10,000. For commercial applications with market potentials of 20 million gyros, the projected per unit costs would be less than \$10 (Ref. 1).

The quartz instruments are larger than the silicon but have simpler electronics and are designed for systems with better performance.

The solid-state inertial sensors have cost, size, and weight advantages over conventional instruments and will result in both redesign of existing systems and conception of new applications. The commercial market is orders of magnitude larger than any contemplated military market. Possible applications for small inertial systems include:

automobiles (the instruments could be used for position location, anti-skid braking systems, air bag deployment, automatic leveling); miniature satellites and spacecraft (where launch weight is a major cost factor); artillery rounds for increased accuracy; camcorders; general aviation; medical electronics; and the largest area-children's toys.

Acknowledgements

Many individuals contributed to the design and construction of the instruments described above. Draper principals include Paul Greiff, Burton Boxenhorn, John Elwell, Dr. Jonathan Bernstein, Lance Niles, James Campbell, Brenda Coletti, Michelle Lind, Dr. Anthony Petrovich, James Sitomer, Anthony Kourepenis, A. Thomas King, Edward Cusson, Kirk Smith, Ralph Haley, and Eric Hildebrant.

References

1. J. Elwell, "Progress on Micromechanical Inertial Instruments", Proceedings AIAA Guidance and Control Conference, August 13, 1991.
2. A. Kourepenis, A. Petrovich, M. Weinberg, "Low Cost Quartz Resonant Accelerometer for Aircraft Inertial Navigation", Proceedings of IEEE 6th International Conference on Solid-State Sensors and Actuators, June 24-28, 1991.
3. W.C. Tang, Electrostatic Comb Drive for Resonant Sensor and Actuator Applications, Ph.D. Dissertation, University of California, Berkeley, 1990.



Figure 1. Silicon gimbaled gyroscope.

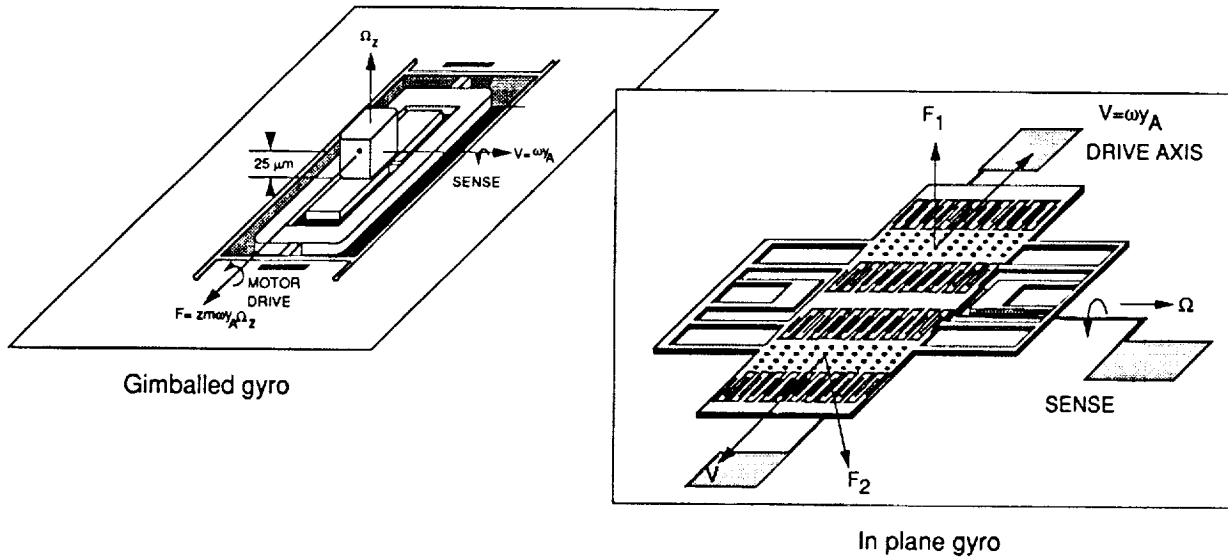


Figure 2. Operation of gimbaled and tuning fork gyro.

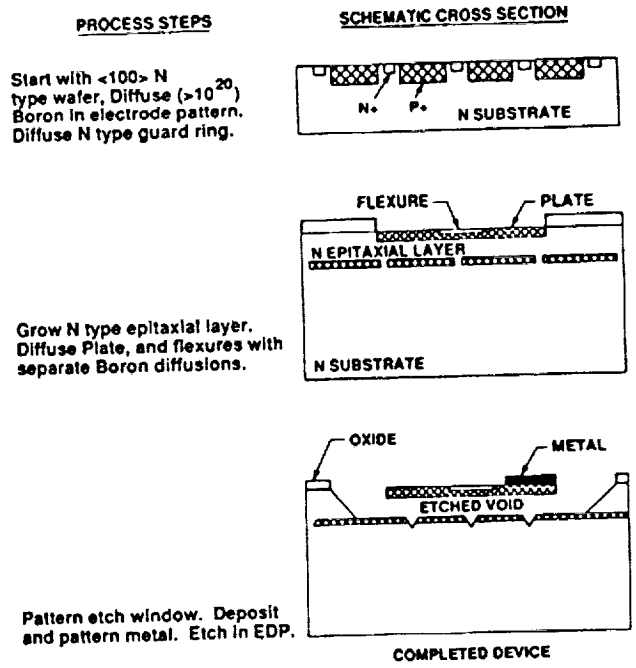


Figure 3. Microfabrication in single crystal silicon.

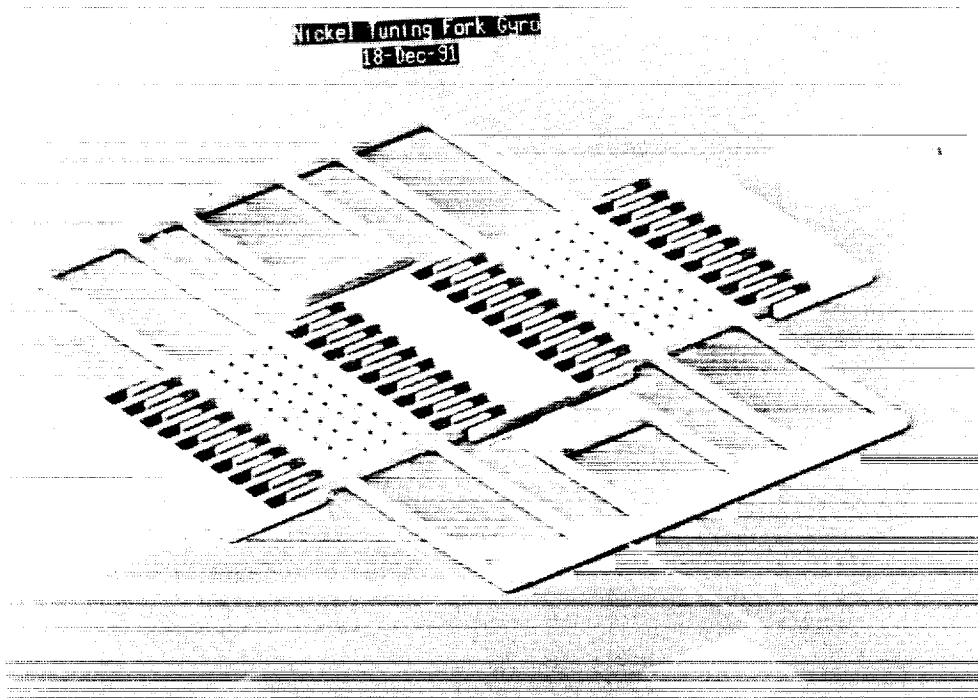


Figure 4. Nickel tuning fork gyroscope.



Figure 5. Silicon force rebalance accelerometer.

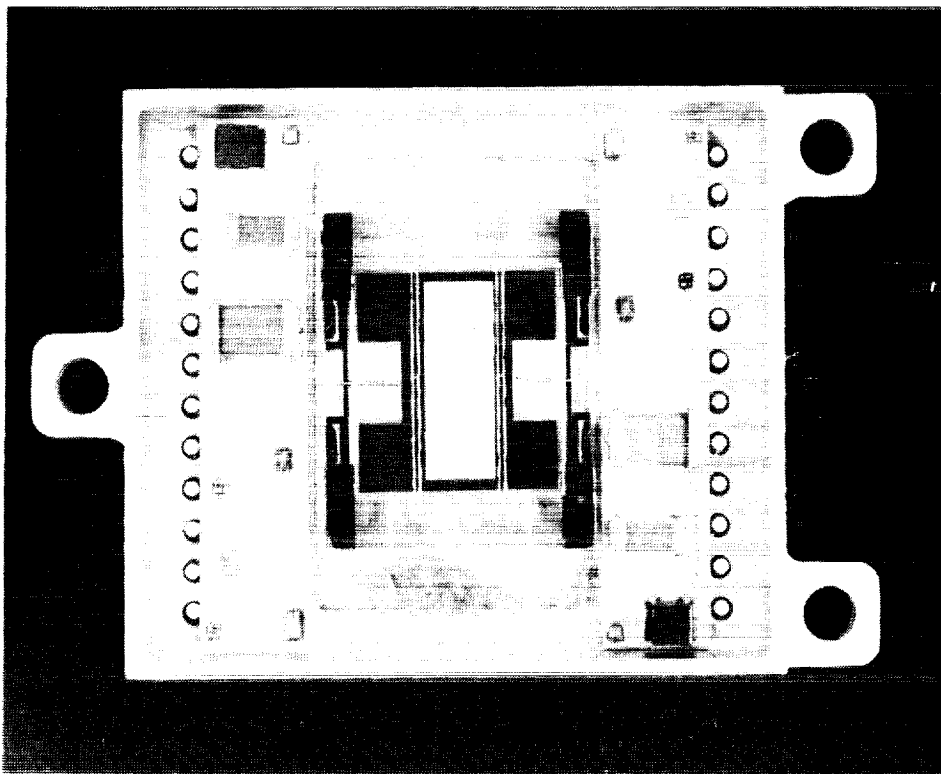


Figure 6. Quartz resonant accelerometer.

MICROMECHANICAL IMU

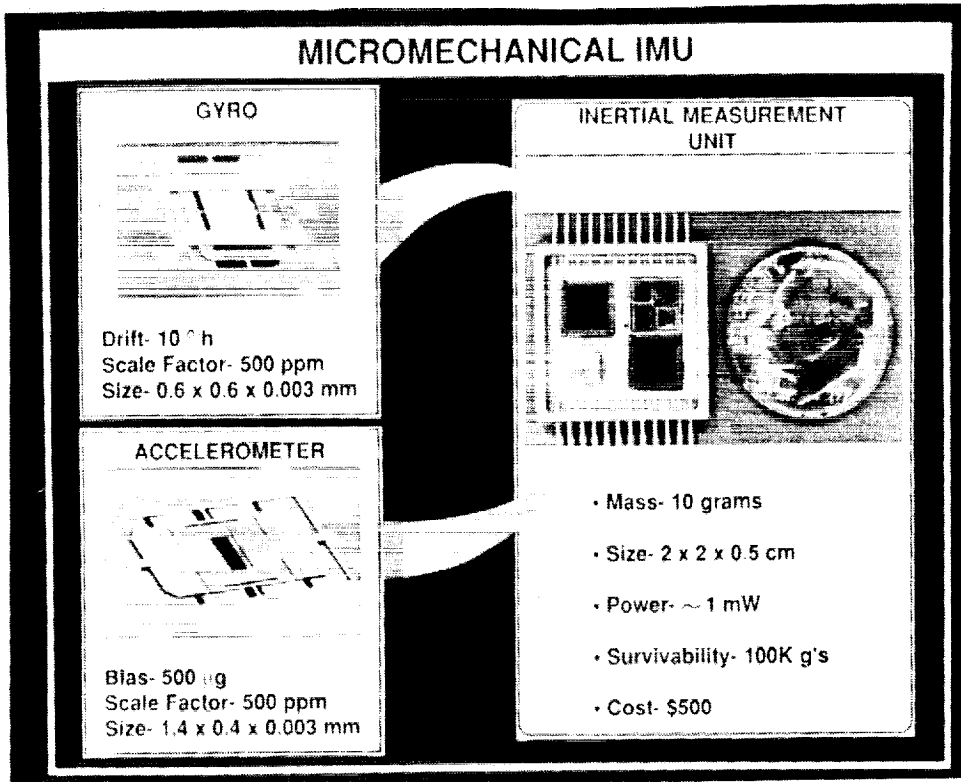


Figure 7. Micromechanical Inertial Measurement Unit.

Integrated Microgyroscope

Timothy J. Hawkey, Richard P. Torti

SatCon Technology Corporation
12 Emily Street, Cambridge, MA 02139

ABSTRACT

SatCon Technology Corporation is developing a prototype electrostatically suspended micromechanical gyroscope in the Small Business Innovation Research (SBIR) program under Contracts 19282, and 19585 from NASA Langley Research Center. This paper presents the results of the Phase I feasibility study and the plans for fabrication in the upcoming Phase II program.

1. INTRODUCTION

SatCon Technology has performed a study of micromechanical gyroscopes. The goals of the Phase I SBIR program were to define a baseline system configuration and establish technical feasibility. In the Phase II program, just beginning, a prototype actuator will be fabricated and tested. This paper presents a micromechanical device overview, a summary of the Phase I results and plans for Phase II.

2. SPECIFICATIONS AND CONFIGURATION

As with all sensors, resolution, accuracy, large dynamic range, low power consumption, small size and high bandwidth are desired. For this technology effort, the obvious primary objective was small size with the goal of eventually developing a complete two-axis rate gyro on a microchip. For this feasibility study, maximum/minimum angular rates of 10 radians/sec and 0.1 radians/sec and 200 Hz bandwidth were chosen as specification goals to approximate what might be required for use on robotic arms. Other performance specifications were determined by process controlled geometries and parameters as discussed in Section 4.

2.1 Suspended gyro configuration

The initial micro-gyro configuration identified is shown in Figure 1. Configured as a rebalance gyro, this microfabricated machine consists of three types of electroquasistatic components - the motor drive, position sensors, and the non-rotary actuators for rebalance and suspension. Like suspended macroscopic gyros, the rotor is spun by a motor to produce angular momentum, suspended and controlled by force and torque actuators, and sensed by various position sensors. As discussed in Section 2, all the sub-components are electric field devices. The term "rebalance" identifies the gyro mode of operation. When acted on by external forces, the control system is designed to hold the gyro in a constant position, rebalancing it. Knowledge of the actuator control signals and dynamics allows the inputs to be determined. Since the controlled mass (the gyro rotor in this case) is held to a nearly constant position, the linearity of the sensors and actuators is improved, and the overall dynamics are simplified. A system block diagram is shown in Figure 2.

The electrostatic force can be written in linearized form for a fixed potential as:

$$F = \frac{1}{2} V^2 \frac{\partial^2 C}{\partial X^2} \Delta X$$

where ΔX represents the excursion about the equilibrium position, and the coefficient is positive. Since the force increases with decreasing distance, the motion is unstable and without other compensation requires closed loop control. In the case of a fully suspended rotor, this control must be effected in both axial and radial directions (five unstable degrees of freedom). There are, therefore, four sets of actuator/sensors - two for the upper and lower axial suspension and two for upper and lower radial rebalance actuator/sensors - and the motor driver actuator; hence the multilayered configuration of the figure.

The fabrication of such a multi-actuated, multi-sensed device requires at least five sets of alternating insulating/conducting layers on the rotor. For reasonable capacitive bias currents and actuator forces, the facing areas must be at least 1-2 μm high with radial gaps of the same order. The height of this rotor will accumulate to over 5 μm . Present technology, however, only makes feasible aspect ratios (rotor thickness to gap) of up to 2/1, with 1/1 being typical. This gap in fabrication technology will have to be bridged to allow successful fabrication of a fully suspended micro-gyro.

2.2 Motor configuration

The electrostatic production of torque has long been considered for motor drives. Four classes of electroquasistatic motor actuators have emerged which have analogues with magnetically operated devices - variable capacitance, electrostatic induction, permanent electret, and electric hysteresis. In the work by Bart, induction and variable capacitance motors were studied in detail with attempts made to fabricate both axial gap and radial gap variable capacitance motors. Radial gap variable capacitance motors have been successfully built and tested at both MIT and Berkeley. Our system therefore baselined a radial gap motor as fabricated at MIT².

2.3 Sensor configuration

The baseline sensor configuration chosen was capacitive position sensing using a superposition of high frequency signals between the axial control electrodes and the rotor. Decomposition of the four sensor signals (one for each axial stator electrode) provides the signals needed to control the rotor. Capacitive position sensing is commonly used in macroscopic devices, and has also been successfully applied to other micromechanical devices. The basic concept is to drive a constant current across an air gap (whose capacitance varies inversely with gap distance) and read the resulting voltage which is linearly proportional to the gap. High frequency modulation and demodulation allow good noise immunity. Though the capacitance of the microgyro axial gap will be very small (about 3×10^{-14} farads), the placement of FETs (field effect transistors) on the silicon substrate as preamplifiers as done by Schmidt should allow reasonable measurements to be made³.

3. ELECTROMECHANICAL DESIGN

The design of the motor drive and rebalance actuator is based on the specifications discussed in Section 3, many of which were derived from known fabrication constraints

and experience. Dimensions were generally conservatively chosen given the uncertainty in fabricating devices with this technology. In practice, some or all of these dimensions may be changed in the prototype development effort. These sizing numbers, however, represent what would be required for engineering development of a useful instrumentation sensor.

3.1 Sizing

The overall rotor diameter, $200\ \mu$, was chosen as the largest size that could be fabricated without significant warpage due to residual stress buildup during fabrication. The rotation rate is constrained by stress limits in the rotor and electronics limits in the motor driver circuitry. A rate of 500,000 rpm (8.3 kHz) was chosen as a reasonable extension of current motor rates (about 50,000 rpm). This is well below the ultimate spin rate (about 10,000,000 rpm) determined by material strength limits and is limited by motor drive electronics. The required electronics frequency, 25 kHz, is attainable without excessive noise problems. The motor height was set to $2.2\ \mu$, the same height as currently fabricated micromotors. The maximum value of total rotor thickness is limited by fabrication technology to about 2 times the radial gap of $1.5\ \mu$. The axial gap between substrate and rotor was set at $2\ \mu$. This represents a tradeoff between gap capacitance and rotor unstable frequency. A smaller gap would make sensor measurements more accurate at the cost of raising the unstable frequency and complicating the control problem. The $2\ \mu$ gap gives a 300 Hz unstable frequency.

3.2 Sensor/Actuator

The four segment rebalance sensor/actuator electrode design is similarly derived from the specifications. While it was not attempted to optimize the pattern for torque, depositing the conducting region from $0.7\ R$ to $1\ R$ gives adequate rebalance torques and adequate capacitance for sensing inclinations as small as 0.008° . A possible difficulty is the actually attainable depth and uniformity of the implanted electrodes since the thermal noise limit is sensitive to circuit resistance. The sensor capacitance between each of the four electrodes and the rotor is approximately $3 \times 10^{-14}\ F$. With a typical commercial oscillator frequency of 100 kHz, the sensor current is about 15 nA for operation at 0.8v. Since commercial devices sense capacitance in the same range (although with larger electrode and gaps) it should be possible to use standard techniques for angle information.

3.4 Summary

The tables below give a summary of the dimensions and parameters predicted for the two degree of freedom microgyro with specifications as discussed in Section 2.

| | |
|----------------------------------|--|
| Spin Angular Speed | 500 kRPM |
| Spin Moment of Inertia | 1.5×10^{-18} kgm-m ² |
| Precession Moment of Inertia | 8×10^{-19} kgm-m ² |
| Minimum Angular Rate | 0.01°/s |
| Thermal Sensor Noise | $< 0.4 \times 10^{-3}$ v |
| Angular Sensitivity | $< 0.008^\circ$ |
| Sensor Electrode Capacitance | 3×10^{-14} F |
| Sensor Operating Current (0.8 V) | 15×10^{-9} A |
| Nominal Drive Actuator Potential | 0.5 v |
| Drive Torque Per Pole | 10-11 N-m |
| Rotor Radius | 50 μ m |
| Radial Gap | 1.5 μ m |
| Vertical Gap | 2 μ m |
| Rotor Thickness | 2.2 μ m |
| # Stator Poles | 12 |
| # Rotor Poles | 8 |

4. CONTROL AND ELECTRONICS DESIGN

4.1 Control System

This section presents the controller design philosophy. For a more detailed description of the controller, the reader may refer to Reference 4. As shown in Figure 2 the system block diagram consists of the actuator and plant (gyroscopic) dynamics, the sensors, the controller, and the decomposition electronics. One of the goals of the controller is to keep the orientation of the rotor fixed, in the null position, relative to the orientation of the "stator" frame of the gyroscope. In addition, the controller must provide accurate measurement of the torque that is required to maintain the rotor in the null relative orientation. As usual, the simplest controller that can meet the performance objectives is desired in order to minimize hardware complexity. In particular, a fixed-gain, linear controller is desired that can be easily implemented in analog electronics. This will force some performance and stability robustness tradeoffs, in particular because the plant dynamics are a strong function of the operating speed and are open-loop unstable. Because of the open-loop unstable nature of the plant -- an inverted pendulum at low speeds -- closed-loop control is required from zero speed to the full operational speed. The challenge, then, is to find a fixed gain controller that will provide adequate performance at all speeds.

The design approach to develop a fixed-gain controller for this speed varying plant was to first examine how optimal, full-state feedback controllers change with changing plant speed. These full-state feedback controllers assume knowledge of the position and velocity of the rotor in both radial directions. Based on the behavior of these parameter-varying, full-state feedback controllers and the addition of some physical insight, a fixed-gain, full-state feedback controller can be chosen that provides reasonable performance over the full speed range. This full-state feedback controller is then implemented as an output feedback controller using lead-lag compensators to provide estimates of the velocity.

4.2 Electronics

4.2.1 Sensor electronics

The capacitance of the position sensor varies inversely with the distance from the sensor to the target. Over the specified measurement range, the sensor varies in capacitance from approximately 0.027 picofarads (pF) to 0.033 pF. Any stray capacitance on the sensor leads will effect the linearity of the measurement unless the leads are appropriately guarded. The ability to detect position accurately is also hampered by any load placed on the sensor capacitance by the measurement electronics.

A block diagram of the sensor electronics is shown in Figure 3. The sensor is driven by a 100 kHz current source so that the resultant voltage is proportional to the sensor impedance. The AC voltage produced across the sensor is buffered by a "guard" loop, full-wave rectified, and low-pass filtered to produce a DC output voltage directly proportional to distance. The effects of stray capacitance on the sensor leads are greatly reduced by driving the shield of the sensor cable with a "guard" loop. The guard loop drives the shield with a voltage identical to that across the sensor, and thus no current flow is possible. The impedance of the shield is a capacitance greater than 200 pF to ground. In order to drive this load, the voltage across the sensor is buffered by the FET input stage, a high-bandwidth differential op-amp, and a high-current buffer. The bandwidth of this follow-up loop must be high to reduce any effects of the guard capacitance upon the sensor capacitance. To reduce the input capacitance of the sensor electronics, a Field Effect Transistor (FET) input stage is used. This input stage presents a very high resistance and low capacitance load to the sensor. The FET input stage is configured as a source-follower where the source signal will exactly follow the gate (input) signal. The source terminals of the FETs are each loaded with a transistor current source. The high impedance of the current sources reduces the effect of any gate-to-source capacitance. The drain of the FETs are capacitively coupled to the buffered sensor voltage to reduce the effects of any gate-to-drain capacitance. Stray capacitance on the circuit board would be reduced by placing the buffer-loop circuitry on a copper-clad board with the copper clad driven by the guard voltage. The output of the sensor guard-loop is bandpass filtered to eliminate both DC drift and high-frequency noise effects. The signal is then full-wave rectified and low-pass filtered to produce a DC output voltage.

4.2.3 Motor drive electronics

The gyro wheel-motor is a three-phase bipolar variable-capacitance motor. Since this motor type is synchronous, i.e., produces torque only when the rotation frequency and excitation frequency are the same, it requires a variable-frequency drive source. In addition, the push-pull excitation required for each of the three bipolar phases will require six high-voltage output stages. The motor is driven with balanced bipolar voltages so that the rotor will remain near ground potential. Any voltage induced on the rotor will cause it to be strongly attracted to the grounded substrate because of its large surface area.

Motor start-up will require that the excitation frequency start at the sub-Hertz level and ramp up to the full-speed value of 25 kHz. This will be accomplished with a ramp generator and voltage-to-frequency (V/F) converter. The bipolar three-phase generator takes the single-phase output of the V/F converter and produces three square-waves with 120 degrees phase difference and their complementary signal for driving the output stages. In addition, the circuit generates the signal pair which develops the bipolar waveforms. The output circuit contains six high-voltage drivers and can deliver up to 120V.

5. FABRICATION

Fabrication is a major challenge with micromechanical systems. Overall system feasibility and functionality are more closely tied to fabrication methods than with macro scale systems. For this program, it is planned to use the microsystems fabrication facilities at MIT and base the motor design on those developed there. The program will be broken into three technology demonstration steps aimed at verifying component technologies before integration into a complete system.

The first step will be the fabrication of a capacitive sensor demonstration unit. This will consist of a microfabricated cantilever beam and a differential field effect transistor pair. The FETs will be connected to an electrode below the cantilever and serve as the capacitive sensor pre-amplifier as discussed in Section 5. Optical methods will be used to independently verify the position of the cantilever.

The next technology demonstration will be a non-rotating closed loop suspension of microfabricated plate. These prototypes will be used to develop specific mechanical, electrical and control designs and fabrication sequences for the integration of sensor technology into a micro-suspension system. Testing will verify actuator and control characteristics and allow the development of a rotating micro-suspension

Finally, after the first two tasks, the rotating, suspended microgyro will be developed. This will extend the non-rotating suspension with a motor drive and additional electronics. It is anticipated that substantial process development may be necessary for the successful completion of this task.

6. CONCLUSIONS

The results of the feasibility study were very positive. Though extensions of fabrication technology will be required for fabrication of the prototype device, the potential for successful development is very good. An operational micromechanical gyroscope would have many applications in commercial, aerospace, and military sectors.

7. REFERENCES

1. Howe, et al, "Silicon Micromechanics: Sensors and Actuators On A Chip", IEEE Spectrum, July 1990.
2. Bart, S.F., Modeling and Design of Electroquasistatic Microactuators, Ph.D. Thesis, MIT, September 1990.
3. M. Schmidt, et al, "Surface Micromachining of Polyimide/Metal Composites For a Shear Stress Sensor", in IEEE Micro Robots and Teleoperators Workshop, Hyannis MA 1987.
4. Hawkey, T, and Torti, R. "An Integrated Microgyroscope", Final Report, contract NAS1-19282, SatCon Technology Corporation, Cambridge, MA July 1991.

8. FIGURES

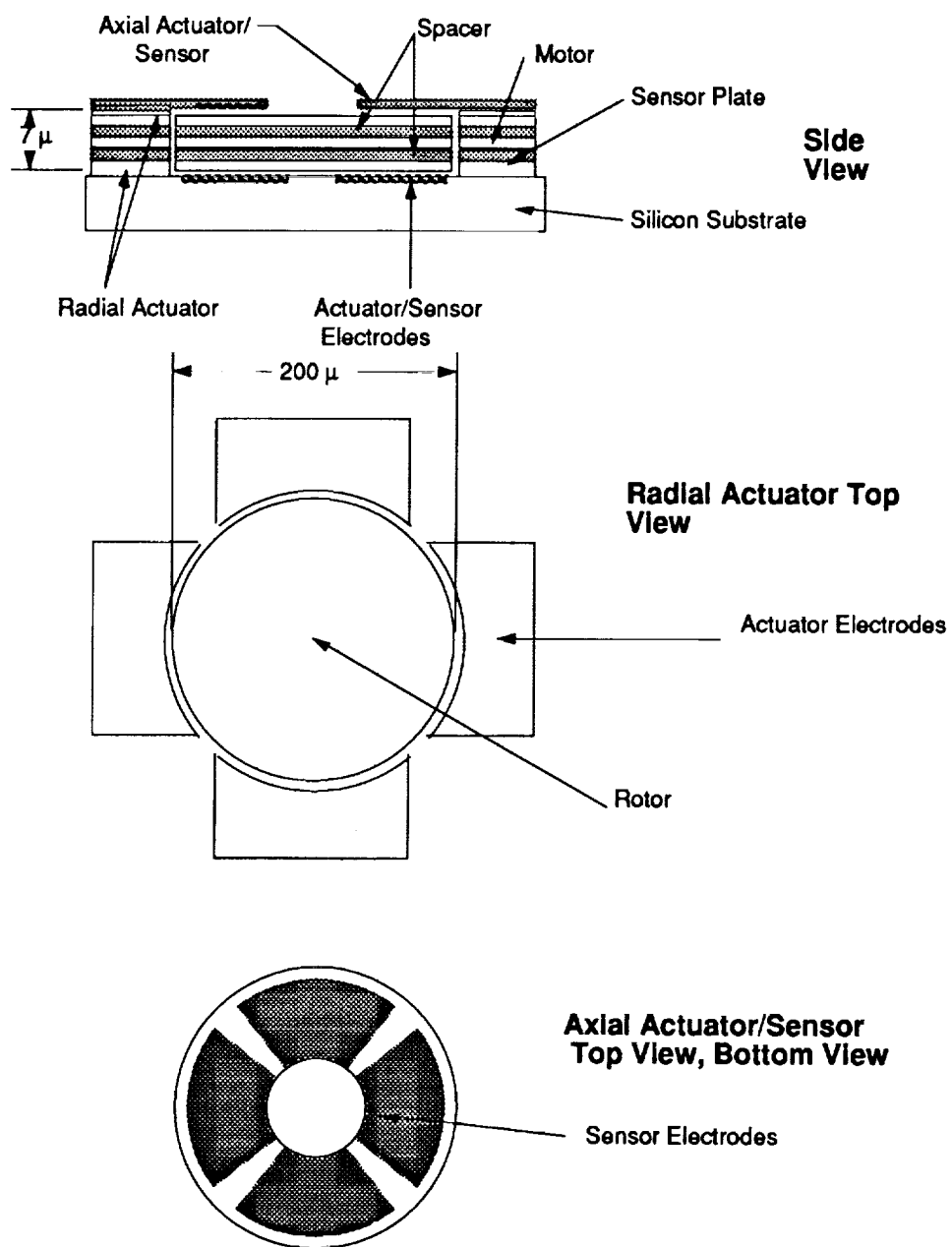


Figure 1. Suspended Microgyroscope Configuration

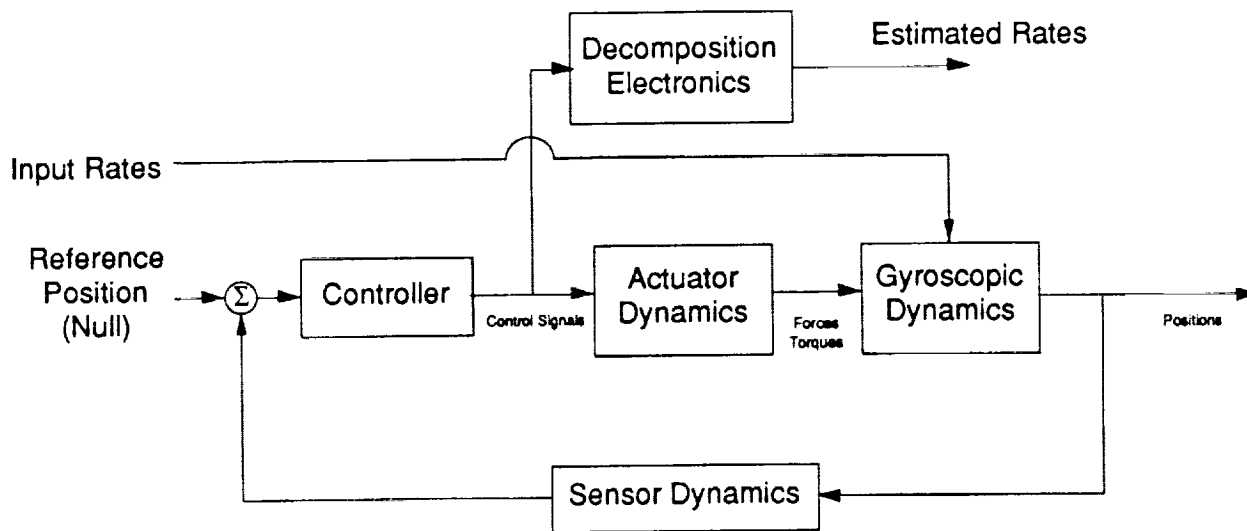


Figure 2. Microgyro Block Diagram

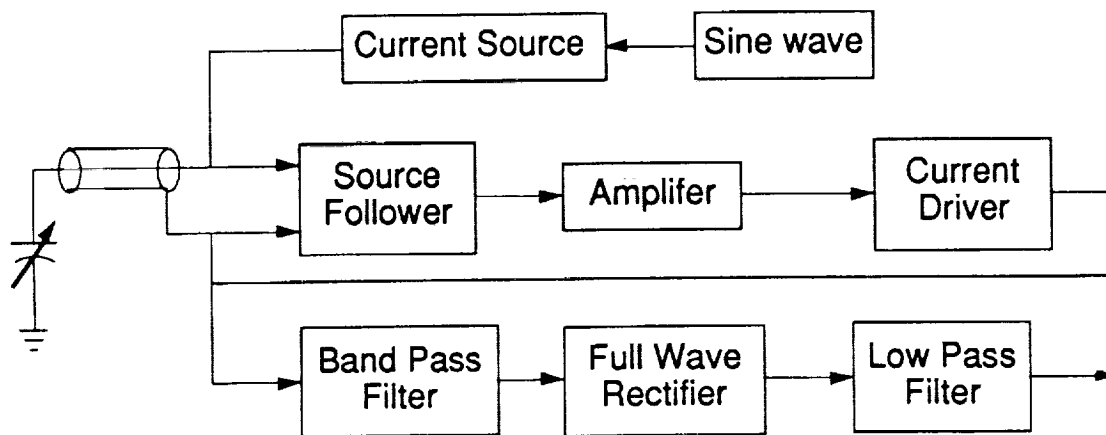


Figure 3. Sensor Electronics Block Diagram

GEC FERRANTI PIEZO VIBRATORY GYROSCOPE

J. D. NUTTALL

GEC FERRANTI, Silverknowes, Edinburgh, EH4 4AD Scotland

Summary

Prototypes of a piezo-electric vibratory angular rate transducer (gyroscope) (PVG) have been constructed and evaluated.

The construction is on the lines suggested by Burdess (reference 4). The sensitive element is a cylinder of radially poled piezo-electric ceramic. The cylinder is metallised inside and out, and the outer metallisation is divided into eight electrodes. The metallisation on the inside is earthed.

A phase locked loop, using two pairs of the electrodes, causes the cylinder to vibrate in one of its two fundamental, degenerate modes. In the presence of rotation, some of the vibration is coupled into the other mode. This can be detected, or suppressed with a closed-up technique and provides a measure of rotation rate.

This gyroscope provides a number of advantages over rotating mass and optical instruments: low size and mass, lower power consumption, potentially high reliability, potentially good dormancy, low cost and high maximum rate.

1. Introduction

The measurement of angular rate (relative to inertial space) is often a significant problem in spacecraft, (and other) system's development. Gyroscopes (angular rate sensors) are perceived as large, heavy, expensive, unreliable or some combination of these. Although the perception is not well-justified, the moves towards lighter space craft suggest that gyroscope technology is ripe for change.

There is a sizeable market (not confined to space craft) for gyros capable of measuring high angular rates, with a null accuracy of around a degree per second, and a scale factor accuracy of around one percent. Such instruments have to be cheap, small and robust. The GEC-Ferranti Piezo-Vibratory Gyro (PVG) is being developed for such a market. The target specification is reproduced below.

| <u>Parameter</u> | <u>Design Aim</u> |
|----------------------------|---|
| Full scale rate | ± 100 deg/sec to ± 5000 deg/sec* |
| Full scale output | ± 10 volts d.c. |
| Over-Range | 25,000 deg/sec |
| Excitation | ± 15 Volts d.c. |
| Power Consumption | 1 Watt/axis |
| Null | ± 1 deg/sec after temperature consumption |
| Temperature Range | - 40 deg. to + 80 deg. C |
| S/O to S/O Repeatability | <0.05 deg./sec |
| Hysteresis | <0.05 deg./sec |
| Resolution | <0.05 deg./sec |
| Threshold | <0.05 deg./sec |
| Linearity | 0.25 % of Full Scale |
| Scale Factor | 0.25 % after temperature compensation |
| Start-up Time | 100 mS |
| Bandwidth | 25Hz to 200Hz* |
| Noise | <0.04 [deg./sec]/ $\sqrt{\text{Hz}}$ |
| Size (in single-axis pack) | 25mm ϕ x 25mm long |
| Size of three axis pack | 40mm cube max. |

*Adjustable by change to electronics only.

Additionally, for a gyro of this type, low cost, high reliability, long operating time, and the capability of working in severe environment, are regarded as of particular importance.

2. Choice of technology

Traditionally, rotation sensors have been based on spinning wheels, but gyroscopes using either optical techniques and/or vibrating masses have become practical in recent years.

Existing spinning-mass gyros are unsuitable for this specification because of:-

- (a) Cost: they are either expensive, or cost-cutting measures have unacceptable effects on lifetime or performance.
- (b) Maximum rate: usually spinning-mass instruments cannot cope with more than (say) 100 degrees/second, and/or there is considerable increase in heat dissipation with rate.

Optical gyros are unlikely to meet the requirement because of both cost and size, although they are expected to do well in more demanding applications (e.g. better than 10 degrees/hour).

This leaves vibratory gyros, which have considerable potential, especially in terms of cost, size, weight, maximum rate, lifetime, bandwidth, power consumption and reliability.

3. Design Considerations in Vibratory Gyroscopes

There have been a number of attempts to develop vibratory gyros, dating back over the last thirty years. Examples include the Sperry "Gyrotron", RAE's experimental tuning-fork gyro, GE's vibrating beam gyro, and Honeywell's vibrating wire-gyro. The major problems with these devices, as far as we can tell, have been associated with the need to get the two resonant frequencies near identical, the need to prevent the vibration leaking away through the support, and various problems associated with the piezo-electric transducers which were bonded to metal vibrators.

The motion of any vibrating body is, in general, affected by the presence of rotation, through the Coriolis coupling [Reference 1]. The Coriolis effect depends on rotation rate, and therefore, in principle, any vibrating body can be used to detect rotation, i.e. as the basis of a gyroscope.

As an example, for educational purposes only, consider the vibrating cantilevered beam shown in Figure 1. The effect of the rotation is to introduce an out-of-plane vibration, as shown. This induced ['secondary'] vibration is at the same frequency as the primary vibration. Thus, to build such a gyro one would need a method of sustaining the primary vibration of the beam, and of detecting its out-of-plane [secondary] motion which is a direct measure of rotation rate. Both of these requirements can be met by pairs of piezo-electric transducers: one pair arranged to bend the beam and one pair to detect the strain in the other plane.

It is clear that to get a primary vibration of reasonable amplitude from the rather weak piezo-electric effect, one needs to make use of a mechanical resonance in the primary direction. To avoid difficulties with the resonant frequency variations [from component manufacturing tolerances or temperature, for example], it is necessary to incorporate the beam itself into the oscillator as the frequency-determining component. Similarly, it is clear that the secondary must be operated on resonance, and thus ideally one should have the two resonances at the same frequency. In practice, the frequency split between the two resonances needs to be rather smaller than the width of the resonances.

As the mechanical resonator is the frequency-determining part of the oscillator, it is desirable to have a resonator with a high Q factor. This situation gives a rapid change of phase with frequency, and thus a stable oscillator with little phase noise. Of course, to get a high Q factor, it is necessary to minimise the losses: in this case the power lost as vibration leaking out of the gyro. [A further reason for minimising the energy loss from the gyro is to reduce the risk of the cross-talk between the gyros].

In the educational example given above, one would expect therefore a gyro with that particular configuration would be unsuccessful. However, there are several better possibilities, including tuning forks, H-shapes and cylinder.

4. Description of the GEC-Ferranti Piezo-Electric Vibratory Gyro

GEC-Ferranti at Silverknowes, Edinburgh in Scotland, has been developing a vibratory gyro for around 3 years. The initial phase included a study of possible configurations and a tolerancing study.

An early decision was to avoid problems with bonding piezo-electric transducers to a metal resonator, by making the resonator itself from piezo-electric material, and by plating metal electrodes onto it. For each configuration considered, the possible materials and the directions of the piezo-electric properties, were considered. The outcome of this study was the decision to work primarily on a cylindrical configuration, with one open end and one closed end. The support was to be at the node at the centre of the closed end. As the cylinder's piezo-electric properties have to be cylindrically symmetric materials which are naturally piezo-electric cannot be used. Instead, we have been working with the sintered piezo-electric ceramic, which can be radially poled. [The material is sold under various names including "PZT"]

Once the ceramic cylinder has been ground to the correct dimensions, it is plated with metal on both the inside and outside. The outside plating is divided up into eight electrodes, which cover virtually all the area, but which are divided by small earthed strips. The metal on the inside is earthed. Figure 2[a] illustrates the configuration.

Several authors have described how such a configuration can be used as a gyro [reference 2]. A cylinder has, of course, a large number of natural modes, but most of these are unsuitable for use in the gyro. Figure 2[b] illustrates the primary mode excited, and the secondary mode detected, in the GEC-Ferranti gyro.

Before we started work on a cylinder gyro, Burdess had already patented [Reference 3] and published [Reference 4] the idea of the cylindrical vibratory gyroscope in piezo-electric ceramic and the ownership of the patent was with the British Technology Group [BTG]. GEC-Ferranti has made a licensing arrangement with BTG.

This cylinder gyroscope has much in common with the one described by Harris [Reference 5]. The major difference between that device and the Ferranti one is that in the former one the piezo-electric transducers are bonded onto the resonator, but in the GEC-Ferranti device the piezo-electric material is the resonator.

There are a number of advantages with the GEC-Ferranti arrangement, mainly to do with its simplicity, and hence its reliability. If a metal cylinder is used, piezo-electric elements have to be bonded onto the cylinder, and wires taken from them, near the point of maximum vibration. By contrast, there is no bonding to the vibrating part of the piezo-electric cylinder: the electrical connections can be made near the node.

Further advantages come from the fact that, in the piezo-electric cylinder, the electrodes are positioned by dividing up the plating, and this position can be trimmed later by removing more metal. This process is potentially more accurate than ones involving bonding the piezo-electric elements in place with adhesives.

The motion of the cylinder is too small and too fast to be seen by normal techniques, but it can be investigated by interferometric holography [Reference 6]. Such a technique gives a photograph of a fringe pattern, with the fringes being contours of equal vibration amplitude. Figure 3 is a line drawing traces from such an interferogram, showing the vibration node, and antinodes of around 1200 nm peak-to-peak.

5. Electronics

A block diagram of the gyro electronics is given in Figure 4. It can be divided into two areas

- (a) Primary drive circuit
- (b) Secondary detection and output circuit

The primary drive circuit is required to establish and sustain the cylinder's fundamental mode of vibration. This is achieved by using the resonant characteristics of the cylinder as the frequency selective parameters of a phase-locked, amplitude-stabilised oscillator. This configuration ensures fundamental-mode operation over a wide temperature range, since the cylinder's temperature-sensitive parameters are automatically compensated for.

As the rotation-induced secondary vibration is in phase with the primary vibration, it is possible simply to demodulate the output from any secondary electrode pair, with respect to the primary vibration, and to use this as the gyro output. However this 'open-loop' detection system is inherently non-linear.

To give an output which is linear with applied rate, a closed-loop secondary system is used. This system acts as a null-seeking servo, which suppresses the secondary vibration by applying a feedback-derived voltage to the secondary drive electrodes. This voltage is a linear function of applied rate.

6. Some results obtained with prototypes

To date, prototype PVGs have been characterised over ± 1000 degrees/second [scale factor of 10mV/[degree/second]], or over ± 100 degree/second [scale

factor 100mV [degree/second]]. Examples of the results of rate tests are given in Figures 5 and 6. In each case the upper figure gives the output voltage as a function of input rate, and the lower figure the deviation of the data from the best straight line. The lower plots are over the range $\pm 0.5\%$ of full rate. For the ± 100 degree/second data, the worst deviation is 0.1% full scale, and the errors seem randomly distributed. For ± 1000 degree/second data, the worst deviation is 0.3% full scale. There is a systematic element to this error, and we believe we understand the nature of the constructional inaccuracies which lead to this. Even so, the r.m.s. non-linearity is only 0.15% full scale.

Figure 7 shows the in-run drift of the gyro on a static overnight run. A simple model has been used to eliminate temperature effects. The data all lies within ± 0.02 o/sec ($\pm 72^\circ$ /hour)

Figure 8 shows the variation of scale factor with temperature. Although the actual variation is rather large, the effect has good linearity, and there is every prospect that the temperature effect can be cancelled out.

References

1. 'Dynamics' by F.P. Beer and E.R. Johnston
McGraw-Hill, pp 621-612
2. C.H.J. Fox
DGON Gyro Symposium 1988, Paper 5
3. UK Patent BG 2 154 739 B
4. J.S. Burdess, Proc I Mech E Vol 200 (C4), pp 271-280 and UK Patent GB
2154739B
5. D.G. Harris, DGON Gyro Symposium 1988, Paper 6
6. R.J. Parker and D.G. Jones, Optical Engineering Vol 27 [1], January 1988

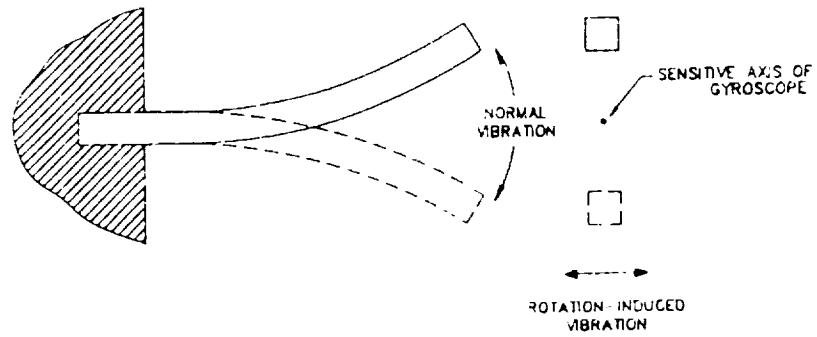


Figure 1

A hypothetical vibrating-beam gyroscope illustrating the principles of all vibratory gyros. The beam is caused to vibrate at its resonant frequency. The figure shows two views of the system with the solid and hatched beams representing the two extremes of the vibration. Rotation about the axis shown induces an out-of-plane vibration as indicated in the diagram.

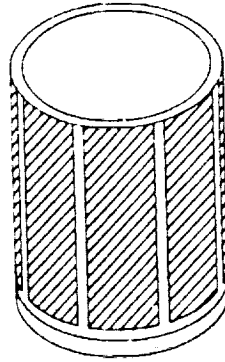


Figure 2a

The GEC-Ferranti Piezo-Electric Vibratory Gyro, showing the vibrating cylinder, made from piezo-electric material, and also the plated electrodes whose position is denoted by the hatched areas.

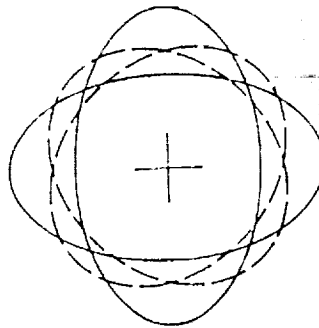


Figure 2b

The modes in a cylinder gyroscope. The primary mode comprises oscillation between the two solid ellipses. The secondary [rotation induced] mode is an oscillation between the two dashed ellipses.



Figure 3

Laser interferogram of the vibratory cylinder. The fringes are lines of constant amplitude. [This is a line drawing produced from the interferogram].

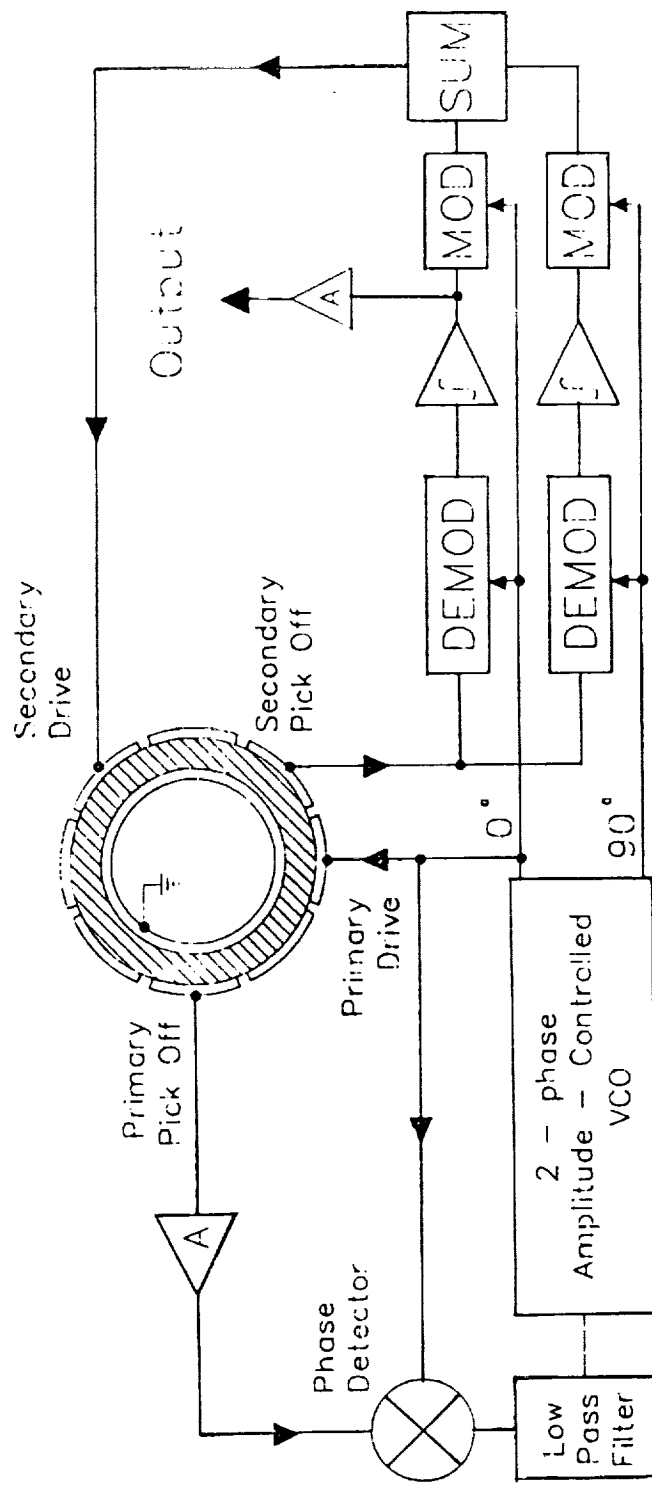


Figure 4

PVG Electronics.
 Note that each electrode is connected in parallel with the one opposite.

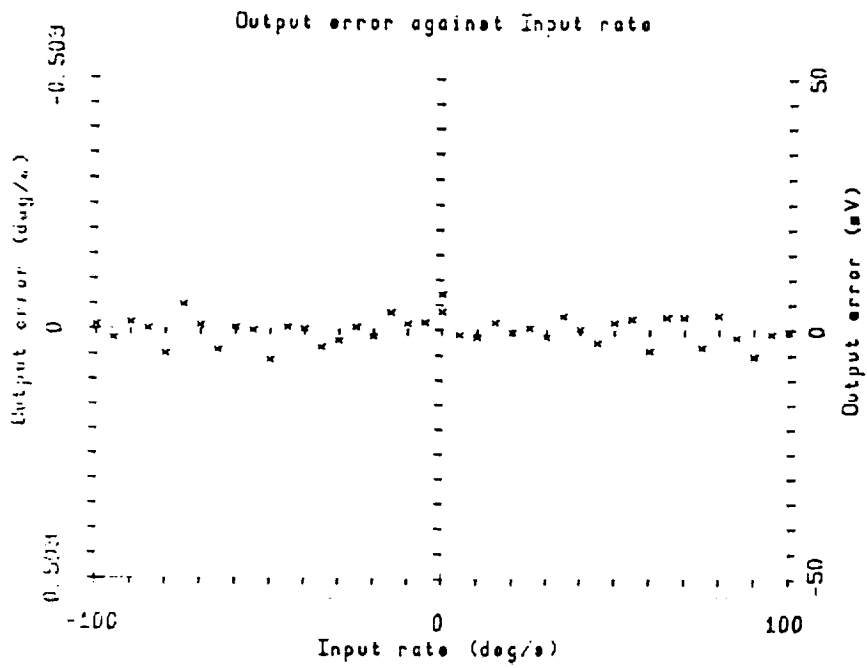
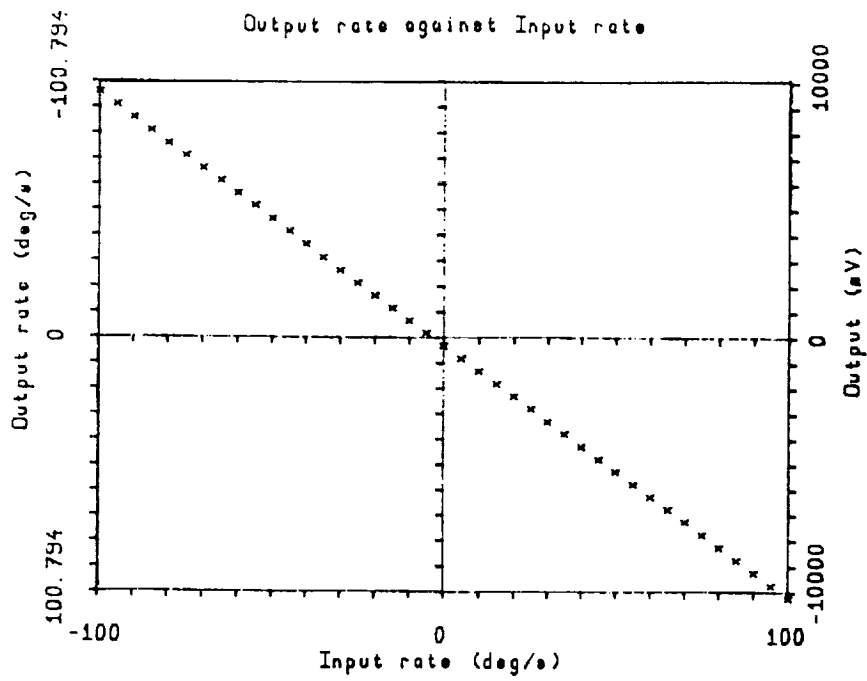


Figure 5

Result of rate test over ± 1000 degrees/second on GEC Ferranti Piezo Vibratory Gyro

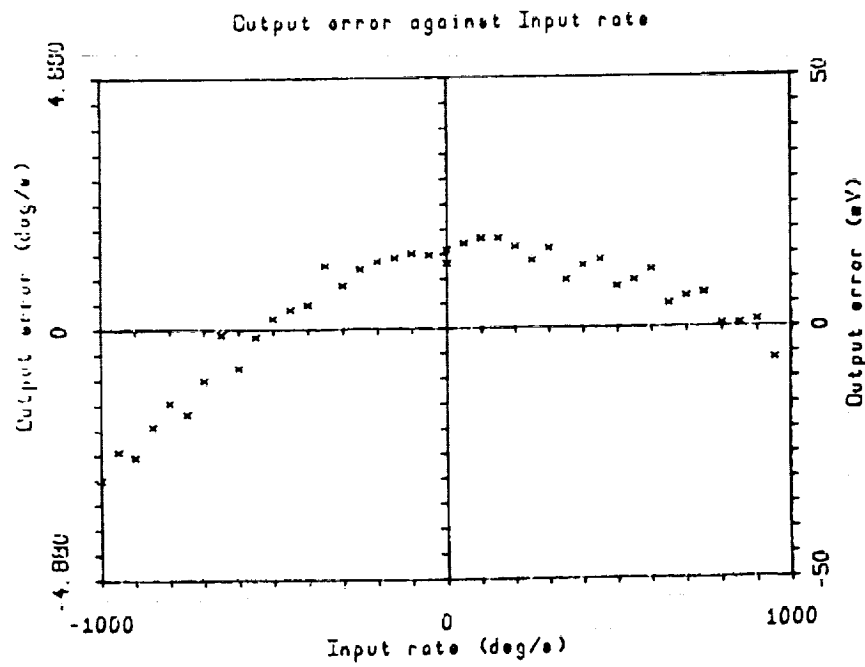
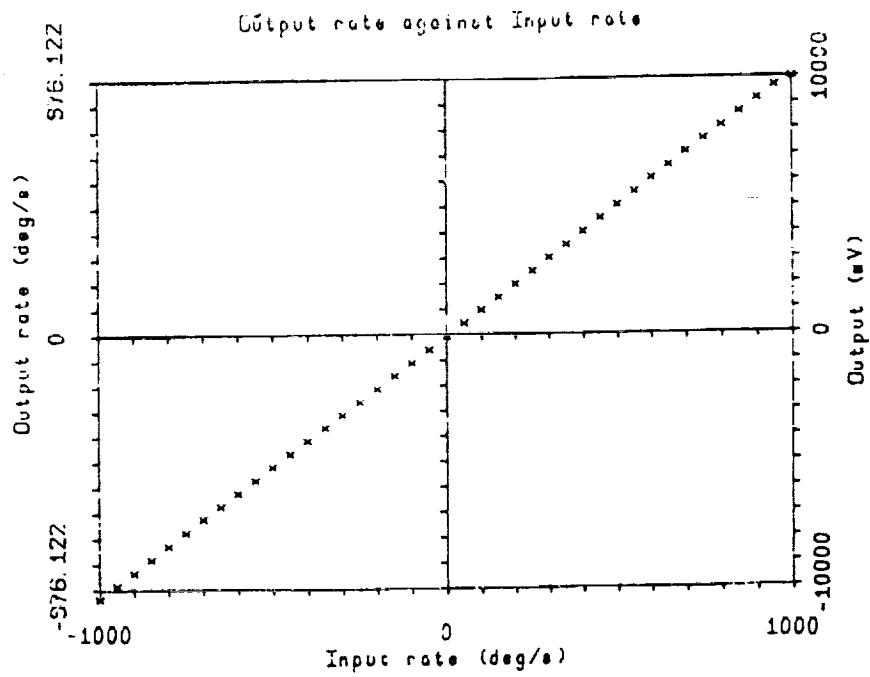
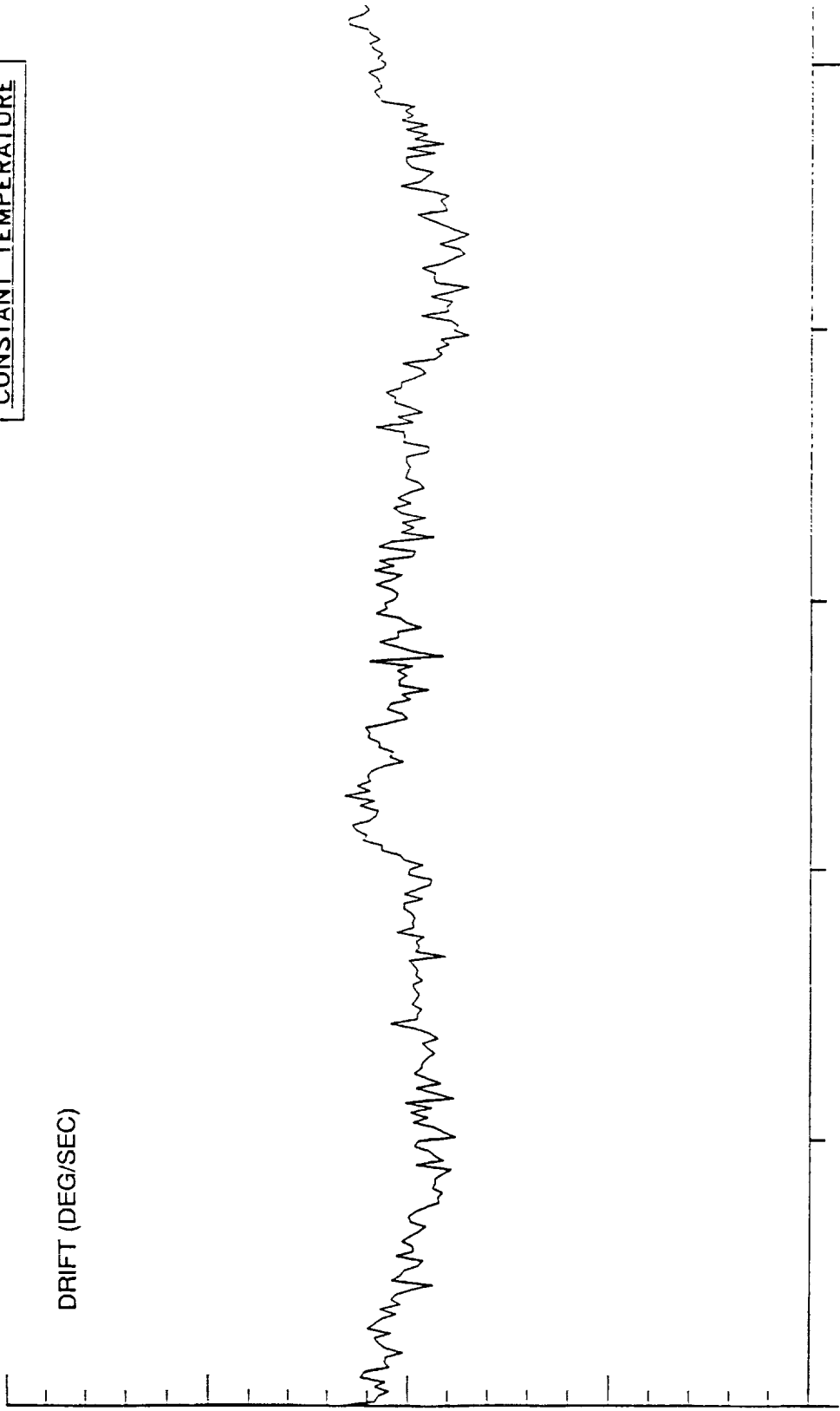


Figure 6

Result of rate test over ± 1000 degree/second on GEC Ferranti Piezo Vibratory Gyro

GYRO DRIFT AT
CONSTANT TEMPERATURE



14.5 HOURS (OVERNIGHT TEST)

Figure 7

Result of drift test on GEC Ferranti Piezo Vibratory Gyro

GYRO 203 : SCALE FACTOR AGAINST TEMPERATURE.

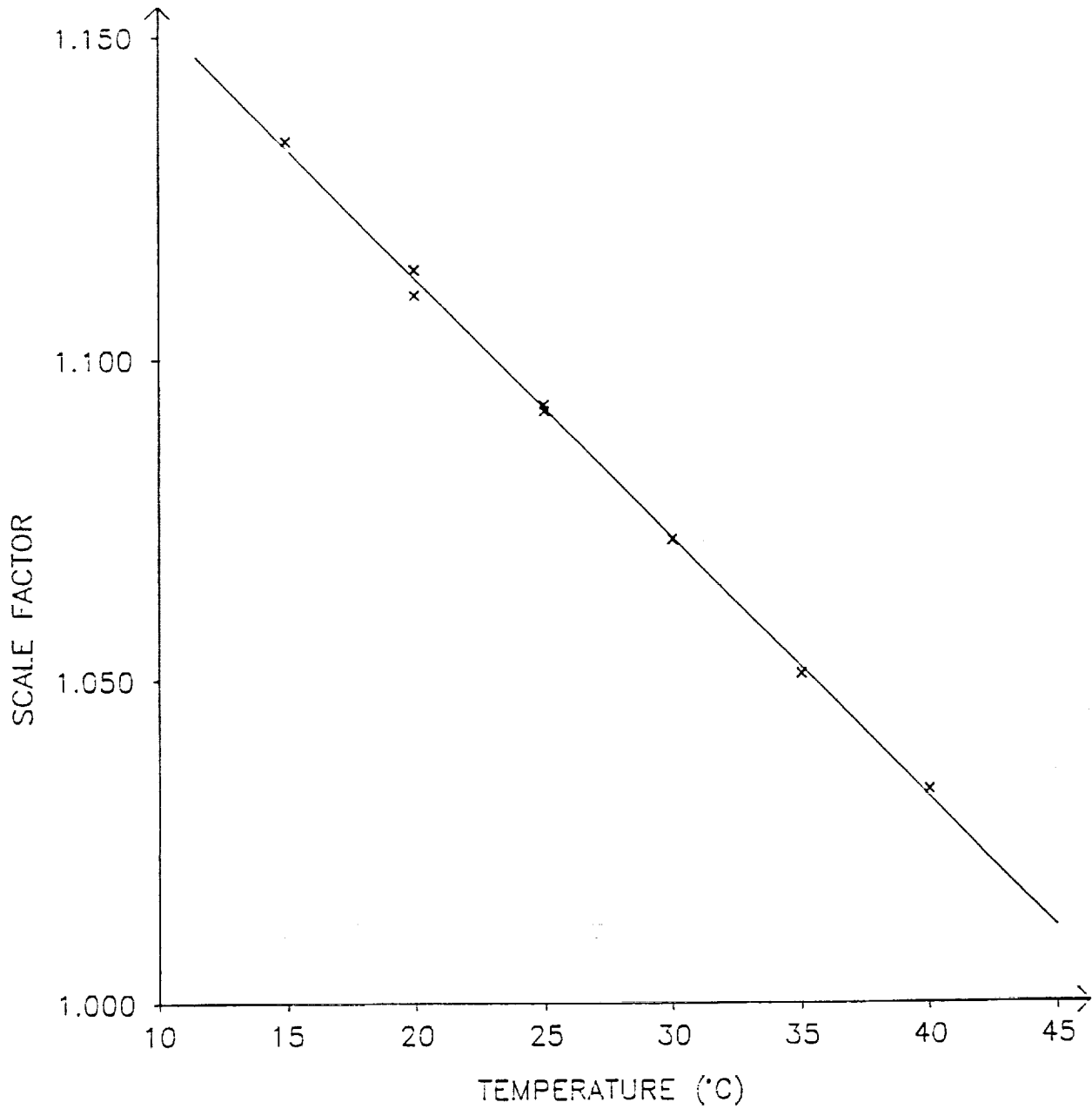


Figure 8

Results of a scale factor temperature sensitivity test on a GEC Ferranti Piezo Vibratory Gyro

The Application of Micromachined Sensors to Manned Space Systems

Aldo Bordano, NASA Johnson Space Center, Houston, TX
Gary Havey, Jerry Wald, Hatem Nasr,
Honeywell Systems and Research Center, Minneapolis, MN 55420
(612) 887-4036

Abstract

Micromachined sensors promise significant system advantages to manned space vehicles. Vehicle Health Monitoring (VHM) is a critical need for most future space systems. Micromachined sensors play a significant role in advancing the application of VHM in future space vehicles. This paper addresses the requirements that future VHM systems place on micromachined sensors such as: system integration, performance, size, weight, power, redundancy, reliability and fault tolerance. Current uses of micromachined sensors in commercial, military and space systems are used to document advantages that are gained and lessons learned. Based on these successes, the future use of micromachined sensors in space programs is discussed in terms of future directions and issues that need to be addressed such as how commercial and military sensors can meet future space system requirements.

Introduction

The application of smart micromachined sensors to vehicle health management VHM is the focus of this paper. The paper presents examples of how smart micromachined sensors have been applied to VHM. Future uses of micromachine sensors are then discussed.

The VHM Requirements

The focus of VHM is to ensure that the system under management is available for mission use at scheduled times and has the ability to 'stay on course' during its mission. The requirements for manned launch systems include a high degree of operational readiness, efficient/automated ground servicing and inspection operations as well as a great deal of near real-time decision making and reaction capability to avert mission threatening events. Manned transfer/rescue vehicles pose additional requirements because they may remain in a dormant state for years, only to have operate normally on demand.

Studies are now deriving microsensor requirements from these large system level requirements^{1 2 3 4 5 6}. Figure 1 represents one such derivation that is based on health management of the man-rated NLS. Notice that from the system level requirements for reliability, distributed test and fault isolation, maintainability, autonomy, and low cost come microsensor requirements for data recording and formatting, time stamping, threshold detection, significant event detection, local data qualification, local processing, communication and fault detection.

Examples of Microsystems for Vehicle Health Monitoring

The following are three examples of complete Health Monitoring microsystems that combine the micromachined sensors with the signal processing, health monitoring

data analysis, data reduction and data recording functions for failure analysis. The extremely small size and very low power requirements of these microsystems allow comprehensive vehicle health monitoring in applications where it was previously impossible or impractical. In a VHM application these microsystems, with the micromachined sensors in them, would be distributed throughout the manned space system.

Micro Time Stress Measurement Device

An example of a VHM microsystem is the Micro Time Stress Measurement Device (Micro TSMD)^{7 8}. The Micro-TSMD is an integrated diagnostic system for embedding into electronic systems. It is packaged as a 1" x 2" x 0.2" hybrid. The Micro TSMD senses and records vibration, shock, temperature, voltage transients, and DC voltage stress events. These forms of external stresses can be correlated to system failures. This approach is key to solving persistent problems and "cannot duplicate" failures that are externally caused. Once failure causing environments are characterized the data can be used for prognostics of systems in use or dormant.

A photo and block diagram of the Micro TSMD is shown in figure 2. An internal micromachined accelerometer senses vibration and shock. An internal microcomputer processes the data. The stress data is time-tagged and histograms recorded for lifetime exposure. In the case of vibration, a fast-Fourier transform (FFT) is performed on the data, saving accumulated time exposure at different frequencies and energy combinations of vibration.

The Micro TSMD, developed under an Air Force contract, is targeted for avionics at the Line Replaceable Unit level, but its use is appropriate in any high-integrity, complex electronics system.

Environment Stress Monitoring Device

A Health Monitoring microsystem similar to the Micro TSMD is the Environmental Stress Monitoring Device (ESMD). The ESMD is smaller than the Micro TSMD and is designed to monitor at the module level. The ESMD is a hybrid ceramic 0.9" x 0.9" in size (see figure 3). This ceramic can be used in a number of different application specific packages with micromachined sensors. The ESMD performs the sensor signal processing, data processing, and data storage. The device is suitable for placing in standard hybrid packaging and mounting on a circuit card assembly (CCA) or in a small stand-alone box customized for the user's application. The collected data is read out via a serial bus. A block diagram of the ESMD is shown on figure 3.

The ESMD requires no external components to monitor temperature, voltage transients and DC voltage. These sensing functions are designed into the ESMD. In addition to these parameters the ESMD has seven analog inputs that can interface to many types of external sensors: temperature, humidity, corrosion, air flow, EMI detectors, strain gauges, electrochemical sensors, magnetic field, and electric current. Signals are multiplexed in the ESMD into a 10-bit analog-to-digital (A/D) converter with 4-V reference. To collect data from a specific external sensor, an embedded software modification would be prepared to scale and histogram the data recording.

Reliability Assessment Tool

A more general purpose health monitoring microsystem is the Reliability Assessment Tool (RAT). The module is only 2"x 3"x 0.5" in size. A photo and block diagram is shown on figure 4. The RAT is currently in development at Honeywell under an Air Force contract. The base line RAT will monitor three channels of vibration (continuously performing FFTs), temperature and electric power quality of the system being monitored. Additional sensors such as humidity, corrosion, air flow, EMI detectors, strain gauges, electrochemical sensors, magnetic field, and electric current can be used with it.

The RAT uses a 16 bit fixed point digital signal processor to perform analysis on three channels of vibration and shock data. This type of information can be used to monitor the health of many forms of mechanical and electrical systems. The health of rotating equipment would be a good example. Vibration spectrums can show the health of bearings or out of specification changes in loads. Three miniature accelerometers are included inside the RATs 2" x 3" x 0.5" package. Remote accelerometers can also be used. In addition to these sensors the baseline device has internal and external temperature sensors and the ability to capture the peak of voltage transients. It captures positive or negative voltage transients for two channels. This would be used to monitor power quality of a system being monitored. It also multiplexes in 4 general purpose analog signals. Two of these channels are used for temperature sensing in the package. One is connected to the case and the other is isolated from the case to measure ambient temperature.

In order to achieve this level of miniaturization Honeywell has developed a mixed signal CMOS IC which places all the analog and digital interface functions required for the sensors on to one chip. This IC can interface to three vibration sensors inside the package or three vibration sensors outside. These vibration signals are filtered to prevent aliasing errors and have a peak hold circuit to capture mechanical shock peaks.

Future Micromachined Sensors for VHM

The examples of Microsystems for Vehicle Health Monitoring presented above focuses on vibration, shock, and temperature sensors. These sensors are most often required for health monitoring applications. Beyond acceleration and temperature are a range of other sensors which are more systems specific. The following is a discussion of these parameters and their sensors.

Air Flow—The absence of proper air flow for cooling can cause failure due to over heating. In addition various stages of the environmental control and life support system should be monitored for proper correct flow. Honeywell has developed micromachined silicon airflow sensors⁹. These sensors operate as a hot thin film microanemometer. Their small size and long term stability make them ideal for use as a monitor in manned space applications.

Infrared Radiation—Placing temperature sensors on large systems of interest could be a problem due to cost, configuration management, interference with operation etc. Temperature can be remotely monitored with IR radiation sensing. Honeywell has developed an uncooled IR imaging array using an array of micromachined microbolometers¹⁰. These uncooled IR cameras could be used much like CCD video

cameras to observe the IR radiation from a complete system. Less than a tenth of degree C resolution is possible.

Current—Current is a system parameter that identifies a problem's cause or source. An example would be IC failure leading to latchup, causing excessive current flow. Current spikes indicating arcing can occur in a traveling wave tube¹¹. The spectrum of the current waveform of an electric actuator can be used to show degradation of the actuator. An integrated magnetic field sensor can sense the current without decreasing reliability by adding another component electrically connected in the system. A hall-effect IC or one with a magnetoresistive thin film could be used.

Electrostatic Discharge—Electrostatic discharge can cause failure in the I/O circuits of microcircuit device by causing breakdown in the oxide insulation. Microsensors for ESD have been developed to show one time occurrences of ESD events (Zero Corp.). Interfaced to a health monitoring system the time and frequency of events can be recorded. With this information potentially damaged equipment can be identified and action can be taken to prevent further ESD.

Pressure—Examples of problems associated with pressurized systems include leakage of gases or fluids from sealed enclosures, rupture of sealed container, changes in properties of low-density materials, overheating due to reduced heat transfer, evaporation of lubricants, failure of hermetic seals and malfunction of equipment due to arcing. This is of key concern to systems that are dormant for many years. Micromachined silicon pressure sensors can be packaged in a small enough form to be embedded into systems to monitor their readiness.

Humidity—Moisture can cause physical and chemical deterioration of material. Temperature changes and humidity may cause condensation inside of equipment. Typical problems that can result from exposure to a warm, humid environment include swelling of materials due to moisture absorption, loss of physical strength, changes in mechanical properties, degradation of mechanical and thermal properties in insulating materials, electrical shorts due to condensation, binding of moving parts due to corrosion or fouling of lubricants, oxidation and/or galvanic corrosion of metals, loss of plasticity, accelerated biological activity, and deterioration of hygroscopic materials. Different types of integrated humidity sensors exist that would be applicable to health monitoring. The small size of integrated humidity sensor makes it possible to embed them into the systems.

EMI— The presence of large amounts EMI can cause unexplained electronic system failures. Miniature broadband antennas and receivers can be distributed in a system and made part of the health monitoring system. A failure can be correlated to a change in the local EMI. Action can then be taken to solve the problem.

Microcracks—Structural failure can be detected by monitoring of the acoustic emission caused by microcracks. Miniature smart acoustic emission sensors can be distributed through key structural components. The acoustic emission sensors can identify microcrack acoustic emissions. Recent Honeywell work has investigated using a micromachined sensor with a fiber optic interface to detect microcracks¹². The health monitoring system would identify when the number of events reach an unacceptable threshold.

Microgravity - The quality of the microgravity environment can be considered important to health monitoring if the mission is performing microgravity experiments. Honeywell has twice flown on the shuttle a microgravity monitoring sensor¹³. This has been used with microgravity processing experiments to record the environment during the processing steps.

Single Event Upset (SEU)- SEU is a transient radiation effect. SEU is of concern for any space mission. An ionized atom can pass through an integrated circuit causing the state of digital data to change. The frequency of this occurring can change with solar activity, orbit or changes in equipment placement. A measure of SEU activity can be a useful input to the health monitoring system. RAM memories with known SEU sensitivities can be used as sensors.

Chemical Contaminants—Chemicals can cause many diverse failures in mechanical and electronics systems. These problems include corrosion of electronic or mechanical components or the contamination of parts of the crew systems. Salt Fog is a specific subset of chemical contamination. The effects of exposure of materials to an environment where there is an aqueous salt environment can be divided into corrosion, electrical, and physical effects. The effects include impairment of electrical equipment due to salt deposits, production of conductive coatings, corrosion of insulating materials and metals, clogging of moving parts, blistering of coatings, and formation of acidic/alkaline solutions. There are a wide variety of ways to sense different forms of chemical contamination. Micro versions of the sensors that measure the presence of chemicals are being developed by many sources. Recent work has used these types of sensors to detect the presence of a corrosive environment instead of the after effects^{14 15}.

Conclusion

This paper has presented examples of microsystems that use micromachine sensors for Vehicle Health Monitoring. Examples of VHM sensor needs for air flow, IR, electric current, ESD, Pressure, Humidity, EMI, Microcracks, SEU and Chemical Contaminants were also presented.

References

- 1) Dr. J.Wald, J.Schoess, G.Hadden " Distributed Health Management Systems Technology for Future Propulsion Control Systems" Aerospace Technology Conference and Exposition, Sept 23-26, 1991
- 2) K. Nelson , G Hadden "A State-Based Approach to Trend Recognition and Failure Prediction for the Space Station Freedom" Space Operations, Applications and Research Symposium, 1991
- 3) G. Hadden, D. Toms, J. Harrington "ACS MDS: Maintenance and Diagnostic Systems for Space Station Freedom" Proceedings of the Fifth Conference on Artificial Intelligence for Space Applications 1990
- 4) J. Schoess, R. Sawamura "Advanced Sensor Architecture for Reuseable Space Launch Vehicles" AIAA/SAE/ASME/ASEE 26th Joint Propulsion Conference July 16-18 1990
- 5) J. Schoess "Smart Sensor Technology for Advanced Launch Vehicles" AIAA/ASME/SEA/ASEE 25th Joint Propulsion Conference, July 10-12 1989
- 6) J. Schoess, "A Distributed Sensor Architecture for Advanced Aerospace, Systems," SPIE Vol. 931, Sensor Fusion, Orlando, Florida, April 4, 1988.
- 7) G. Havey, J. Schoess, R. Olson, J. Carney, T. Tanji and S. Buska, "Microminiature Intelligent Sensor Systems", Government Microelectronics Conference, 1989.

- 8) G. Havey, J. Herrlin, and D. Kampf, "The Integrated Time and Stress Measurement Device Concept", 23rd Annual Proceedings of Reliability Physics 1985, pp. 252.
- 9) U. Bonne, G. Havey, "Versatile Flow Control Microsensor Structure and Application" 22nd Int'L Conference on Environmental Systems, 13-16 July 1992
- 10) R Wood, B. Cole C. Han and R. Higashi "Monolithic Silicon Uncooled Focal Planes for High-Density Array Development (HIDAD) Program" Aug 6 1991
- 11) F. Scafuri and, G. Havey, "Instrumented TWT", 1986 Microwave Power Tube Conference.
- 12) J. Schoess, C. Sullivan "Conformal Acoustic Waveguide Technology For Smart Aerospace Structures" 1st European Conf. on Smart Structures and Materials Glasgow 1992
- 13) J. Schoess, D. Thomas, B. Dunbar "Measuring Acceleration In a Microgravity Environment" Sensors Vol. 7 No. 1, Oct 1990
- 14) T. Anguish, P. Janavicius and J. Payer "Development of a Multiple Element Sensor for Localized Corrosion of Stainless Steel" 1989 tri-Service Conference on Corrosion
- 15) R. Glass, W. Clarke, K. Dolan, W. Thompson, D. O'Brien "Electrochemical Sensors Based upon Multielement, Microelectrode Arrays for Smart Structures" 1991

Vehicle Requirements

- Fault avoidance
- Reduced maintenance on schedule/demand



System Requirements

- Automated checkout
- Real-time monitoring
- Integrated maintenance
- Fault prognosis/diagnosis
- Information management and control



Subsystem Requirements

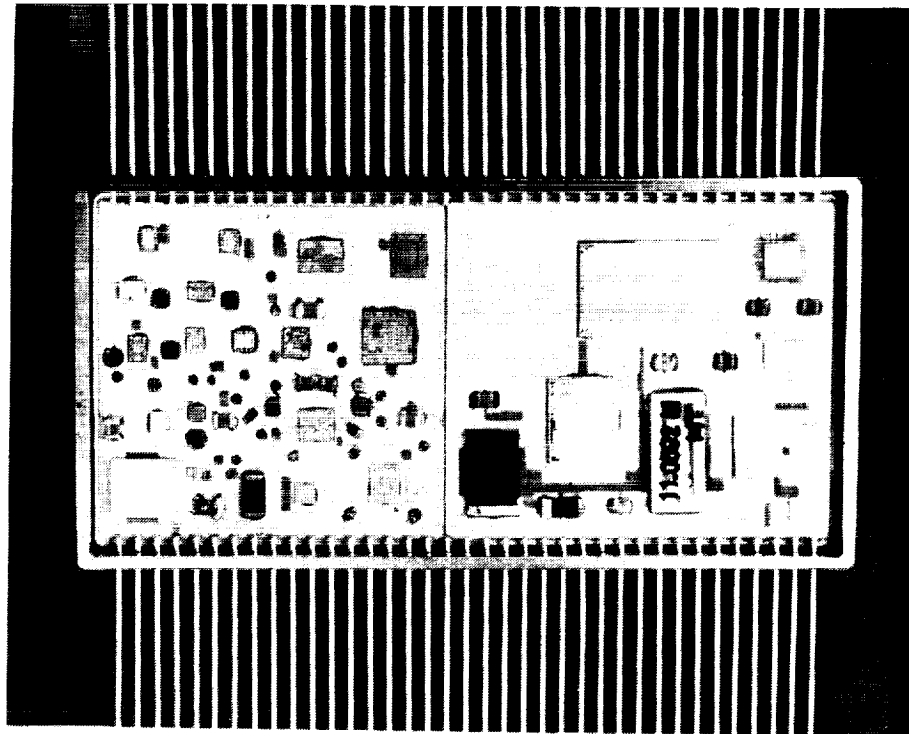
- Remaining life measurements
- Fault prediction, detection, isolation
- Redundancy management
- Local data
- Local data management and control
- Timestamping of events



Smart Sensor

- Fault detection isolation
- Self-test
- Local data acquisition, filtering and processing/health status assessment
- Timestamping of data

Figure 1 Derivation of smart micromachined sensors requirements for VHM



The internal accelerometer is in the lower left-hand corner.

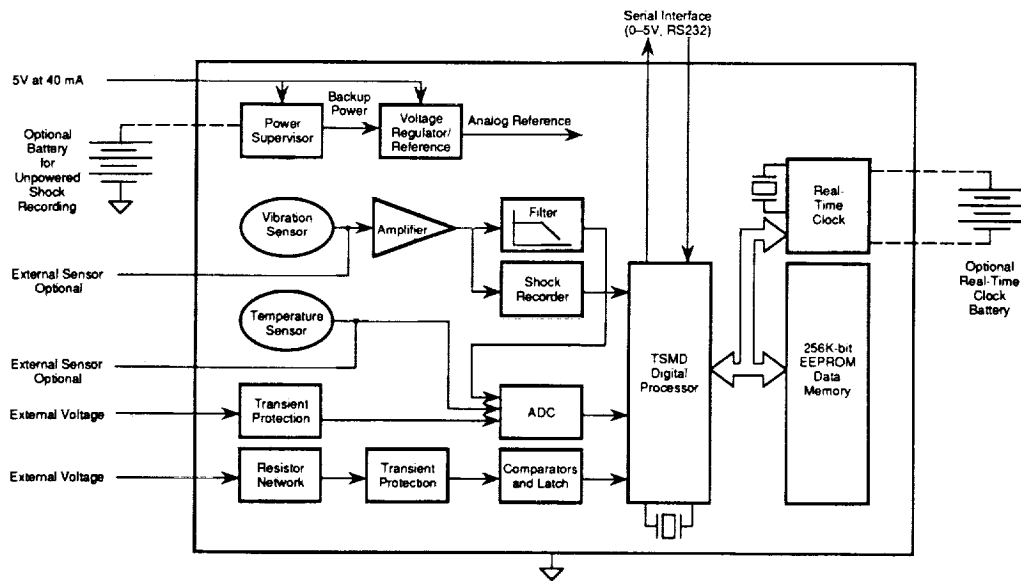


Figure 2 Micro-Time Stress Measurement Device photo and block diagram

Environment Stress Monitoring Device (ESMD)

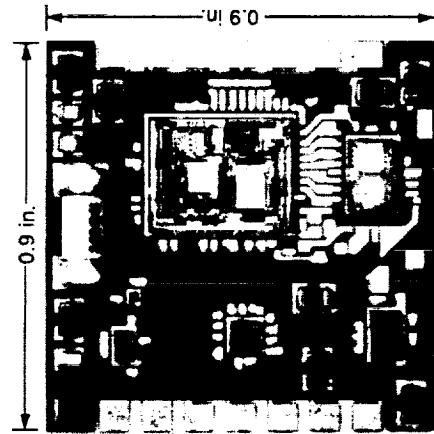


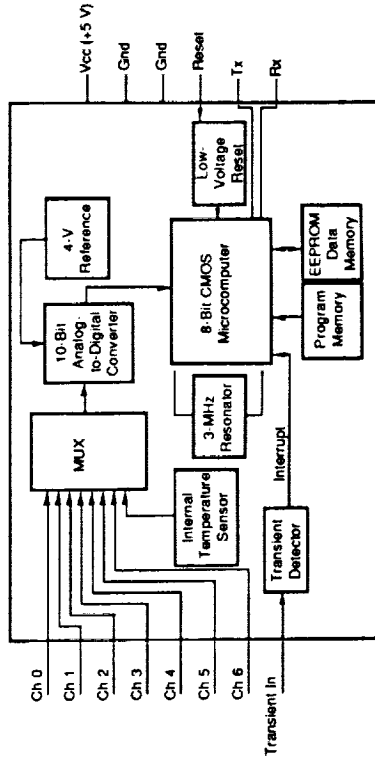
Photo of ESMD

A low-cost device to accumulate long-term histories of failures that cause stress on an electronic system

Baseline Software Recording Functions

- Elapsed "power on" time monitor, (1-min resolution)
- Number of on/off cycles
- Temperature for the last 250 samples (samples selectable from 1-255 min)
- Temperature histogram (5°C bins)
- Temperature cycle histogram
- Voltage transient counter
- Temperature during voltage transient

ESMD Block Diagram



Examples of Possible External Sensors

- Humidity
- Corrosion
- Strain gauges
- Air flow
- ESD
- Mechanical shock
- Current (dc and transients)

Applications

- Electronic assemblies
- Warranty verification
- Intrusion monitoring
- Product development testing
- Process trend monitoring
- Shipment monitoring
- Waste storage monitoring
- Equipment usage monitoring

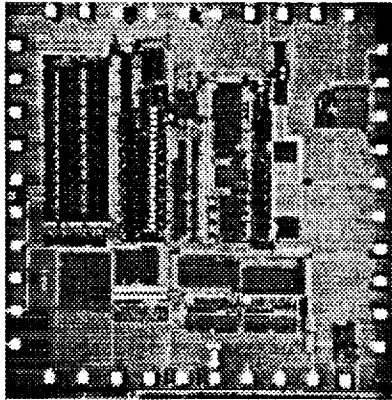
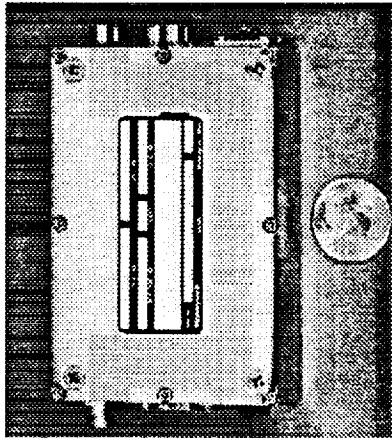
Systems and Research Center

Figure 3 Environmental Stress Monitoring Device

Honeywell

8920158-02

Vehicle Health Monitoring Microsystem with Internal Digital Signal Processor



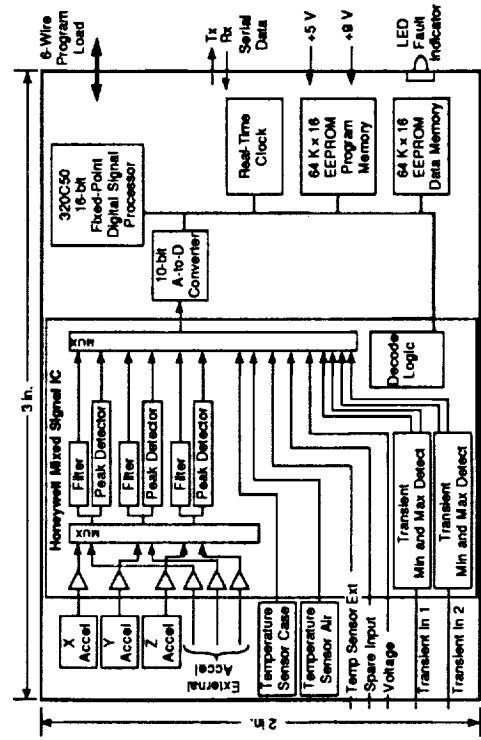
Function
 Monitors 3-axis vibration, shock, temperature, voltage and voltage transient conditions of a system and can record a time history

- Features**
- Small size—2" x 3" x .05"
 - Two internal temperatures
 - Internal 3-axis vibration sensors
 - 2-voltage transient detect
 - 10-bit A to D converter
 - 16-bit fixed point digital signal processor
 - Nonvolatile data memory
 - Real-time clock
 - Serial interface

- Applications**
- System health monitoring
 - System evaluation tests

Honeywell-Designed Custom CMOS Mixed Signal IC for Sensor Interfacing

Vehicle Health Monitoring Microsystem



Block Diagram

Figure 4 Reliability Assessment Tool



MICRO GUIDANCE AND CONTROL SYNTHESIS: NEW COMPONENTS, ARCHITECTURES AND CAPABILITIES

Edward Mettler and Fred Y. Hadaegh

Jet Propulsion Laboratory
California Institute of Technology

ABSTRACT

New GN&C (guidance, navigation & control) system capabilities are shown to arise from component innovations that involve the synergistic use of microminiature sensors and actuators, microelectronics, and fiber optics. Micro-GN&C system and component concepts are defined that include micro-actuated adaptive optics, micromachined inertial sensors, fiber-optic data nets and light-power transmission, and VLSI microcomputers. The thesis is advanced that these micro-miniaturization products are capable of having a revolutionary impact on space missions and systems, and that GN&C is the pathfinder micro-technology application that can bring that about.

1. INTRODUCTION

The general trend in communication, signal processing, and computation over the last two decades continues to be towards miniaturization for improved performance, higher reliability, and lower relative cost. However, the engineering difficulties and rapidly increasing expense of interfacing digital microelectronics with conventional sensors and effectors have not allowed this promise to be realized for space GN&C systems.

Research in micro-mechanics sensing and actuation has been very active in the past several years, both in industry and academia. Various commercial micro-sensors have been built to measure humidity, temperature, flow rate, viscosity, pressure, acceleration, chemical reactions, and many other physical parameters. At MIT, U. C. Berkeley Sensor and Actuator Center, the University of Utah Center for Engineering Design, and at Caltech, research is ongoing in integration of micromotors, micromechanical gearing, logic, and transducers.¹⁻¹²

There have been recent advances in the micromachining of silicon through the use of anisotropic etchants with doping controls. These advances have led to the development of a new class of sensors composed entirely of surface micro-machined silicon. Surface micromachining is a much more sophisticated technique than bulk micromachining. Various beams, masses and other structures can be formed by depositing and etching multiple thin films and layers of silicon and silicon oxide. The feature dimensions of such devices are 1-2 μm , roughly the same as conventional electronic circuits.

Recent progress in the integration of established batch fabrication techniques for VLSI microelectronics with new silicon surface-micromachining methods has now made it feasible to incorporate on-chip the supporting circuitry for microsensors and microactuators (i.e., amplification, compensation, conversion, multiplexing, and interfacing functions). As an example, this technology has recently been used to develop the Analog Devices ADXL-50 accelerometer¹³ shown in Figure 1.

While the present version of this sensor has an advanced level of integration, it is not an "inertial guidance grade" accelerometer in accuracy. It does represent the functional form of "smart" micromachined devices that are evolving rapidly through a marriage with VLSI microelectronics.

The Analog Devices' part breaks new ground by using a surface micromachining process that lets the company integrate a capacitive, force rebalance, acceleration sensor, as well as control circuitry, on the same die. The device features on-chip signal conditioning and self-test circuitry. The sensor measures $500\ \mu\text{m} \times 625\ \mu\text{m}$. The capacitor plates are approximately $115\ \mu\text{m}$ long and about $4\ \mu\text{m}$ wide. The on-chip signal-conditioning circuitry produces a scaled-referenced and temperature-compensated output voltage. In addition, a digitally controlled self-test function lets the sensor deflect at any time, producing a precise output voltage corresponding to the equivalent g-force for a healthy sensor.

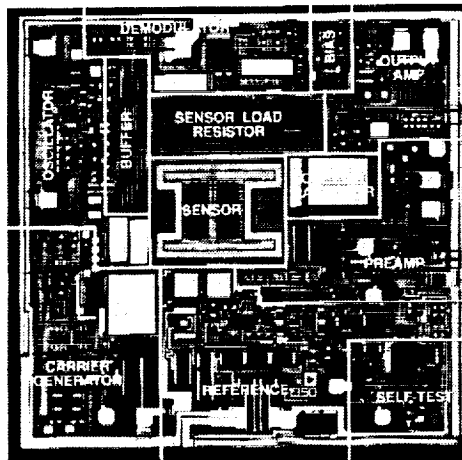


Figure 1. ADXL-50 Accelerometer

In this paper, these device features along with higher integration levels of micro-devices with local DSP for distributed architectures are proposed for new GN&C architectures.

2. SPACE APPLICATIONS

In the subsequent discussions, we present an advocacy for the development of micro-GN&C and describe an approach for the utilization of new microengineering technologies to achieve major reductions in GN&C mass, size, power, and costs to meet the needs of future space systems.

It would not be an overstatement to forecast the outcome of integrating the emerging fields of micro-optoelectronics and micro-electromechanics with advanced microelectronics as a revolutionary change, rather than an evolutionary improvement. The potential payoffs in the metric-space of cost-performance-risk are very impressive: 100/1 reductions in size, mass, and power; 10/1 reduction in recurring costs and cost growth-rates; solid-state reliability and lower performance risk; and robustness to temperature, vibration, and radiation environments.

To fully appreciate the impact that micro-miniaturization can have on intelligent-system implementation costs (i.e., systems like GN&C and robotics with sensors, computation/logic, and effectors), we have only to apply a conservative scaling to the dollars per kilogram and per watt for current unmanned spacecraft equipment: approximately 100 K \$/watt and 100 K \$/kilogram for today's planetary probes. Then, without even factoring in the multiplier for improved performance and reduced risk with a micro-technology implementation, we observe that the recurring cost improvement of 10/1 and greater can be taken as an achievable objective based only on the mass, power, and fabrication economics of microelectronics.

Several major NASA programs will directly benefit from these technology advances and therefore they provide an important motivation for this research: The Lunar and Mars Exploration initiatives contain both Micro-Spacecraft and Micro-Lander/Rover elements as key capabilities required to realize cost effective exploration and science return.

In a discussion of "micro-size" systems, we must define the metric that distinguishes "micro" from "small" or "light" spacecraft and rovers. As a reference, typical spacecraft fall into a range of 1500 to 3000 kg, and large rovers are in the 500 kg range. Then by "small" or "light" we mean a reduction of about 10/1 in mass, and by "micro" we mean a 100/1 or greater mass reduction. This scaling places the mass of micro-spacecraft in the range of 15-30 kg, and micro-rover mass at about 5 kg.

On the large space-systems scale, the future astrophysics advances from Space Interferometers and Multi-aperture Reflectors will be made feasible by the capability to actively control these spatially distributed optomechanical systems and integrated structures to nano-precision levels without imposing instrumentation mass, power and cost penalties proportional to system size and complexity.

Cost-constrained remote sensing platforms, for both missions to planet Earth and deep space, and manned space stations will all benefit from the new microelectromechanics technology that will become ubiquitous in applications for both microsystems and macrosystems.

The GN&C application needs for these future space systems have been identified as follows:

Micro-Spacecraft, Micro-Landers, & Micro-Rovers

- Attitude & Maneuver Control System
- Micro-Inertial References
- Microelectro-optics for miniature cameras & remote sensors
- Inertial Navigation Systems
- Heading Reference Units
- Mini-Camera Pointing & Stabilization
- Antenna Pointing & Stabilization

Remote Sensing Platforms, Interferometers, & Deployable Reflectors

- Distributed Micro-Sensor System Identification
- Multivariable Control of Structural Dynamics
- Distributed Shape & Position Control of Mirror Arrays
- Embedded Stabilization of Telescope & Instrument Optics
- Distributed Micro-Inertial References
- Embedded Health Monitoring of GN&C Effectors

3. MICRO GN&C CORE INNOVATIONS

The core microengineering innovations needed to realize the above micro-GN&C architectures and functions can be combined into a set of six micro-technology products that would serve as enabling building blocks for the new GN&C subsystems. The following products include component and system implementations that are synergistic and would involve contributions and coordinated activities of NASA, industry, and academia.

- Massively distributed microsensing for system ID & control
- Light powered remote processing network for microsensing
- Micro-GN&C for microspacecraft and microrovers
- Six degree-of-freedom micro-inertial measurement unit

- Actively controlled micromachined deformable mirrors
- Embedded health monitoring for GN&C effectors

3.1 Massively Distributed Micro-Sensing for System ID & Control

For a massively distributed system ID-sensing approach for active structure control to be practical, the basic sensing system has to be, of necessity, mass efficient, low power, micro-g sensitive, of low complexity and cost, fault tolerant, and have generic applicability to future missions.

The fully integrated sensing system (Figure 2) will consist of high sensitivity micromachined sensing elements with distributed data communication, signal conditioning and processing electronics, connected together over a fiber-optic network. The high bandwidth fiber optic network provides digital data interfaces with high EMI immunity, and serves as the source for sensor power through optical to electrical power conversion. This obviates the need for multiple conductors for data and signal as in conventional networking technology. Fault tolerance and redundancy can be provided with multiple sensing elements per sensor as well as with a suitable choice of network topology and communication protocol.

The proposed smart sensor system will be implemented using a micro-accelerometer as the basic sensing element. Typical deployable space structures depend on flexible beam-truss structures assembled out of rod elements interconnected with joints (e.g., high gain communication antennas, instrument booms, basic truss support structures for segmented reflector telescopes, and spaceborne interferometers). Three-axis accelerometers will be mounted on the connecting joints of a truss structure, or single axis accelerometers will be installed along the length of flexible ribs.

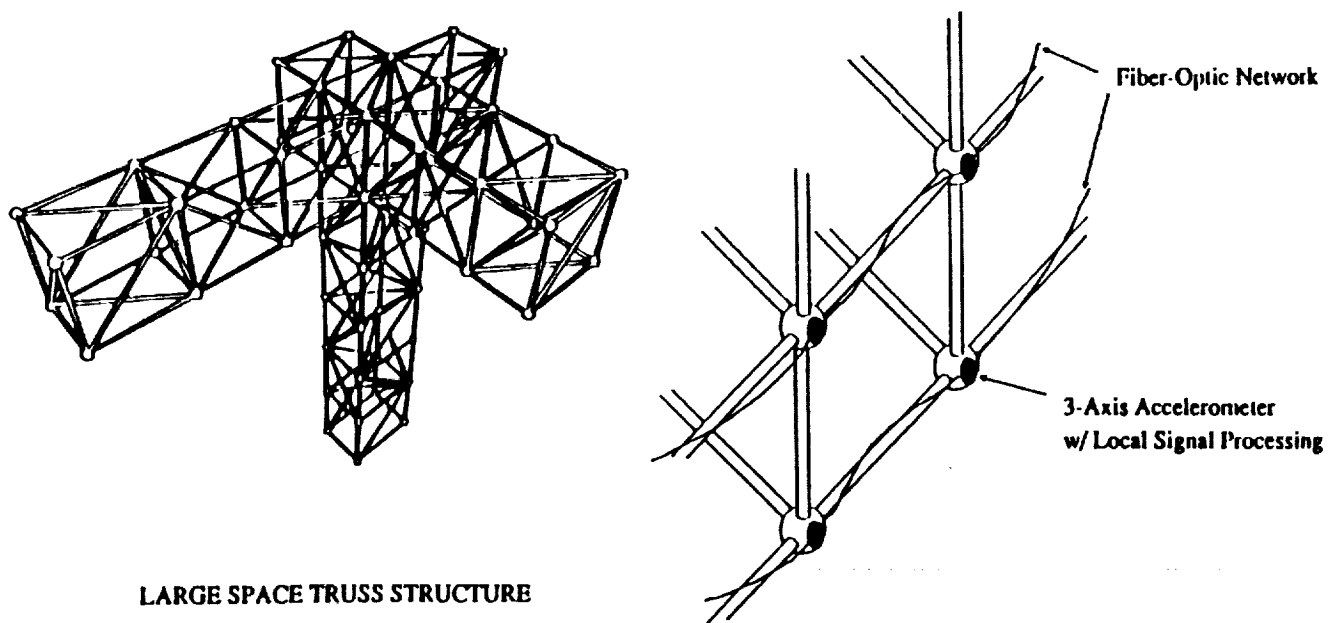


Figure 2. 3-Axis Integrated Sensing System

3.2 Light-Powered Remote Processing Network for Micro-Sensing

It will be necessary to develop the microtechnology that will enable the full integration of micro-sensors with their electronics, and will enable the adaptation of fiber-optic networks for communicating with, and powering of, microsensor systems. This work is described in two parts: **Microsensor Electronics**, and **Fiber Optic Networks**.

3.2.1 Microsensor Electronics

The development of integrated sensor electronics will provide a self-contained motion sensor with a very small form factor and low cost and power. This will enable the use of multiple sensors to sense three-axis linear accelerations. The system will read the multiple sensor outputs, process the information for velocity/ acceleration vectors, and format the output for serial I/O interfaces that transmit/receive information over fiber optics in a large massively distributed system. Figure 3 illustrates the various components of such a system. The amount of data management electronics will enable diverse system architectures to be produced from the same microelectronic building blocks.

The sensor electronics are programmable in gain and mode of operation. The sensor output is digital so the sensor has a bi-directional digital interface. Enhanced versions of integrated sensor electronics will include:

- Standard serial and parallel interfaces.
- Two-wire interface where power is obtained from the interface.
- Signal processing on the sensor to integrate its acceleration signals for velocity, and correct for offsets in the system.
- Gain control of the sensor electronics to maximize their dynamic range.
- Optical power and interface designs that isolate the sensor from the control electronics.

The off-sensor control electronics will provide for the use of multiple-axis sensor systems and further enhance the sensor performance through hardware signal processing by special purpose local integrated circuits.

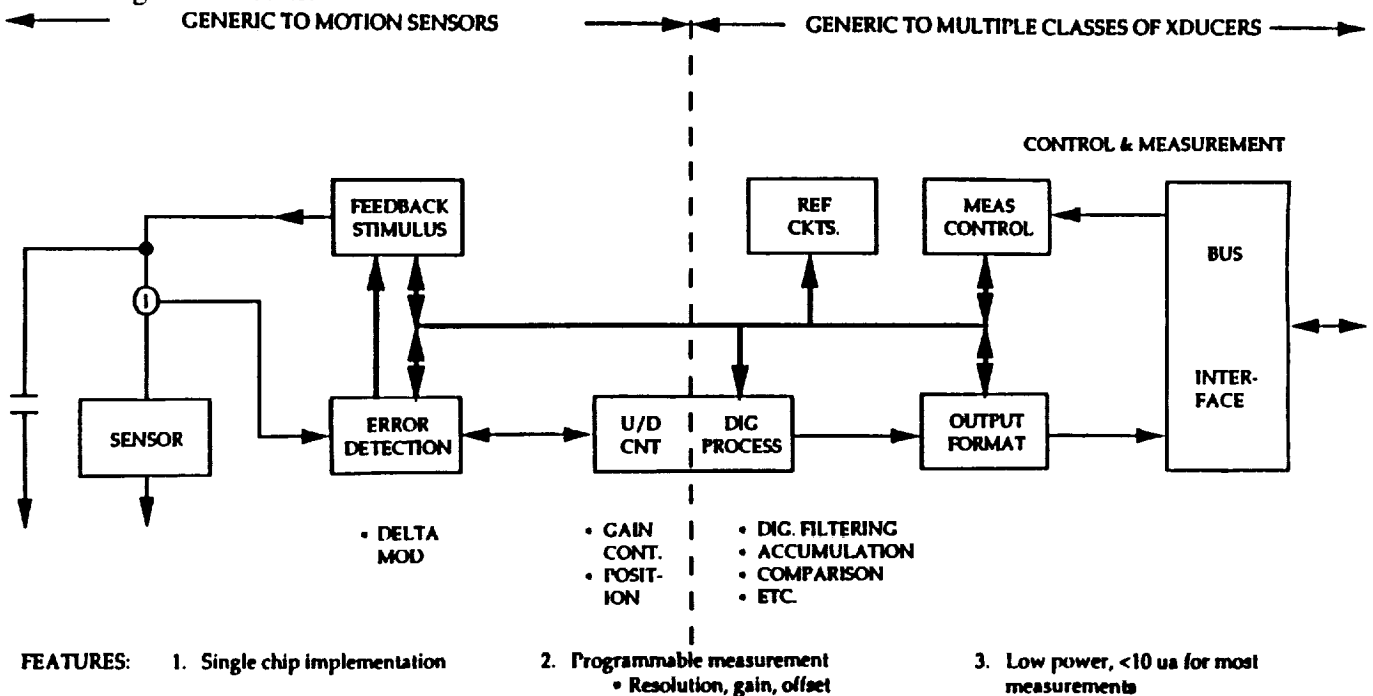


Figure 3. Remote Signal Processor for Motion Sensors

The development of on-chip electronics for the micromachined sensor will be directed toward generic electronics. These electronics will be integrated directly on the silicon sensor with conventional CMOS circuit fabrication technology. Their proximity to the microsensors mechanism will provide maximum overall sensitivity through noise minimization in the high impedance circuit; and equally significant, they will provide a small self-contained sensor at a low recurring cost.

These integrated sensor electronics will allow future system evolution so that on-chip enhancements will use the sensor as a cell, and external enhancements will have sufficient measurement and control interface access. In addition to low power, the design goal will include low voltage operation so that the chip can be powered from a single photo-detector which would be integrated on the sensor.

The addition of data management functions would include the further integration of sensor-specific processing functions and the interfacing with a distributed microcomputer. This microcomputer may make use of the technology that has been developed at JPL for a Common Flight Computer (CFC). The CFC makes use of a VLSI chip set jointly developed by Sandia National Labs and JPL. The CFC is a high performance computer contained on a single board. It will be further miniaturized by redesigning the packaging configuration to a high-density hybrid multi-chip module containing unpackaged chips on ceramic substrates.

The 16 bit data path computer is designed in a 1.25 μm CMOS (Complementary Metal-Oxide Silicon) technology and is based on Sandia's SA3300 microprocessor, a Rad Hard Single Event Upset resistant microprocessor which executes the National Semiconductor NSC 32016 instruction set. The chip set includes a Floating Point Unit (FPU), Interrupt Control Unit (ICU), two Direct Memory Access Co-processors (DMACs), Control Unit (CU), and Fault Management Unit (FMU). The FMU will transparently correct single-bit errors and perform bit-plane sparing to replace single bits of memory which might fail over time. Figure 4 shows a block diagram of the computer and its interfaces to other hardware functions.

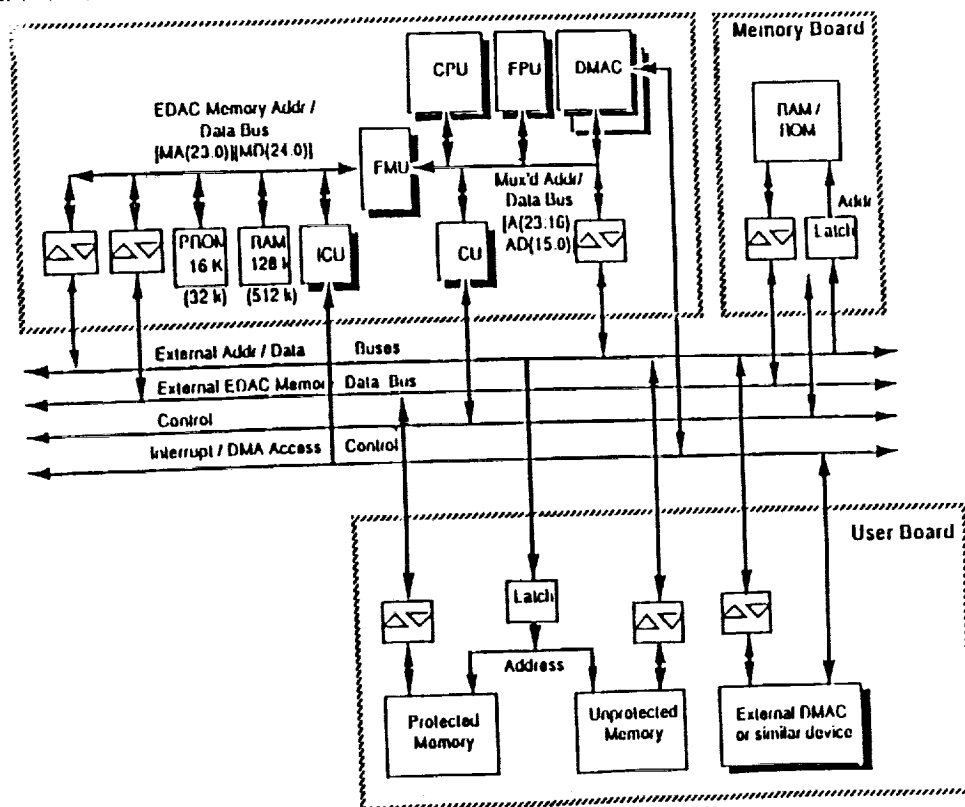


Figure 4. Common Flight Computer Architecture

3.2.2 Fiber Optic Networks for Microsensing

The general objective is to implement the remote-processing network with optical fiber rather than with electrical conductors. The small mass and low power consumption of microsensors make them the natural choice for many system-identification and control applications, and the use of remote processing enhances these advantages by a large factor. However, these advantages are largely lost if the interconnection must be done with conventional multi-conductor copper cable.

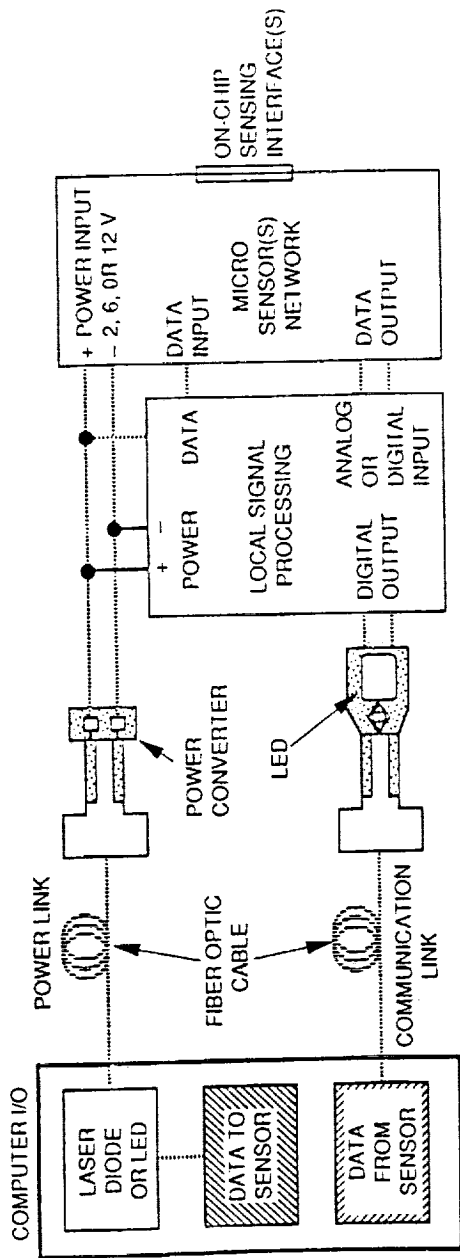
The network connects the microprocessors associated with each microsensor to one or more central processors. In this function it is a data bus of very high bandwidth. It is also a power-distribution system in which the power is distributed in the form of optical radiation. The optical power will travel through the same fiber as the data. The network will be constructed for the most part from existing components. These components include, besides the fiber itself, electrical-to-optical and optical-to-electrical interfaces as well as couplers, taps, etc. Although the optical powering of a pilot's headset, or the equivalent, has been demonstrated, the powering of an entire network has not been demonstrated, and some of the components may need continued development.

Semiconductors that convert light into electrical power have typically been characterized by a low output voltage that requires step-up transformers and amplifiers. Varian Research recently introduced its PR6C power converter¹⁴ that offers a breakthrough solution. The monolithic device converts optical power into electrical power sufficient to drive ICs as well as sensors. When driven by light sources such as laser diodes, either directly or via fiber-optic cable, the new converter can produce an output power of up to 1 W, with output voltages up to 12 V. To generate such an increase in power output, Varian combined its GaAs solar cells with GaAs IC design and manufacture.

As an example, the 6-V version of the converter has an active-area diameter of 3 mm that is divided into six equal sections. Each section is essentially a GaAs solar cell, operating as an independent photodiode with an output of 1 V. These sections are electrically isolated by a trench measuring 20 μm . Interconnecting along the surface is not possible as the higher voltages require a topology too deep for this process. The solution is an "air bridge" or metal strip which spans the trenches, producing a sum of 6 V between the first and the last cell. The output voltage can be increased by simply increasing the number of 1-V cells. For a 6-V device, a 250 mW light input at a wavelength of 800 nm can produce an output power of about 111 mW at 5.8 V, giving an efficiency approaching 50%.

In one example of a "Power down/Data back" transmission strategy, light is sent from a control system, via fiber optics, to the converter. This light powers a sensor, as well as a diode, to send data back along the same fiber to be processed by the controller. Figure 5 shows a distributed microsensing system example based on Photonic Power Systems'¹⁵ application of the power converter under license from Varian.

The overall topology of the network is also an important consideration. It is in part determined by the specific sensing problem being addressed, but it is also determined by reliability considerations. Figure 5.1 shows an example of network topologies. A linear bus implemented with two fibers is shown at (a). The use of dual fibers simplifies the design of the taps. A star network is shown at (b). The central star may be either active or passive depending on requirements. Ring networks both parallel and counter-rotating are shown at (c) and (d). The increased redundancy of the counter-rotating ring gives it improved reliability. A significant effort will be devoted to analysis of alternate network topologies for GN&C applications, including their effectiveness and their reliability.



FEATURES:

- NOISE-FREE FIBER OPTICS FOR POWERING REMOTE SENSORS AND CONTROL SYSTEMS
- COMPLETE POWER ISOLATION, i.e., TOTAL AVOIDANCE OF POWER AND SIGNAL GROUND LOOPS
- TOTAL IMMUNITY TO NOISE CAUSED BY ELECTROMAGNETIC AND RADIO FREQUENCY INTERFERENCE
- NO VOLTAGE "STEP-UP" CONVERSION IS NEEDED SINCE VOLTAGE LEVELS ARE AVAILABLE AT 2, 6, OR 12V
- SENSOR INPUT POWER LEVELS AVAILABLE FROM 1 mW TO 150 mW DEPENDING ON LIGHT SOURCE
- MULTIPLEXING BOTH POWER AND SIGNAL FOR MULTIPLE SENSORS AND CONTROLS
- LIGHTWEIGHT CABLING

*COURTESY OF
photonics
 POWER SYSTEMS, INC.

Figure 5. Light Power and Communication for Distributed Microsensing

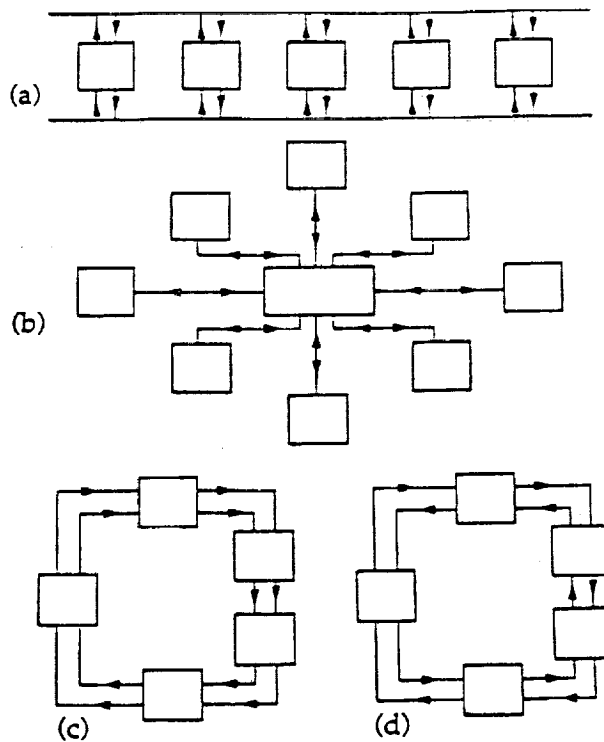


Figure 5.1. Candidate Network Topologies

3.3 Micro-GN&C for Micro-Spacecraft and Micro-Rovers

Advances in the miniaturization of sensors and computers with increases in performance allow the development of a miniaturized GN&C subsystem that enables a new class of micro-spacecraft and planetary roving vehicles.

3.3.1 Micro-Spacecraft

The functionality of an entire GN&C subsystem for a micro-spacecraft will be implemented in the miniaturized VLSI common flight computer. This includes the interfaces with CDS (the command and data subsystem), sensors, and actuators. Information will be processed into appropriate actuator commands (Figure 6).

The CDS interface will include input commands and output telemetry. The sensor inputs needed by the GN&C subsystem include gyros and accelerometers (from the 6-DOF IMU), star tracker or micro-imaging system (for attitude position and rate), sun sensor, and encoder position (for at least one articulating element). The sensor inputs and CDS commands will be processed by the computer to produce driver outputs suitable for actuators including reaction wheels, thrusters, and articulation motors.

The primary GN&C functions for a spacecraft are given below. The actual functions implemented in the micro-spacecraft GN&C subsystem will be a subset of these. The functions are broken up into three main areas:

Attitude Determination: This set of functions takes sensor data (such as sun sensor, IMU, and encoder information) and determines spacecraft attitude (to various levels of accuracy depending on the sensor), attitude rate, the articulation angle and rate of any appendages, and the vector (in the spacecraft frame of reference) to important bodies (sun/earth/bright bodies/target body).

Attitude Control: This includes various spacecraft functions such as sun acquisition and pointing, HGA pointing (pointing the radio antenna towards the earth), commanded turns, axial/lateral delta-v burn control, thrust vector control, and momentum unloading.

Articulation Control: Given an articulated appendage such as a camera, there are various modes that it needs to be commanded in, such as celestial pointing (based on inertial data), relative pointing (based on encoder data), target motion compensation, and closed loop target body tracking.

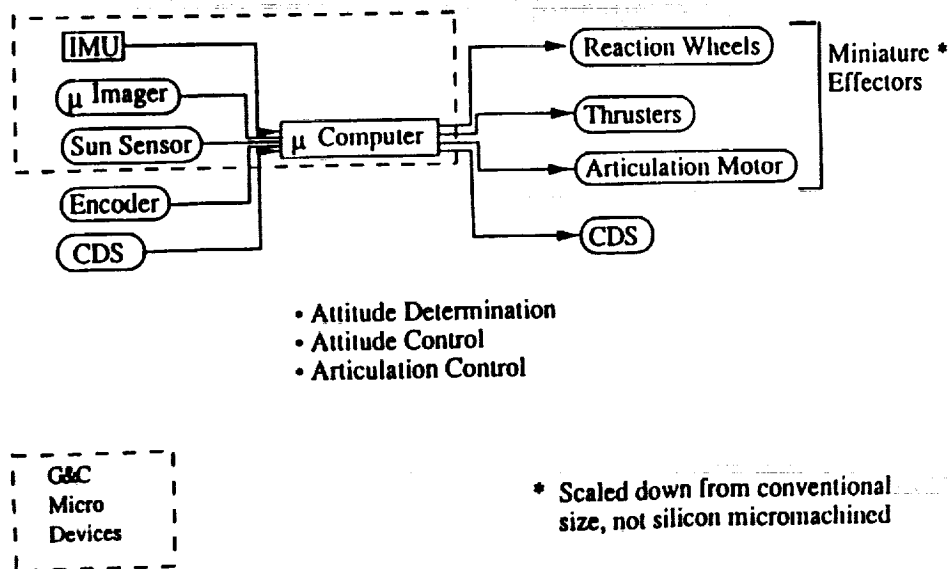


Figure 6. Micro-Spacecraft GN&C

3.3.2 Micro-Rovers

The GN&C functionality appropriate to a rover is quite similar to that for the micro-spacecraft, including an interface to CDS, sensors, and actuators (Figure 7). The CDS interface will include input commands and processed sensor information (such as processed landmark information from a micro-imaging system), and output telemetry and guidance information. The sensor input needed by the GN&C subsystem includes gyros and accelerometers (from the 6-DOF IMU), odometer, and encoder position (from an articulated appendage). The sensor inputs and CDS commands will be processed (in the common flight computer) to give articulation control commands, and navigation information suitable for processing to appropriate vehicle steering commands, path-planning, and telemetry.

The GN&C functions we will consider for the micro-rover are a subset of the following:

Attitude and Position Determination: This set of functions takes sensor data (such as IMU, odometer, landmark position information from an imager, and encoder information) and determines rover attitude, attitude rate, the articulation angle and rate of any appendages, and rover position.

Path Guidance: Given information on a path to be followed, and the current position, the path guidance function determines the high level steering commands needed to follow the path.

Articulation Control: Given an articulated appendage such as a camera, there are various modes that are required such as relative pointing (based on encoder data), rover motion compensation, and closed loop feature tracking.

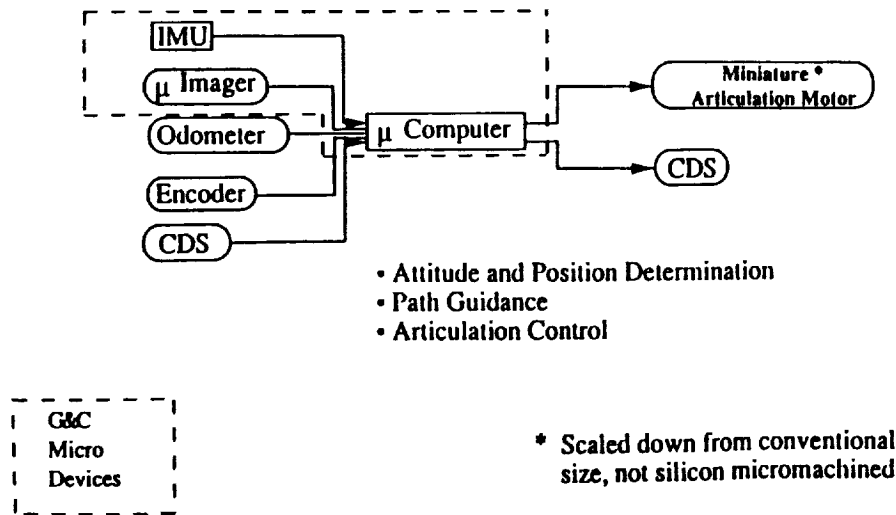


Figure 7. Micro-Rover GN&C

3.4 Actively Controlled Micro-Machined Deformable Mirrors

As the size and sophistication of optical instruments increases, instrument designers are turning to deformable mirrors as a means of compensating for distortions in elements of the optical train and/or in the instrument's field of view. The resulting adaptive optical systems have applications in large space interferometers and multi-aperture reflectors.

In the case of imaging instruments intended for space applications, a deformable mirror should be small, lightweight and highly pixelated (i.e., deformations having high lateral resolution can be made); it should also consume little electrical power, thereby minimizing undesirable thermal effects on the controlled surface as well as overall spacecraft power requirements. Figures 8 and 9 show an example construction.

This effort will exploit micromachining technology to develop a deformable mirror with the above characteristics. The mirror may be realized as a "flip chip" type assembly, consisting of two matched, micromachined structures mounted face-to-face and fused together along their peripheries. The key elements of the mirror will be simple, easily-replicated, capacitively-driven linear actuators, each responsible for pulling on a small section of a thin flexible mirror. Electronic element access, and perhaps even control circuitry, will be monolithically integrated into the mirror.

The initial performance goals for the mirror will be 10 nm control of a 32 x 32 pixel flat mirror. Once these goals have been achieved, efforts will be directed at extending the number of pixels/control elements until 10 nm control can be effected over a 1024 x 1024 pixel surface.

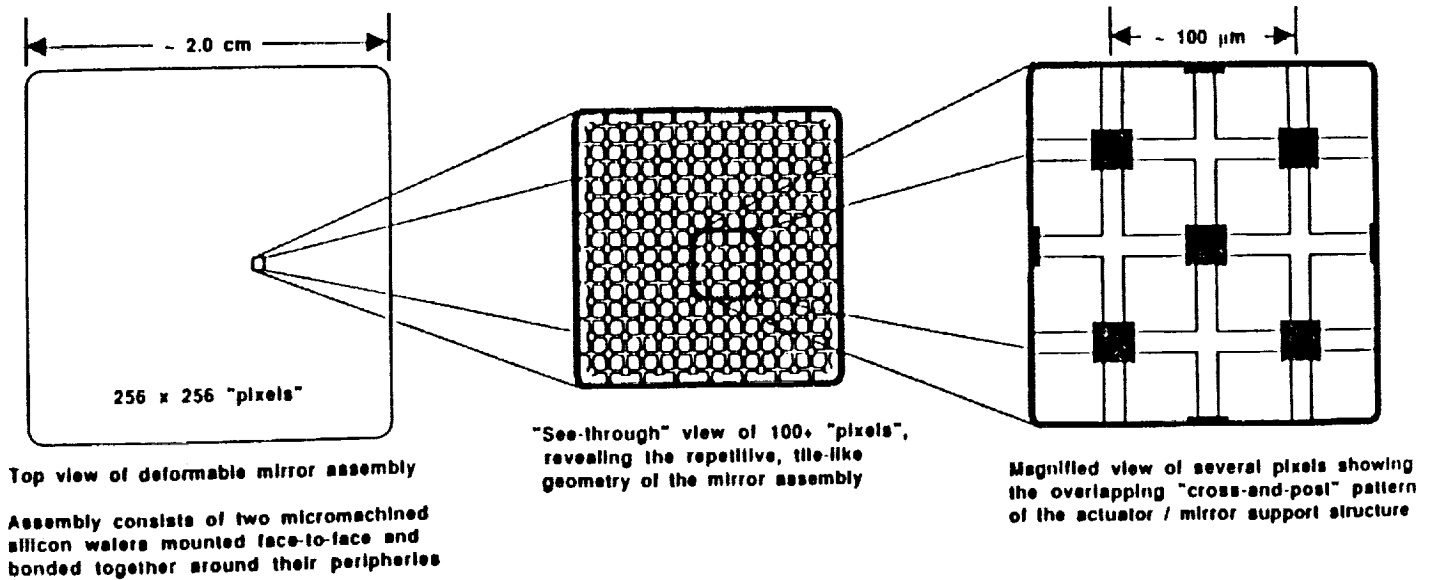
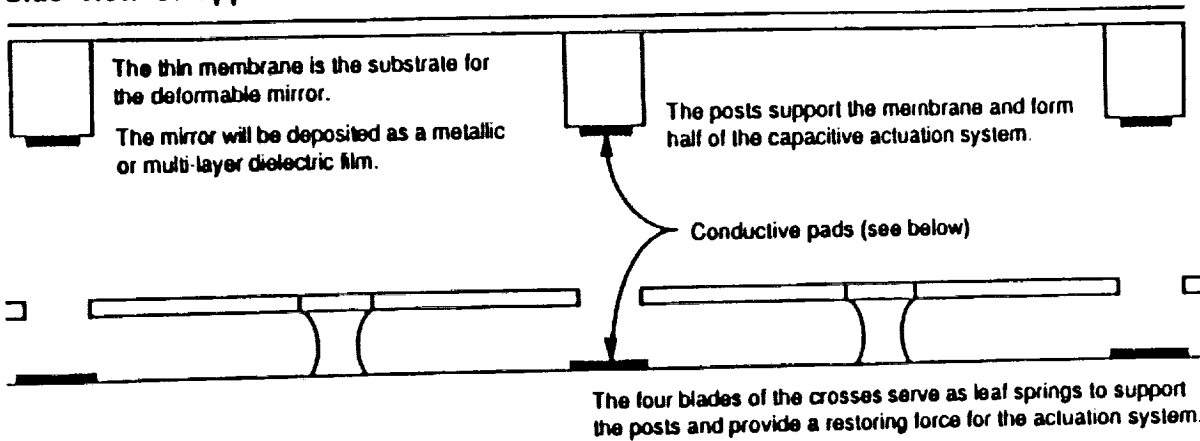
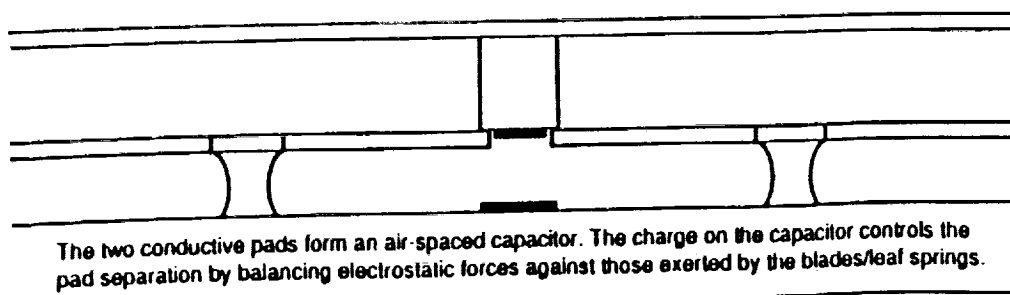


Figure 8. Micromachined Deformable Mirror

Side view of upper wafer



Side view of the lower wafer



Side view of the mirror assembly

Figure 9. Micromachined Deformable Mirror

3.5 Six-Degree of Freedom Micro-Inertial Measurement Unit

The IMU is composed of three orthogonal micro-gyros (micromachined devices integrated with VLSI sensor electronics), and three orthogonal micro-accelerometers with integrated sensor electronics. The sensor array mountings and 3-D packaging will be defined as part of the basic technology development effort. Functionally, the IMU will contain the necessary power and signal interfaces, conditioning electronics, the gyro and accelerometer capture loops, and any required local circuits for bias correction or temperature sensitivity compensation. The sensor outputs to the attitude determination and control, trajectory correction, and navigation functions of the micro-spacecraft or micro-rover will be delta (incremental) attitude angle and delta velocity in each axis with resolution dependent on the quantization achievable in the sensor capture loops.

3.5.1 Micromachined Vibratory Gyroscopes

Vibratory gyros are based on Coriolis-force-induced coupling between two modes of a two-dimensional mechanical oscillator. This basic principle has been extended to other two-dimensional mechanical oscillators to obtain gyros of greater utility than the elegant but unwieldy Foucault Pendulum. In particular, gyros have been based on tuning forks as well as vibrating strings, triangular and rectangular bars, cylinders and hemispheres. The performance capabilities of some of these gyros can be quite impressive. Hemispherical resonator gyro development has achieved navigational-grade performance: bias stabilities of 0.005 degree/hr, angular random walk levels of 6×10^{-5} degrees/square root hr, scale factor stability of 0.02 ppm, and readout noise of 0.02 arcsec.

Precise electron beam lithography and silicon micromachining capabilities, combined with high resolution interferometric displacement measuring techniques, suggest a new variation on the vibratory gyro theme. A micro-machined, vibrating silicon beam would serve as a rate-integrating vibratory gyro; readout of the integrated rotation angle would be performed by two orthogonal interferometric displacement measuring systems. The latter would be based on solid state lasers and fiber-optic/integrated-optics technology, and could be integrated with the vibrating beam into a very small package. Despite the gyro's small size and relatively simple design, impressive performance capabilities appear to be attainable: interferometric metrology systems are capable of measuring vibration amplitudes with precision on the order of 1 fm/square root Hz. Thus, given an overall vibration amplitude as small as 1 μm , the gyro would, in principle, be capable of nanoradian angular resolution at 1-Hz update rates.

Given the nature of the individual components, the gyros should also be relatively inexpensive, readily testable and highly reliable. The availability of unusually small, reliable and inexpensive navigational-grade gyros will have a profound impact on guidance and control applications. Inertial guidance systems will find entirely new uses in systems ranging from planetary microrovers to stabilized video cameras. Traditional gyro applications will enjoy the direct benefits of reduced mass, power, volume, and cost, and will further exploit these reductions to realize improved reliability and simplified environmental control requirements.

3.5.2 Micromachined Accelerometers

The designs for micro-miniaturized transducers have differed radically from scaled down versions of conventional sensors. The laws of scaling of the various physical phenomena have become critically important. For example, the scaling laws favor electrostatics over electromagnetics as the dimensions of a structure are reduced. In addition, the sensitivity of conventional sensors typically degrades with spatial reduction, and theoretical limits to transducer sensitivity impose practical constraints. The development of new transducers which scale favorably as the dimensions of the

structure are miniaturized can allow substantial improvements over the performance of conventional technology.

At JPL's Center for Space Microelectronics Technology a breakthrough device has been designed and constructed -- an Electron Tunnel Motion Sensor with a currently measured noise floor of $1.0 \text{ E}^{-8} \text{ g}$ and near term capability of a nano-g¹⁶.

This novel motion sensor takes advantage of the mechanical properties of micromachined silicon. For the first time, electrostatic forces are used to control the tunnel electrode separation, thereby avoiding the thermal drift and noise problems associated with all other tunneling devices which use piezoelectric control of the electrodes. The electrostatic forces induce deflection of a micromachined silicon cantilever spring with an integral tip electrode. For a typical construction, the tunneling current varies by an order of magnitude for each Angstrom change in electrode separation. Since tunneling only occurs in regions where the electrode tip is within several Angstroms of the other surface, the active area of the device is microscopic and relatively immune to radiation and charged particle environments common to space missions.

3.6 Embedded Health Monitoring for Electromechanical Effectors

Many spacecraft effectors, particularly rotating and scanning equipment, experience gradual bearing degradation rather than sudden catastrophic failure. For example, bearing wear can be due to micro-fatigue, contamination, hermetic seal leakage, lubricant chemical breakdown or thermal gradient driven migration, retainer whirl instability, and bearing resonances tuned to certain shaft rotation speeds or structural vibration modes. The torque noise produced by these phenomena is often a limiting condition on the jitter level of the spacecraft and its instrument-pointing-system precision.

There is a need for real-time methods to monitor and analyze the effector torque signature, vibrations of the bearings and structures, internal pressures and molecular by-products of chemical decomposition, temperature gradients, and motor current signatures to obtain an important advance in space system reliability and maintainability.

At present, health monitoring of these critical effectors (they are often not a block redundant resource) relies mainly on the download of telemetry reports. Often the only way the flight controllers have of detecting degraded performance of an effector is the indirect cause/effect behavior of the vehicle dynamics as measured by an attitude sensor or smear in a reconstructed imaging sequence. While telemetry may include data on temperature and motor current, these data are used in after-the-fact analysis and do little to predict the onset of poor health. The health-monitoring system would detect, identify cause, and select corrective actions for the spacecraft fault management system, whether located onboard or in the ground control center.

Important considerations in the design and implementation of a health monitoring system are that it should be embedded but non-intrusive, not draw significant power, not interfere with the primary function of the device being monitored, not impose significant mass and space penalties, and be highly reliable. We therefore see the direct compatibility of micromachined sensor technology with the practical constraints of an onboard health-monitoring system design.

3.6.1 Health-Monitoring Architecture

An architecture of embedded microsensors for health monitoring in the space environment will take advantage of integrated electronics to provide information not previously available to spacecraft operations. For example, monitoring of device parameters is available only at a very low

bandwidth because of telemetry constraints, and monitoring bearing noise becomes impossible because of the bandwidth limitation. If processing of higher frequency data could be done on the spacecraft with a DSP chip designed for the particular application, the processed data could then be passed to the ground at the slower rate.

The case of health monitoring in a reaction wheel, depicted in Figure 10, is a particularly good example because the primary mode of performance degradation is bearing wear. The emphasis here is on designing the health monitoring by using existing bearing modeling and analysis techniques, while taking full advantage of microsensor and integrated electronics technology.

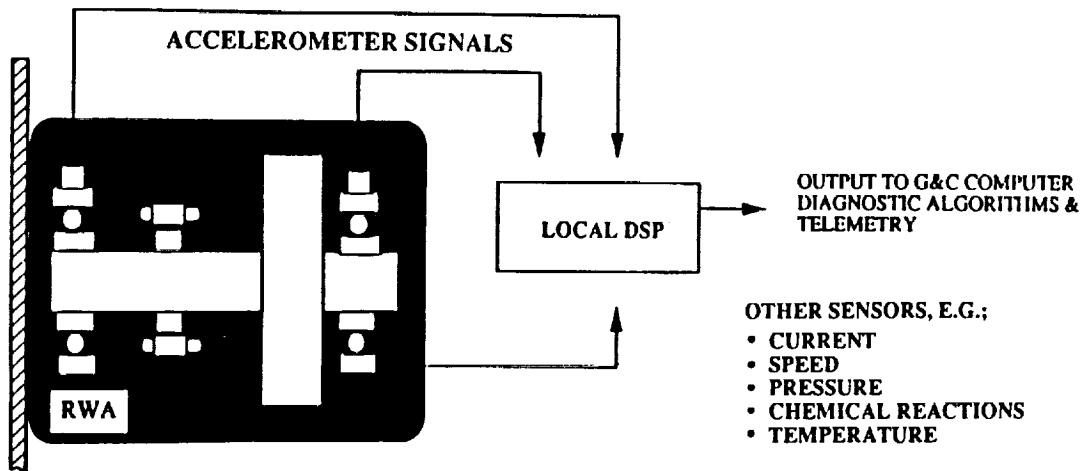


Figure 10. Reaction Wheel Health Monitoring

4. CONCLUSIONS

This paper has presented an advocacy for the development of micro-GN&C that would involve contributions and coordinated activities of NASA, industry, and academia. An approach has been described for the utilization of new microengineering technologies to achieve major reductions in GN&C mass, size, power, and costs to meet the needs of future space systems. New GN&C system capabilities were shown to arise from component innovations that involve the synergistic use of microminiature sensors and actuators, microelectronics, and fiber optics. Micro-GN&C system and component concepts were defined that include micro-actuated adaptive optics, micromachined inertial sensors, fiber-optic data nets with light-power transmission, and VLSI microcomputers. The thesis is advanced that these micro-miniaturization products are capable of having a revolutionary impact on space missions and systems, and that GN&C is the pathfinder micro-technology application that can bring that about.

5. ACKNOWLEDGEMENTS

We wish to gratefully acknowledge the technical contributions of the following people at JPL: Asif Ahmed, Randy Bartman, Louise Jandura, Paula Grunthner, William Kaiser, Tom Kenny, Edward Litt, Robert Nixon, Robert Schober, Sam Sirlin, and Eldred Tubbs.

This work was performed at the Jet Propulsion Laboratory, California Institute of Technology, under contract with the National Aeronautics and Space Administration.

6. REFERENCES

1. IEEE Micro-Robots and Teleoperators Workshop (1987): Proceedings, Hyannis, MA, 11/9-11, IEEE Publication 87T0204-8.
2. IEEE Solid State Sensors and Actuators Workshop (1988): Technical Digest, Hilton Head Is., SC, 6/6-9, IEEE Publication 88TH0215-4.
3. R. H. Price, J. E. Wood, S. C. Jacobsen, "Modelling Considerations for Electrostatic Forces in Electrostatic Microactuators," *Sensors and Actuators*, 20 (1989), 107-114.
4. "IC Fabrication Techniques Sculpt Silicon Sensors," *Electronic Design*, October 1989, 39-46.
5. *Sensors and Actuators*, Vol. 20, nos. 1 & 2, 11/15/89.
6. *Sensors and Actuators*, Vol. 20, no. 3, 12/1/89.
7. *Sensors and Actuators*, Vol. A23, nos. 1-3, 4/1/90.
8. "Micro-Machines," *Research and Development*, Vol. 32, no. 12, 12/1990, 36-40.
9. "Semiconductor Sensors and Microstructures in Automotive Applications," *Sensors*, Vol. 8, no. 3, 3/1991, 23-31.
10. "Micromachined Sensors for Automotive Applications," *Sensors*, Vol. 8, no. 9, 9/1991, 54-63.
11. "New Developments in Chemical/Gas Sensing, Part II: Other Technologies," *Sensors*, Vol. 9, no. 1, 1/1992, 34-39.
12. "An Integrated Capacitance Based Pressure Sensor," *Sensors*, Vol. 9, no. 2, 2/1992, 34-35.
13. Analog Devices Corporation, Norwood, MA; and *Computer Design*, November 1991, 42-45.
14. Varian Associates, Palo Alto, CA; and *Electronic Products*, 1/1991, 26-27.
15. Photonic Power Systems, Inc., Palo Alto, CA.
16. T.W. Kenny, S.B. Waltman, J.K. Reynolds, W.J. Kaiser, "Micromachined Silicon Tunnel Sensor for Motion Detection," *Journal Applied Physics Letters*, Vol. 58, January 1991, 100-102.

Micro-Opto-Mechanical Devices and Systems Using Epitaxial Lift Off

C. Camperi-Ginestet, Young W. Kim, S. Wilkinson, M. Allen and N. M. Jokerst
School of Electrical Engineering
Microelectronics Research Center
Georgia Institute of Technology
Atlanta, GA 30332-0250

Introduction

The integration of high quality, single crystal thin film gallium arsenide (GaAs) and indium phosphide (InP) based photonic and electronic materials and devices with host microstructures fabricated from materials such as silicon (Si), glass, and polymers will enable the fabrication of the next generation of micro-opto-mechanical systems (MOMS) and optoelectronic integrated circuits. Thin film semiconductor devices deposited onto arbitrary host substrates and structures create hybrid (more than one material) near-monolithic integrated systems which can be interconnected electrically using standard inexpensive microfabrication techniques such as vacuum metallization and photolithography. These integrated systems take advantage of the optical and electronic properties of compound semiconductor devices while still using host substrate materials such as silicon, polysilicon, glass and polymers in the microstructures. This type of materials optimization for specific tasks creates higher performance systems than those systems which must use trade-offs in device performance to integrate all of the function in a single material system. The low weight of these thin film devices also makes them attractive for integration with micromechanical devices which may have difficulty supporting and translating the full weight of a standard device. These thin film devices and integrated systems will be attractive for applications, however, only when the development of low cost, high yield fabrication and integration techniques makes their use economically feasible. In this paper, we discuss methods for the alignment, selective deposition, and interconnection of thin film epitaxial GaAs and InP based devices onto host substrates and host microstructures.

In integrated systems, it is often advantageous to utilize a variety of materials, each suited to a particular purpose. Compound semiconductors are useful for optical and optoelectronic devices, and silicon, polysilicon, glass, metals and polymers have been widely investigated for microstructure and microelectronic systems. High quality compound semiconductor devices, particularly those suited for optoelectronic applications, are generally grown lattice matched or near lattice matched. For the integration of GaAs onto single crystal Si, heteroepitaxial growth has been intensively investigated [1]. However, the crystal quality of this material is often insufficient for many optical applications. To integrate compound semiconductor devices with host materials which have no periodicity, however, such as polysilicon, glass, metals and polymers, the compound semiconductor cannot be grown directly upon such a host. In many cases, the substrate which is used as a nucleation seed for lattice matched growth is not essential to the performance of the epitaxial device. In fact, some device structures can be significantly improved upon if the growth substrate is removed from the lattice matched epitaxial device layers. These thin film epitaxial devices are light weight and the device designer has access to both sides of the epilayer, uninhibited by the substrate.

Bellcore first reported the separation of epitaxial layers from the lattice matched growth substrate using selective etches, and named the process epitaxial liftoff (ELO) [2]. A thin aluminum arsenide (AlAs) sacrificial layer is grown lattice matched onto a GaAs substrate, and GaAs device epilayers of interest are grown on top of this AlAs layer. The GaAs lattice matched epilayers are separated from the growth substrate by selectively etching the AlAs sacrificial layer. These epilayers are then mounted onto a variety of smooth substrates and this sheet of material is subsequently etched to define individual devices. This ELO material is very high quality [2]; devices tested before and after ELO show no degradation in device performance. These materials are currently being used for the integration of GaAs materials onto host substrates such as Si, glass, lithium niobate, and polymers [2-5].

Although the Bellcore technique yields high quality material, it has several problems, including the inability to align and selectively deposit the thin film devices, smoothness constraints on the host substrate, and difficulties in contacting both sides of the patterned device. In this paper, we report two modified ELO techniques which enable the alignment and selective deposition of a device or array of devices onto a host structure, and also allows the devices to be processed on both the top and bottom of the epitaxial sample while under support. The smoothness constraints on the host substrate are also relaxed since the devices are deposited individually or as an array and not, in contrast to the Bellcore process, as a continuous sheet of material. This alignment and selective deposition also places the relatively expensive compound semiconductor GaAs and InP based devices only where needed, thereby producing an inexpensive integrated system. The thin film epitaxial devices and the host structures can be independently optimized and tested, leading to high performance and high yield. This technique also enables the formation of large scale, repairable arrays of devices as well as the integration of thin film compound semiconductor devices with microstructures.

Integration Process Technology

In the first of the two Georgia Tech ELO techniques, the GaAs and InP based device layers (Figure 1a) are defined on the growth substrate using mesa etch processing (Figure 1b). Processing steps such as contact definition can also occur on these mesa defined devices either before or after the mesa etch (Figure 1c). These devices are then coated with Apiezon W (Figure 1d) and, for the GaAs based devices, are exposed to a standard HF:H₂O (1:10) etch solution to separate the epitaxial devices from the growth substrate (Figure 1e). High Al composition layers can be included in the ELO devices, since these layers are protected from the ELO etch solution. The array of mesa defined epitaxial devices is embedded in the surface of the Apiezon W carrier, which is approximately 100 μm thick and can be easily handled. At this point it is not possible to align these ELO devices with respect to features on a host substrate since the Apiezon W is opaque.

To overcome this difficulty, the ELO devices are VDW bonded to a transparent polyimide diaphragm which serves as an alignment and selective deposition transport for the ELO devices (Figure 1f). The polyimide diaphragm is fabricated using standard micromachining techniques. Silicon wafers are coated with approximately 4 μm of polyimide, which is spin-cast from a commercially available polyamic acid solution (DuPont PI-2611), baked at 150 °C in air for 30 minutes, and cured at 400 °C in nitrogen for one hour. The central portion of the wafer is then etched from the backside using a single sided etching technique [9] and 6:1:1 HF:HNO₃:H₂O as the etchant to form a polyimide diaphragm

approximately 4 μm thick and ranging from 3 mm to 25 mm in diameter, supported by a silicon 'ring' at its perimeter. The diaphragm fabricated in this manner is transparent, taut, and mechanically tough, and is ideal as a carrier for the liftoff layers. Mylar transparent diaphragms have also been used at Georgia Tech for this process. The ELO devices on the Apiezon W carrier are then brought into contact with the polyimide, and through VDW bonding, the ELO devices are attached to the polyimide (Figure 1f). The Apiezon W is dissolved with trichloroethylene, leaving the ELO devices bonded to the top of the polyimide. Note that the pre-liftoff processing (for example, contacts) applied to these devices now lies on the top of the ELO devices supported by the polyimide diaphragm. The devices can now be aligned through the transparent diaphragm and selectively deposited to the host structure as shown in Figure 1g.

The second Georgia Tech ELO process utilizes a spun on film of transparent polyimide (DuPont PI-2611) as the handling layer instead of the opaque Apiezon W. The epitaxial devices are mesa etched, the polyimide is spun on, a support ring is placed upon the polyimide before curing, and the polyimide is cured to form the protective handling layer. This assembly is then placed in the HF etch solution to release the epitaxial device. The devices can now be aligned and selectively deposited onto the host structure.

An etch as highly selective etch as that which enables the ELO process in GaAs-based compounds has not yet been identified for InP based compounds. We have demonstrated the formation of thin film epitaxial devices in InP based compounds, namely, InP, InGaAs and InGaAsP, using a slightly different etching sequence. This technique uses a single or a pair of selective etches and etch stop layers to dissolve the substrate, leaving behind the epitaxial layers of interest. An InGaAsP (bandgap of 0.95 eV) etch stop layer is grown lattice matched onto the InP substrate. The epitaxial devices are mesa etched, the handling layer is applied, and the assembly is placed into the HCl etch solution, which selectively etches the InP. The stop etch InGaAsP is subsequently removed with $\text{H}_2\text{SO}_4:\text{H}_2\text{O}_2:\text{H}_2\text{O}$ (1:1:1) if this layer is not part of the functional epitaxial device. The alignment and deposition of these InP based devices then proceeds identically to the GaAs based devices.

Results

Figure 2 is a photomicrograph of InP/InGaAsP/InP pin double heterostructure detectors mounted on a polyimide transfer diaphragm in a top view with illumination through the transparent diaphragm. The dark squares are the thin film devices on the diaphragm. This transparent diaphragm enables the user to align the ELO devices with respect to the host substrate prior to deposition. Current alignment and deposition capability is to within 1 μm . After deposition, the uncontacted side of the ELO devices faces up, and conventional photolithographic and processing techniques can be used to apply contacts to this side of the devices. This process sequence is important, as we have noted some difficulty with processing steps such as contact deposition if these thin ELO samples are not supported by a substrate during deposition.

Since the ELO devices are on the order of 2-3 microns thick, the surface profile of the devices on the host substrate is nearly monolithic, and conventional processing techniques can be used to electrically connect the devices to the host substrate. Figure 3 shows a photomicrograph of a GaAs/GaAlAs light emitting diode (LED) structure which has been mesa etched, preprocessed, lifted off, transferred, deposited onto Si and post processed using

the Georgia Tech ELO technique. This LED structure was patterned into mesas and ohmic contact was deposited while the ELO sample was still on the growth substrate. After lift off and adhesion to the polyimide diaphragm, the devices were adhered to a Si host substrate which had previously been coated with Au. The n-type material, now available on the top of the device, then had an ohmic contact deposited onto it, and a window was opened in the contact using photolithography. The contact was rapid thermal annealed, which also bonded the bottom contact to the Au on the Si host substrate for enhanced adhesion of the ELO device to the host substrate. Figure 3 shows this device emitting infrared light under forward bias, illustrating the successful liftoff, transfer, and electrical contacting of this device.

The alignment and deposition of single thin film devices or arrays of devices can be performed using the Georgia Tech ELO process. To form large (wafer scale) arrays of devices, subarrays of devices can be aligned and deposited to form larger arrays. This eliminates the need for wafer-scale growth uniformity of devices for wafer-scale integration. Figure 4 shows a 4 X 4 array of InP/InGaAsP/InP pin detectors which have been deposited onto gold pads which lie on Si.

For high yield in integrated systems, the ability to repair devices is of paramount importance. The lower right hand element shown in the array in Figure 4 was slightly offset due to a particule which was included during deposition. This defective device was removed, and a new device was aligned and selectively deposited onto that bare pad, as shown in Figure 5. Thus the demonstrated integration technology allows the replacement of defective devices.

Micro-Opto-Mechanical Systems

For applications from sensors to packaging, the combination of optoelectronic devices and microstructures is extremely attractive. The integration tools described herein will prove to be particularly usefully for the integration of micromechanical structures with thin film GaAs and InP based devices to form micro-opto-mechanical systems (MOMS). The integration of high quality single crystal semiconductor optical devices such as emitters, detectors and modulators directly on top of or into moving microsensors and microactuators is currently limited by the heavy weight and/or large thicknesses of the optical devices. The elimination of the substrate material decreases the weight and thickness of the optical device, thus making them ideal for integration with micromachines. The deposition of these thin film devices results in the monolithic integration of these devices, so standard microfabrication processes are used to connect the devices to the micromechanical device and to adjacent control circuitry. This use of standard processing for interconnect produces high reliability, low cost, manufacturable integrated MOMS.

To demonstrate the utility and manufacturability of MOMS, we are developing the MOMS technology through a variety of test vehicles, including an accelerometer and a fiber optic automated alignment package. Both of these designs are based upon micromachined movable platforms coupled with thin film semiconductor optoelectronic devices. The accelerometer is a self-contained optical Fabry-Perot interferometric acceleration sensor. The thin film optical emitter is integrated directly onto an optically transparent movable platform which responds to acceleration by changing its Fabry-Perot cavity spacing. The highly sensitive interferometric output of this device is detected by an optical sensor integrated in the surface of the silicon underneath the movable platform. Due to the ability to sense small deflections interferometrically, the platform structure can be made very stiff, potentially allowing sensing

bandwidth on the order of 1 MHz. The dynamic range is tuned through the initial position of the platform, which determines the tuning point on the Fabry-Perot curve, thereby setting the platform movement necessary to produce an output.

The fiber optic positioner utilizes a micromachined movable platform to position an emitter or detector with respect to an optical fiber. One such micromachined platform fabricated at Georgia Tech, shown in Figure 6, has the capability to move in three dimensions, thereby aligning the emitter, detector or modulator with respect to the fiber. We have begun our MOMS integration by aligning and depositing a GaAs/GaAlAs double heterostructure detector onto a micromachined platform, shown in Figure 7. An added advantage of this system is the fact that the feedback signal from the fiber to the platform can be processed using circuitry integrated into the silicon substrate upon which the platform is fabricated. This type of inexpensive, automated alignment of optical components with fibers may significantly reduce the packaging cost of optoelectronic components which are fiber coupled.

Conclusions

The integration of high quality thin film GaAs and InP based optoelectronic devices with micromechanical structures expands the functional operation of micromechanical integrated systems into the realm of optical applications, which includes sensors and packaging for photonic interconnect such as optical fibers. Epitaxial lift off processes which utilize a transparent polyimide diaphragm have been developed to realize the alignable, selective deposition of epitaxial GaAs and InP based lift off material onto host structures comprised of materials such as Si, glass, and polymers. This transparent diaphragm can be used to align and selectively deposit the thin film GaAs and InP based devices as individual devices from the array or as an entire array onto the host substrate. The use of the polyimide transfer diaphragm also allows both the bottom and the top of the device to be processed while under substrate support. These thin film devices can be removed if they are defective, and replaced with aligned and deposited replacement devices. This low cost integration technology, which produces thin, light weight devices, is being coupled with micromechanical structures. These micro-opto-mechanical systems will introduce optical functions into microstructures, thereby addressing applications needs from sensors to low cost packaging.

Acknowledgements

The authors wish to acknowledge valuable technical discussions with Professor M. Brooke, S. Fike, B. Rashidian and C. Ahn of Georgia Tech. Financial support was provided by the Newport Corporation, Digital Equipment Corporation, and the National Science Foundation. Microfabrication was carried out in the Microelectronics Research Center of Georgia Tech with fabrication assistance from the staff.

Figure Captions

Figure 1. Georgia Tech epitaxial lift off process. (a) Starting substrate with grown layers; (b) after mesa etching; (c) after contacting; (d) after Apiezon W application; (e) after selective etch; (f) after adhesion to silicon supported polyimide diaphragm and removal of Apiezon W; (g) after selective deposition onto host substrate. Individual devices or the entire array can be aligned and deposited onto host substrates.

Fig 2: Photograph of an array of 250 μm x 250 μm x 4 μm thick InP/InGaAsP/InP double heterostructure lifted-off devices on a 6 μm thick mylar diaphragm. a) top illumination, b) bottom illumination (through the transparent diaphragm).

Figure 3. An epitaxial liftoff LED, emitting radiation, which has been selectively deposited from the polyimide diaphragm onto a Si host substrate.

Figure 4. Four by four array of InP/InGaAsP/InP pin detectors on Si.

Figure 5. Defective device from Figure 4 was removed and replaced with new device aligned and deposited.

Figure 6. Micromachined movable platform onto which a thin film optoelectronic device will be integrated.

Figure 7. GaAs/GaAlAs detector integrated onto a micromachined platform.

References

1. H. Choi, J. Mattia, G. Turner, and B.Y. Tsauer, *IEEE Electron Dev. Lett.*, 9, 512 (1988).
2. E. Yablonovitch, T. J. Gmitter, J. Harbison, and R. Bhat, *IEEE Phot. Tech. Lett.*, 1, 41 (1989).
3. A. O'Donnell, I. Pollentier, P. Demeester, P. Van Daele, and P. Carr, *Elec. Lett.*, 26, 1179 (1990).
4. E. Yablonovitch, T. J. Gmitter, J. P. Harbison, and R. Bhat, *Appl. Phys. Lett.*, 51, 2222 (1987).
5. W. Chan, A. Yi-Yan, and T. J. Gmitter, *IEEE J. Quant. Elec.*, 27, 717 (1991).
6. L. Buydens, P. De Dobbelaere, P. Demeester, I. Pollentier, and P. Van Daele, *Opt. Lett.*, 16, 916 (1991).
7. I. Pollentier, L. Buydens, P. Van Daele, P. Demeester, *IEEE Phot. Tech. Lett.*, 3, 115 (1991).
8. J. Y. Pan and S. D. Senturia, *Society of Plastics Engineers Technical Papers: ANTEC '91*, 37, 1618 (1991).
9. G. P. Anderson, S. J. Bennett and K. L DeVries, *Analysis and Testing of Adhesive Bonds*, Academic Press, 1977.

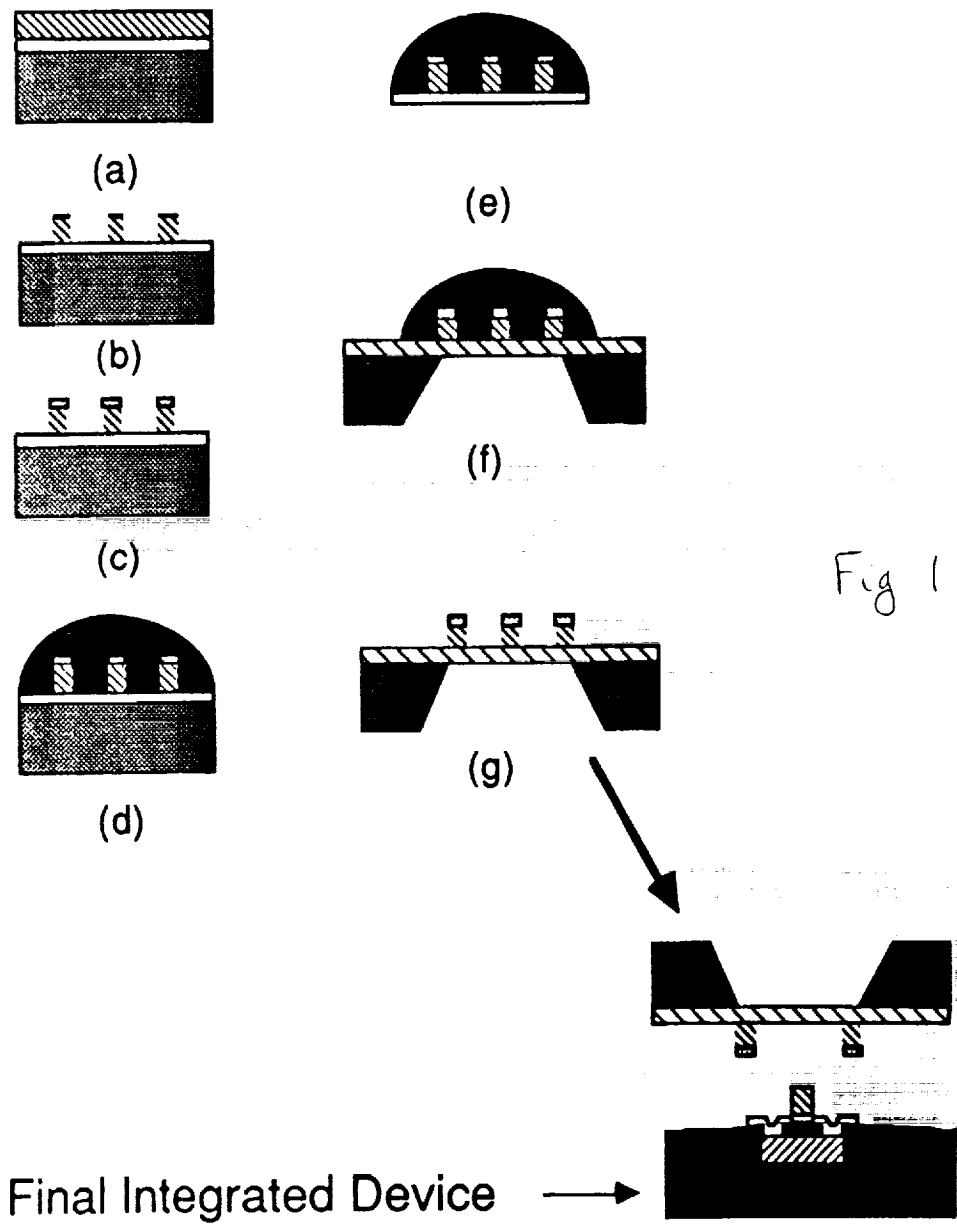


Fig 1

Fig. 1

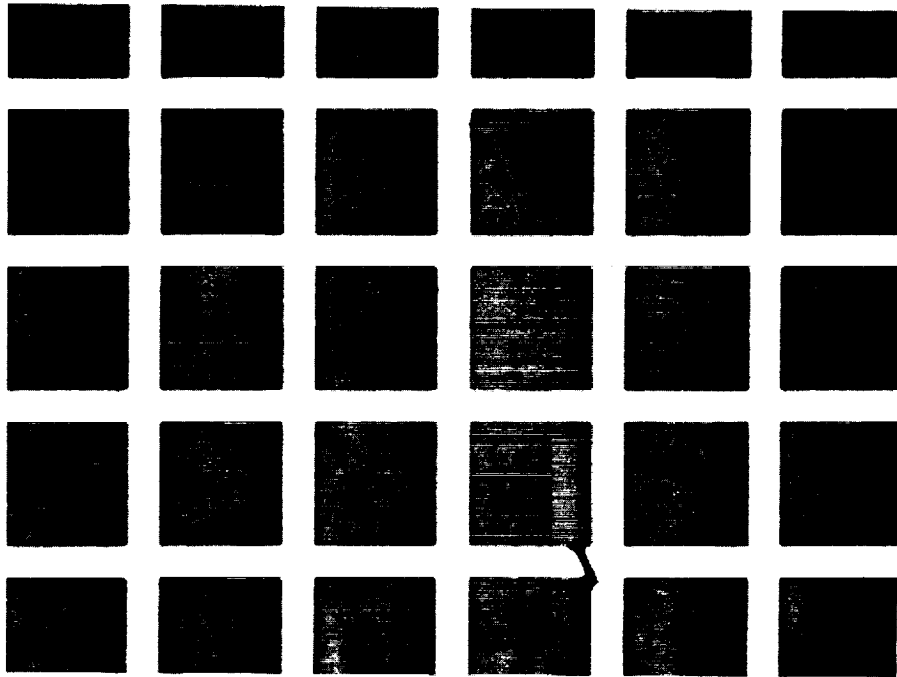


Fig. 2



Fig. 3

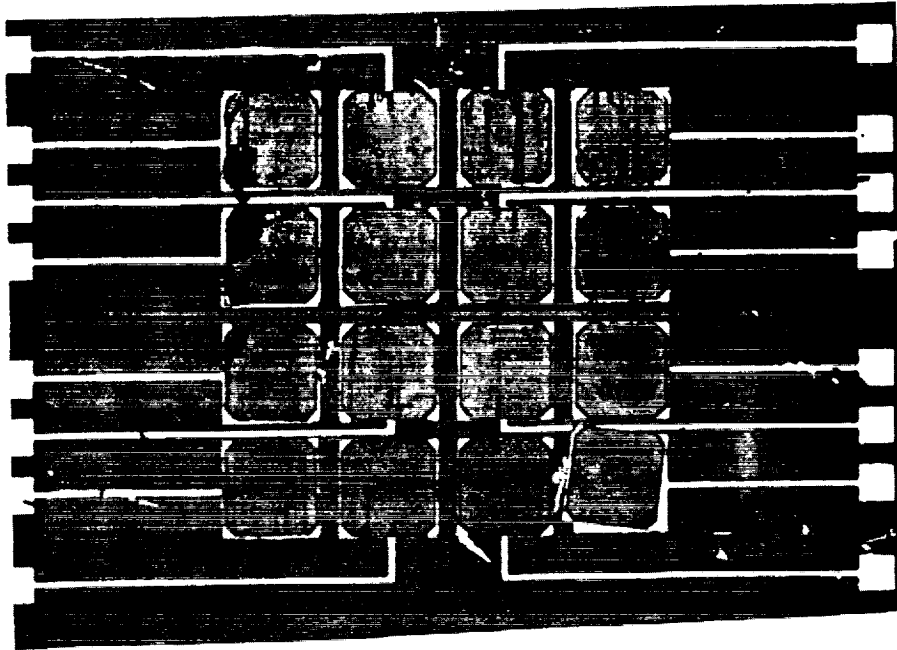


Fig 4

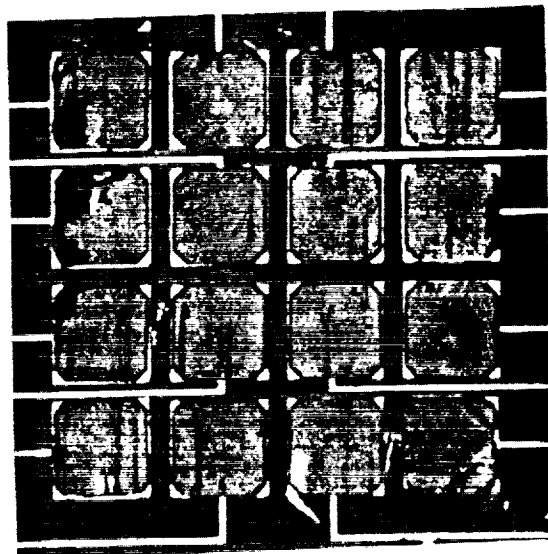


Fig 5.

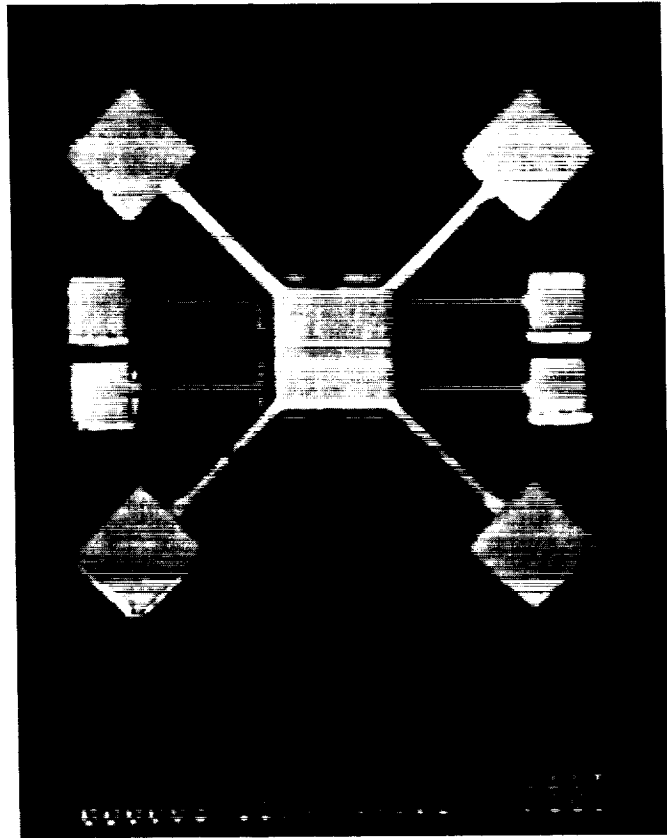


Fig. 6

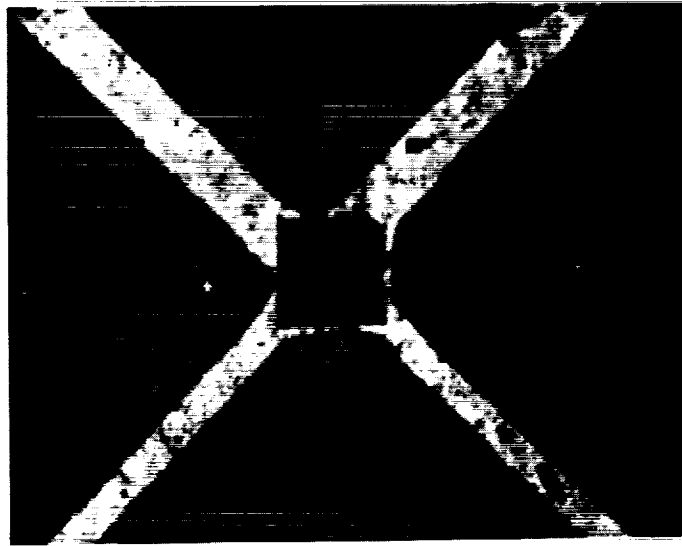


Fig 7

Miniature Wide Field-of-View Star Trackers for Spacecraft Attitude Sensing & Navigation

William McCarty, Senior Staff Engineer

Eric Curtis, Vice President, Technical Director

Anthony Hull, Vice President, Engineering

William Morgan, Business Development Manager,
Space and Science Programs

OCA Applied Optics, Inc.

7421 Oranewood Avenue

Garden Grove, CA 92642

714/895-1667

Abstract:

Introducing a family of miniature, wide field-of-view Star Trackers for low cost, high performance spacecraft attitude determination and navigation applications. These devices, derivative of the WFOV Star Tracker Camera developed cooperatively by OCA Applied Optics and the Lawrence Livermore National Laboratory for the Brilliant Pebbles program, offer a suite of options addressing a wide range of spacecraft attitude measurement and control requirements. These novel sensors employ much wider fields than are customary (ranging between 20 and 60 degrees) to assure enough bright stars for quick and accurate attitude determinations without long integration intervals. The key benefits of this approach are light weight, low power, reduced data processing loads and high information carrier rates for wide ACS bandwidths.

Devices described range from the proven OCA/LLNL WFOV Star Tracker Camera (a low-cost, space-qualified star-field imager utilizing the spacecraft's own computer for centroiding and position-finding), to a new autonomous subsystem design featuring dual-redundant cameras and completely self-contained star-field data processing with output quaternion solutions accurate to $100 \mu\text{rad}$, 3σ , for stand-alone applications.

Miniature Wide Field-of-View Star Trackers for Spacecraft Attitude Sensing & Navigation

William McCarty, Senior Staff Engineer

Eric Curtis, Vice President, Technical Director

Anthony Hull, Vice President, Engineering

William Morgan, Business Development Manager,
Space and Science Programs

OCA Applied Optics, Inc.

7421 Oranewood Avenue

Garden Grove, CA 92642

714/895-1667

1.0 LLNL/OCA STAR TRACKER CAMERA

The LLNL/OCA Star Tracker Camera was developed in support of the SDI Brilliant Pebbles (BP) program by the Lawrence Livermore National Laboratory and OCA. The BP Star Tracker Camera was designed to acquire star-field imagery from which spacecraft attitude information could be derived for navigation and to update and calibrate Inertial Measurement Unit (IMU) attitude data. The WFOV Star Tracker Camera is unusual in that it employs very wide field-of-view optics (nearly 60°), much greater than is customary for Star Trackers. This wide-field design evolved from trade-studies early in the BP program that showed this approach to be significantly more mass-efficient than traditional narrow field designs. Its advantage results from the unique balance the design achieves between FOV, aperture, focal plane sensitivity and the spatial distribution of bright stars in the sky. Prototypes of this new class of sensor weighing just a few hundred grams routinely achieve better than 200 microradian accuracy as reported recently by Lewis et al¹.

The generic WFOV Star Tracker Camera uses a 55° FOV concentric lens. The concentric design-form maximizes relative aperture and eliminates lateral color effects that can introduce stellar color temperature dependent centroid shifts. The focal surface in this design is spherical, requiring the use of a fiber-optic faceplate (FOFP) with a spherically curved front surface to flatten the field for interface to the CCD imaging device. This design approach delivers a fast optical system in a very compact, low mass package with a

relative aperture almost twice as large as flat-field design-forms of comparable performance.

Both intensified and unintensified versions of the WFOV Star Tracker Camera have been prototyped and tested. The intensified variants employ a gated, second-generation, proximity-focused image intensifier between the lens and the CCD to increase sensitivity enough to allow a corresponding decrease in integration time. This configuration assures full performance on vehicles with relatively high attitude drift rates by using its short integration time (typically, 30 to 50 msec) to avoid degradation from image smear. Unintensified versions are much lighter (weighing less than 130 grams) and achieve full performance on platforms with drift rates up to about $1^\circ/\text{hour}$ (where integration periods as long as 400 msec are practical). With current commercial focal plane readout noise levels as low as 40 to 60 electrons, unintensified cameras perform well with integration periods of about 100 msec. Advanced technology focal planes reduce that period considerably. In the presence of limiting background flux (where the net signal-to-noise ratio becomes background limited), the unintensified array will actually allow shorter integration times than an intensified camera because of its superior quantum efficiency and broader spectral bandwidth.

The basic Wide Field-of-view Star Tracker concept has several important advantages over traditional approaches. Key among them is that the probability of finding bright stars increases with the solid angle surveyed (FOV). Therefore, as field-of view increases, so too will the number of bright stars included within it. Further, since there are relatively few bright stars in the sky (less than 500 brighter than $M_v = 4$), a large FOV assures that only a small catalog of the very brightest need be considered for navigation. With such a small star map to manage, it is quite practical to use fast pattern-matching techniques to reliably determine the orientation of a spacecraft in near real-time.

With the focal plane stray light flux distributions anticipated in typical service, WFOV Star Tracker imagery ordinarily requires processing to subtract the average local background signal from each pixel. This is automatic where the signal amplitude distribution of a cluster of pixels is found to match the nominal blur energy distribution of an imaged point source (probable star). Star Tracker maximum stray light limits are imposed by either saturation effects (where the sum of signal and background fluxes exceed CCD well capacity or the dynamic range of subsequent signal electronics) or by the shot noise of the background. In the case of dim stars, shot noise limits the maximum background flux before saturation becomes a problem. Stray light analyses using the APART code indicate

maximum point source transmittance (PST) for a typical baffle is about 1×10^{-7} for all sun angles beyond the solar exclusion angle. For sun positions just approaching the solar exclusion angle, the exact magnitude of the stray light becomes a major factor in determining minimum integration times for both the intensified and unintensified sensors. Inside the solar exclusion angle, one or more optical surfaces will be directly illuminated by the sun and the stray light signal increases dramatically, overwhelming the dimmer stars.

The image processing algorithm identifies stars by evaluating the amplitude characteristics of candidate pixel clusters. The key discrimination criteria require that, 1), the peak pixel amplitude(s) remain below saturation (normally the case, except for the very brightest stars) and 2) that the character of the intensity profile of the pixel cluster match the expected point-spread function (PSF) of a normal image. Thus, a single, isolated pixel will not be identified as a star, even though it exhibits appropriate signal amplitude, because the amplitude of its neighboring pixels won't conform to the expected PSF intensity contour. It is important to note that the sub-pixel centroiding accuracy of the Star Tracker's image processing algorithms, nominally about 1/10 pixel, would not be possible if the star's blur diameter were not larger than a single pixel. The unique concentric optic of the WFOV Star Tracker Camera not only provides the proper image scale for optimum centroiding, but maintains essentially perfect scale uniformity across its full working format.

Once all of the potential star images within a data field have been located, the brightest are grouped into candidate star-triangles, iteratively compared against star catalog data and ultimately resolved into confirmed star-triangle matches. The algorithm typically uses a minimum of five star-triangle matches (requiring at least five detectable stars per data field) in order to establish the attitude of the sensor within prescribed error limits. The orientation of the Star Tracker's optical axis (and thus the spacecraft's attitude) is ultimately expressed as an output quaternion developed from the individual rotation quaternions for each of the star triangle matches in the ensemble (and in which any residual star position errors have been evenly distributed).

WFOV Star Trackers can reliably establish their orientation with only a relatively simple corrective term to standardize the position-finding algorithm for hardware variances. Just three quantities are needed for this correction; 1) the as-manufactured effective focal length, 2) static boresight position error and 3) the two-dimensional distortion characteristics of the basic optical design (each quantity being referenced to the origin of the focal plane coordinate system and expressed to an accuracy $\leq 3 \mu\text{m}$). No special measurement or

specific correlation of actual (individually measured) PSF variations across the field-of-view is needed to achieve nominal angular precision.

1.1 WFOV Star Tracker Optics Assy

The generic WFOV Star Tracker optic is a 3 element $f/1.26$ design yielding a 55 degree diagonal working field. The central, spherical (ball) element is of Schott SSK4 glass and the front and rear concentric shell elements are Ohara SLF02 and Schott LaF20, respectively. A fiber-optic faceplate provides the curved image surface to interface the spherical image front of the lens to the planar CCD array.

1.2 WFOV Star Tracker Focal Plane Electronics

The baseline focal plane detector device for the WFOV Star Tracker Camera is a Thomson-CSF TH7883 CCD array. The TH7883 is derived from the TH7863 array by transforming its storage zone into an imaging area, identical and adjacent to the original imaging zone, thereby doubling its active imaging area. The array is read out as a single field of 576 active lines with 384 active pixels per line. Pixels measure $23\ \mu\text{m}$ by $23\ \mu\text{m}$, yielding an active imaging area of 8.832 mm by 13.248 mm. The pixel instantaneous field-of-view (IFOV) is 1.3 milliradians, square. The array, with its surface-mount readout electronics, is packaged into a compact space-qualified focal plane assembly on a multi-layer flex-print circuit board. Power, control and digital video interfaces are implemented through a single miniature 50-pin connector.

2.0 OCA ADVANCED STAR TRACKER ASSEMBLY

OCA's Advanced Star Tracker Assembly (ASTA) is a new, completely self-contained, light-weight, high-performance star tracker system for space applications. The ASTA design has evolved from its WFOV Star Tracker origins in response to needs for a fully integrated star tracker system able to meet the demanding mass, power and performance goals of next-generation light-weight spacecraft. This new design capitalizes on the unique attributes of the LLNL/OCA Wide Field-of-view Star Tracker Camera, developed originally for the SDI Brilliant Pebbles program, and extends that heritage to realize a wholly self-contained attitude measurement system weighing less than 1.2 kg and nominally accurate to ± 100 microradians, 3σ .

2.1 System Overview

The OCA ASTA is based on dual-redundant CCD star cameras. The analog outputs of the camera's CCD arrays are digitized and uniformity corrected to better than 0.2% of full scale. System control and star image processing is implemented using a 32-bit MIPS R3000 compatible LSI Logic LR33000 microprocessor. The computer manages all internal functions including camera control, analog to digital conversion, pixel uniformity correction, sub-pixel star centroiding, housekeeping, BIT and communications to and from the spacecraft under the RS-422 communications protocol. Star identification and attitude solutions are implemented using Intelligent Decisions, Inc. "Stellar Compass" software. This code, developed for the LLNL Brilliant Pebbles program and proven on all BP test flights to date, has been specifically engineered for this new class of wide-field star tracker and is ideally suited to the task.

ASTA is configured around an orthogonally mounted pair of 23 degree FOV cameras. This narrower, flat-field optical design-form takes advantage of BP simulation and flight-test experience showing that the WFOV Star Tracker Camera's working field could be reduced without compromising performance. Early WFOV Star Tracker operational doctrine was very conservative in its baseline demand for 10 cataloged stars in any given field to assure that a minimum of 5 would be ultimately useful for attitude determination. In practice, PSF matching has turned out to be an excellent way to distinguish legitimate star images from other objects, artifacts and noise spikes. In fact, so fast and robust is this "star-finding" method that ASTA was designed with a significantly narrower field-of-view (now based on a minimum of 5 stars per field in the least well populated high galactic latitudes) and so benefits in three important ways:

- ASTA's flat-field, low distortion lens weighs less and also eliminates the cost, mass and additional complexity of a fiber-optic field flattener.
- Better than 90% optical transmission over its full working field
- Reduced probability of the sun's intrusion into the working field

Figure 2.1-1 illustrates OCA's Advanced Star Tracker Assembly. Prominently visible are the two, orthogonally oriented lens assemblies and (through the cut-away) a portion of the main circuit board inside the housing. Figure 2.1-2 presents a cross-sectional view of the ASTA in orthographic projection. The dual-redundant camera configuration is ASTA's most obvious physical feature. This configuration not only provides the basic redundancy

of two separate and complete cameras (independent optics, focal plane and analog video circuitry) but, more importantly, assures reliable high-accuracy attitude data irrespective of the spacecraft's orientation or rotational axis. If the sun should happen to intrude into one camera's field, attitude measurements may be conveniently made using the other camera rather than by re-orienting the spacecraft. Even more importantly, the dual-camera design avoids the potential for large errors resulting when the spacecraft's instantaneous axis of rotation lies near the optical axis of one of the cameras. This problem arises from the sharply increasing influence of residual star centroid errors on the output quaternion's roll component as the spacecraft's roll axis approaches the sensor's line-of-sight. In practice, ASTA's control software features can select the proper camera based on IMU attitude data from the spacecraft or will automatically switch to the alternate field if the roll axis is found to lie too close to the current sensor's optical axis.

The ASTA optics use the same 14 mm entrance pupil diameter (aperture) typical of the WFOV Camera but take advantage of improved net optical transmission (gained by eliminating the WFOV Star Camera's FOFD field flattener) and new low noise read-out electronics to extend its working range down to stars of $M_v = 5.1$ with normal integration periods of only 20 msec. This configuration still allows a conveniently small star catalog (1024 stars) to assure attitude updates at 33 msec intervals with completely deterministic data latency characteristics.

As an illustration of its robustness it is significant to note that ASTA is designed to deliver its specified performance under worst-case conditions but, in actual practice the statistical distribution of stars is such that it is only necessary to use stars fainter than $M_v = 4.5$ about 4% of the time and, normally, fully half of the stars will be brighter than $M_v = 3.6$.

ASTA optics are baffled externally by a single-stage multi-vane sun-shade with integral capping shutter. The shutter protects against the long-term build-up of scattering contaminants (and atomic oxygen erosion in LEO) and, when closed, provides an active diffuse radiometric calibration stimulus for in situ CCD gain normalization.

Stray light analyses reliably predict a sun equivalent PSNIT = 1×10^{-8} for these optics with the Sun at its closest working (exclusion) angle of 30 degrees. This allows sufficient margin to assure specified performance even with a realistic allowance for degradation due to space contamination build-up over time.

The 6 element, thin section optical design is based on generally available Schott radiation-tolerant (anti-browning) glasses.

2.2 Summary Specifications

| | | |
|-------------------------|-------------------------------------|---|
| Optics | Equivalent Focal Length: | 22 mm |
| | Entrance Pupil Diameter: | 14 mm |
| | Focal ratio: | $f/1.57$ |
| | PSF Energy Distribution: | ~70% central pixel, ~30 % adjacent eight pixels |
| | Ensquared Energy: | ≥ 60% everywhere within working field |
| | Field of View (FOV): | 23°, circular |
| | Instantaneous Field of View (IFOV): | ~1 mrad |
| | Spectral Range: | 500 - 1000 nm (full spectrum) |
| | Transmission: | ≥ 90% within working field (full spectrum) |
| | Image Format: | 8.84 mm, square |
| CCD | Imaging Device: | Thomson-CSF TH7883 CCD |
| | Quantum Efficiency: | ≥ 35% |
| | Pixel dimensions: | 23 μm, square |
| | Pixel arrangement: | 384 (V) x 384 (H) (usable pixels) |
| | Array dimensions: | 8.83 mm (V) x 8.83 mm (H) (usable area) |
| | Readout Noise: | ≤ 40 e ⁻ , 1σ, rms |
| | Integration Time: | variable, 20 msec nominal |
| Frame Rate: | 30 fps (max, full field) | |
| Image Processing | Data Latency: | Integration time dependent, fully deterministic |
| | Stellar Compass Processing Time: | 2 msec (quaternion computation) |
| | Attitude Accuracy: | ±100 μradians, 3σ, for drift rates ≤10°/min |
| | Video Quantization: | 9 bits effective (dim stars) |
| | Offset Uniformity: | Corrected to 0.2% full scale |
| | Gain Uniformity: | Corrected to 0.2% full scale |
| Power | Operating Voltages: | ±5.0, ±15.0, 28.0 ±6 VDC |
| | Nominal Operating Power: | 6.5 W (worst case peak) |
| | Shutter Actuation Power: | 2.2 W peak, 0.5 W holding |
| | Stand-by (idle) Mode: | 0.7 W |
| Mass | Optical Subassembly: | 89 g |
| | Electronics Subassembly: | 640 g |
| | Mechanical Subassembly: | 317 g |
| | STA, Total Mass: | 1,046 g |

¹Lewis, A.Ledebuhr, T.Axelrod, J.Kordas and R.Hills, "WFOV Star Tracker Camera, UCRL-JC-105345, proc. SPIE International Symposium on Optical Engineering & Photonics in Aerospace Sensing, Orlando, FL, April 1-5, 1991.

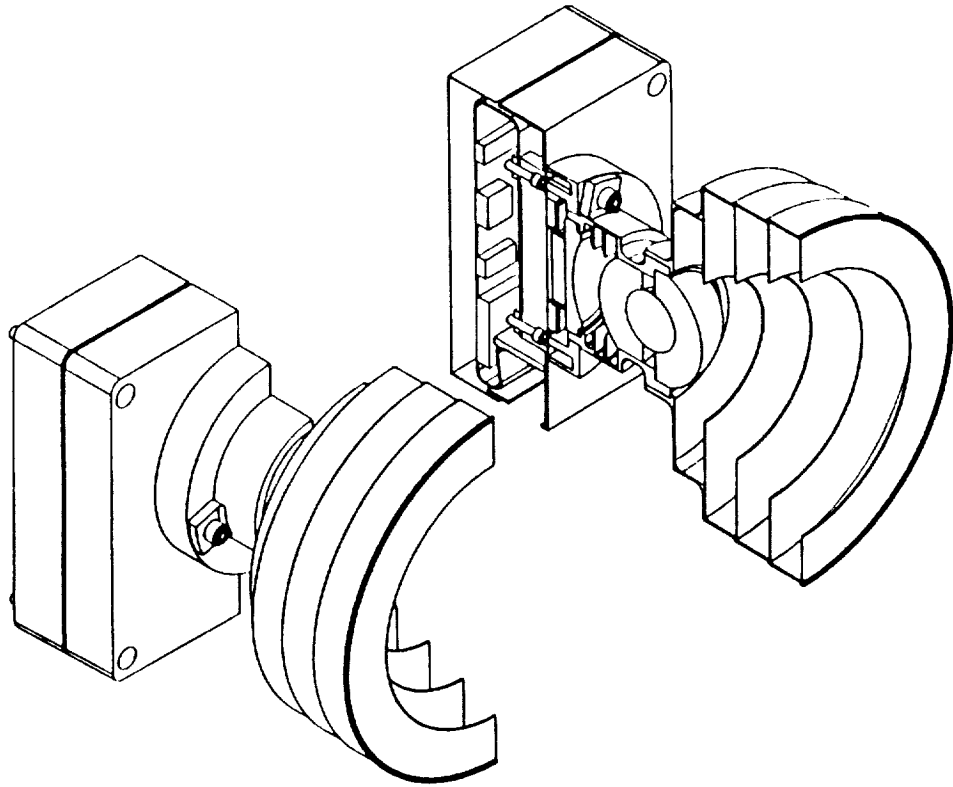


Figure 1.0-1 Cut-away view of the OCA/LLNL Wide Field-of-View Star Tracker Camera showing (in order, front to rear) the multi-vane baffle, WFOV concentric lens, fiber-optic field flattner, CCD and camera electronics.

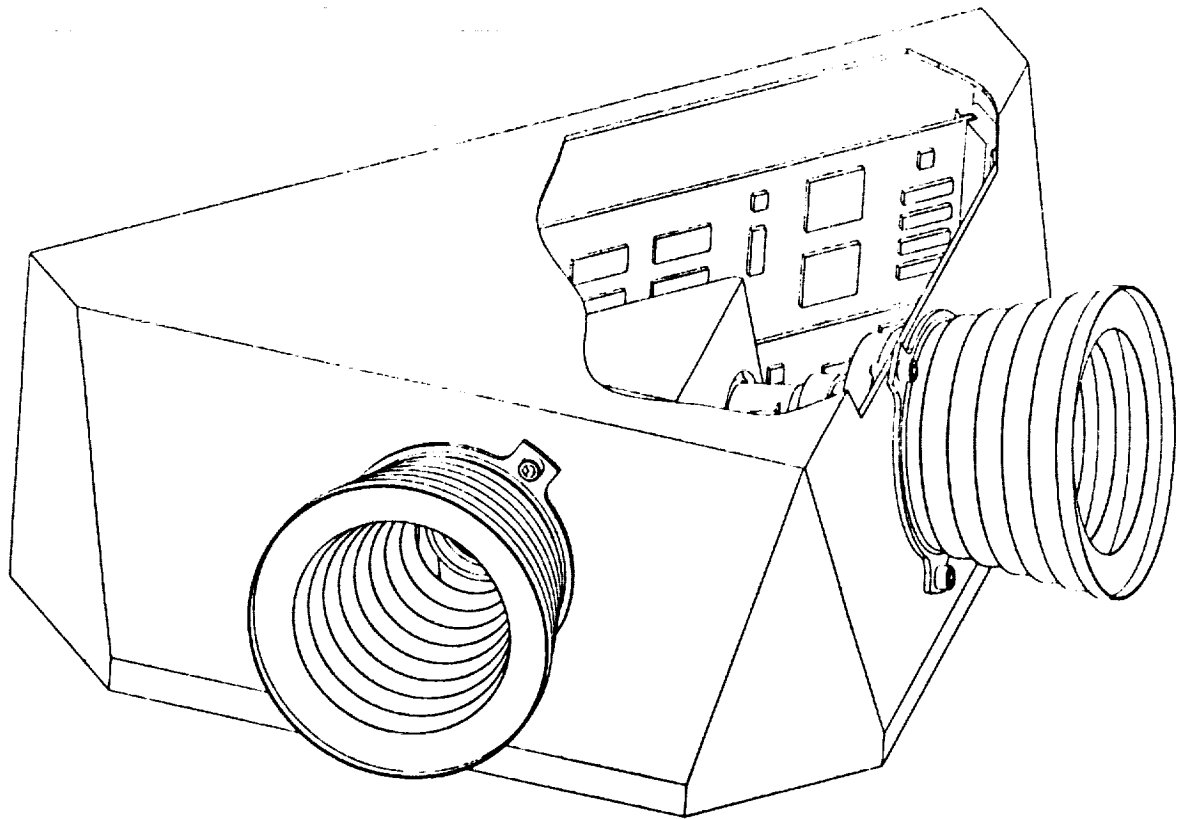


Figure 2.1-1 Cut-away view of the OCA Advanced Star Tracker Assembly (ASTA) illustrating the orthogonally oriented, dual-redundant cameras with optics and baffles.

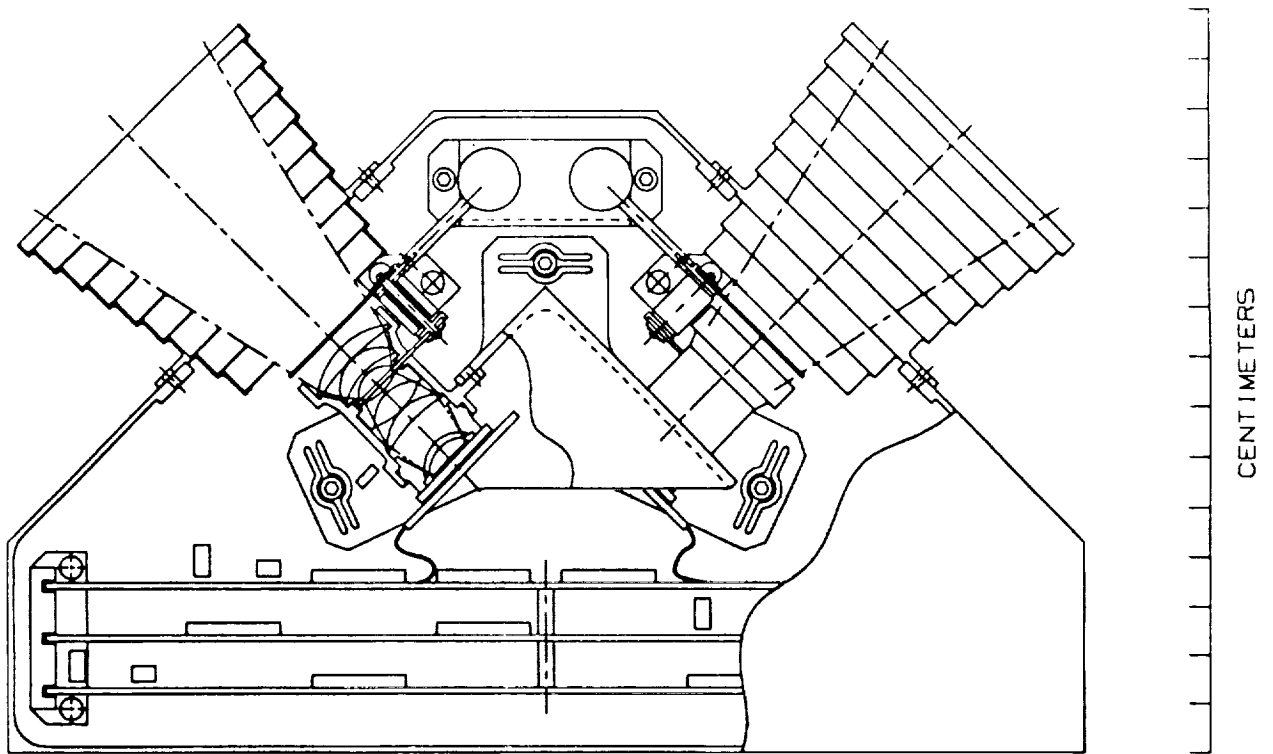


Figure 2.1-2 Cross-sectional orthographic projection of the OCA Advanced Star Tracker Assembly (ASTA) showing details of its 6-element, wide angle, flat-field lens with baffle and integral capping shutter.



NOVEL POSITION SENSOR TECHNOLOGIES
FOR
MICRO ACCELEROMETERS*

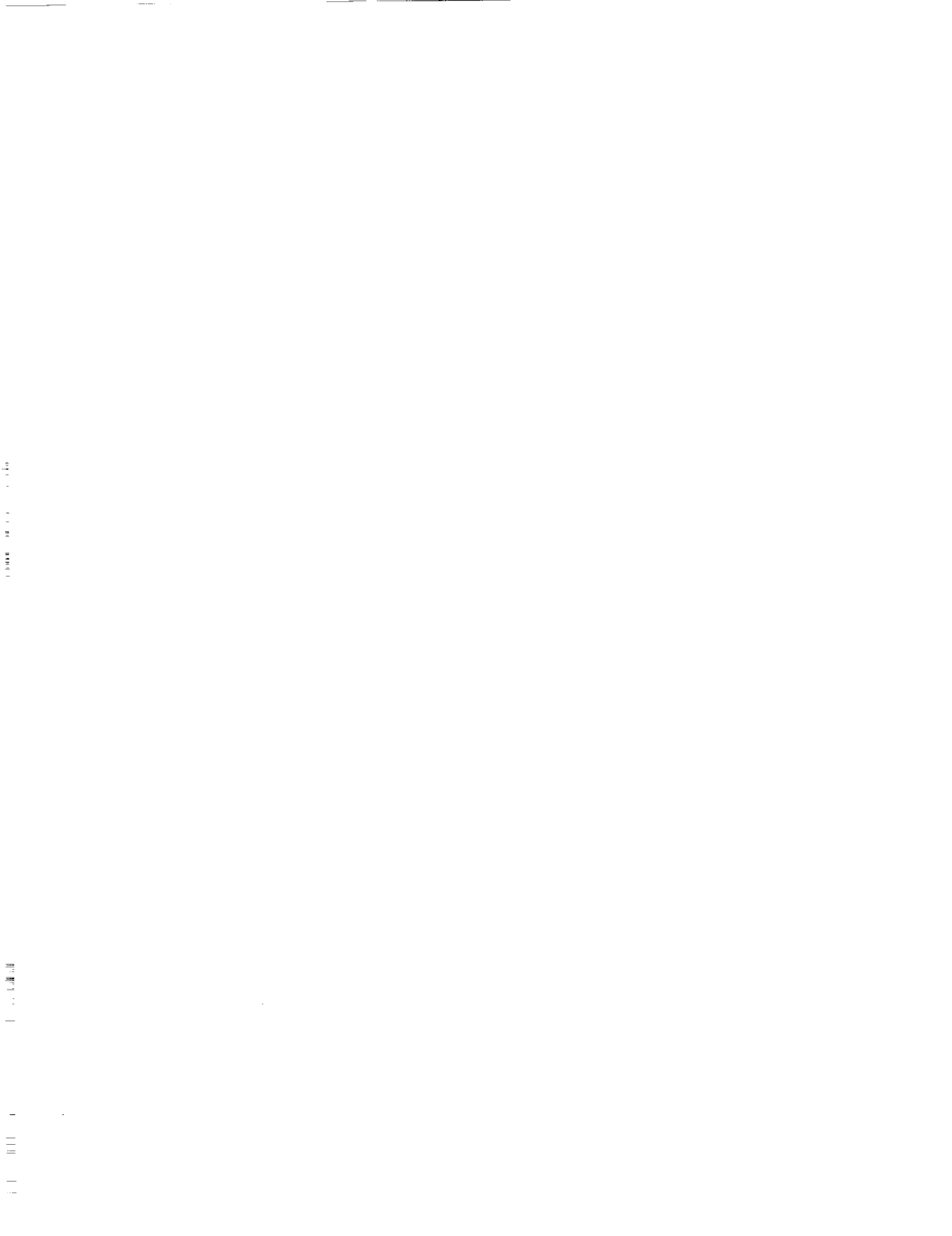
T. R. Van Zandt, T. W. Kenny, and W. J. Kaiser
Center for Space Microelectronics Technology
Jet Propulsion Laboratory, California Institute of Technology
Pasadena, California 91109

ABSTRACT

An important new approach for vehicle guidance and control is based on the use of compact, low-mass, low-cost sensors integrated with the vehicle structure. Many advantages of this approach lead to new capabilities. However, the development of compact guidance and control sensors leads to a variety of fundamental physical problems associated with sensor sensitivity and noise. For example, as sensor size is reduced, it becomes necessary to improve the sensitivity of the sensor signal detection mechanism. For an accelerometer, the position sensor must be more sensitive if the accelerometer proof mass is to be reduced. In addition, as accelerometer proof mass is reduced, thermal noise appears in the motion of the proof mass, thus degrading the resolution of the accelerometer. These challenges to sensor development will be described.

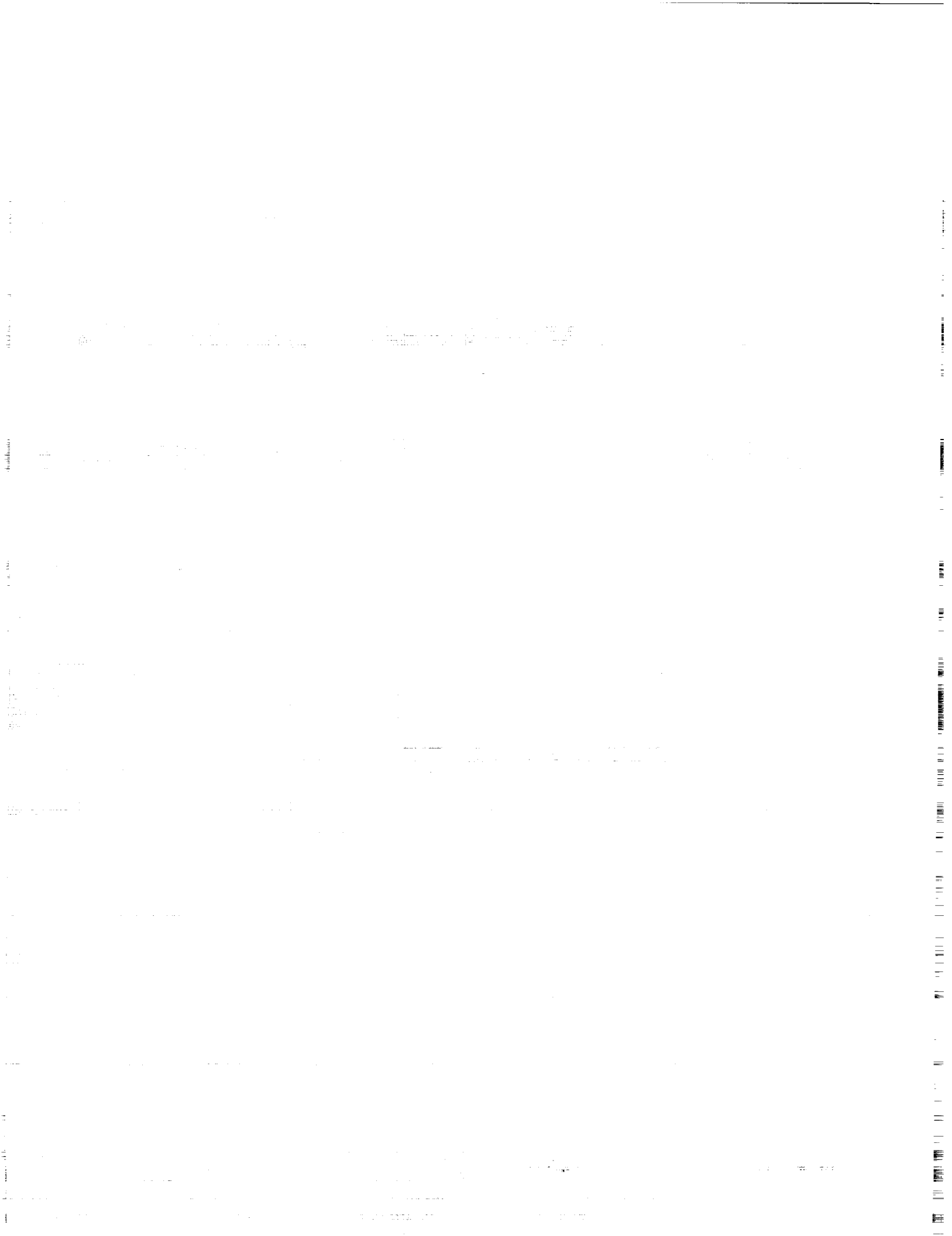
Recent developments at JPL, based on new position sensor principles such as electron tunneling, have produced a series of novel, ultra-high sensitivity microsensors and microinstruments. Included among the applications demonstrated are a high-sensitivity micro-seismometer and micro-accelerometer. In this presentation, the principles and performance of these devices will be described. It will be shown that the implementation of micro instruments using these principles produces systems having performance equivalent to previous conventional instruments, but, with major reductions in mass, volume, and power consumption.

* Research supported by NASA, DARPA, and SDIO/IST.



Microtechnologies
and
Applications to Space Systems Workshop

SUMMARY REPORTS



REPORT OF THE MICROSPACECRAFT PANEL

Chairmen

Ross M. Jones

Jet Propulsion Laboratory, California Institute of Technology

Denis Connolly

NASA Lewis Research Center

This report is based in part on material presented at the
workshop on

MICROTECHNOLOGIES AND APPLICATIONS TO SPACE SYSTEMS

Jet Propulsion Laboratory

California Institute of Technology

May 27 & 28, 1992

Sponsored by:

National Aeronautics and Space Administration
Office of Aeronautics and Space Technology

REPORT OF THE MICROSPACECRAFT PANEL

INTRODUCTION

These findings and recommendations are based solely on the material presented during the Microtechnologies and Applications to Space Systems Workshop, 5/27 & 28/92, and the personal knowledge and judgment of the panel members. These findings and recommendations represent the consensus views of the committee. The mission utility of microspacecraft for NASA space science missions was not an issue that the panel addressed. For the purposes of this panel, a microspacecraft was defined to be a fully functional spacecraft, intended for use on NASA space science missions, whose mass is on the order of 10 kg. During the panel discussions the microspacecraft mass definition was used somewhat loosely to be not less than 10 kg but certainly not more than 100, dependent upon the mission requirements.

PANEL SCOPE

The scope of the panel is presented here in order to put the panel report into context.

"The panel report will attempt to identify areas that need additional development to enable a microspacecraft for NASA space science missions. These areas will span technology development through space qualification of the microspacecraft system. The panel will deal with two top level issues: 1) integrating advances in technology into the microspacecraft system and 2) identifying present limits or obstacles to achieving a microspacecraft. These limits or obstacles will be further defined as either fundamental or only based upon the present state of technology, and therefore a fertile area for improvement with increased resources. The panel will be concerned with all spacecraft subsystems, i.e., instruments, power, propulsion, attitude control, command & data, telecommunications, thermal and structure/cabling/mechanisms."

The scope of the panel evolved somewhat from the above during the discussions on 5/29. Contrary to the what is written above, the panel did not concern itself specifically with (science) instruments.

FINDINGS

- 1) The panel identified no fundamental engineering or physics limitations that would preclude the construction of a microspacecraft.
- 2) There is a large amount of available technology (up to technology readiness level (TRL) 7 which can support microspacecraft given the proper amount of design, validation and qualification.
 - 2a) Some of this technology can be directly and immediately applied to microspacecraft and some will require modification to NASA needs.
 - 2b) This same technology can also be applied to the larger NASA space systems.
- 3) The majority of the technology that can support microspacecraft is programmatically located in the DOD (SDIO, DARPA, etc.) and their contractors.
- 4) There are certain spacecraft components that could be applied to or may be required for certain NASA space science microspacecraft and that have not been addressed by the DOD. Foremost among these components are micro-RTGs, electric propulsion and telecommunications equipment developed for the frequencies used by NASA.
- 5) The following subsystem/box level technologies (see table 1) can support a microspacecraft and are relatively mature (up to TRL 7) in the DOD community.
- 6) Microspacecraft have certain unique technical challenges/needs at the system integration level (see table 2).
- 7) The panel's assessment is that the first application of Micro Electro Mechanical Systems (MEMS) technology to microspacecraft will probably be in the area of sensors (e.g. pressure and temperature), and micro gyros and micro-accelerometers.

Table 1
Technologies Resident at DOD Contractors
that Could Support a NASA Microspacecraft

Structures/Mechanisms

shaped memory actuators - d
composite sandwich panel & trusses (metal & polymer matrix
composites) - d
high thermal conductivity composites & phase change material - d

Power

high efficiency solar cells - d
high energy density battery cells - m

Command and Data

data compression - d/m
opto electronics - m
high capacity bulk data storage parts - d

Telecommunications

active arrays - m
digital receivers - m
Ka band and higher frequencies -m
optical communications - m

Attitude Control

fiber optic and ring laser gyros - d
miniature star cameras trackers - d
lightweight reaction/momentum wheels - d

Propulsion

mono and bi-prop engines - m
high pressure fiber overwrapped propellant & pressurant tanks - d
lightweight valves and regulators - m/d

Electronic Packaging

surface mount technology - d
multichip modules - d
3-D packaging - d
wafer scale integration - m
MMIC - d

d = can be directly applied to NASA microspacecraft (may require
re-qualification for a NASA mission)
m = requires modification and qualification for NASA needs

Table 2
System Level Technology Issues Unique to Microspacecraft

- 1) Improved/Re-partitioned system architectures
- 2) minimization of interconnections (e.g. cabling/connectors)
- 3) common mechanical/electrical/thermal packaging
- 4) power distribution and use at lower system voltages

RECOMMENDATIONS TO NASA
(ranked according to priority)

- 1) Establish a program to flight demonstrate microspacecraft.
 - 1a) Vigorously pursue the transfer, qualification and insertion of DOD developed technologies (defined in finding #5) to NASA missions, systems and subsystems.
 - 1b) In cooperation with NASA codes SL, SS, SZ, SE and QE, support system/mission studies of the microspacecraft concept with the goal of more effectively presenting the applications, requirements and pros and cons of microspacecraft.
 - 1c) Support the development of microspacecraft technologies which are either unique to microspacecraft or which have not been supported by the DOD (defined in findings # 4 & 6).
- 2) Support the MEMS community with a small (~\$0.5) program and encourage investigations into NASA applications.
- 3) Convene a microspacecraft working group to increase communication between users and technologists. This working group should consist of representatives from NASA user centers, NASA technology centers, codes R, S and Q and the DOD contractor community.

JPL

**MICRO GUIDANCE AND CONTROL
PANEL RECOMMENDATIONS**

μG&C

**JOHN DIBATTISTA, CHAIR, NASA HQ CODE RSR
FRED Y. HADAEGH, CO-CHAIR, JPL
CLAUDE KECKLER, CO-CHAIR, LaRC**

MAY 29, 1992

WORKSHOP ON MICROTECHNOLOGIES & APPLICATIONS TO SPACE SYSTEMS

**JET PROPULSION LABORATORY
CALIFORNIA INSTITUTE OF TECHNOLOGY
PASADENA, CALIFORNIA 91109**

WHAT IS MICRO GUIDANCE AND CONTROL?

- MICRO-MINIATURIZED GUIDANCE AND CONTROL COMPONENTS AND SUBSYSTEM (SENSORS, ACTUATORS, CONTROL ELECTRONICS)
- MICRO GUIDANCE AND CONTROL ARCHITECTURE REALIZED BY INTEGRATION OF MICRO-MACHINED DEVICES, ON-CHIP VLSI CIRCUITS AND GUIDANCE AND CONTROL FUNCTIONS

THE GUIDANCE AND CONTROL PANEL WILL FOCUS ON EMERGING MICRO-GUIDANCE AND CONTROL TECHNOLOGIES, USERS AND SYSTEMS ISSUES WITH THE FOLLOWING EMPHASIS.

- MICRODEVICE G&C SUBSYSTEMS FOR SPACECRAFT WILL BE EXAMINED WITH EMPHASIS ON COMPONENT TECHNOLOGY, ATTITUDE AND ARTICULATION CONTROL CAPABILITIES, HEALTH MONITORING AND RECOVERY.
- MICROSENSOR AND MICROACTUATOR DESIGN AND THE ATTENDANT ELECTRONICS, POWER AND INFORMATION PROCESSING WILL BE ADDRESSED. ALSO INCLUDED WILL BE VEHICLE HEALTH MONITORING FOR TRANSPORTATION SYSTEMS.
- FABRICATION TECHNOLOGIES, INCLUDING SILICON PROCESSING, MICRO-MACHINING, TUNNELING TECHNOLOGY, MATERIAL SCIENCE, VLSI OF DEVICES AND SUPPORTING CIRCUITRY "ON-CHIP" WILL BE COVERED.
- DISTRIBUTED ARCHITECTURE ISSUES WILL BE DISCUSSED INCLUDING DATA HANDLING, POWER TRANSMISSION AND DISTRIBUTED MICROSENSING ARCHITECTURES.
- PLATFORM APPLICATIONS WILL INCLUDE
 - SYSTEM IDENTIFICATION, HEALTH MONITORING, AND REMOTE SENSING APPLICATIONS
 - VEHICLE GUIDANCE, NAVIGATION AND CONTROL, AND SHAPE CONTROL FOR MULTI-USE VEHICLES AND LARGE INSTRUMENTS LIKE RADIOMETERS
- THE SCIENCE MISSION APPLICATIONS WILL INCLUDE SYSTEM IDENTIFICATION, OPTICAL FIGURE CONTROL FOR GROUND/SPACEBORNE TELESCOPES AND INTERFEROMETERS, AND INSTRUMENT POINTING/SENSING/ISOLATION.

JPL MICRO G & C TECHNOLOGY **PURPOSE AND OBJECTIVES**



OVERALL PURPOSE:

- DEVELOP NEW MINI/MICRO GUIDANCE AND CONTROL SYSTEM ARCHITECTURES AND COMPONENTS THAT MEET THE NEEDS OF FUTURE SPACE SYSTEMS

KEY OBJECTIVES:

- DEVELOP THE GUIDANCE AND CONTROL MICRO-SENSING, COMPUTATION, AND CONTROL ARCHITECTURES AND COMPONENTS THAT WILL ENABLE:
 - INCREASED RELIABILITY VIA
 - SOLID STATE TECHNOLOGY
 - MASSIVE REDUNDANCY OF MICRO-COMPUTERS

REDUCTIONS

- 100/1 OR MORE IN SIZE, MASS AND POWER
- 10/1 OR MORE IN RECURRING COST AND COST GROWTH RATES

• ARCHITECTURES WITH

- ROBUST PERFORMANCE OVER TEMPERATURE, VIBRATION, AND RADIATION RANGES
- EMBEDDED HEALTH MONITORING
- VIABLE DISTRIBUTED FAULT TOLERANT G & C

JPL MICRO G & C TECHNOLOGY
**G & C APPLICATION NEEDS FOR
FUTURE SPACE SYSTEMS**



MICRO-SPACECRAFT, MICRO-LANDERS, MICRO ROVERS

- ATTITUDE & MANEUVER CONTROL SYSTEM
- MICRO-INERTIAL REFERENCES
- MICROELECTRO-OPTICS FOR MINIATURE CAMERAS & REMOTE SENSORS
- INERTIAL/CELESTIAL NAVIGATION SYSTEMS
- HEADING REFERENCE UNITS
- MINI-CAMERA POINTING, ARTICULATION & STABILIZATION
- ANTENNA POINTING, ARTICULATION & STABILIZATION
- INTEGRATED OPTICAL TRACKING

REMOTE SENSING PLATFORMS, INTERFEROMETERS, & DEPLOYABLE REFLECTORS

- DISTRIBUTED MICRO-SENSOR SYSTEM IDENTIFICATION
- MULTIVARIABLE CONTROL OF STRUCTURAL DYNAMICS
- DISTRIBUTED SHAPE & POSITION CONTROL OF MIRROR ARRAYS
- EMBEDDED ARTICULATION AND STABILIZATION OF TELESCOPE & INSTRUMENT OPTICS
- DISTRIBUTED MICRO-INERTIAL REFERENCES
- EMBEDDED HEALTH MONITORING OF G&C EFFECTORS
- INTEGRATED OPTICAL TRACKING

**MICRO G & C TECHNOLOGY
CORE BUILDING BLOCKS**

JPL

μ G&C

- **CORE INNOVATIONS NEEDED FOR THE NEW MICRO-G & C ARCHITECTURES**
 - **MASSIVELY DISTRIBUTED MICROSENSING FOR SYSTEM ID AND CONTROL**
 - **LIGHT POWERED REMOTE PROCESSING NETWORK FOR MICROSENSING**
 - **MICRO-G & C FOR MICRO-SPACECRAFT AND MICRO-ROVERS**
 - **SIX DEGREE-OF-FREEDOM MICRO-INERTIAL MEASUREMENT UNIT**
 - **ACTIVELY CONTROLLED MICROMACHINED DEFORMABLE MIRRORS**
 - **EMBEDDED HEALTH MONITORING FOR G & C EFFECTORS**
 - **NEW ARCHITECTURES FOR FAULT TOLERANCE AND TO INTEGRATE DIVERSE SUBSYSTEMS**

JPL

**MICRO G&C TECHNOLOGY
TECHNOLOGY AVAILABILITY**



CURRENT READINESS LEVEL: 2-3 (COMPONENT), 1 (SYSTEM)

LAB DEMONSTRATION:

3 YEARS FROM FUNDING START

FLIGHT DEMONSTRATION:

**5 YEARS FROM FUNDING START
(SUBSYSTEM LEVEL)**

MICRO G&C TECHNOLOGY

JPL G & C PANEL RECOMMENDATION

μG&C

THE GUIDANCE AND CONTROL PANEL CONCLUDES THAT THE DEVELOPMENT OF MICRO GUIDANCE AND CONTROL TECHNOLOGIES WILL HAVE A REVOLUTIONARY IMPACT ON NASA SPACECRAFT AND MISSIONS.

THE PANEL RECOMMENDS THAT NASA UNDERTAKE AS SOON AS POSSIBLE THE DEVELOPMENT OF THE MICRO G&C TECHNOLOGY CORE BUILDING BLOCKS, IDENTIFIED IN THIS REPORT, IN ORDER TO EXPLOIT AND SHAPE THE DIRECTION OF INDUSTRIAL AND ACADEMIC ADVANCES IN MICROT TECHNOLOGIES.

EXPEDITE CRITICAL ANALYSIS OF MICROT TECHNOLOGY VIABILITY FOR G&C

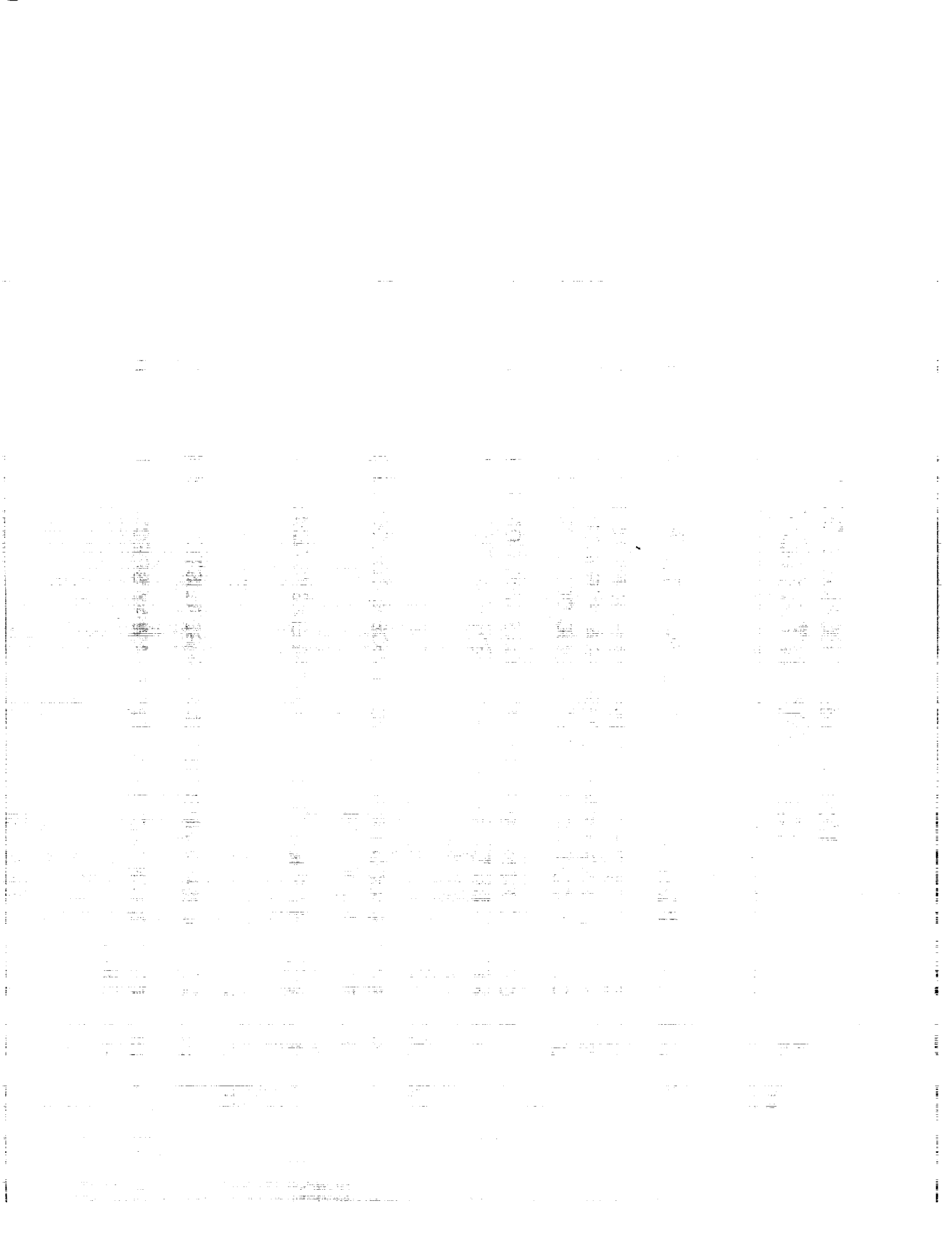
- EXAMINE STATE-OF-THE-ART IN MICRO-DEVICES ACROSS VARIOUS DISCIPLINES AND AGENCIES FOR LEVERAGING INTO G & C INCLUDING MEDICAL, AUTOMOTIVE, BIOLOGICAL, AVIATION AND CONSUMER PRODUCT ADVANCES
- CONDUCT G & C BENEFITS, APPLICATIONS AND CONCEPTUAL STUDIES TAKING INTO ACCOUNT THE MULTIDISCIPLINARY TECHNOLOGIES INVOLVED

FABRICATE

- PURSUE AND SUCCESS PROMISING DEVICES, CONCEPTS (E.G., ELECTROSTATIC, ELECTROMAGNETIC, ETC.)
- BUILD AND TEST PROTOTYPE INTEGRATED SYSTEMS

VALIDATE

- SUBJECT PROMISING SUBSYSTEMS TO REALISTIC ENVIRONMENT
- CONDUCT FLIGHT EXPERIMENTS (GET-AWAY SPECIALS, PIGGY-BACK, ETC.) FOR VALIDATIONS



**WORKSHOP PROCEEDINGS:
MICROTECHNOLOGIES AND APPLICATIONS TO SPACE SYSTEMS**

Workshop Summary Report

Study Coordinator and Proceedings Editor: B.A. Wilson
Jet Propulsion Laboratory, California Institute of Technology

Workshop Chairs: F.Y. Hadaegh, W.J. Kaiser and B.A. Wilson
Jet Propulsion Laboratory, California Institute of Technology

Microtechnologies offer the potential of enabling or enhancing NASA missions in a variety of ways. Following in the footsteps of the microelectronics revolution, the emerging micro-electro-mechanical systems (MEMS) technology, which offers the integration of recent advances in micromachining and nanofabrication techniques with microelectronics in a mass-producible format, is viewed as the next step in device and instrument miniaturization. In the course of identifying the major areas of impact for future space missions, the following three categories emerged:

- **Miniaturization of components and systems, where the primary benefit is a reduction in size, mass and/or power. (Example: Microspacecraft.)**
- **New capabilities and enhanced performance, where the most significant impact is in performance, regardless of system size. (Example: Optical domain image processing.)**
- **Distributed (multi-node) systems and missions, a new system paradigm in which the functionality is enabled through a multiplicity of elements. (Examples: Distributed networks of sensors for mapping, constellations of microspacecraft, or distributed health management sensor systems.)**

The first category is the most obvious, and, not surprisingly, encompasses many of the important applications identified in this report. Nevertheless, there are also numerous examples of significant impact in the other two categories, and because they are more likely to be overlooked in a cursory survey, represent some of the most significant contributions of this study.

MINIATURIZATION OF COMPONENTS AND SYSTEMS

It is generally recognized that future large flagship missions will be fewer and farther between, and that we have entered an era in which smaller, lower budget missions will dominate NASA's space exploration suite. Consequently, there is a critical focus on making everything smaller, lower mass and lower power, preferably with little or no sacrifice in capability or performance. The near-term targets are for Pegasus-launched microspacecraft, for which the total mass allocation, all subsystems and instruments combined, is 10 - 400 kg. Instruments for microspacecraft missions must be concomitantly small, typically under 1 kg. The feasibility of small (< 20 kg) and miniature (< 2 kg) planetary rovers is also being considered.

The Microspacecraft panel reviewed requirements for and obstacles to achieving a 10 - 400 kg, first-generation microspacecraft, and no *fundamental* engineering or physics limitations were identified. Much of the required technology has already been developed, primarily within the DoD community. Key technology developments yet required include micro radioisotope thermoelectric power generators, electric propulsion, Ka-band communication systems, and embedded physical

sensors. Space and mass limitations on a microspacecraft may preclude conventional modular approaches, calling for additional systems integration issues to be addressed. Other technologies such as high-density batteries, data compression techniques, mono-, bi- and solid propellant engines and various mechanical, optoelectronic and communication systems, require further modification to meet specific NASA requirements.

A number of overall recommendations were generated concerning the development and implementation of a first-generation microspacecraft. Ranked in order of priority, these are:

- Establish a program to flight demonstrate microspacecraft.
 - Vigorously pursue the transfer, qualification and insertion of DoD-developed technologies to NASA missions, systems and subsystems.
 - In cooperation with NASA Codes SL, SS, SZ, SE and QE, support system/mission studies of the microspacecraft concept with the goal of more effectively presenting applications, requirements, and pros and cons of microspacecraft.
 - Support the development of microspacecraft technologies that are either unique to NASA or have not been adequately supported by DoD.
- Support the micro-electro-mechanical systems R&D community with small programs and encourage investigation into NASA applications.
- Convene a Microspacecraft Working Group to increase communication between users and technologists. This working group should consist of representatives from NASA user centers, NASA technology centers, Codes R, S and Q, and the DoD contractor community.

The Guidance and Control (G&C) Panel concluded that the development of micro G&C technologies will have a revolutionary impact on future generations of NASA spacecraft and missions. Micro G&C architectures can be achieved through the integration of micromachined devices, on-chip VLSI circuitry and guidance and control functions. The core building blocks include a six-degree-of-freedom micro inertial measurement unit (IMU), actively controlled deformable mirrors, distributed microsensor systems, embedded health monitoring, and light-powered, fault-tolerant processing networks. The overall recommendations in the area of G&C encompass three phases from the planning stages to the flight experiments:

- Expedite critical analysis of microtechnology viability for G&C:
 - Examine emerging state-of-the-art microdevice technologies across various disciplines and agencies for leveraging into G&C implementations, including medical, automotive, biological, aviation and consumer product advances.
 - Conduct studies on micro G&C conceptual development, applications, and benefits, taking into account the multidisciplinary technologies involved.
- Develop and fabricate components & systems:
 - Pursue and succor promising concepts and devices, e.g. electrostatic, electromagnetic, etc.
 - Build and test prototype integrated systems.
- Validate system performance:
 - Subject promising subsystems to realistic environments and operating conditions.
 - Conduct flight experiments for validation, e.g. "get-away specials," "piggy-back," etc.

Miniaturization of planetary rovers will enable a wide range of future planetary exploration missions. Rovers can be considered planetary surface "spacecraft," and much of the discussion in the spacecraft section applies equally to rovers. There are also some additional requirements, primarily in the areas of motility, including path planning and navigation, and articulation of components. Enhanced autonomy is also desirable, which requires additional microsensors and on-board processing capabilities.

The implementation of microtechnologies in sensors and science instruments is already under way, and represents a rapidly evolving area of development with the promise of additional revolutionary advances in the future. The primary impact on science instrument size is expected to result from the development of micromachined transducers, micromechanical structures, and chip-level photonics coupled with fiber optics. The integration of electronics, photonics, and micromechanical functionalities into "instruments-on-a-chip" will provide the ultimate size advantage. The near-term advantages will most likely occur through the insertion of micromachined sensors and actuators, on-focal-plane electronics, discrete photonic components, and nanofabricated optical elements. Overall, the Science Instruments Panel of the workshop found reason for excitement in the potential of emerging microtechnologies to significantly reduce the size and power of future science instruments. Just as in the microelectronics revolution of the previous 20 years, during the next 20 years we may witness vast reductions in the cost of mass-produced items, in this case based on micromechanical and integrated MEMS technologies. This is particularly encouraging as we enter a future in which we anticipate significantly smaller missions with concomitantly reduced cost ceilings. Consequently, this panel strongly urged NASA to focus attention on the development of these technologies to permit their insertion into space missions as rapidly as possible.

NEW CAPABILITIES AND ENHANCED PERFORMANCE

In many cases, the insertion of microtechnologies and/or miniaturized systems can actually *improve* system performance or even enable new science returns. In the case of microspacecraft, for example, the smaller mass and potentially increased robustness against higher accelerations, can be translated into increased maneuverability. This can mean more direct trajectories and shorter trips, which, in turn, reduces restrictions on the viability of instruments suffering from limited component lifetimes. It also increases the possibilities for multi-destination missions. Enhanced performance may also be possible for individual spacecraft subsystems such as communications, data management, G&C, and embedded sensor systems, which could be used to advantage in micro and conventionally sized spacecraft alike. Micromechanical structures are particularly promising for improving the capabilities of inertial sensors and robotic manipulators.

Increased sensitivity, frequency response, dynamic range, resolution and robustness can often be achieved in science sensors through the use of microtechnologies. One of the key components is the micromachined transducer. A prime example is the tunnel sensor, an ultra-sensitive new transducer based on electron tunneling between a micromachined tip positioned a few Å above an underlying surface, the entire structure fabricated from a single silicon wafer. Reconfigured as a transducer, tunneling structures can reveal changes in the tip-surface separation with accuracies of 0.1 Å or better, representing an increase in sensitivity of many orders of magnitude over conventional transducers. Nanofabrication and lithographically defined transducer structures offer large enhancements in sensitivity over conventional approaches. Microchemical sensors offer the possibility of in-situ chemical sensing. A second technology area of critical importance to future science instruments is the application of micro and nanofabrication techniques to optics and optical systems. Microactuators will play a key role in advanced optical systems. Micromachining techniques offer significant enhancements in X-ray imaging resolution, and new opportunities in electrostatic imaging and vacuum electronics for chip-level particle detection and analysis. Nanolithography of optical surface structure is another key element. Lithography on the nm scale is also required for the fabrication of high-frequency receiver components, phased-array antennas and chip-level photonic devices.

DISTRIBUTED SYSTEMS

Perhaps the most stimulating and provocative opportunities for new mission capabilities and science return emerging from the workshop fall into this category. We are at the threshold of the MEMS revolution, anticipated to have as far-reaching an impact on the miniaturization and cost reduction of components as the microelectronics revolution we have already experienced. With the

availability of mass-produced, miniature instrumentation comes the opportunity to rethink our fundamental measurement paradigms. It is now possible to expand our horizons from a single instrument perspective to one involving multi-node or distributed systems. As the largest departure from conventional approaches, advances in this area are the hardest to predict, but may be the most far-reaching.

Given the possibility of launching suites of microspacecraft, it is appropriate to consider the benefits of multi-spacecraft missions. Advantages for Eos-type missions include simultaneous multi-swath mapping. Placing two or more satellites at appropriately phased intervals in the same orbit enables direct active measurements through the atmospheric layers of interest. Multiple spacecraft can also be used as nodes along an extended interferometric baseline, or as points of a gigantic linear unfilled aperture array. Distributed sensor systems offer performance advantages in health management for conventional and microspacecraft. The greatest impact is expected for fuel and propulsion systems, G&C systems and life-support systems, which will require the development and insertion of physical, chemical and biological sensors. Propulsion and fuel systems would benefit from suites of temperature, pressure and specific chemical sensors for leak detection.

One of the most exciting ideas that emerged from the workshop is the concept of utilizing distributed sensor systems for extending the scope of possible science measurements. Similar to the breakthrough in science return offered by focal-plane arrays versus discrete detector elements, distributed arrays of sensors can provide extended sets of information that lead to new levels of understanding of the underlying phenomena. Multi-node sensor systems enable both imaging/mapping activities, as well as the acquisition of time-phased/dynamic information unavailable from a single-sensor measurement mode. For example, while a single seismometer can only indicate the local ground acceleration, multiple sensors distributed across the planetary surface can lead to a detailed understanding of global seismic activity and the nature and structure of the planetary interior. Examples of science instruments where the advantages of distributed arrays are on the horizon include seismometer arrays, free-flying magnetometers, planetary surface constituent analysis, and fiber-optic-linked, free-space interferometers. Complex science instruments may also benefit from embedded arrays of microsensors to monitor their system functionality.

MICROTECHNOLOGY DEVELOPMENT RECOMMENDATIONS

An integrated assessment of the panels suggests that the predominant near-term impact of microtechnologies on NASA space missions is most likely to occur in two areas: (i) the implementation of miniature systems utilizing existing technology; and (ii) the insertion of micromachined sensors and actuators. The miniaturization of spacecraft, planetary rovers and science instruments can proceed rapidly with the incorporation of miniature technologies that have already been developed at the component level, but not yet integrated into appropriately designed miniature systems. Compact packaging technologies will also assist in this process. New miniaturization opportunities are offered by emerging micromachined sensors and actuators, selected chemical sensors, discrete photonic devices, and lithographically defined micro-optics technologies.

Further miniaturization and performance enhancement of spacecraft, planetary rovers and science instruments will be possible as the on-chip integration of micromechanical and electronic components becomes feasible. Coupled with the development of appropriate processing networks, this should enable the first distributed sensor systems for health management applications. Other important mid-term impact areas include the incorporation of binary and adaptive optics and the development of space-qualifiable high-speed electronic systems for Ka-band communications and adaptive processing networks. More fundamental advances are likely to provide additional system advantages further downstream. To ensure that areas relevant to space applications emerge in a timely manner, it is recommended that NASA consider base-program support in selected areas of

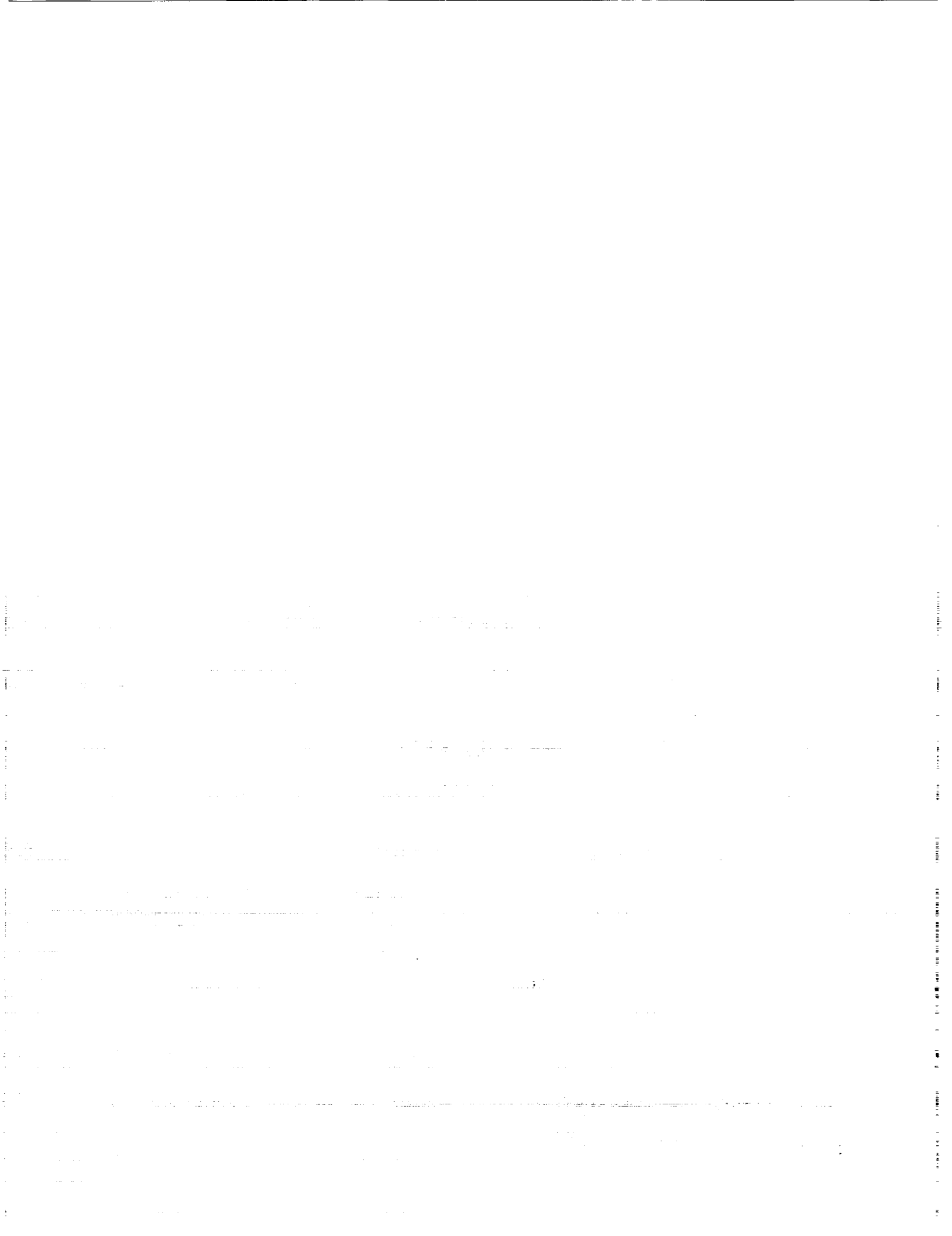
long-term pay-off. These include micromachining and nanofabrication techniques of greater sophistication and in new materials including binary optics, chemical and biological microsensor development, vacuum electronics components, integrated photonic technologies, and fundamental advances in concurrent processing architectures.

CONCLUSIONS

As the first forum spanning the emerging microtechnologies and bringing together the technology and space systems experts across the country, the workshop was enthusiastically supported by all parts of the community. Over 225 people participated in this workshop, drawn from universities, industry, NASA centers, and other government laboratories and agencies. The workshop was chaired by Fred Hadaegh, Bill Kaiser and Barbara Wilson, with presentations overviewing emerging microtechnology developments coordinated by Frank Grunthaner. Following the workshop, a set of recommendations to NASA in support of the key technology development areas was generated as an interim internal report, which was subsequently incorporated into the NASA technology planning process.

Microtechnologies
and
Applications to Space Systems Workshop

APPENDIX



MICROTECHNOLOGIES AND APPLICATIONS TO SPACE SYSTEMS WORKSHOP

AGENDA

DAY 1: May 27, 1992

WELCOME - Barbara Wilson, Session Chair

8:00 am *Workshop Welcome*
8:15 am *Workshop Overview*

Terry Cole, JPL
Wayne Hudson, NASA Code RS

FUTURE VISIONS - Gordon Johnston, Session Chair

8:30 am *Future Trends in Small Missions and Need for Microtechnology*
8:50 am *The NSF Microtechnology Program, or Robots on the Head of a Pin*
9:20 am *Silicon Micro-Instrumentation*

Charles Elachi, JPL
George Hazelrigg, NSF
Kurt Petersen, Lucas NovaSensor

NASA MISSION & SCIENCE GOALS - Wayne Hudson, Session Chair

10:10 am *The Solar System Exploration Program: Goals, Strategy, and Plans*
10:30 am *Science Goals & Constraints of MESUR*
10:50 am *The Fast Flyby Pluto Mission: Completing the Reconnaissance of the Solar System*
11:10 am *Space Physics Mission Needs*
11:30 am *Mission & Science Goals of Lunar Outpost Missions*

Corinne Buoni, SAIC
Arthur Lane, JPL
Paul Henry, JPL
Jim Randolph, NASA Code SS
Jeffrey Plescia, JPL

MICROTECHNOLOGY PROGRAM OVERVIEWS PART I - Frank Grunthaner, Session Chair

1:00 pm *Micro Electro Mechanical Systems (MEMS) and Their Impact on Future Robotic Systems*
1:20 pm *SDI Development of Miniaturized Components*
1:50 pm *DoD Advanced Space Technology Program Challenge*
2:10 pm *Code R Microtechnologies*
2:30 pm *Micromechanics Program at Sandia: Micromechanical Sensors, Actuators and Devices*
2:50 pm *Micromanufacturing: Recent Developments in this Country and Abroad*
3:10 pm *Microsensors and Microinstruments: New Measurement Principles and New Applications*

Stephen Jacobsen, Univ. of Utah
Mick Blackledge, SDI/TN
Al Wheatley, DARPA
Dave Lavery, NASA Code RS
Ned Godshall, Sandia
Robert Warrington, Louisiana Tech Univ.
William J. Kaiser, JPL

MICROTECHNOLOGY PROGRAM OVERVIEWS PART II - William Kaiser, Session Chair

5:00 pm *Micro-Sensors, -Actuators, -Systems: Accomplishments & Prospects*
5:20 pm *National Nanofabrication Facility and Nanoelectromechanics*
5:40 pm *Microactuator Production via High Aspect Ratio, Edge Acuity Metal Fabrication Technology*
6:00 pm *Overview of Microoptics: Past, Present and Future*
6:20 pm *Microsensors, Smart Sensors, Sensor Arrays, and the Artificial Nose*

Richard White, UC Berkeley
Noel MacDonald, Cornell Univ.
Henry Guckel, Univ. of Wisconsin-Madison
Wilfrid Veldkamp, Lincoln Laboratory, MIT
Joseph Stetter, Transducer Research Inc.

PRECEDING PAGE BLANK NOT FILMED

DAY 2: May 28, 1992

APPLICATIONS OVERVIEWS PART I - John DiBattista, Session Chair

| | | |
|---------|---|--|
| 8:00 am | <i>Micromechanical Actuators</i> | William Trimmer, Princeton Univ. & Belle Mead Research |
| 8:30 am | <i>In Situ Meteorological Sensors for Earth and Mars Applications</i> | James Tillman, Univ. of Washington |
| 8:50 am | <i>Silicon Flexural Microelectromechanical Devices</i> | Kaigham Gabriel, NRL |
| 9:10 am | <i>Micromachining the Future</i> | Marc Madou, Teknekron |
| 9:40 am | <i>Learning from Biology - Motor Systems at all Scales</i> | M.G. Littman, Princeton Univ. |

APPLICATIONS OVERVIEWS PART II - Fred Hadaegh, Session Chair

| | | |
|----------|---|---|
| 10:20 am | <i>Micro-Software for Micro-Robots</i> | David Miller, MIT |
| 10:40 am | <i>Spacecraft Telecommunications Technology for Microspacecraft</i> | Charles Kyriacou |
| 11:00 am | <i>Microspacecraft: A Concept</i> | Ross Jones, JPL |
| 11:20 am | <i>Micro-Guidance and Control Technology Overview</i> | Glen Kissel, JPL |
| 11:40 am | <i>Health Management Issues for Space Systems</i> | Stephen Johnson, Martin Marietta Astronautics |

PARALLEL SESSION ON SCIENCE INSTRUMENTS

SESSION AND PANEL CHAIRS: Benton Clark, Gregg Vane & Louis Watts

| | | |
|---------|---|--|
| 1:00 pm | <i>Trends in X-Ray Fluorescence Instruments</i> | Benton Clark, Martin Marietta |
| 1:20 pm | <i>Miniaturization in X-Ray and Gamma-Ray Spectroscopy</i> | Jan Iwanczyk, Xsirius, Inc. |
| 1:40 pm | <i>Backscatter Mossbauer Spectrometer (BaMS) for Extraterrestrial Applications</i> | David Agresti, Univ. of Alabama |
| 2:00 pm | <i>A Sub-cm Micromachined Electron Microscope</i> | Alan Feinerman, Univ. of Illinois at Chicago |
| 2:20 pm | <i>Differential Scanning Calorimetry for Planetary Surface Exploration</i> | Douglas Ming, JSC |
| 2:40 pm | <i>Micro-Sensors for in-situ Meteorological Measurements</i> | David Crisp, JPL |
| 3:00 pm | <i>A Broad-Band Microseismometer for Planetary Applications</i> | Bruce Banerdt, JPL |
| 3:40 pm | <i>The Miniature X-Ray Telescope ALEXIS</i> | Bill Priedhorsky, Los Alamos |
| 4:00 pm | <i>Imaging Spectrometry for the Earth and Other Solar System Bodies</i> | Gregg Vane, JPL |
| 4:20 pm | <i>Smart Focal-Plane Technology for Micro Instruments and Micro Rovers</i> | Eric Fossum, JPL |
| 4:40 pm | <i>Evolution of Miniature Detectors and Focal Plane Arrays for Infrared Sensors</i> | Louis Watts, SAIC |
| 5:00 pm | <i>Photonics Devices for Microinstruments</i> | Robert Lang, Spectra Diode |

PARALLEL SESSION ON MICROSPACECRAFT

SESSION AND PANEL CHAIRS: Denis Connolly, Ross Jones

| | | |
|---------|---|-------------------------------------|
| 1:00 pm | <i>Asteroid Investigation with Microspacecraft (AIM)</i> | Ross Jones & Christopher Salvo, JPL |
| 1:20 pm | <i>Fundamental Limits on Earth Remote Sensing from Small Spacecraft</i> | David Rider, JPL |
| 1:40 pm | <i>Development of MMIC Technology for SATCOM Applications</i> | John Berenz, TRW |
| 2:00 pm | <i>Spacecraft Telecommunications Technology for Microspacecraft Applications</i> | Charles Kyriacou, JPL |
| 2:20 pm | <i>Power Subsystem State-of-the-Art Assessment and Miniaturization Technology Needs</i> | Robert Detwiler, JPL |
| 2:40 pm | <i>The Application of Micro Technology to Spacecraft On-Board Computing</i> | Leon Alkalaj, JPL |
| 3:20 pm | <i>Command & Data Subsystem Technology</i> | Richard Grammier, JPL |

| | | |
|---------|--|-------------------------------|
| 3:40 pm | <i>Electronic Packaging for Microspacecraft Applications</i> | David Wasler, JPL |
| 4:00 pm | <i>Microspacecraft Attitude Control</i> | George Sevaston, JPL |
| 4:20 pm | <i>Miniaturized Propulsion Systems</i> | Dale Hook, TRW |
| 4:40 pm | <i>Lightweight Structures and Mechanisms for Microsatellites</i> | Robert Wendt, Martin Marietta |
| 5:00 pm | <i>SDI Flight Tests of Integrated Microsystems</i> | Rich Matlock, SDI/TN |

PARALLEL SESSION ON SPACE STATION, SHUTTLE & PROPULSION

SESSION AND PANEL CHAIRS: **W.T. Powers, Gerald Voecks**

1:00 pm - 6:00 pm Roundtable Discussions and presentations

PARALLEL SESSION ON MICROROVERS

SESSION AND PANEL CHAIRS: **Kaigham Gabriel and Subramani Venkataraman**

| | | |
|---------|---|--|
| 1:00 pm | <i>Role of Microrovers in Planetary Exploration</i> | Corinne Buoni, SAIC |
| 1:25 pm | <i>Robotic Vehicles for Planetary Exploration</i> | Brian Wilcox, JPL |
| 1:50 pm | <i>Application of Behavior Control Technology to Planetary Rovers</i> | Rajiv Desai, JPL |
| 2:15 pm | <i>Difficulties Inherent in Miniaturizing Current Rover Technologies for Use as Planetary Explorers</i> | Gerald Roston, CMU |
| 2:40 pm | <i>Micromachining Technologies for Automotive Applications</i> | William Tang, Ford Motor |
| 3:05 pm | <i>Microtechnology on Minirovers</i> | Donald Bickler, JPL |
| 3:50 pm | <i>Silicon Flexural Microelectromechanical Devices</i> | Kaigham Gabriel, NRL |
| 4:15 pm | <i>Micromechanical Actuators</i> | William Trimmer, Princeton Univ. & Belle Mead Research |
| 4:40 pm | <i>Toward Milli-Newton Electro- and Magneto-Static Microactuators</i> | Long-Shen Fan, IBM Almaden |
| 5:05 pm | <i>Micro Structures and Micro Actuators for Implementing Sub-Millimeter Robots</i> | Ronald Fearing, UC Berkeley |
| 5:30 pm | <i>Coordinated Control of Legged Locomotion via Nonlinear Oscillators</i> | P. Krishnaprasad, Univ. of Maryland |

PARALLEL SESSION ON MICROTECHNOLOGIES OF THE FUTURE

SESSION AND PANEL CHAIRS: **Frank Grunthaler, John Hines and Brent Mott**

1:00 pm - 6:00 pm Roundtable Discussions and presentations

PARALLEL SESSION ON GUIDANCE & CONTROL

SESSION AND PANEL CHAIRS: **John DiBattista, Fred Hadaegh and Claude Keckler**

| | | |
|---------|--|---|
| 1:00 pm | <i>Control of Micro-Machined Deformable Mirrors</i> | P.K.C. Wang, UCLA |
| 1:25 pm | <i>Emerging Technologies in Microguidance and Control</i> | Marc Weinberg, C.S. Draper Laboratory |
| 1:50 pm | <i>An Electrostatically Suspended, Micro-Mechanical Rate Gyroscope</i> | Timothy Hawkey, Satcon Technology Corp. |
| 2:15 pm | <i>GEC Ferranti Piezo Vibratory Gyroscope</i> | John Nuttall, GEC Ferranti |
| 2:55 pm | <i>The Application of Micromachined Sensors to Manned Space Systems</i> | Gary Havey, Honeywell Systems & Research |
| 3:20 pm | <i>Micro Guidance and Control Synthesis: New Components, Architectures and Capabilities</i> | Edward Mettler, JPL |
| 3:45 pm | <i>Microoptomechanical Devices & Systems using Epitaxial Lift-Off</i> | Mark Allen, Georgia Inst. of Technology |
| 4:10 pm | <i>Miniature Wide Field-of-View Star Trackers for Spacecraft Attitude Sensing & Navigation</i> | William McCarty, OCA Applied Optics, Inc. |
| 4:35 pm | <i>Novel Position Sensor Technologies for Micro Accelerometers</i> | Thomas Van Zandt, JPL |

WORKSHOP PANELS

PANEL ON SCIENCE INSTRUMENTS

PANEL CHAIRS: Benton Clark, Gregg Vane & Louis Watts

PANEL MEMBERS

Arden Albee, Caltech
James Bradley, JPL
Benton Clark, Martin Marietta
Eric Fossum, JPL

Raymond Goldstein, JPL
Gordon Johnston, NASA Code RSS
William Kaiser, JPL
James Tillman, Univ. of WA

Gregg Vane, JPL
Wilfrid Veldkamp, MIT Lincoln Labs
Louis Watts, SAIC

PANEL ON MICROSPACECRAFT

PANEL CHAIRS: Denis Connolly, Ross Jones

PANEL MEMBERS

Leon Alkalaj, JPL
John Berenz, TRW
Corinne Buoni, SAIC
Richard Cheng, Hughes
Denis Connolly, LeRC
Robert Detwiler, JPL
Terry Gamber, Martin Marietta

Rick Grammier, JPL
Dale Hook, TRW
Ross Jones, JPL
Charles Kyriacou, JPL
Robert Lafferty, Motorola
Rich Matlock, SDI/TN
John McIver, Boeing

Rich Reinert, Ball Aerospace
George Sevaston, JPL
Dave Stevens, JPL
David Wasler, JPL
Robert Wendt, Martin Marietta

PANEL ON SPACE STATION, SHUTTLE & PROPULSION

PANEL CHAIRS: W.T. Powers, Gerald Voecks

PANEL MEMBERS

David Blackburn, NIST
Rod Bogue, Ball Aerospace
Thurman Henderson, U. of Cincinnati
Richard Higgins, GA Tech Res. Inst.
Stephen Johnson, Martin Marietta

Kevin Kellenberger, KSC
C.C. Liu, Case Western Reserve
Wally Parce, Molecular Devices
Marc Porter, Iowa State Univ.
Greg Schunk, MSFC

John Simpson, Rocketdyne
Raoul Tawel, JPL
W.T. Powers, MSFC
Dave Venezky, NRL
Gerald Voecks, JPL

PANEL ON MICROROVERS

PANEL CHAIRS: Kaigham Gabriel and Subramani Venkataraman

PANEL MEMBERS

Rajiv Desai, JPL
Long-Shen Fan, IBM, Almaden
Kaigham Gabriel, NRL

Dave Lavery, NASA Code RS
Michael Sims, ARC
Bill Tang, Ford Scientific Res. Lab.

Subramani Venkataraman, JPL
Brian Wilcox, JPL

PANEL ON MICROTECHNOLOGIES OF THE FUTURE

PANEL CHAIRS: Frank Grunthaner, John Hines and Brent Mott

PANEL MEMBERS

Robert Hughes, Sandia
Stephen Jacobsen, Univ. of Utah
Seun Kahng, LaRC
Thomas Kenny, JPL
Ned Godshall, Sandia
Frank Grunthaner, JPL

John Hines, ARC
Mark Madou, Teknekron
M. Mehregany, Case Western Res.
Harvey Moseley, GSFC
Brent Mott, GSFC
Kurt Petersen, Lucas NovaSensor

Stephen Senturia, MIT
Joseph Stetter, Transducer Research
Yu-Chong Tai, Caltech
Joseph Warner, LeRC
Robert Warrington, LSU
Richard White, UC Berkeley

PANEL ON GUIDANCE & CONTROL

PANEL CHAIRS: John DiBattista, Fred Hadaegh and Claude Keckler

PANEL MEMBERS

Randy Bartman, JPL
Frank Bauer, GSFC
John DiBattista, NASA Code RSR
Nelson Groom, LaRC
Fred Hadaegh, JPL

Gary Havey, JSC
Dean Jacot, Boeing
Claude Keckler, LaRC
Glen Kissel, JPL
Henry Lum, Jr., ARC

John Shackelford, General
Dynamics
Henry Waites, MSFC

TECHNICAL REPORT STANDARD TITLE PAGE

| | | | | | |
|---|--|--|--|--|-----------|
| 1. Report No. 93-8 | | 2. Government Accession No. | | 3. Recipient's Catalog No. | |
| 4. Title and Subtitle Proceedings of the Workshop on Microtechnologies and Applications to Space Systems | | | | 5. Report Date June 15, 1993 | |
| | | | | 6. Performing Organization Code | |
| 7. Author(s) None credited on cover | | | | 8. Performing Organization Report No. | |
| 9. Performing Organization Name and Address JET PROPULSION LABORATORY California Institute of Technology 4800 Oak Grove Drive Pasadena, California 91109 | | | | 10. Work Unit No. | |
| | | | | 11. Contract or Grant No. NAS7-918 | |
| | | | | 13. Type of Report and Period Covered JPL Publication | |
| 12. Sponsoring Agency Name and Address NATIONAL AERONAUTICS AND SPACE ADMINISTRATION Washington, D.C. 20546 | | | | 14. Sponsoring Agency Code RE 156 BK-506-49-21-00-00 | |
| 15. Supplementary Notes | | | | | |
| 16. Abstract During FY'92, the NASA Code RS System Analysis RTOP funded a study to evaluate the potential impact of emerging microtechnologies on future space missions. As part of this study, a workshop, "Microtechnologies and Applications to Space Systems" was held May 27-29th, 1992, in Pasadena, CA. This volume serves as the Proceedings of this workshop. It contains the manuscripts provided by plenary and parallel session presenters, and summary reports generated from this material and from information presented during the panel discussions. Where manuscripts were not provided, extended abstracts, if available, have been included. The order of the papers follows the original workshop agenda. | | | | | |
| 17. Key Words (Selected by Author(s)) Spacecraft Communications, Command, and Tracking Spacecraft Design, Testing, and Performance Spacecraft Instrumentation Spacecraft Propulsion and Power | | | 18. Distribution Statement Unclassified; unlimited. | | |
| 19. Security Classif. (of this report) Unclassified | | 20. Security Classif. (of this page) Unclassified | | 21. No. of Pages 370 | 22. Price |

